Coiled-Coil-Templated Acyl Transfer Reactions on the Surface of Living Cells

Dissertation

to obtain the academic degree
doctor rerum naturalium
(Dr. rer. nat.)

in Chemistry

submitted to

The Faculty of Mathematics and Natural Sciences
Humboldt-Universität zu Berlin

by Georgina Clare Gavins

President of Humboldt-Universität zu Berlin
Prof. Dr. Julia von Blumenthal

Dean of Faculty of Mathematics and Natural Sciences
Prof. Dr. Caren Tischendorf

Reviewers:
1. Prof. Dr. Oliver Seitz
2. Prof. Dr. Annette Beck-Sickinger
3. Prof. Dr. Christoph Arenz

Date of viva voce: 17.01.2023

Coiled-Coil-Templated Acyl Transfer Reactions on the Surface of Living Cells

Dissertation

zur Erlangung des akademischen Grades
doctor rerum naturalium
(Dr. rer. nat.)

im Fach Chemie

eingereicht an der

Mathematisch-Naturwissenschaftlichen Fakultät
der Humboldt-Universität zu Berlin

von Georgina Clare Gavins

Präsidentin der Humboldt-Universität zu Berlin
Prof. Dr. Julia von Blumenthal

Dekan der Mathematisch-Naturwissenschaftlichen Fakultät
Prof. Dr. Caren Tischendorf

Gutachter:
1. Prof. Dr. Oliver Seitz
2. Prof. Dr. Annette Beck-Sickinger
3. Prof. Dr. Christoph Arenz

Tag der mündlichen Prüfung: 17.01.2023

The experimental work presented in this dissertation, was carried out between June 2016 and January 2021 in the research group of Prof. Dr. Oliver Seitz at the Institute of Chemistry, Humboldt University of Berlin.

Acknowledgements

There are numerous people I am thankful to for helping me on my PhD journey and enjoying 5 marvellous years in Berlin and I trust that at least a few of them will know they are included in this. I am thankful to you for all the things I have learned, experiences I have had, ridiculous topics debated, new outlooks realised, and for hopefully coming out the other side as a better, more thoughtful scientist and human.

Some names relating directly to this work do warrant mentioning: Firstly, thanks go to Prof Dr. Oliver Seitz for giving me this opportunity in the beginning, and from whom I have learnt a whole lot about the world of academia. Next to the invaluable work of the technical assistants, especially Sophie Neuber and Christina Klotz. Thirdly, to people involved in my project and fruitful collaborations: Philipp Wolff (Universität Leipzig), Dr. Michael Bartoschek (LMU), and Dr. Katherina Gröger. I also want to thank the marvellously meticulous proof-reading of Yannic Altricher. And of course, a big thanks to the whole Seitz group for being the best bunch of people I could ask to work, laugh, drink coffee, and grumble with. It was brilliant.

Thanks to all my family and friends who have no interest in chemistry or academia, who have on occasion provided some much needed perspective, whilst also sometimes reminding me how exceptional it is to be a scientist.

Abstract

Live-cell fluorescent labelling techniques allow biologists to glimpse into a complex biological environment and derive information about a specific target in a near-native environment. Thanks to a concerted effort from the scientific community, a plethora of commercially available, genetically encodable tags and reporters for fluorescence microscopy exist. However, few live-cell methods allow direct conjugation of nucleic acids with proteins despite the robust DNA technologies carried out on cell surfaces using oligo-antibody conjugates. Another aspect of labelling which is often limiting is the ability to selectively multiplex targets. In this study, a method of tag–probe labelling was developed that accomplishes selective, simultaneous labelling of two distinct targets with two peptide nucleic acid (PNA) strands. The technique uses a pair of coiled-coil peptides to guide conjugation of a PNA group to a target protein expressing a peptide tag and using orthogonal coiled-coil enables multiplexing.

Initially, the labelling of synthetic tag-peptides analysed by liquid chromatography revealed the orthogonal dual transfer of PNA to be selective, quantitative, and rapid. PNA conjugation of exemplar membrane receptors followed by hybridization with complementary fluorophore-DNAs achieved straightforward live-cell dual receptor visualization. Finally, using simple molecular tools that form the basis of DNA nanotechnology, recruitment of multiple DNAs facilitated progressively brighter labelling, and erasable surface labelling allowed quantitative study of receptor internalisation.

The presented work borrows from nature two major biomacromolecule building blocks – α-helical coiled-coil peptides and oligonucleotides. The versatile labelling technique uses one of the smallest peptide recognition tags for multiplexed covalent labelling to date and is one of the few reported methods to directly marry the world of genetically encoded proteins with that of nucleic acid technology. Moreover, it preserves the important criteria of being rapid, quantitative, and specific.

Zussamenfassung

Fluoreszenzmarkierungstechniken für lebende Zellen ermöglichen es Biologen, einen Blick in eine komplexe biologische Umgebung zu werfen und Informationen über ein bestimmtes Ziel in einer nahezu natürlichen Umgebung zu erhalten. Dank der konzertierten Bemühungen der wissenschaftlichen Gemeinschaft gibt es eine Fülle von kommerziell erhältlichen, genetisch kodierbaren Markern und Reportern für die Fluoreszenzmikroskopie. Allerdings gibt es nur wenige Lebendzellmethoden, die eine direkte Konjugation von Nukleinsäuren mit Proteinen erlauben, obwohl es robuste DNA-Technologien gibt, die mit Oligo-Antikörper-Konjugaten auf Zelloberflächen durchgeführt werden. Ein weiterer, oft einschränkender Aspekt der Markierung ist die Fähigkeit, Ziele selektiv zu multiplexen. In dieser Studie wurde eine Methode der Tag-Probe-Markierung entwickelt, die eine selektive, gleichzeitige Markierung von zwei verschiedenen Zielen mit zwei Peptid-Nukleinsäure-Strängen (PNA) ermöglicht. Diese Methode verwendet ein Paar von Coiled-Coil-Peptiden, um die Konjugation einer PNA-Gruppe an ein Zielprotein zu steuern, das ein Peptid-Tag exprimiert. Die Verwendung orthogonaler Coiled-Coils ermöglicht Multiplexing.

Die Markierung von synthetischen Tag-Peptiden, die mittels Flüssigchromatographie analysiert wurden, hat gezeigt, dass der orthogonale duale Transfer von PNA selektiv, quantitativ und schnell ist. Die PNA-Konjugation von exemplarischen Membranrezeptoren, gefolgt von der Hybridisierung mit komplementären Fluorophor-DNAs, ermöglichte eine unkomplizierte Visualisierung von dualen Rezeptoren in lebenden Zellen. Durch den Einsatz einfacher molekularer Hilfsmittel, die die Grundlage der DNA-Nanotechnologie bilden, konnte durch die Rekrutierung mehrerer DNAs eine zunehmend hellere Markierung erreicht werden und die löschbare Oberflächenmarkierung ermöglichte eine quantitative Untersuchung der Rezeptorinternalisierung.

Die hier vorgestellte Arbeit lehnt sich an zwei wichtige Biomakromolekül-Bausteine aus der Natur an - α-helical coiled-coil Peptide und Oligonukleotide. Diese vielseitige Markierungstechnik verwendet einen der bisher kleinsten Peptiderkennungsmarker für die kovalente Multiplexmarkierung und ist eine der wenigen Methoden, die die Welt der genetisch kodierten Proteine direkt mit der der Nukleinsäuretechnologie verbindet. Darüber hinaus werden die wichtigen Kriterien der Schnelligkeit, Quantität und Spezifität beibehalten.

Conltents

1. Introduction

For decades biologists have used fluorochrome-labelled proteins to study living cells, in an effort to gain insight into the workings of biological systems. Fluorescence is a phenomenon ideally suited to sensitive, non-invasive detection and fluorescence microscopy or spectroscopy techniques provide a broad scope for delving into the protein microcosm. In the span of just one generation, advances in molecular biology, organic chemistry and imaging technology have paved the way for a live-cell imaging toolbox that includes an unprecedented number of creative and novel ways to label, manipulate, visualize, and analyse proteins in situ. [2,3] Chemical biological methods facilitate labelling with a plethora of different reporter dyes to suit the particular task. [4-6] Multiparameter studies of protein localization, interaction, dynamics, or local environment can now be obtained with exquisite spatiotemporal control. [7,8] Multiple targets may be examined in unison, [9] single molecules can be imaged, [10] and resolution below the diffraction limit has been realized. [11] Fluorescence imaging is now an essential biochemical method for protein analysis and with these tools, complex cellular processes that would otherwise be difficult to analyse are being carefully unpicked.

The first stage in the process is having an effective way to connect a reporter group with the target protein. A common approach for this is the 'tag–probe' method, where a genetically encoded peptide tag is later addressed with a labelling probe leading to a non-covalent or covalent interaction with a reporter group; [12] a field where great advances have been observed in the past 20 years. At the same time, DNA nanotechnology has emerged as a tool for manipulating or barcoding biomolecules in live cells. The nature of oligonucleotide hybridization means that the end product is easily programmed and due to the strong bonding between complementary strands, specificity is maintained in the presence of other oligonucleotides. These features have facilitated the use of DNA labelled proteins for novel applications such as DNA based super resolution microscopy[13] and proximity-triggered fluorescence assays. [14] Currently, protein labelling with oligonucleotides is limited to the use of DNA-antibody or DNA-ligand conjugates, [15] or with the use of large fusion proteins. [16,17] It is apparent that more elegant means to link oligonucleotides to surface proteins, with small tags and fast kinetics, would be of use to the scientific community, and this present work aims to address this gap in the research. The thesis will outline a general and flexible method of live-cell labelling, which uses a proximity induced acyl transfer reaction to

specifically label proteins with a peptide nucleic acid (PNA) molecule to facilitate DNA nanotechnology on the surface of cells.

2. Theoretical Background

2.1. Live-cell Imaging

Before the discovery of fluorescent proteins (FPs), identifying gene expression was only possible with limited methods such as antibody labelling, microinjection of in vitro modified proteins, [18,19] or as bioluminescent luciferase fusions. [20,21] The innovation of using FPs as genetically encoded reporters began with the valiant undertaking by Shimomura et al. in the 60's to collect and purify the 'squeezate' of 10,000 jellyfish, in an effort to isolate the bioluminescent *Aequorin*. [22] The incidental discovery of a protein "exhibiting a very bright, greenish fluorescence in the ultraviolet" prompted the characterization of a green fluorescent protein (GFP). [23] Later, Prasher, [24] Chalfie, [25] and Tsien[26,27] established the use of GFP as a fluorescent marker of gene expression. This was a revolution for cellular imaging since it provided observable fluorescence of any almost any heterologously expressed protein as a GFP fusion, without the requirement of external cofactors (Figure 1B). Rational design and directed evolution produced a selection of fluorescent proteins with diverse spectra allowing for multiplexing, increased brightness, and faster maturation of the chromophore. [28] Accordingly, various microscopic techniques were developed to derive information on FP localization, mobility (FRAP; fluorescence recovery after photobleaching), protein-protein interactions (FRET; fluorescence resonance energy transfer), and to achieve resolution beyond diffraction limits (PALM; photoactivated localization microscopy). [29] The GFP revolution has led to ubiquitous use of FPs and revealed fascinating images of biological systems such as those derived from multicolour mapping of neuronal circuits in the so-called Brainbow (Figure 1A). [30] The significance is reflected in the Nobel Chemistry Prize awarded in 2008 "for the discovery and development of the green fluorescent protein, GFP", [31] echoing the importance of fluorescence microscopy largely. Though FP fusion technology is still favoured today due to its simplicity and intrinsic specificity, there are some basic limitations. The large size (28 kDa) is an obvious constraint; not only does it limit the resolution when using super resolution microscopy (SRM) techniques, but it was shown in some cases that FPs negatively effect the function, [32] localization, [33] stability, [34] and speed of folding[35] of the target protein. Another constraint is the lack of appropriate spatial and temporal control; an inevitable

consequence of a genetically encoded reporter which renders the whole of the target population fluorescent. An assortment of FPs are presently available to complement a

Figure 1 Progress in the field of fluorescence microscopy A) Multicoloured labelling of neurons in transgenic mice using fluorescent proteins. Lichtman et al. developed a novel method of multicolour neuron staining ("brainbow"),which co-integrates combinations of fluorescent proteins, resulting in over 150 potential colours. Image adapted with permission from Springer Nature[36] **B)** Early example (1995) of a fluorescence gene expression marker in living mammalian cells. NMDAR1 (*N*-methyl-D-aspartate subunit 1 receptor)

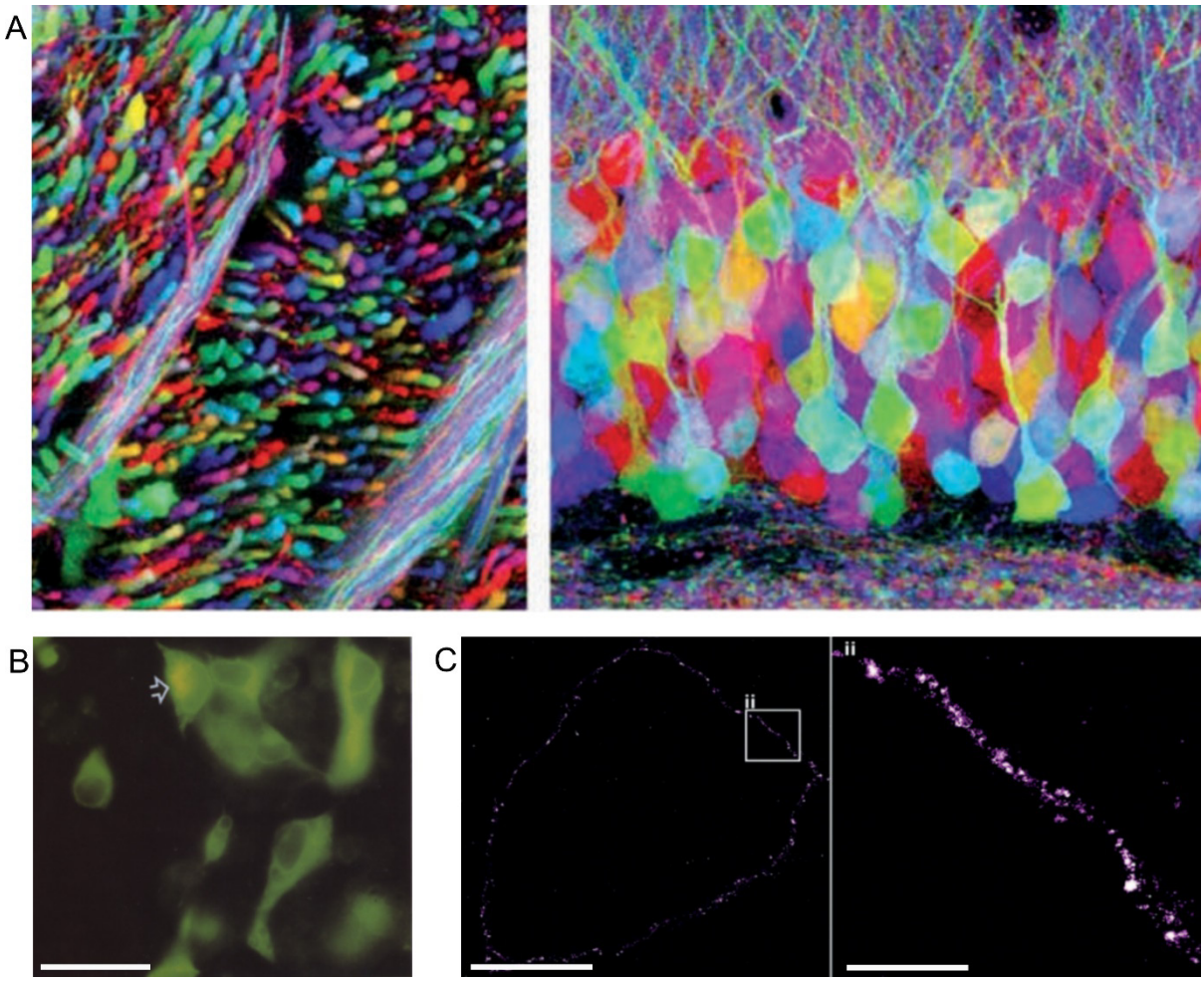

expressed as a fusion of GFP (green fluorescent protein, green) in HEK293 cells. Scale bar= 16 µM. Image adapted with permission from Elsevier[37] **C)** More recent example (2018) of super resolution *d*STORM (direct stochastic optical reconstruction microscopy) imaging of NMDAR1 NR1 domain on live HEK298 cells. Genetic code expansion facilitated labelling of Y392TAG-NR1 (purple) at non-canonical trans cyclooctene (TCO) amino acid with a tetrazine-Cy5 derivative via strain-promoted inverse electron-demanding Diels–Alder cycloaddition reaction. Scale bar= 2.5 µM (left) and 0.5 µM (right; inset). Image adapted with permission from John Wiley and Sons. [38]

range of experimental set-ups and to address some of the drawbacks, [28] yet they cannot compete with what is achievable through chemical synthesis.

Post-translational Labelling

In 1998, alongside the development of GFP, Tsien and co-workers developed another style of fluorescent labelling as a complement to FPs that used chemical recognition of a tetracysteine (TC) peptide tag expressed on the target protein. [39] The FlAsH-EDT_2 (Fluorescein Arsenical Helix binder bis EDT adduct; though later it was discovered hairpin binding is favoured over helical[40]) was a minimal, 6 amino acid long, 0.7 kDa genetically encodable peptide tag able to bind biarsenical fluorescein derivative FlAsH. Though initial methodology was plagued by problems such as unspecific binding, troublesome washing and requirement of reduced peptide, the concept of a hybrid system that uses genetically encoded recognition tags addressable with a chemical probe was a novel concept with obvious advantages. Not only did the magnitudes smaller tag overcome a key weakness of FP technology, it also hinted at the possibility of having chemical and temporal control over the reporter and thereby widening the scope of protein tagging.

Accordingly, the development of labelling techniques that target chemical reporters to genetically encoded tags has been the focus of much research and innovation in the past 20 years and many post-translational labelling strategies have evolved, which allow superior imaging abilities with minimal tags (compare Figure 1B and 1C). The use of chemical probes rather than biological fluorophores provides freedom and flexibility over the reporter, whose properties may be molecularly optimized for particular tasks. [41] This includes organic fluorophores with superior photon output, [42] photostability, [43] preferable absorption and emission spectra[44] or special photophysical properties such as photo switching, two-photon excitation or ion detection. [45-47] As an example of how organic fluorophores can be designed for highly specialized roles, the near infrared (NIR) ‘turn on’ probe for in vivo imaging of Cu(II) was designed by Li et al. It was known that some metal detector probes that increase fluorescence output upon binding to metal ions do so by suppression of an intramolecular photo-induced electron transfer (PET), which normally quenches photon emission. The design of the new probe was approached logically, combining an existing NIR Cyanine fluorophore with a 2,2'-azanediyl bis(N-hydroxyacetamide) side chain capable of switching PET on or off upon binding Cu(II). [48] Aside from organic fluorophores, a non-encoded reporter may grant access to biorthogonal handles for the conjugation of biomolecules (e.g. biotin, oligonucleotides) or reagents (e.g. for cross-linking[49]) to the target; or to super bright quantum dots (QDot) with size-tuneable spectra. [50]

Membrane Protein Labelling

Though only 22% of the human genome codes surface proteins, 60% of current drugs are targeted them. [51] Their roles of recognizing extracellular stimuli, transducing signals or transporting material are a vital to link the extracellular world to the intracellular. Since lipid composition of the membrane bilayer has a strong effect on dynamics and thermodynamics of membrane protein domains[52,53] and membrane composition is markedly complex, [54,55] in situ investigation is necessary for meaningful investigation. For surface protein labelling, a chemist enjoys a larger freedom in the physical properties, chemistries, reactive moieties, and size of the labelling probes they may use. Moreover, the tightly controlled membrane barrier can be advantageous since it makes cell surface specific labelling possible with non-lipophilic, membrane impermeable probes. Because of fewer associated constraints, development of membrane specific labelling methods was natural. [56,57] Moreover, for many medicinally relevant membrane receptors, such as GPCRs (G-protein coupled receptor) and RTKs (receptor tyrosine kinase), the extracellular domain is N-terminal, so N-terminal tagging methodologies are more common. [56] This thesis will relate exclusively to N-terminal, extracellular labelling. For such methods the option of intracellular labelling is merely a bonus, though it may explain the success of widely adopted methods such as the 'SNAP tag' methodology, which will be introduced later in Chapter 2.2.

2.1.1. The Labelling Toolbox

The goal of the ever-growing live-cell labelling toolbox is to find methods that are easily adaptable to many targets. An essential prerequisite is that the tag is addressable in a biorthogonal reaction or provides an interaction without significant off-target labelling. Other requirements may be balanced according to the application, some of which will be introduced in this section.

For instance, use of a small, non-perturbing recognition tag is of increasing importance after the perturbing effect of larger tag fusions has called into question validity of several studies. [32-35] High spatial resolution afforded by smaller probes and tags may also become critical for super resolution microscopy when the resolution limit approaches the size of proteins. Another factor is speed of labelling; quick labelling of the target is a practical advantage, such as for pulse-chase studies where the speed of the chase label is limiting. [58] Stable labelling under the experimental conditions may be essential or a merely a practical advantage, but in some cases the opposite is desired.

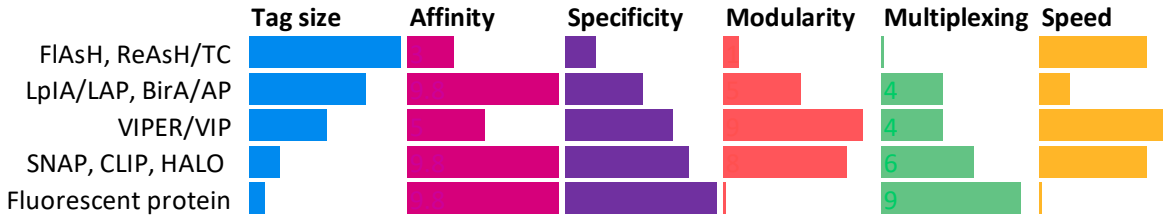

Figure 2 The balance of live-cell protein labelling methodologies. Each criterion was given an estimated score based on published data, with a larger bar representing more favourable score. Labelling methods include fluorescent proteins[28] or post translational methods: FlAsH/ReAsH metal-ion complexes affinity tagging; [39] enzymatic labelling with LpIA or BirA on LAP/AP tags; [60] coiled-coil labelling with VIP[61]/VIPER[62]/miniVIPER tags; [63] Self labelling fusion tags SNAP[64]/CLIP[65]/HALO[66].

Whilst covalent interactions facilitate long lasting experiments and subsequent biochemical analysis, super resolution microscopy can depend on low affinity binders such as the transient peptide interactions used in peptide-PAINT imaging. [59] Multiple target labelling (multiplexing) is crucial to study complex protein systems, yet is markedly lacking in current methods due to difficulties in developing orthogonal labelling reactions/interactions that are also highly specific at low biological concentrations. Modularity of the system, in which the reporter can be easily changed without much labour is essential for a method to be widely employed, given that switching to different methods requires new validation, and consumes both time and money. Modularity also more easily supports study of specific functionalities such as pH sensitive fluorophores, crosslinkers or other biomolecules.

Like any chemical reaction, not all labelling reactions are applicable to all experiments. Encompassing all desirable criteria into one technique is unrealistic, and some methodologies will always favour certain applications. As one criterion is optimized this may come at the detriment to another (Figure 2). This is easily understood when comparing FP and FlAsH methodology. In this case there is a trade-off between tag size and specificity, a common concession. Alternatively, a method with rapid reaction rates may depend on synthetically obscure or toxic probes, or non-commercial enzymes. Thus, aside from the essential traits of being non-perturbing to function and sufficiently specific, other attributes should be prioritized in a manner dependent on the application, and the method picked accordingly.

2.2. Tag–probe Labelling

Recognition tag labelling, so called 'tag–probe' labelling involves expression of the target as a genetically engineered fusion with a tag which is later addressable by a specific probe molecule. There are several different approaches, which can be broadly split into two categories: peptide or protein domain affinity. The latter takes advantage of high affinity binding between proteins and either natural or synthetic ligands and can be further split into non-covalent protein domain interactions or self-labelling strategies, where the protein enzymatically forms a covalent bond. Peptide affinity labelling maintains an advantage over protein domains as it uses smaller tags, but predictably this usually results in a lower specificity. The interacting probes can be metal complexes, [39,40] other peptides, [57] small molecules[64] or even protein domains as for the case of split luciferases or split-FPs. [67] In the case of small molecule and peptides probes, covalent labelling can be mediated by chemoenzymatic labelling via an exogenously added enzyme. These strategies usually evolve from proteins that install post-translational modifications, reworked to accept more useful reporters. Affinity labelling may also be used to enhance the effective molarity of two reactive moieties, triggering a covalent bond-forming reaction. This usually takes place at cysteine thiolate due to its unmatched nucleophilicity[68] but can also be targeted to histidine [69] or lysine. [70]

The technology presented in this thesis will use coiled-coil peptides as the basis of recognition, but to understand the significance of the method, it is important to learn about alternative methods that are currently available and widely used. The following chapter thus outlines some relevant methods available for N-terminal surface protein labelling.

2.2.1. Peptide Recognition Tags with Metal-ion Complexes

Since the first report of the FlAsH-EDT_2/TC tag in 1998 the concept of metal-chelation to a short peptide tag has expanded to a range of metals and reporters (Figure 3). [71] Though all of these methods rely on a coordinate metal-ligand bonds, which can dissociate in aqueous conditions, the most recent iterations have achieved nanomolar or picomolar affinities. The prototype biarsenical binder FlAsH with the 'CCRECC' tag (Figure 4A) has a sufficiently slow k_{off} rate that staining is stable for days in the absence of dithiols, but reversible with millimolar concentrations. [40] An additional advantage is the practical non-fluorescence of the bis-EDT (bis-1,2-ethandithiol) complex. This

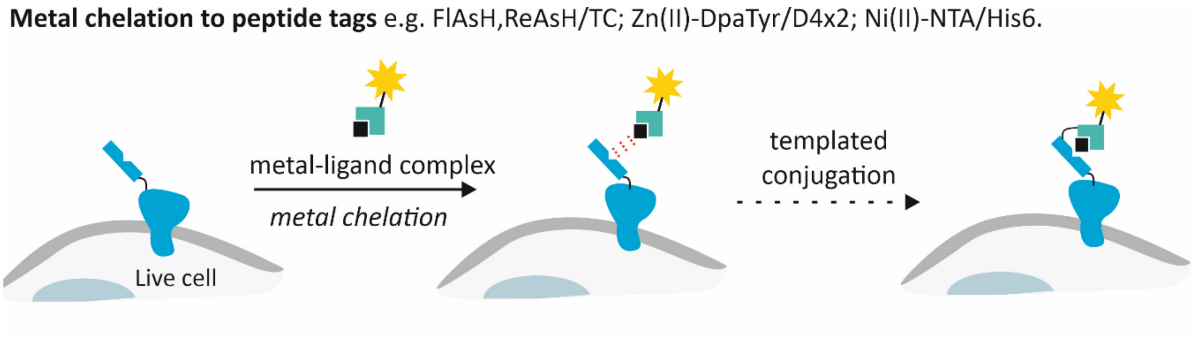

Figure 3 Tag-probe live-cell surface protein labelling using metal chelation. Blue: target protein with tag; Yellow star: reporter group e.g. fluorophore; Green: ligand; Black square: metal (e.g. Zn(II)); Dotted arrow: potential pathway for a proximity triggered reaction, resulting in a covalent linkage to the target.

means removal of unbound FlAsH-EDT_2 by washing is technically not necessary, however due to the prevalence of cysteine residues, stringent 1,2-dithiol washes are still required to counter toxic off-target binding. [39] Background staining is still a weak aspect of the strategy, with the original CCPGCC sequence only being able to resolve up to 20 µM target. Nevertheless, optimization of the tag to a 12mer has improved contrast 20 fold by allowing more stringent washing. [72] What makes the approach compelling is the development of ReAsH, a red-shifted resorufin analogue of FlAsH. [40] Not only does this allow pulse-chase experiments, but ReAsH can also photo-oxidize diaminobenzidine into electron-rich precipitates: a prerequisite to correlate light microscopy with electron microscopy (EM). Exploiting this, Gaietta et al. studied the life cycle of connexin43, a protein that builds gap junction plaques. Using FlAsH for pulse labelling and ReAsH for the chase, they were able to distinguish an abrupt

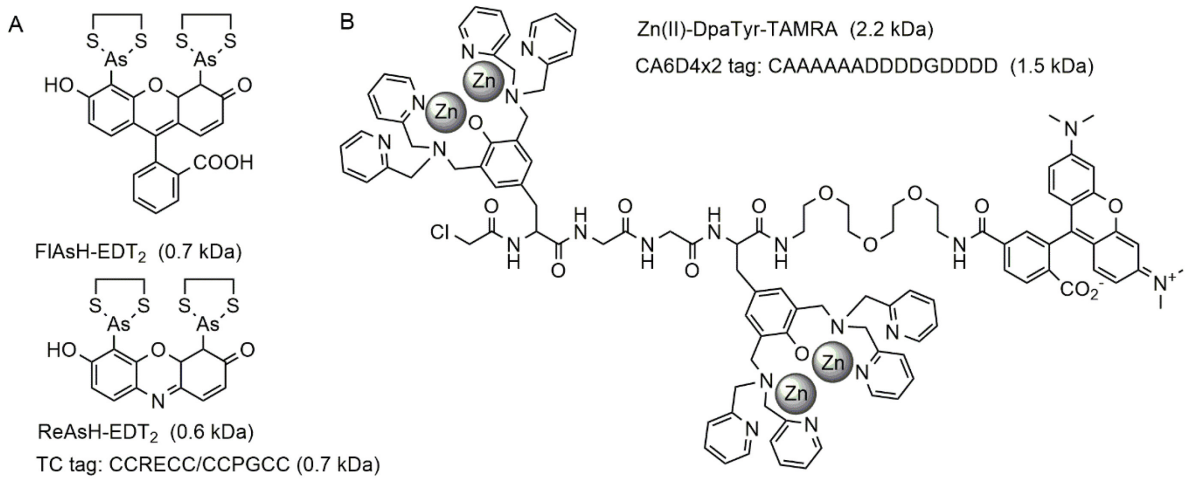

Figure 4 Examples of metal ion complexes that recognise peptide tags A) FlAsH-EDT_2 probe for labelling the TC tag. [39] **B)** Tetranuclear Zn(II)-Dpa-Tyr ligand bearing a TAMRA as the reporter, and a chloroacetyl moiety for covalent labelling of the CA6D4x2 peptide tag via its N-terminal cysteine. [73]

boundary between old and newly formed connexin. They then performed EM on chase-labelled connexin to visualize in higher definition only the newly formed vesicles, gaining insight into delivery of newly formed connexin to the membrane. [74] Another useful application is FRET sensing of protein dynamics, where FlAsH/ReAsH tags can act as a less bulky alternative to the commonly used FP biosensors. Using FlAsH/ReAsH biosensors for quantitative measurements of protein dynamics in cellular studies, Gelman et al. showed that fusion of a GFP was consequential to folding rates. [35] The FlAsH/ReAsH/TC system is a useful method when a large fusion perturbs the protein of interest, and FlAsH and ReAsH kits are commercially available.

Other groups followed suit to create new metal-tag pairs. The Hamachi group created a new, biorthogonal 9mer 'D4x2' oligo-aspartate tag, to which multinuclear Zn(II)-DpaTyr complexes multivalently bind with submicromolar affinity. [75] Unlike FlAsH, Zn(II) ligands have the advantage of tolerating a number of different reporters groups, making the method more adaptable. Crucially, in 2010 Nonaka et al. adjusted the Zn(II)/D4x2 system to allow covalent labelling. With the aim of developing a proximity induced nucleophilic substitution reaction they appended an α-chloroacetyl moiety to the ligand, which reacted with a cysteine sulfhydryl on the modified 16mer 'CA6D4x2' tag (Figure 4B). [73] This was one of the first instances where chemical recognition of a short peptide tag was able to drive a covalent modification of a surface protein with a small molecule probe.

In cooperation with the Ojida group, Hamachi and colleagues also reworked a previously reported recognition pair, the His6-tag/Ni(II)-nitrilotriacetic acid (NTA) system, to similarly enable quantitative covalent labelling. His6 was already a commonplace affinity tag that had previously been applied for reversible membrane protein labelling in a live-cell system, [76,77] but Piehler and co-workers had reported that the multivalency effect could make subnanomolar His-tag binders of Ni(II) coordination complexes, [78] from formerly micromolar mononuclear binders. Building upon this, Takahira et al. used a binuclear Ni(II)-iminodiacetic acid (IDA) complex bearing an α-chloroacetyl group to achieved labelling of membranous Cys-His6 tagged GPCRs in just 30 minutes. [79] Unfortunately, a significant downside to Ni(II)/His6 systems is that Ni(II) is toxic, and acts as a partial fluorescence quencher.

Generally, an increase in binding specificity can be afforded with larger recognition tags, however multivalent metal ligands allow their complementary tags to remain some of the smallest available (<1 kDa for His6; 1.5 kDa for CA6D4x2). Conversely, the high

affinity Zn(II) and Ni(II) complexes are often much larger than the tags (1.3 kDa for bimolecular Ni(II)-IDA[79]; >2 kDa for Zn(II)-DpaTyr probes), and toxicity of nickel and arsenic remains a concern.

2.2.2. Peptide recognition tag with chemoenzymatic labelling

Nature has provided a wealth of enzymes for modification of proteins with biological small molecules and scientists have successfully applied some of them to chemoenzymatic modification of proteins in vitro, and in cellular experiments (though mainly for surface labelling; Figure 5). Such enzyme-mediated labelling protocols usually require micromolar amounts of exogenously added enzyme and substrate, are highly specific (though may recognize natural ligands) and often afford covalent labelling in under one hour. Protein engineering has the potential for providing increased activity, whilst decreasing tag size, and to widen specificity of the enzymes toward substrates which make more useful reporters. Groups have reported biotin ligase[80], sortase[81] and transglutaminase[82]-mediated, N-terminal labelling of proteins. A couple of notable examples are mentioned below.

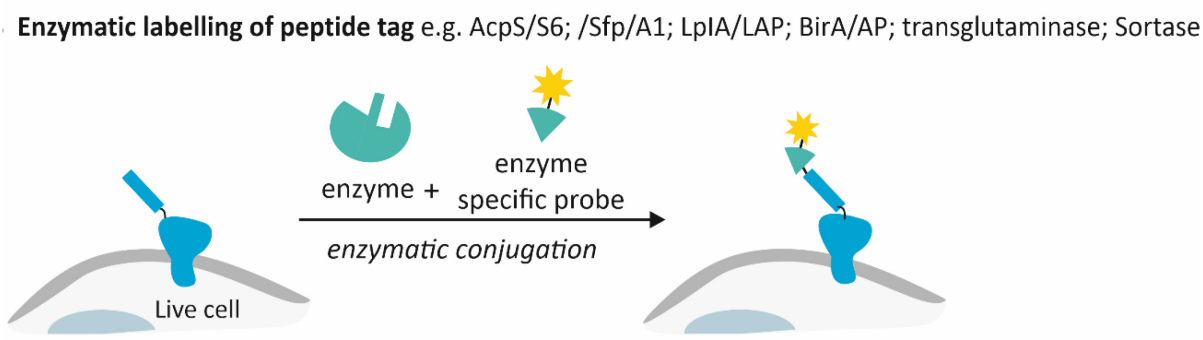

Figure 5 Tag-probe live-cell surface protein labelling using enzymes. Blue: target protein and tag; Yellow star: reporter group, e.g., fluorophore/biotin.

Phosphopantheteinyl-transferases

An established surface labelling method is one mediated by phosphopantheteinyl-transferases (PPTase) AcpS and Sfp. The acyl/peptidyl carrier protein domains ACP (AcpS) [83] or PCP (Sfp) [84] were simultaneously developed for tag–probe labelling in the Johnsson and Walsh labs in 2004, and both recognize coenzyme A (CoA) substrates or CoA derivatives including fluorophores, peptides or biotin (Figure 6A). The 1.4 kDa acyl/peptidyl carrier protein tags (S6 and A1) allow direct conjugation of a pantetheine phosphate to a serine residue in the presence of micromolar amounts of PPTase,

substrate and millimolar Mg(II). The two methods were used for sequential orthogonal labelling of surface proteins TfR1 (Transferrin receptor 1) and EGFR (epidermal growth factor receptor) in under one hour. [85] Surface specificity depends on membrane impermeability of substrates, as CoA is ubiquitous intracellularly, but a recent publication pointed out that cytosolic uptake of CoA substrates, especially of more hydrophobic dyes, restricts the use of this system for methods requiring low background. [86]

Lipoic acid ligase

Lipoic acid ligase (LplA) lipoylates natural protein substrates (E2o, E2p, H protein) at a conserved lysine residue of a ß-sheet. The Ting lab demonstrated that LpIA would accept azido-modified alkanoic acid derivatives, and a second biorthogonal conjugation at the azide (CuAAC, Staudinger ligation) effectively gives the user complete choice of reporter group (Figure 6B). The group redesigned a 22 aa, 1.6 kDa LAP tag after screening various peptide segments of the natural substrate lipoyl domain. After showing the effective labelling, they also demonstrated that the system is orthogonal to biotin ligase BirA/AP tag system (a two-step labelling system based on a mechanistically similar catalytic enzyme, developed in the same lab) and since labelling conditions are comparable, they may be used in unison. [60]

The original system was limited by low activity and yield, but through protein engineering, LpIA/LAP enzymatic labelling has been improved. The group used a 12-mer yeast display library of potential new LAP tag candidates, fixing some important residues and randomizing the non-conserved ones. Their best candidate, “LAP2 tag”, was able to match the labelling efficiency of the original E2p protein on the surface of HEK293 cells. [87] The group also managed LAP2 conjugation of a 7-hydroxycoumarin or resorufin derivative with the mutants ^{W37V}LplA or $^{E20A/F147A/H149G}$LplA, respectively. [88,89] They proved the technique to be faster, more specific and less toxic than the FlAsH methodology for intracellular labelling. [88] Other biorthogonal handles have also been identified; Baalman et al. screened a library of norborene derivatives against ^{W37V}LplA to identify a derivative with equal activity as lipoic acid. This allowed the use of the rapid inverse-electron-demand Diels–Alder [4+2] cycloaddition reaction (DA_{inv}). [90] The LAP2 tag is short and biorthogonal handles allow flexibility in labelling, however the initial enzymatic reaction can take up to one hour and requires micromolar PPTase and lipoic acid derivative.

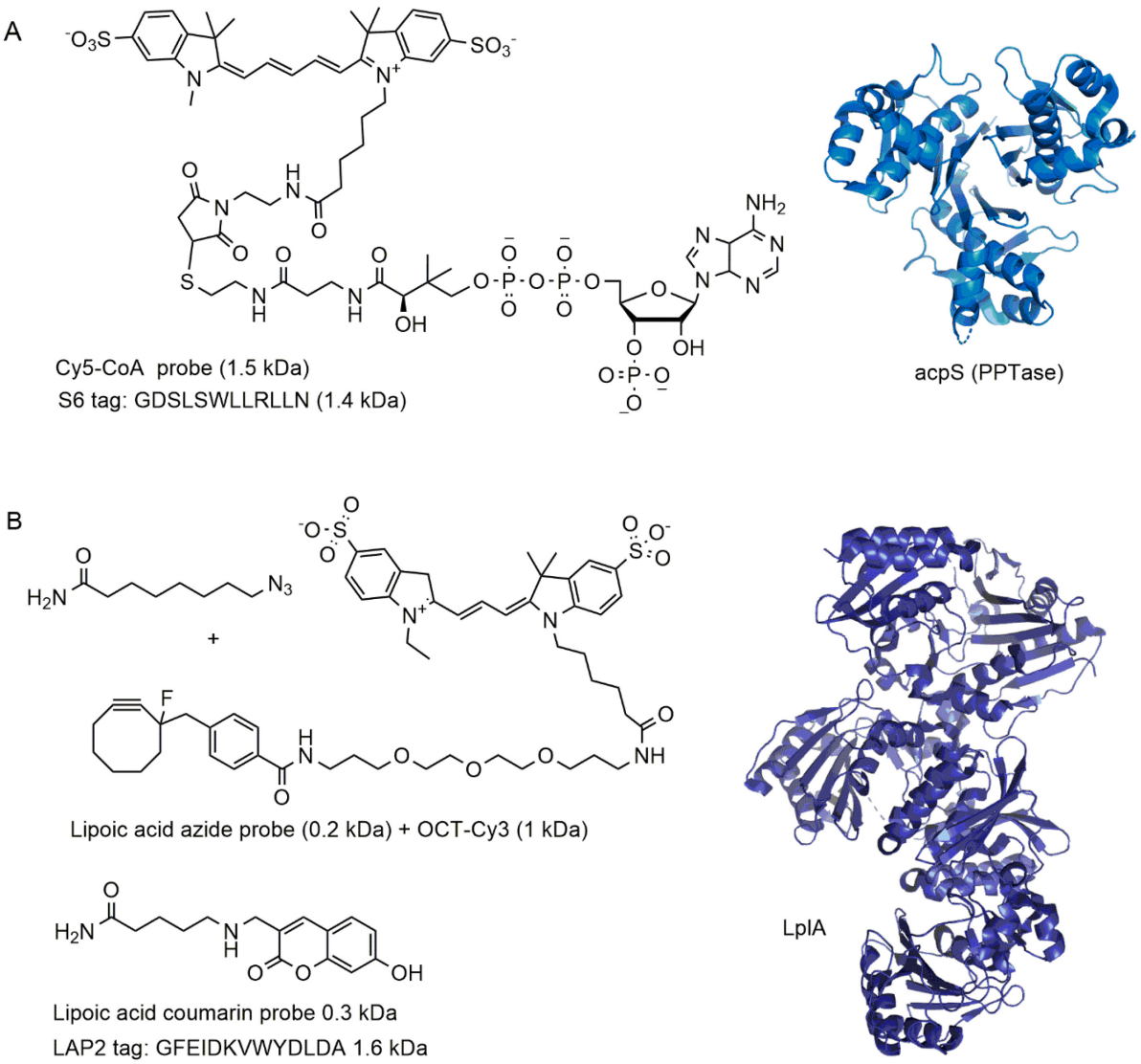

Figure 6 Examples of chemoenzymatic labelling of peptide tags. In each case, a reporter group is conjugated to a peptide tag by an exogenously added enzyme A) PPTase mediated labelling of the 'S6' tag with AcpS (PBB:3hyk) and a coenzyme A (CoA) derivative probe.[83] B) Lipoic acid ligase-mediated labelling of the LAP2 tag with LplA (PDB: 1X2G). Two lipoic acid derivatives are shown: An azide derivative which is addressable in a biorthogonal strain-promoted azide-alkyne cycloaddition reaction, or a coumarin derivative which allows one-step labelling.[60] Crystal-structure images made on PyMOL v2.5.1.

2.2.3. Protein Domain Tags

The most relevant current example of recognition tag labelling, despite their relatively large size, are the self-labelling SNAP[64]/CLIP[65] (20 kDa) and HALO[66] (33 kDa) fusion tags (Figure 7). Pioneered by the Johnsson group in 2003, the SNAP tag was reported first and uses a mutated form of DNA repair protein O^6-alkylguanine-DNA alkyltransferase (hAGT) to promote the irreversible conjugation of a benzyl-guanine

(BG) derivative to a cysteine thiol (Figure 8). [64] The most recent mutant was able to do so in only five minutes with 2.5 µM of BG-Cy3 substrate. [1] CLIP is a mutated form of SNAP which accepts O^6-benzyl cytosine (BC) derivatives, albeit with a 20-fold lower rate constant, discovered by directed evolution. HALO is a haloalkane dehalogenase enzyme capable of covalently linking chloroalkane- reporters (also irreversibly) to cysteine. Many BG/BC/chloroalkane derivatives for each method are tolerated and indeed many are commercially available, including an array of fluorophores; moieties such as azides, which can rapidly undergo bioconjugation reactions; and biotin. [91] In each case labelling is reported to be theoretically quantitative[92] and highly specific, though the HALO tag reportedly exhibits minor off-target labelling. [93]

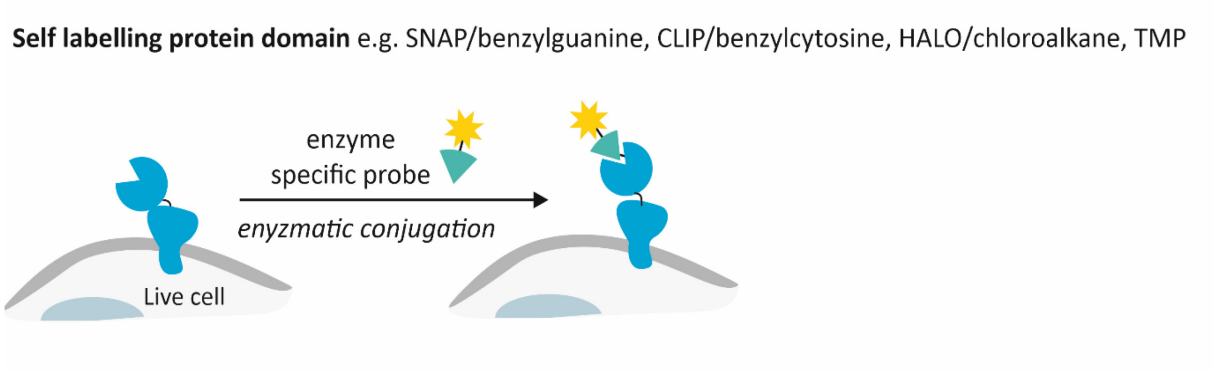

Figure 7 Tag-probe live-cell surface protein labelling using fusion enzymes. Blue: target protein and fusion tag; Cyan: recognition probe; Yellow star: reporter group e.g. fluorophore/biotin.

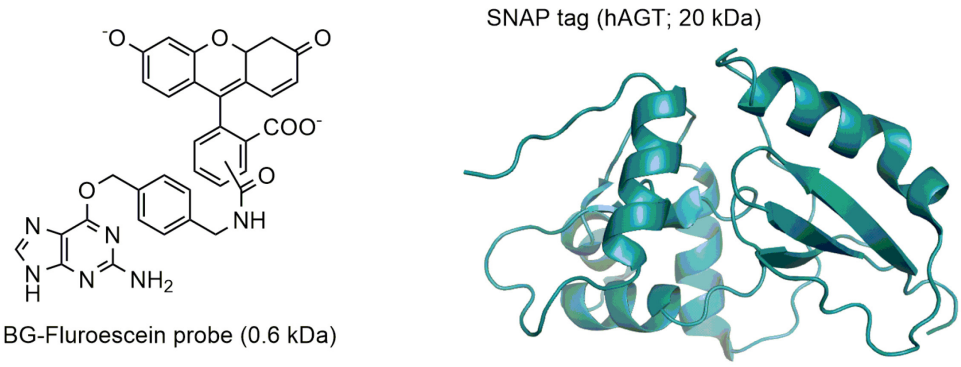

Figure 7 Self labelling SNAP tag. The human DNA repair protein O^6-alkylguanine-DNA transferase (PDB: 6GA0), right, and O^6-benzyl guanine (BG) fluorescein derivative, left, used for SNAP tag labelling. The SNAP tag fusion protein irreversibly transfers the benzyl group and the connected fluorescein from the substrate probe to a cysteine residue. [1] hAGT crystal structure made on PyMOL v2.5.1

Still large, but smaller than FPs, the SNAP tag has appropriated the function of GFP in many experiments. This is due to its superior selection of reporters, membrane permeable probes, rapid labelling, and the option to multiplex with HALO or CLIP. [98,99] This multiplexibility is an important advantage but it should be noted that there is minor promiscuity of the SNAP tag towards the benzyl cytosine CLIP reagents, [93] and the

selection of three proteins still does not compete with the wide range of FPs available. The prospect of a general method allowing conjugation of a target with almost any small molecule derivative has however allowed previously established practices to be quickly repurposed for use in a variety of biological applications. Just a few examples show the broad utility: appending short DNA strands onto SNAP and HALO for super resolution tagPAINT, [100] proximity ligation assays with SNAP and CLIP, [101] organelle-targeted H_2O_2 detection using boronate-caged Tokyo Green derivatives of benzylguanine, [102] a wash-free membrane stain based on Nile Red, [103] crosslinking assays, [104] quantitative internalization assays using a combination of membrane permeable and impermeable HALO ligands, [105] and single molecule tracking of SNAP tagged proteins with highly photostable organic dyes. [106,107] If at all possible, similar experiments would previously have depended on many individual systems such as reporter-conjugated antibodies on fixed cells (PAINT, [13] proximity ligation[108]) or specifically designed fluorescent proteins (H_2O_2 detection[109]).

Other self-labelling tags exist with less general functions such as the HUH-endonuclease tags introduced by Lovendahl, Hayward and Gordon, [16,110] which cleave specific ssDNA sequences to form a covalent 5'-phosphotyrosine linkage. In nature this linkage is intermediary, however when the domain is isolated, the bond persists. Since the HUH super family spans a wide range of endonucleases with different biological functions of which many are literature described, [111-113] the group was able to identify domains recognizing five different oligo sequences, making multiplexing an option. [16] The HUH tags were derived from different bacteria and viruses with varying fusion sizes (13-36 kDa), specificities (some displayed cross reactivity), and conjugation yields (25-75%). They also demonstrated that a covalent oligo 'barcode', as for oligo linked antibodies, can offer a range of applications in fixed or live cells. For example, hybridization of Cy3- and Cy5-conjugated DNA to two different ssDNA-labelled transmembrane HUH tags could be used for one-pot orthogonal imaging, while DNA-linked magnetic beads allowed selective labelling of membrane Notch receptors with the beads. [16] For enzymatic fusions, size remains the major drawback but until another technique that is as generally applicable and easily implemented as the SNAP/CLIP/HALO fusion tags, the methodology is to stay a fast favourite.

2.3. Coiled-Coil Peptide-based Recognition Tags

To tackle specific deficiencies in other available labelling methods, namely the balance between tag size and labelling specificity, Matsuzaki's lab pioneered the use of coiled-coil peptides in tag–probe labelling (Figure 9). The peptide folding motif is ubiquitous in expressed proteins, [114,115] but only recently a broad structural understanding has enabled its *de novo* design, [116,117] which is amenable to optimization of affinities, directions, self-assemblies and also of orthogonal pairs. [118-120] These aspects mean the motif has been the focus of much research interest in the past years and have allowed it to be used as a genetically encoded structural building block and is increasingly used in biomaterial design[121,122] and synthetic biology. [123]

The higher order structure of the coiled-coil motif is made from at least two α-helical peptides assembled into a superhelix. Each peptide is made of a repeating heptad amino acid pattern denoted as *abcdefg* (Figure 10). Burial of hydrophobic residues between both peptides at the *a* and *d* positions in a knob-into-hole manner provides the thermodynamic driving force for supercoil formation. In a heterodimeric coiled-coil, electrostatic or polar interactions at positions *e* and *g* provide stabilization, whilst also maintaining selectivity between different coiled-coil sets, deciding the orientation, and the preference for homo- or hetero oligomerization. Variation of the remaining residues can modulate stability and alignement. [124]

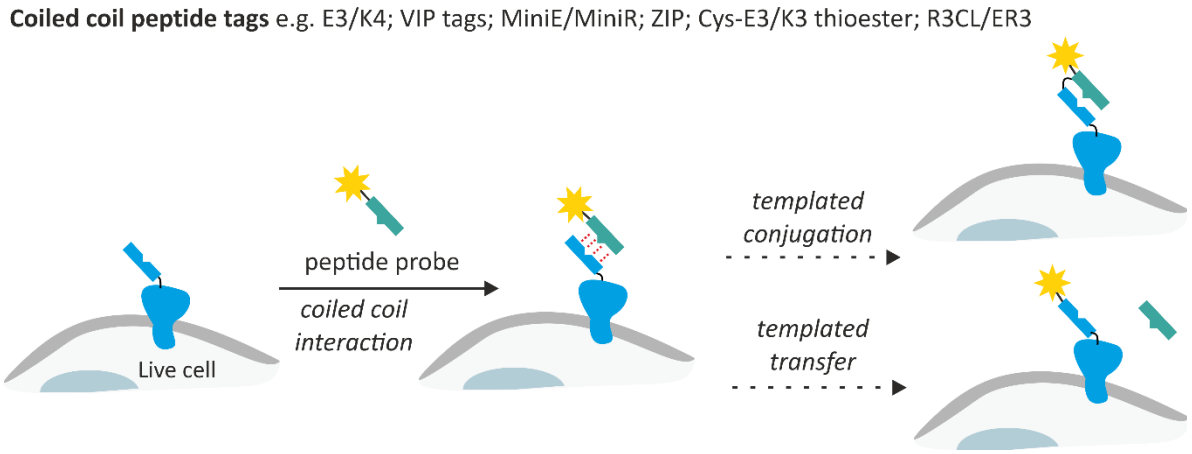

Figure 8 Coiled-coil mediated labelling of a target protein. Blue: Protein of interest/ Coil A (tag); Cyan: Coil B (probe); Yellow star: reporter group, e.g., fluorophore/biotin; Dotted arrows: potential pathway for a proximity triggered reaction, resulting in a covalent linkage to the target.

2.3.1. Non-covalent Coiled-Coil Labelling

Yano et al. [125] first reported the use of a peptide-peptide coiled-coil interaction for labelling in 2008 with the 'IAAL' E/K coil (Figure 11). [116,117] The affinities were demonstrated to be 6 nM for the E3/K4 coil, where the 'K4' labelling peptide was made of four repeated heptads and the fusion tag-acceptor peptide 'E3' three repeated heptads; and 60 nM for the E3/K3 coil, for which both peptides were three heptads long. The system had stronger affinities than the initial metal-ion complex tags,* but not as strong as protein domain interactions or covalent tags. Conversely, the tags were larger than those recognized by metal-ion complexes such as FlAsH, but smaller than fluorescent proteins and SNAP tags. Coiled-coil tag methodology therefore filled a new niche, where membrane proteins fitted with a small-to-mid-size non-perturbing tag should be post-translationally labelled with high specificity and intermediate affinity. The 2.3 kDa E3-tag afforded fast labelling in one minute, allowed use of a non-toxic K3- or K4-probe at nanomolar concentration and required no additional enzymes or special buffers (Figure 12A). Another advantage was that the K-probe could be synthesized with absolute choice of fluorophore or reporter through widely available custom peptide synthesis, making it more accessible than other non-commercialized methods, which may require organic synthesis of their respective probes (such as the Zn(II)-DpaTyr/D4x2 system) or the use of a recombinantly expressed enzyme (Such as LpIA). Additionally, the tags are short enough to be facilely copied into a plasmid by assembly PCR. [126]

The group demonstrated the usefulness of the method in a series of publications delving into the oligomerization[127-129] and internalization[130,131] of GPCRs and RTKs. A compelling example was the development of tools to distinguish receptor oligomerization and its relationship with ligand-based activation. GPCR oligomerization has been extensively studied due to its implication on receptor activation. Though Class C GPCRs are generally reported in the literature to activate through dimer formation, for Class A and B receptors a general consensus has not been reached and literature is plagued with inconsistencies, with the previous assumption of

*The affinities of the E3/K3 and E3/K4 are, however, comparable to the more recently published high affinity metal chelation systems, which also have larger tags and large metal-ligand complexes compared with the tetracysteine/FlAsH system.

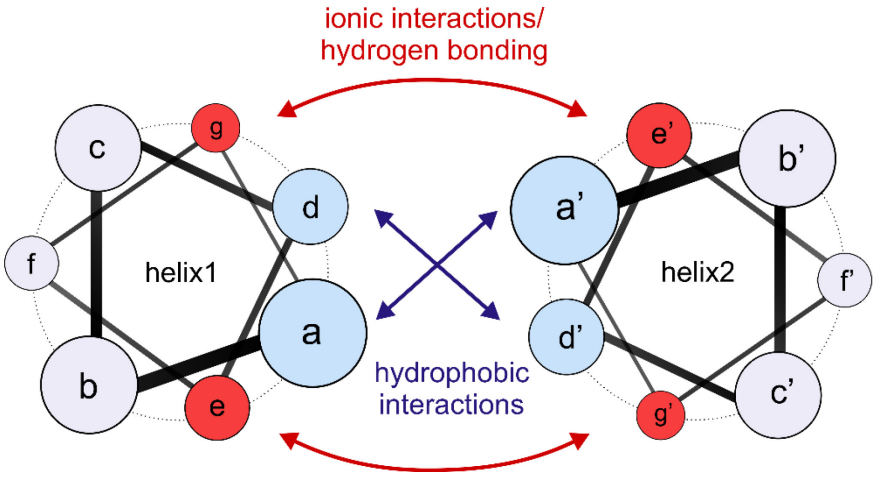

Figure 9 Helix orientation of a parallel coiled-coil heterodimer. Interaction of the two peptides is mediated by the hydrophobic interface (blue) and adjacent ionic or hydrogen bond interactions (red), which stabilize the motif. The individual peptides form α-helicals 'coils', which again wrap around one another, hence the name 'coiled-coil'.

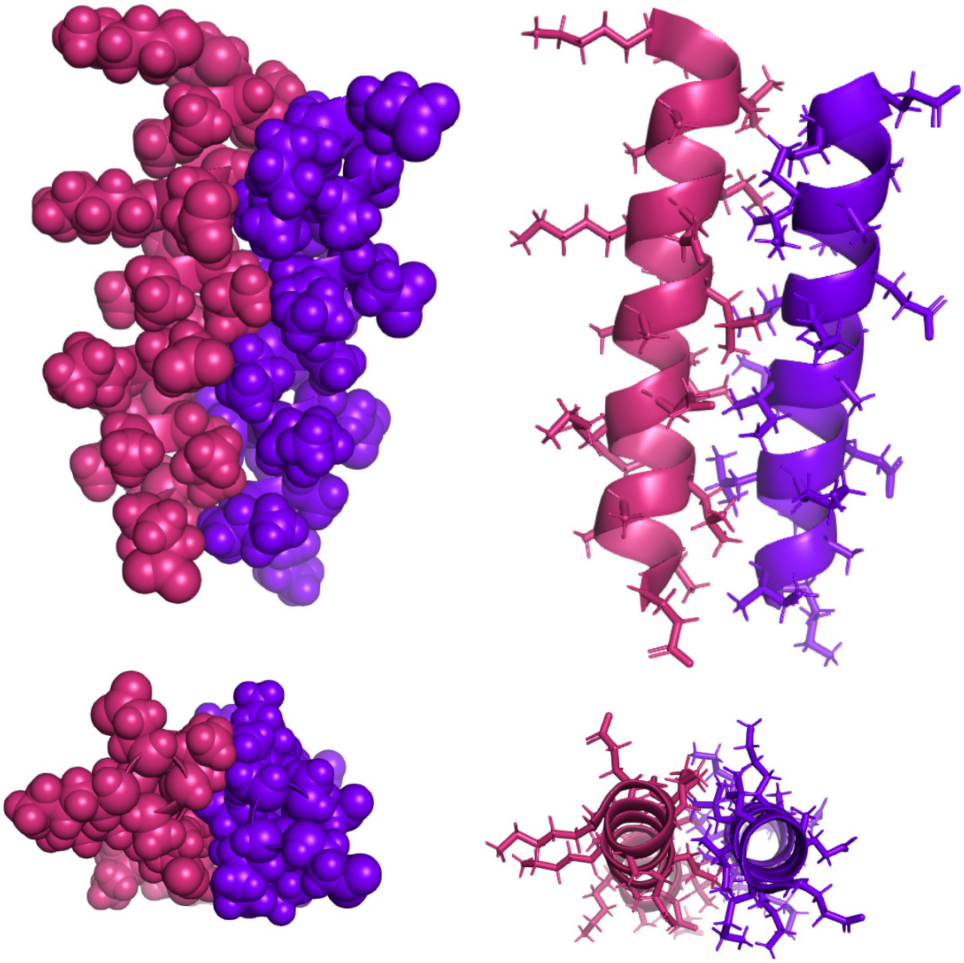

Figure 10 Crystal structure of the parallel heterodimeric E3/K3 'IAAL' coiled-coil. E coil (pink): $(EIAALEK)_3$; K coil (blue): $(KIAALKE)_3$. Left picture shows side chains as spheres, right image shows ribbon structure with stick side chains. Structures are shown in two planes (top and bottom). PBD: 1U0I. Image made on PyMOL v2.5.1

constitutive dimers in contention. [132-136] A major obstacle for clarification is the lack of reliable in situ measurement methods. Immunolabelling has the disadvantage that it can detect artefacts of aggregation after detergent solubilization. [137] BRET (Bioluminescence resonance energy transfer) with FPs has been used as a more reliable alternative, but quantitative analysis is tricky due to poor definition of acceptor/donor ratio, background signal from intracellular protein and a large tag with the potential to aggregate/perturb localization. Since oligomerization is calculated from the dependence of RET on donor/acceptor ratio, this point is critical. An alternative FRET method using E3/K4 labelling reported by Kawano et al. would address the drawbacks of BRET, and weigh into the long-standing debate of whether β2ARs (ß2-adrenic receptors, a Class A GPCR) require homo-oligomerization for activity, which has been differentially reported in literature. [136,138] They found that not only is ß2AR still functionally active without homodimerization, but monomers (or heterooligomers) are the main active form for most of the agonists tested. Importantly, the method was verified and calibrated using standard surface proteins of known oligomeric state, and functional analysis was possible. [127] A follow-up study reported on a number of other Class-A GPCRS, and found that these, too, were active monomers, but reported clustering events that were not related to receptor activation: a probable factor for previous contention. [128]

These findings were clearly valuable and have echoed results from other post translational labelling studies. In fact, the study had followed earlier work by Vogel et al. who used the ACP tag for an analogous FRET methodology to examine NK1R (Neurokinin 1, a Class B GPCR) oligomerization. They found no evidence of constitutive or ligand induced homodimers or oligomers, as well as a dependence of expression level on FRET signal, though unlike Kawano et al., did not use calibration standards. [139] A recent study using single molecule FRET to detect oligomers of 'typical' Class A, B and C GPCRs agreed with both groups. [135] They found monomers, density dependent dimers and dimers in the respective examples. This study used N-terminal SNAP tag labelling which, by comparison is larger but since the authors used single molecule FRET, results had the advantage of not being affected by 'averaging' effects. It should be noted that while SNAP (20 kDa), ACP (9 kDa after tagging) and K/E coiled-coil (5 kDa after tagging) systems both showed that oligomers were not necessary for functional signalling of GPCRs, these studies relied on N-terminal peptide tags. Such tags, though allowing selective membrane labelling, have the potential to disrupt oligomerization therefore presence of functional oligomers could not be completely ruled out, only shown to be non-essential for signalling. Nevertheless, the

need of distinct functional studies to form a consensus on this topic is clear, and even smaller tags or alternate methods would be of use to exclude tag perturbation.

In recent years, remarkable work has been done by the Beatty group in presenting coiled-coil labelling as a multifunctional labelling tool. They first reported Versatile Interacting Peptide (VIP) tags[61] based on a coiled coil designed in the Keating group[140] (5–6 kDa), which were used as interchangeable membrane labelling probes for fluorophores or QDots. The interchangeability was owing to the pI balance of the two peptides, which constitutes an advantage over the K/E system. This was shortly followed by VIPER tags[62] based upon picomolar affinity coils (CoilE/CoilR) from the Vinson group. [141] The group demonstrated how, using a CoilE tag, one could carry out stable live-cell labelling with a range of CoilR fluorophores, perform dynamic pulse-chase imaging, achieve intracellular imaging following cell permeabilization of fixed cells, or use correlative light electron microscopy (CLEM) in conjunction with CoilR-QDots. This methodical validation of the multifunctionality of coiled-coil labelling revealed the ease at which the method was adapted. Furthermore, the tag size remained small; CoilE is 5.2 kDa and CoilR, 7.5 kDa.

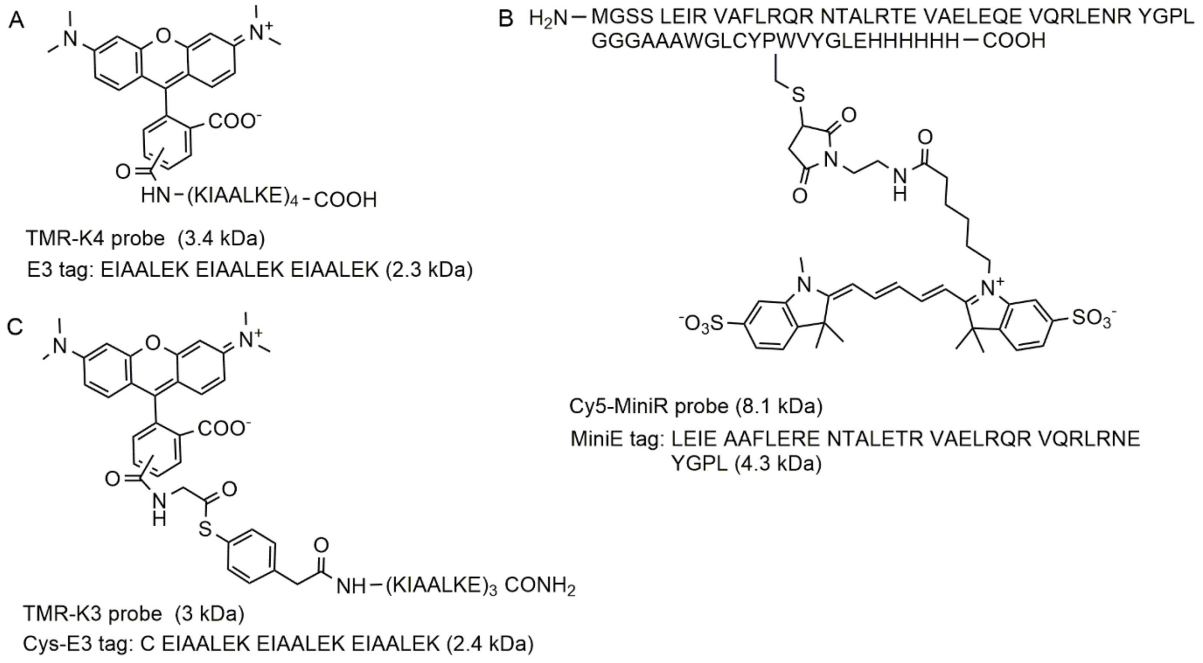

Figure 11 Coiled-coil tag–probe pairs used for live-cell surface labelling. A) E3/K4 coiled-coil labelling with TAMRA-K4 probes[125]. **B)** Cy5-MiniR probe and MiniE tag. The tag and probe can be interchanged. **C)** E3/K3 coiled coil covalent acyl transfer labelling. Only the TAMRA moiety is transferred to the Cys-E3 tag. Spaces are given between coiled-coil heptads for clarity. [142]

Just two years later, Doh et al. reported a modification of the 5 heptad VIPER, dubbed miniVIPER. [63] Losing one heptad and balancing the pI yielded the smaller (4.3 kDa), interchangeable MiniR and MiniE coils (Figure 12B). Additionally, target proteins TfR1-MiniR and H2B-CoilE could be simultaneously visualized through sequential labelling, with MiniE probe treatment on the live-cell surface followed by intracellular labelling of permeabilized fixed cells using a CoilR probe. Since the MiniR and CoilE tags can force protein dimerization, simultaneous labelling was limited to surface target matched with an intracellular target. On the other hand, MiniR-MiniE tag dimerization was used to force 'VIP mediated' protein translocation to the nucleus: another use of the VIP tags. Chemically induced dimerization is a common investigative biological tool[143,144] and coiled-coil-mediated dimerization was already shown to be a valid method of guiding protein interactions. [145,146] This is not surprising as this is often the function of coiled coils in native proteins. [147]

Low-affinity coiled-coil pairs have also been designed for specific applications, such as the E/K peptides used in peptide-PAINT (point accumulation for imaging in nanoscale topography), an SRM method dependant on transient 'on-off' binding of a probe. The method was first established with transient DNA duplexes, [148] but it was shown that the k_{off} rate of the coil peptides could also be fine-tuned for effective super resolution imaging with an E3 tag and a 17 amino acid (less than 3 heptad) long K-peptide imager. [59]

Another notable and more recent example of tuneable coiled-coils sets was reported from the Jerala group, who rationally designed a set of six orthogonal heterodimeric coiled-coil pairs and demonstrated their functionality in mammalian cell experiments. The peptides sets were shown to interact predictably and selectively, with no cross reactivity, in an assay where functional transcription factors for a reporter gene were generated by a coiled coil pairs interaction. One coiled coil (CC) was fused to a transcriptional activation domain VP16 (CC:VP16) and the other CC fused to a DNA binding domain that guided VP16 to the specific reporter gene (TALE:CC). The correctly matching CC:VP16 and TALE:CC fusions were able to trigger gene expression of the target to different levels depending on the CC set used. Furthermore, they showed that gene expression levels could also be modulated by either manipulating the affinity of the coiled coils with increased length or residue substitutions, or by using peptide repeats to recruit multiple transcriptional activators. [149]

To show that the sets could be used simultaneously, another experiment was carried out using three of the sets (P3:P4, P5:P6 and P7:P8) to translocate three FPs into three different cellular compartments in a single cell. One peptide from each set was expressed as a fusion to a signal peptide, and the other from the set to the FP. The mutual orthogonality was confirmed when the FPs were targeted to their corresponding cellular compartments. [149]

2.3.2. Covalent Coiled Coil labelling

Though coiled coils with picomolar affinities, such as the VIPER system, have demonstrated stable enough labelling for pulse-chase experiments, some assays require covalent linkages. Naturally, as for other affinity tag methods, coiled-coil-induced proximity has been employed to trigger a specific ligation reaction. The first of such an approach was demonstrated in 2009 by the Tamamura group, who adapted their previously reported ZIP coiled-coil probes to undergo a cross-linkage. The original method was based on a three stranded leucine zipper coiled coil. [150] This motif was appended to a 4-nitrobenzo-2-oxa-1,3-diazole (NBD), a dye which is quenched in polar environments. When the dimeric tag was treated with the third coiled-coil NBD-peptide, the dye was embedded in a hydrophobic pocket and became fluorogenically active, and did not require washing away of the peptide. [151]Adding a cysteine residue to the encoded tag and an *N*α-chloroacetyl group to the probe, analogous to the approach used by the Hamachi group, conjugation was possible in 15 minutes. [152]

This was the first instance of coiled-coil-induced crosslinking and benefited from a no wash method, but the choice of fluorophore was limited to NBD. The ZIP tag was only slightly heavier than the E3/K4 system, weighing 7.5 kDa after tagging; 5 kDa before tagging, whereas the E3/K4 coil was 5.7 kDa after and 2.3 kDa before.

The next significant step in this field was the acyl transfer reaction developed in the Seitz lab. [142,153] Reinhardt et al. used the prototype E3/K3 interaction to enable a proximity driven reaction. Here, the K3 probes were equipped with a reactive aryl-thioester moiety, which could undergo a reaction with an N-terminal cysteine similar to a native chemical ligation (NCL) (Figure 12C). Thiolysis followed by transthioesterification would result in the acyl group being transferred to the E3 tag via a stable peptide bond. Importantly, the transfer was traceless: the increase in mass after labelling was owing to the reporter group only. Covalent linkages to GPCRs human neuropeptide Y2 (hY_2R) and Y5 receptor (hY_5R) were afforded in two minutes,

comparable the original non-covalent tagging with K4 peptides, whilst using the smaller K3 donor probe. After the transfer, the interacting K3 peptide was washed away with mildly basic solution. A number of reporters were tested, exhibiting differing reactivities and reaction yields in test tube reactions. [153] The remarkable point about this acyl transfer reaction was its high speed and selectivity, despite the relatively small tag size. With this improved covalent labelling method, Lotze et al. [58] were able gain new insights in the hY_2R trafficking via pulse-chase experiments. It was not previously known, whether subsequently trafficked hY_2Rs were treated differently by the cell, but the authors showed that pulse and chase-labelled vesicles internalised independently, and had fused within ten minutes. The study was made feasible by the: i) stable covalent linkage; ii) labelling faster than the vesicle trafficking; and iii) modularity of reporter group allowing multicolour experiments.

Other coiled-coil-templated conjugations reactions have been developed, albeit with slower reactivities and without the benefit of a traceless transfer. Wang et al. developed a crosslinking method based on a 'VAAL' E3/K3 coiled-coil pair analogous to the 'IAAL' E3/K3 coil used by Matsuzaki. This enabled a stable *N*α-chloroacetyl-cysteine cross-linkage with flexible choice of fluorophore and the in vitro reaction reaching a maximum labelling efficiency of 75% in 45 minutes. [154] Yano et al. chose to differentiate from cysteine crosslinking strategies, using a sulfosuccinimidyl ester, which is susceptible to aminolysis. A modified 'IAAL' E3/K3 pair was used, in which the lysines were substituted for arginine (R3CL/ER3 coil), except for one reactive lysine for the cross-linkage. The use of aminolysis as a means for transfer meant that reduction of the cysteine could be skipped, an extra step reported to be explicitly required for tetracysteine tags[39] and conjugation to CA6D4x2/Zn(II)-DpaTyr[73] and CHis6/Ni(II)-IDA[79] metal chelation tags. A prior 10 minute TCEP treatment was also reported by Wang et al. [154] and twice by the Seitz group, [142,153] however in these cases the reduction step was not rationalized. In the pulse-chase studies reported by Lotze et al., the acyl transfer labelling was performed without prior TCEP preincubation, instead the reduction was included in the three-minute labelling step. It is also worth noting that compared with transient labelling using the coiled coils, ligations and transfer reactions have used shorter (3 heptad) peptides. The micromolar-nanomolar interactions of these peptides were still sufficiently strong to increase the effective molarities and trigger stable ligation, whilst the non-templated 'background' labelling remained negligible.

The high affinity, specificity, and speed of labelling with coiled coils is an advantage, and the peptide probes can be conveniently synthesized in any organic laboratory using

basic SPPS methods. The length of the fusion tags still cannot compare to the very short metal ligand/enzymatic peptide tags and the additional mass from the probe peptide, in addition to the persistence length of the coiled coil formed, its rigidity must be considered. However, the particular strength of coiled-coil-based labelling lies in the programmability of this well-defined motif, often made up of only a handful of repeating amino acid building blocks. FPs and enzymatic tags have, after the discovery of an appropriate naturally occurring enzyme, relied on years of protein engineering to deliver suitable characteristics and tend to serve a specific function. In contrast, coiled-coil pairs can be designed de novo, can be (and have been) rapidly adapted to specific functions, and can easily incorporate other synthetic chemical entities or biomolecules. One considerable advantage held over other methods presented here, is the potential of multiplexing using orthogonal coiled-coil sets.

2.4. Multiplexed labelling

Integral in the deciphering of protein networks is the ability to multiplex- that is target a number of proteins simultaneously. [9] Many current drugs exhibit polypharmacology[51] (i.e., they act on multiple targets or disease pathways) and a molecular understanding of this property is essential to testing rational design of multitargeted drugs. [155] Unfortunately, multiplexing in living cells is difficult. FP represent the easiest route to multi target imaging, but this approach is mainly limited by the broad spectral peak overlaps. Technical advances are improving cross talk issues, giving hope to a colourful future for FP imaging, however these do not always apply to live-cell setups. [156] As mentioned, organic fluorophores are superior when considering spectral overlap and properties, so multiplexed posttranslational labelling with organic fluorophores is desirable. Here, the limitation is the labelling step, be this by the existing bio-orthogonal chemistries or the unique fusion enzymes available. Still, some of the earlier mentioned methods do offer orthogonal strategies.

Simultaneous multiplexing of SNAP, CLIP and HALO and TMP[96] tags was demonstrated on the surface of fixed *Drosophila* brain cells with adequate selectivity despite some of the SNAP tag being labelled with CLIP substrate; [99] a point also noted in the original publication[157] and observed in live-cell dual colour STED-SRM (stimulated emission depletion microscopy) of yeast cells with CLIP and SNAP. [98] Nevertheless, *New England Biolabs* offer SNAP/CLIP as orthogonal techniques. For metal ligand based tagging, in vitro experiments on solubilized proteins demonstrated the orthogonality of an earlier iteration of the His6/Ni(II) and D4/Zn(II) system, but live-cell labelling of two targets remains, to the author's knowledge, elusive. [69] For surface labelling with exogenous proteins, ACP/MCP tags[85] (also offered for orthogonal surface labelling from *New England Biolabs*) can be used for sequential labelling only, since the Sfp recognizes both tags, but AcpS only the ACP tag. LpIA and BirA are a decent orthogonal pair, having the advantage of the same labelling conditions. [60] HUH endonucleases were already used for multiplexed labelling of two targets with different ssDNAs, [16] and a recent publication identified four residues in the crystal structure which could be altered to predictably change sequence specificity- an interesting implication for future multiplexing capabilities of the HUH tags. [110]

Different techniques may of course be combined. Wilmes et al. used HALO to tag with photo-switchable Atto655 for dSTORM after duel colour PALM (Photo-activated localization microscopy) for three-colour live-cell SRM (Figure 13), avoiding spectral

overlap between the limited photoactivatable FPs required for PALM. [158] Though there is the possibility to combine different affinity tag methods with one another, this can be laborious, especially if labelling procedures are not compatible.

Coiled-coil-mediated labelling holds a particular advantage over the aforementioned methods because it used a rationally designed system as the basis of target recognition, and many orthogonal coiled-coil sets already exist. Sophisticated methods of rational design have led to progressively larger sets of *de novo* designed orthogonal coiled coils in publications, [120,159,160] the largest group to date being a set of seven heterospecific coiled coils. [161] However, defining stable orthogonal peptide interactions within a well-characterized and easily managed buffer solution is only the foundation for utilising the peptides in live cell experiments. This introduces additional constraints, the most obvious being unwanted interactions of the peptides with biomolecules such as with charged oligonucleotides or polysaccharides. Impressively, up to six orthogonal coiled-coil interactions have been shown to orthogonally modulate protein interactions within the complex cellular matrix in works by the both the Jerala group in mammalian cells and Baker group in yeast cells, with three of Jerala's sets also used for concurrent protein translocation. Interestingly, not all of the peptide sets that were orthogonal in a native-MS (in vitro) experiments undertaken in the Baker group were orthogonal in the subsequent cellular experiments.

The Beatty group's VIP tags were already used to fluorescently image two targets simultaneously in fixed cells, [61] though this could only be carried out in separate cellular compartments due to the sets not being fully orthogonal. Recognising the potential to apply this chemistry to orthogonal labelling, Katherina Gröger and Marc Reimann from the Seitz group demonstrated in preliminary test tube experiments that orthogonal coiled coils[126] (P1/P2 and P3/P4 from the Jerala group) [119] could be used for simultaneous coiled-coil-based labelling of cysteinyl peptides using the acyl transfer methodology previously presented by the group. These experiments hinted that coiled-coil motif covalent labelling has potential for multiplexed imaging. If the interactions were sufficiently specific, large sets could be utilized for covalent labelling of multiple targets.

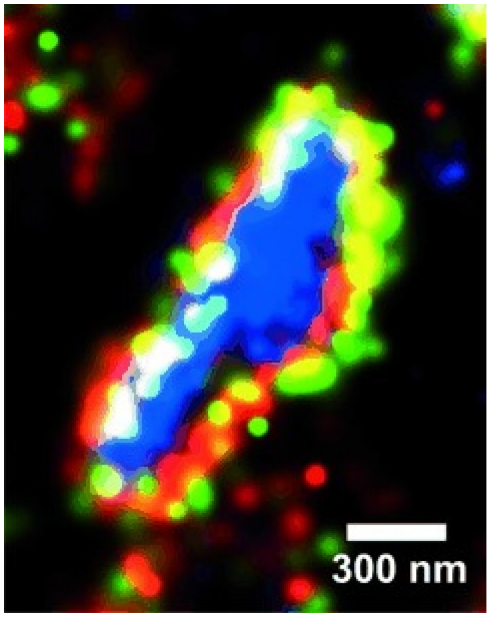

Figure 12 Simultaneous triple-colour live-cell super resolution imaging. Hela cells were transiently transfected with interferon receptors carrying photoactivatable (PA) fluorescent protein tags: IFNAR1-PAGFP (green) and IFNAR2–PAtagRFP (yellow), then treated with Lifeact–HaloTag and HTL–ATTO655 to stain actin (red). Dual colour PALM followed by dSTORM of Atto655 enabled triple colour SR imaging. Image reprinted with permission from John Wiley and Sons. [158]

2.5. Templated Acyl Transfer Reactions for Live-cell Labelling

Many of the labelling techniques described thus far depend on a stable interaction of a tag and probe by hydrophobic interaction, hydrogen bonding or coordinate bonds. In some cases, the structures formed were not the final intent, but used as a template to trigger a covalent bond-forming reaction. Templated chemistry like this is common in bioorganic synthesis and chemical biology, as it delivers specificity to reactions that would otherwise be difficult to perform in the presence of many other biomolecules. [162] The proximity of functional groups brought about by the template means that a quasi-intramolecular reaction can occur at rates many orders of magnitude over the untemplated 'background' reaction, even at very low concentration.

The coiled-coil-templated acyl transfer reaction presented in this work and introduced in the previous chapter (2.3.2) was developed in the Seitz group and was a consequence of the group's focus on nucleic acid templated ligation and in particular, native chemical ligation (NCL). [162] The acyl transfer reaction is an adaptation of a native chemical ligation reaction, which had originally been developed in 1994 by Kent and coworkers[163] as a method of stitching together two or more unprotected peptide fragments to generate a long peptide chain with a native backbone. NCL is considered one of the key developments in the field of synthetic peptide synthesis and has become a standard procedure used to facilitate chemical synthesis and semi-synthesis of peptides and proteins. The key advantages that led to the widespread adoption of the reaction are the native amide linkage, regioselectivity, mild aqueous conditions, and synthetic ease to obtain the peptide fragments. In a typical reaction, a peptide-α-thioester and a sulfhydryl group of an N-terminal cysteinyl peptide react to form a long polypeptide with an amide bond at the junction (Figure 14A). The reaction is highly regioselective for the N-terminal cysteine, allowing selective ligation of unprotected peptides carrying post translational modifications and even of peptides in complex environments, such as in the cytoplasmic matrix. [164]

The scope of NCL has now extended way beyond that of protein synthesis and it is used as a powerful biorthogonal reaction, especially in templated chemistry. [165] In 1996, the Ghadiri group had demonstrated already that coiled-coil peptides were effective for templating the synthesis of larger peptide chains by NCL (Figure 14B). In this work, a 32-amino acid leucine zipper domain was formed from two NCL peptide precursors and a complementary coil peptide template, accelerating production of the peptide 500-fold in the templated reaction compared to non-templated one. [166]

Similar to coiled coils, nucleic acid are self-assembling and programmable scaffolds and are favoured for templated reactions[167] due to their robust, programmable recognition properties; high sequence fidelity; [168] and substantial effective molarity increases. [169] In the same year the Ghadiri group carried out templated NCL, Bruick et al. of the Joyce group made important steps in DNA-templated ligations, when they transferred a peptidyl chain from a thioester-modified DNA to a 3'-amino-terminated oligo, using a DNA template to bring them together. [170]

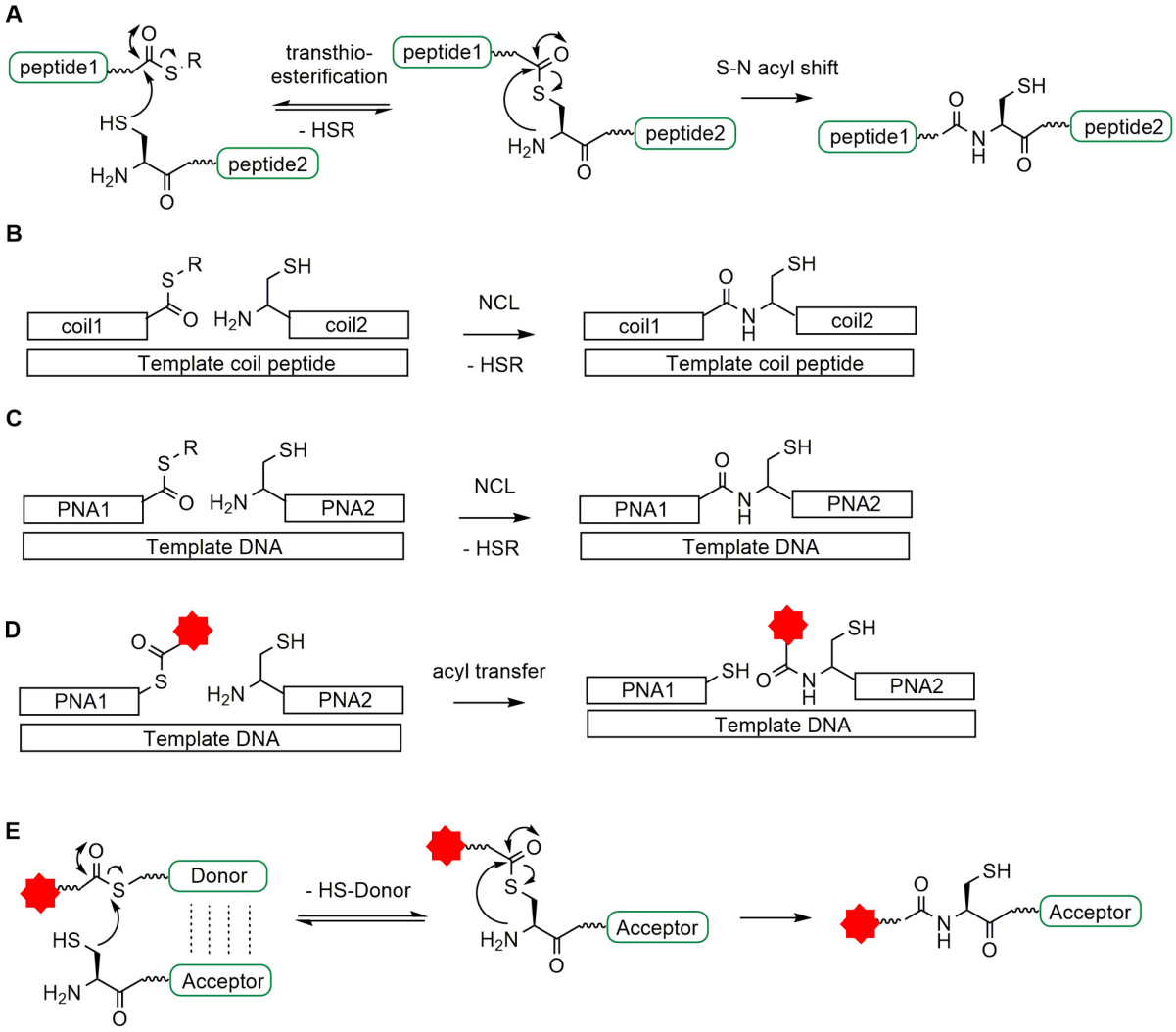

Figure 13 A) Standard native chemical ligation (NCL), used to conjugate two peptide strands. **B)** Coiled-coil-peptide-templated NCL of two peptide strands as carried out by Lee et al. [166] **C)** DNA-templated NCL of two PNA stands as carried out by Ficht et al. [171] **D)** DNA-templated acyl transfer reaction for conjugation of a reporter (red star) as carried out by Grossman et al. [40,172] **E)** Coiled-coil-peptide-templated acyl transfer of a reporter (red star) as carried out by Reinhardt et al. [142] R= alkyl/aryl group.

Later, nucleic acid templated NCL was established in the Seitz lab, [168,171] where a DNA template was used to ligate two nucleic acid (NA) strands for the first time; one bearing

a thioester and one with a terminal cysteine (Figure 14C). Using this system, Ficht et al. achieved a reaction rate faster than the enzymatic ligation: in the presence of template, the reaction was 10^3-times faster than an untemplated reaction, even at 1 µM reactants. In this system, peptide nucleic acid (PNA), a non-ionic and biostable analogue of DNA with a pseudopeptidic backbone (Figure 15) was used for the nucleic acid strands to be ligated. PNA/DNA hybrids form Watson Crick base pairs similarly to a DNA duplex but with increased affinity, allowing the use of shorter PNA segments. [173] Their compatibility with SPPS also makes synthesis of cysteinyl and thioester analogues convenient.

With the aim of developing catalytic, oligonucleotide-templated reaction systems, which do not ligate the two PNA strands, but rather transfer a reporter molecule, the group later reported an analogous acyl transfer reaction. [172] In principle still a NCL, the thioester contained a Dabcyl quencher as the acyl group, rather than a PNA strand; the PNA instead provided the thiol part of the conjugate (Figure 14D). Templated transfer of Dabcyl was achieved without ligation of the templating elements (i.e., the short PNA strands). This meant that the DNA strand could continue to template a new reaction rather than being sequestered, and therefore act catalytically. Furthermore, Erben et al. showed that the DNA-templated (NCL) acyl transfer was also possible in cell lysate: using a DNA template, they demonstrated how a XIAP (X-linked inhibitor of apoptosis protein) antagonist tetrapeptide could be synthesized from a Cys-peptide-PNA conjugate and a thioester linked PNA-peptide, with a readout that allowed reactivation of the formerly inhibited caspase-9. [174] This work showed that acyl transfer reactions could translate into a biologically useful output within a complex biological environment.

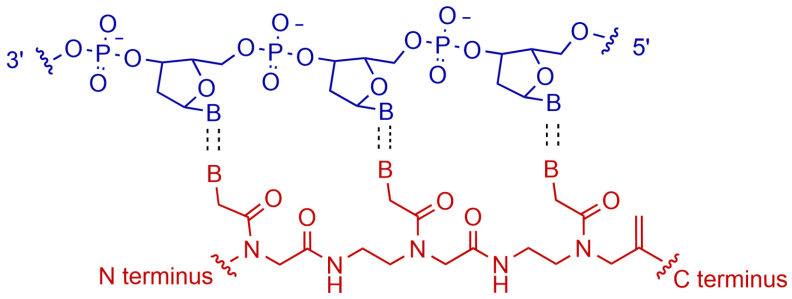

Figure 14 Chemical structure of PNA (red) and DNA (blue) in a double strand. B= nucelobase pair. Dotted lines represent hydrogen bonding between nucleobases

The concept of templated acyl transfers used in DNA-templated chemistry was then adapted for coiled-coil-templated protein labelling. The work of Matsuzaki had

demonstrated that *de novo* designed heterodimeric coiled coils (E3/K3) could be formed on the surface of living cells and used for labelling[175] and the Ghadiri group had used coiled-coil interactions to achieve the effective molarity increases required to trigger native chemical ligations. [166] Building on this work, Reinhardt et al. developed an NCL-type acyl transfer reaction for labelling live cells (Figure 14E). Using a thioester linked fluorophore-K3 peptide conjugate, and validating the method on a number of GPCRs, a fluorophore was successfully transferred onto an N-terminal Cys-E3 tag expressed on the target protein. [142,153] Upon addition of the complementary K3 thioester, a coiled coil was formed with the E3 peptide tag on the surface of the cell. Consequently, a proximity-induced acyl transfer was triggered, forming a covalent linkage between the expressed Cys-E3 tag and the fluorophore in under five minutes. Mercaptophenyl acetic acid (MPAA) thioesters enable rapid transthioesterification (the rate limiting step in NCL) [176] at biological pH, whilst still being relatively hydrolytically stable. All thioesters are highly reactive towards amines and sulphides, but relatively unreactive to oxoesters and water. [177] Though more reactive than their alkyl counterparts, MPAA thioesters still remain stable in mildly acidic buffer and can therefore be safely purified and stored over time without significant hydrolysis.

Unlike with other methods of covalent coiled-coil-templated conjugation presented in Chapter 2.3.2, this resulted in transfer with a minimal mass increase due to no additional mass from the coil peptide. The group also showed that multiple different fluorophores could be transferred, with varying yields. Theoretically any acyl group could be transferred, and Gröger et al. expanded the scope to include PNA transfer; a thioester linked PNA-K3 peptide was used to transfer a 3-mer or an 11-mer PNA strand onto Cys-E3 peptides in under 10 min, and the same methodology was used to image Cys-E3 tagged EGFR protein after hybridization of a complementary fluorophore-labelled PNA or DNA. [126]

2.6. Oligonucleotides as reporter groups

Nucleic acids are one of the three principal building blocks found in nature. By design, they are carriers of information that is translated into complex functionality of proteins via the gene expression mechanism. Using only four nucleobases and two interacting pairs adenine-thymine (or uracil for RNA) or guanine-cytosine, an enormous amount of information can be stably stored in DNA. It is unsurprising then, that through knowledge of nucleobase interactions, global melting temperatures and computational design, scientists have exploited its use not just for genetic engineering but as a programmable building block for assembling structural motifs and enabling new technologies in the nanoscale, such as DNA molecular machines, genetic barcoding, and protein assembly. [178]

The potential of oligonucleotide technology for cellular assays and imaging is large and varied. Immuno-PCR uses oligo-antibodies to combine the specificity of antibodies with the amplification power of PCR and sensitivity is up to 10^5 fold higher in comparison to antigen detection methods. [179] The Jungmann group has used DNA-conjugated antibodies for super resolution PAINT (Point Accumulation for Imaging in Nanoscale Topography) imaging, an alternative method of super resolution microscopy. They used the transient binding of short imager ssDNA to DNA docking strands on the antibody to create the prototypical 'blinking' effect required for super resolution methods such as those used in dSTORM and PALM. [13,148] Using orthogonal DNA sequences, Wade et al. showed that 124 orthogonal DNA sequences could be imaged simultaneously by PAINT. [180] Oligo labelling is also not limited to dsDNA; often modified nucleic acids probes such as LNA (locked nucleic acid) or PNA are used in place of standard DNA due to having increased affinity[181] and DNase resistance. [182]

Antibody-nucleic acid conjugates have the downside of difficult synthesis and the requirement for cell fixation. For this reason, post-translational labelling methods have also been used for nucleic acid-labelling of proteins. HALO tags have been used to produce DNA barcodes for screening interactions of GPCRs in solid phase asssays. [183] In a live-cell setting, SNAP tags have been used to append EGFR with short DNA strands on live HEK293 cells. [17] Using a dimerization DNA, Liang et al. were able to pre-organize the receptors into homodimers, and showed that these dimers, though activated by phosphorylation, differed in downstream activity from those formed by ligand stimulation. Methods of conjugating nucleic acids to proteins are integral to link DNA technology to biological applications. [184] Unfortunately, very few methods which

allow conjugation of oligonucleotides to live cells are reported in recent literature; one being the above mentioned SNAP tag method in a 2-step fashion, [17] and more notably the HUH domains from the Gordon group mentioned in chapter 2.2.3. [16]

3. Objective

Recognition tag labelling depends on chemical or biological recognition of a specific protein secondary or tertiary structure. The reliance on amino acids as the tag is driven by our ability to easily genetically encode any given amino acid sequence into the target protein. Using our knowledge of preferred chemical bonding and interactions, biorthogonal peptide tags can be rationally designed and targeted with external probes. The coiled-coil structural motif is one such example of a programmable tag, which has been used to label[175] and to manipulate expressed proteins on live cells. [149] Previous work in the Seitz group in collaboration with the Beck-Sickinger group focused on a method of covalent live-cell labelling of surface proteins expressing 2 kDa 'Cys-E3' acceptor peptide tags. Formation of a coiled-coil motif with a complementary donor K3 peptide-thioester triggered an acyl transfer reaction able to rapidly label the target with a various organic fluorophores (Figure 14E). [142,153] This technique proved to be advantageous for pulse-chase labelling due to its rapidity. [58] To increase the scope of this reaction, work by Katherina Gröger and Marc Reimann examined the use of orthogonal coiled-coil sets from the Jerala group, [119] who used computational design to optimize four sets of completely orthogonal peptide pairs. Using two of these sets (P1/P2 and P3/P4), Marc Reimann showed that transfer of two different fluorophores to synthetic acceptor peptides was possible in a one-pot reaction in buffer. [119]

Another programmable biomacromolecule, which has gained increasing prominence as a tool for nanotechnology in the live-cell setting, is DNA or nucleic acid analogues. [178] Given the recent advances of DNA nanotechnologies, and the fact that the number of live-cell DNA conjugation techniques is still limited, development of a general nucleic acid labelling method would be a useful addition to the labelling toolbox. Initial work by Dr. Katherina Gröger examined the same live-cell labelling reaction to transfer a peptide nucleic acid (PNA) to EGFR, finding that a 3-mer and an 11-mer strand could be transferred in under five minutes to synthetic peptides, and that selective live-cell labelling could be achieved by hybridization of complementary fluorophore-ssDNA strands.

The objective of this work was to develop the method of live-cell PNA labelling, establishing the system as a versatile and general oligonucleotide conjugation method, and to demonstrate the practicality of the nucleic acid tag in a biological setting. The

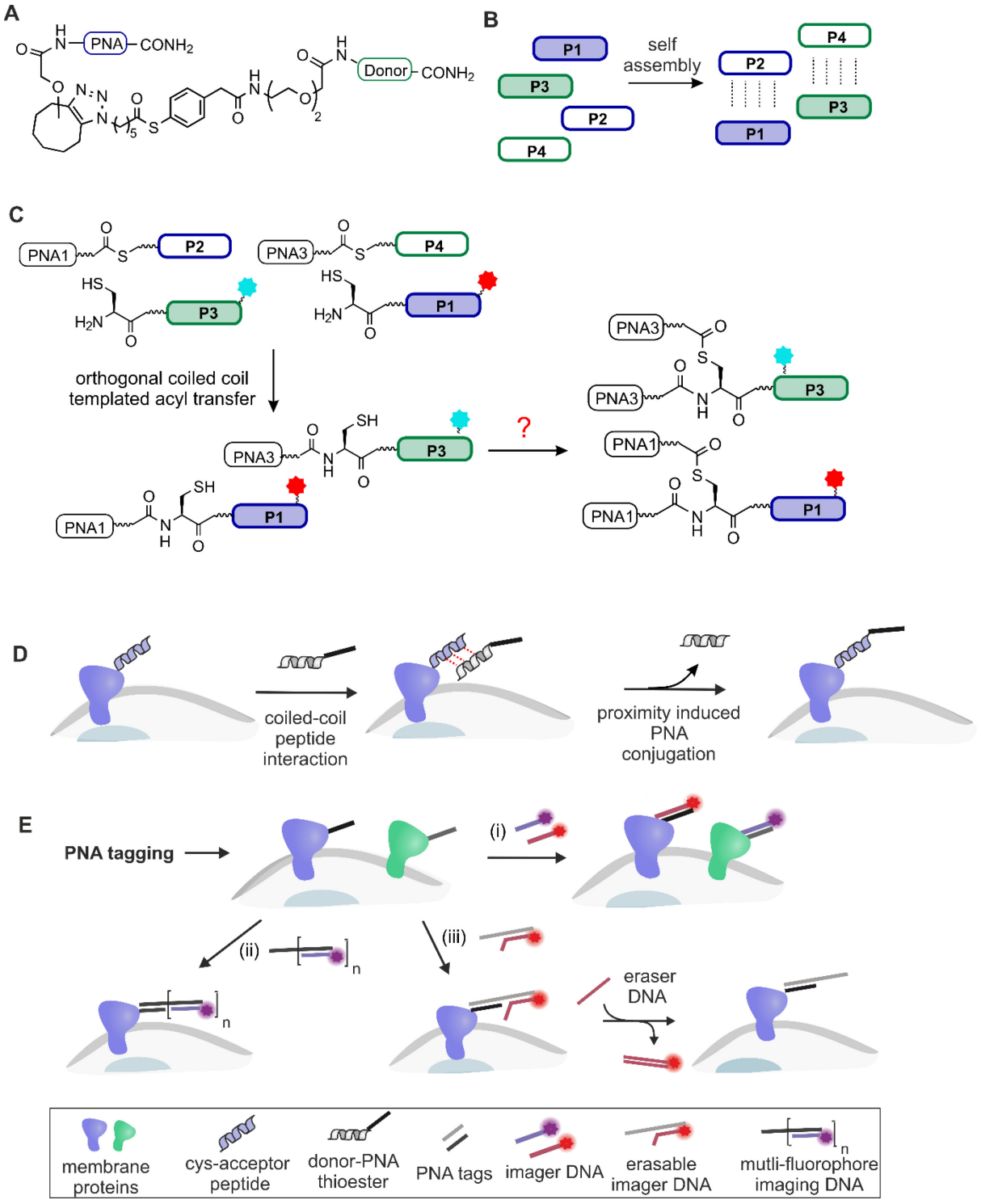

Figure 15 A) PNA-donor probe to be used for live-cell acyl transfer reaction. **B)** Self assembly of orthogonal coiled coils P1/P2 and P3/P4. **C)** Selective acyl transfer of PNA to acceptor peptides facilitated by coiled-coil assembly. Acceptor peptides are labelled with a fluorophore (red/blue star) to enable analysis via fluorescence. A potential side reaction is a second acylation of the product. **D)** Live-cell PNA tagging of a single surface receptor facilitated by coiled-coil assembly. **E)** Live-cell orthogonal PNA tagging (coil peptides not shown for clarity) followed by DNA hybridisation. After PNA tagging, hybridisation of: (i) complementary fluorophore-labelled DNA strands will allow simultaneous imaging of two target receptors; (ii) adaptor DNA strands will facilitate imaging with multiple fluorophores; (iii) adaptor DNA strands which are subsequently removed via toehold-mediated strand displacement by application of an 'eraser DNA' strand.

key goals were firstly to carry out simultaneous orthogonal labelling of two different proteins with PNA; then through hybridization of DNA adaptors and imagers, to achieve both brighter and erasable labelling.

First, we would investigate the orthogonal acyl transfer of two 15-mer long PNA strands in test tube reactions. For this, synthesis of the thioester-linked PNA-donor peptide probes would be carried out, incorporating coiled-coil peptides P2 and P4 (Figure 16A). These 'donor' peptides are known to self assemble with P1 and P3 'acceptor' peptides, respectively, (Figure 16B) and the interaction would be used to guide the reaction. The orthogonal acyl transfer of PNA from the PNA-donors to synthetic cysteine-acceptor peptides would be analysed by liquid chromatography, facilitated by fluorophore labelling of acceptor peptides (Figure 16C). A critical aspect was that the reactions should be carried out at low concentration and possible cross-reactivities be analysed. Previous acyl transfer reactions on synthetic peptides had not confirmed that quantitative labelling of acceptor peptides was feasible, despite the importance of a well-defined population in biological labelling experiments. An additional point to be considered at this stage was the presence of a side product bearing two reporter (PNA) strands (Figure 16C, second reaction step). This side product was reported in all previous work, but never fully addressed. In some experiments, this product could be a concern and a means to limit its formation should be investigated.

The second objective was to validate the method in live-cell imaging experiments (Figure 16 D and E). Several surface receptors: EGFR, ErbB2 (epidermal growth factor receptors 1 and 2) and ET_BR (endothelin receptor B) would be hybridized with DNA-fluorophore imagers after PNA conjugation of the receptors. The specificity of both the PNA conjugation and the DNA hybridization steps was to be examined by simultaneous labelling of tyrosine kinases EGFR and ErbB2. Universal applicability of the method to surface receptors would then be substantiated on a G-protein coupled receptor, ET_BR. To demonstrate the potential of the PNA tag, hybridization of DNA adaptors carrying multiple DNA-imagers were to be analysed by flow cytometry to determine the brightness gains. Subsequently, DNA-imagers with toehold sections would be removed using toehold mediated strand displacement. Erasable labelling would be used in combination with ligand stimulated receptor internalization, to aid the analysis of receptor trafficking.

The experiments presented in this thesis were previously published by Gavins et al.[185,186]

4.1. Synthesis

The first objective of this work was to validate a surface labelling method whereby a PNA tag is covalently linked to a target protein. In this labelling method an acyl transfer reaction occurs following heterogenous coiled coil formation of a 'tag–probe' (Acceptor–Donor) peptide pair. Three different coiled-coil pairs (P1/P2, P3/P4, E3/K3; Table 1) [116,119] were studied for tag–probe labelling. The PNA-donor probes used for the acyl transfer consisted of a PNA section and a donor peptide section, joined by an aryl thioester. The PNA strand would be the reporter group, and the donor peptide the basis of recognition, being one half of a coiled-coil heterodimer. The design of such probes was based upon previous work carried out in the Seitz group. [126] Briefly, both PNA-cyclooctyne and donor peptide-thioester were synthesized by Fmoc SPPS chemistry, and joined in strain-promoted azide-alkyne cycloaddition (SPAAC) reaction. A synthetic method was developed to carry this out completely on the resin, to good effect. The acceptor peptides would take part in an acyl transfer via an N-terminal cysteine residue, which would be analysed by liquid chromatography. For this, fluorophore-labelled Cys-acceptor peptides were synthesized by SPPS (Solid-phase peptide synthesis). For further studies of the acyl transfer reaction, Ac-Gly-donor thioester, N-terminal thiol donor peptides, and N- and S-acylated acceptor peptides were also synthesized by SPPS.

Table 1 Amino acid sequences of coiled-coil peptides used for tag–probe labelling.

Name	Role	Sequence
E3	acceptor	EIAALEK EIAALKE EIAALKE EIAALKE
K3	donor	KIAALKE KIAALKE KIAALKE KIAALKE
P1	acceptor	EIQALEE ENAQLEQ ENAALEE EIAQLEY
P2	donor	KIAQLKE KNAALKE KNQQLKE KIQALKY
P3	acceptor	EIQQLEE EIAQLEQ KNAALKE KNQALKY
P4	donor	KIAQLKQ KIQALKQ ENQQLEE ENAALEY

Sequences are written from N-terminus to C-terminus and include spaces between coiled-coil heptads for clarity.

4.1.1. Synthesis of PNA-donor Thioesters

For the PNA, two orthogonal 15-mer strands PNA1 and PNA3 were designed (Table 2) with PNA/DNA duplex melting temperatures of over 60°C, ensuring stable hybridization under biological conditions. Melting temperatures were predicted according to the literature: after determination of the analogous DNA–DNA duplex melting temperature by nearest neighbour approach, assuming 1 mM Na^+ concentration, [187,188] an empirical formula to predict $T_{m(PNA/DNA)}$ from $T_{m(DNA/DNA)}$ was applied. [189] At 200 nM oligonucleotide concentration, predicted melting temperatures were: $T_{m(pred.)}$ (PNA1/DNA1) = 65.8°C; $T_{m(pred.)}$ (PNA3/DNA3) = 64.3°C.

Table 2 Sequences of PNA and DNA duplexes and their predicted melting temperatures.

	PNA1/DNA1	PNA3/DNA3
PNA Sequence	gac tct gga tga cgc	ctg gta agt ggt gtc
DNA Sequence	GCG TCA TCC AGA GTC	GAC ACC ACT TAC CAG
$T_{m(pred)}$ (°C)	65.8	64.3

For synthesis of PNA-donor thioester probes, a modular ligation strategy was used to join the PNA and peptide part via SPAAC as designed by Katherina Gröger for PNA_n-K3 probes (Scheme 1). [126] The donor azido-peptides included an aryl thioester, the thioester having been formed from a final condensation with azidohexanoic acid. The strained cycloalkyne ALO (aryl-less octyne) was connected to the PNA via the carboxylate group. The final SPPAC joined the two precursors, whilst keeping the thioester intact. ALO was chosen for its relative stability, meaning storage would be less problematic and HPLC purification would not result in significant acid catalysed triple bond hydration.

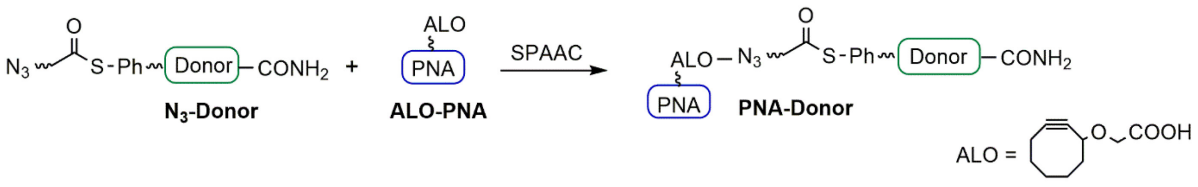

Scheme 1 General ligation strategy for PNA-donor thioesters. SPAAC: Strain-promoted azide-alkyne cycloaddition.

Azido-donor peptides (N_3-donor)

For synthesis of the azido-thioester-donor peptides (N_3-donor**,** Scheme 2), the 22-mer donor K3, [116] and 29-mer donors P2 and P4[119] were prepared by automated SPPS on TentaGel® Rink amide (RAM) resin using Fmoc-amino acid building blocks activated with a mix of the uronium based coupling reagent HCTU (2-(6-Chloro-1-H-benzotriazole-1-yl)-1,1,3,3-tetramethylaminium hexafluorophosphate, NMM (*N*-methylmorpholine) base, and OxymaPure®, to prevent racemization. Double coupling steps were used after the 8th amino acid and between coupling steps, capping with Ac_2O/2,6-lutidine/DMF (5:6:89) ensured uncoupled amino termini were not extended in subsequent cycles. Fmoc deprotection was carried out in 20% piperidine in DMF. Manually, the final three acids were coupled: firstly, a linker of either 6-(Fmoc-amino)hexanoic acid (Ahx) or [2-[2-(Fmoc-amino)ethoxy]ethoxy]acetic acid (Fmoc-AEEAc) was activated (5 eq acid, 5 eq PyBroP, 10 eq DIPEA in DMF; 4 min) and coupled twice for 1 h. 6-aminohexanoic acid had previously been found a sufficiently long linker for the acyl transfer and it was reasoned that the similar length polyethylene glycol (PEG) type chain of AEEAc could improve final aqueous solubility. Next, 4-mercaptophenylacetic acid (MPAA) was protected with the very acid labile 4-monomethoxytrityl (Mmt) protecting group using Mmt-Cl, [190] then similarly coupled. Mmt was removed through washing with 2% TFA (trifluoroacetic acid) with 1% carbocation scavenger TIS (triisopropylsilane) before coupling 6-azidohexanoic acid (Azhx) to form the thioester (5 eq acid, 4.8 eq HATU and 8 eq DIPEA in DMF; 5 min preactivation; 3x 1 h). After global deprotection and cleavage (TFA/TIS/H_2O 94:3:3, 2 h) the resin was rinsed with TFA and DCM and after precipitation of the combined washes and HPLC purification, the N_3-donors were obtained in 42% (**1**), 8% (**2**), 9% (**3**), and 12 % (**4**) yield.

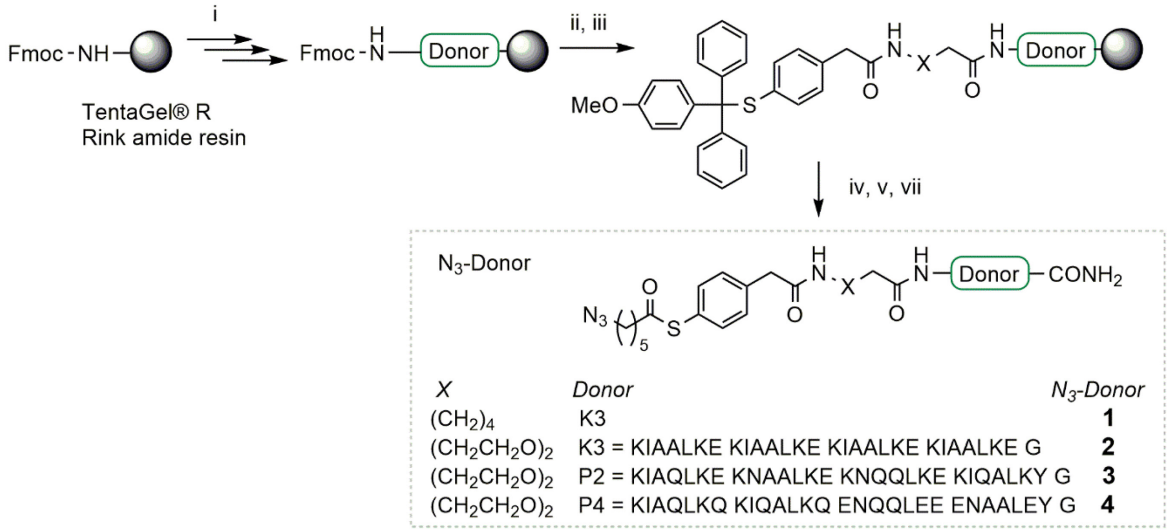

Scheme 2 Synthesis of N_3-donor peptides (i) automated Fmoc/tBu SPPS: 20% piperidine/DMF 5+4 min Fmoc deprotection; Fmoc-aa, OxymaPure, HCTU, NMM, DMF, 1 x 30 min (aa 2-7) or 2 x 30 min coupling (aa 1; 8 onwards); Ac_2O/2,6-lutidine/DMF (5:6:89) 5 min capping. (ii) 20% piperidine/DMF 5+5 min; 6-(Fmoc-amino)hexanoic acid or Fmoc-AEEAc, PyBroP, DIPEA, DMF 2 x 60 min (iii) 20% piperidine/DMF 5+5 min; Mmt-MPAA, PyBroP, DIPEA, DMF 2 x 60 min (iv) DCM/TFA/TIS, 97:2:1 wash (v) 6-azidohexanoic acid, HATU, DIPEA, DMF 3 x 60 min (vi) TFA/TIS/H2O 94:3:3, 2 h.

ALO-PNA and PNA-donors — Strategy 1

The cyclooctyne-carboxylic acid building block ALO was synthesized from heptene as previously described. [191] For ALO-PNA synthesis and subsequent cycloaddition to the azido-peptides, two strategies were attempted. The first was carried out similarly to Gröger[126] and produced a 15-mer PNA with C-terminal lysine for in-solution peptide coupling to ALO, and subsequent SPAAC to the K3 azide.[†] Following Strategy 1 (Scheme 3A), the sequence PNA1H, bearing a C-terminal lysine and an acetylated N-terminus, was synthesized by automated SPPS on TentaGel® RAM resin. The automated method was similar to that used previously for peptide couplings, but with all double couplings, no OxymaPure, and with a more activating pyridinium analogue of HCTU: HATU (1-[Bis(dimethylamino)methylene]-1H-1,2,3-triazolo[4,5-b]pyridinium 3-oxid hexafluorophosphate). The crude ether precipitate obtained after cleavage was coupled to ALO with N,N′-diisopropylcarbodiimide (20 eq ALO, 20 eq DIC, DMF 15 min preactivation) to the ε-amino group of lysine, yielding ALO-PNA1H

[†] ALO was preferred at the C-terminus of PNA since it would position the 3' end of a hybridized DNA away from the labelled protein, which was believed advantageous if the DNA were to be used for rolling circle amplification, which extends the 3' end of the DNA primer. This application appeared in the project grant proposal but was not carried out in this thesis.

5 after purification. Addition of 3 eq of N_3-donor **1** in MeCN/H_2O/TFA (60:40:1) for 3 days followed by HPLC purification produced the final PNA1H-K3 conjugate **6** (30%, 5% overall).‡ It was noted that **6** was prone to adsorption (see later Chapter 4.2.2). Addition of charged residues to the termini is a frequently used approach for introducing positive charges to PNA either for aiding in cellular delivery[192] or enhancing aqueous solubility. [193] To alleviate potential solubility and aggregation issues later on, the PNA strand was redesigned to include charged residues Arg and Asp at both termini to give the still overall neutral sequence PNA1S.

It was speculated that, after introduction of Asp and Arg, regioselective in-solution coupling of ALO to the deprotected PNA could still be feasible at Lys, provided sufficient ALO preactivation. This time, ALO coupling of the crude PNA1S was carried out with DCC in DMSO due to its low solubility in DMF, which also indicated a decrease in its hydrophobicity. The overall yield of ALO-PNA1S **7** after HPLC purification was much lower: 1.6% compared with 16% for ALO-PNA **5**, which had lacked the extra amino acid residues. Nevertheless, SPAAC was carried out with **7** and the N_3-donor (10 eq **2** in H_2O/TFA, 100:1). After SPAAC and HPLC, PNA1S-K3 **8** was obtained (22%, 0.5% overall). It was noted that the low overall yield of final PNA-K3 conjugates in both cases was owing in part to a difficult purification of the ALO-PNA but also the final conjugates, particularly with ALO-PNA1S **7**. Still, adding charged residues to the PNA was found to be advantageous (Chapter 4.2.2; 4.3.2).

For orthogonal labelling studies, PNA-donors made from P2 and P4 donor peptides were synthesized. PNA1S-P2 **9** was prepared similarly to **8** with an overall yield of 0.2%, again owing to the poor yield of ALO-PNA1S **7**. Since C-terminal ligation of the PNA to the donor peptide was not a prerequisite to the design of the PNA-donors for live-cell labelling studies, a simpler strategy (Scheme 3B, Strategy 2) was devised, where the whole synthesis, including SPAAC, was carried out on the resin. This was enabled by the fact that ALO would be coupled to the N-terminus rather than the C-terminus, which supported adequate purification of the final product; since ALO would be coupled as the final amide bond condensation before the SPAAC reaction, truncated sequences would not take part in the cycloaddition to the azido-donor peptide.

‡ Calculated from maximum theoretical amino acid loading of the batch of TentaGel® Rink amide resin, which in turn was estimated from coupling Fmoc-Gly-OH onto a known weight of resin and using Fmoc-monitoring to determine the initial functional group loading.

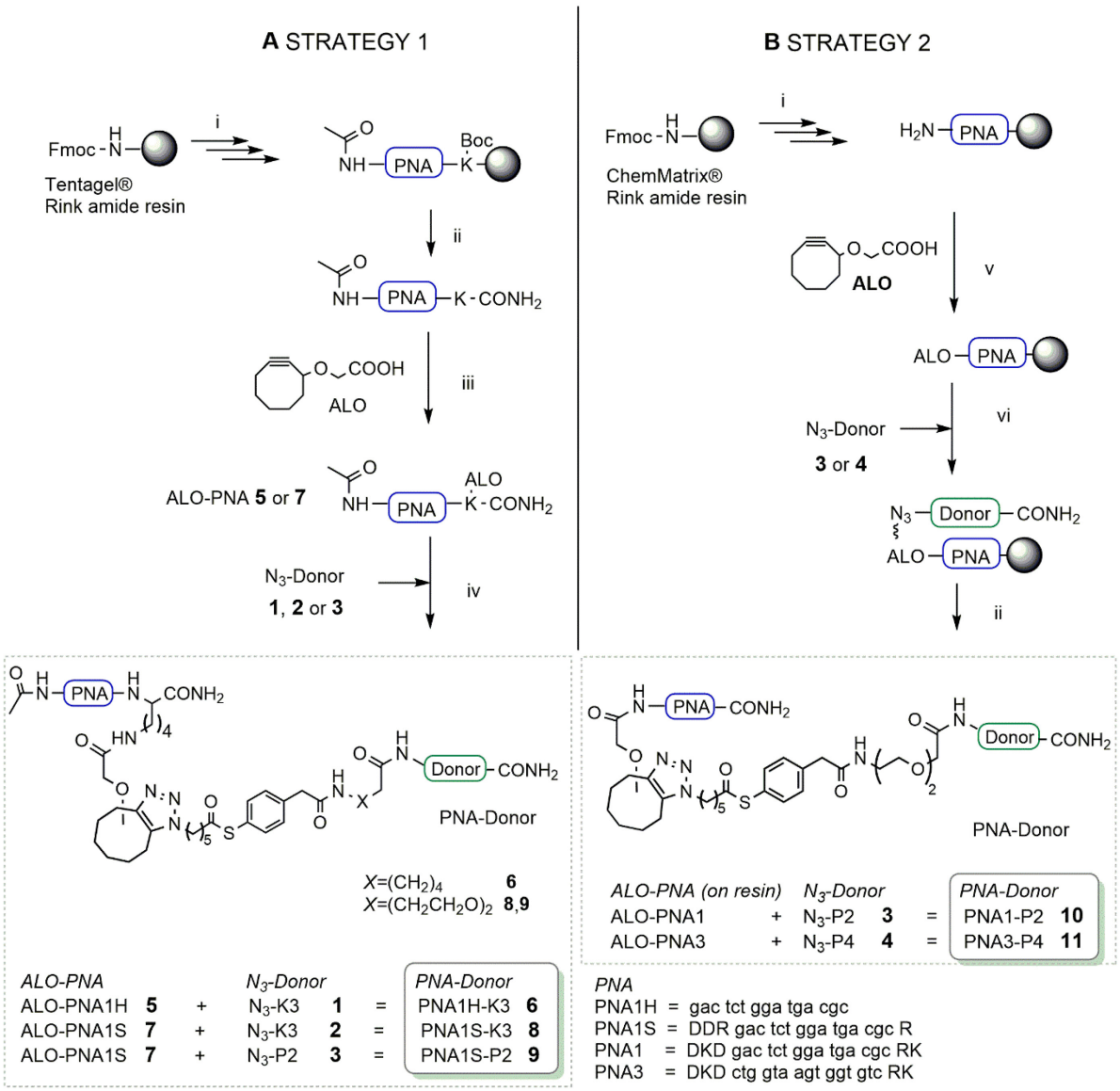

Scheme 3 Synthesis of PNA-donor thioesters. A) Strategy 1, in-solution SPAAC. (i) automated Fmoc/Bhoc/tBu SPPS. Fmoc deprotection: 20% piperidine/DMF, 5+4 min; coupling: Fmoc-PNA monomers (0.08M), HATU, NMM, DMF, 2 x 30 min; capping: Ac_2O/2,6-lutidine/DMF (5:6:89), 5 min (ii) TFA/TIS/H_2O (94:3:3) 3 h; HPLC purification (iii) for ALO-PNA1H **5:** 20 eq ALO, 20 eq DIC, DMF, 15 min preactivation, 2 h coupling; for ALO-PNA1S **7:** 40 eq ALO, 40 eq DCC, 3 eq DMAP, DMSO, 10 min preactivation**,** 20 h coupling (iv) SPAAC for PNA1H-K3 **6:** 3eq **1**, MeCN/H_2O/TFA (60:40:1) 84 h; SPAAC for PNA1S-K3 **8:** 10eq **2**, H_2O/TFA (100:1) 72 h. SPAAC for PNA1S-P1 **9:** 10eq **3**, MeCN/H_2O/TFA (75:25:1) 72 h. **B)** Strategy 2, on-resin SPAAC. (v) Coupling: 10 eq pyBroP, 10 eq ALO, 20 eq DIPEA, DMF, 10 min preactivation, 3 hr (vi) SPAAC: 2 eq **3** or **4** in DMF, RT, 48 h, then 1 eq 35°C 24 h (ii) cleavage: TFA/TIS/H_2O (94:3:3) 3 h; HPLC purification.

ALO-PNA and PNA-donors — Strategy 2

Orthogonal PNA strands PNA1 and PNA3 were to be conjugated with P2 and P4, respectively, with terminal amino acid residues that imparted an overall +1 charge to the PNA strand. For this, PNA was synthesized on a ChemMatrix® RAM resin, a 100% PEG resin intended to minimize aggregation of the long PNA strands, and able to swell in polar solvents. This would be particularly useful in the final SPAAC step. Test cleavages from the synthesis of the PNA3-P4 donor **11** using Strategy 2 were recorded by UV-UPLC and are shown in Figure 17. The UPLC traces were very similar to those obtained in the synthesis of PNA1-P2 donor **10**. For both, after SPPS of PNA1 and PNA3, Fmoc-monitoring was carried out on the final Asp residue to determine an accurate concentration of the terminal amine and thus, the full-length chain (Figure 17A).[§] Next, a small amount of dry resin was weighed (300 and 600 nmol of free amine

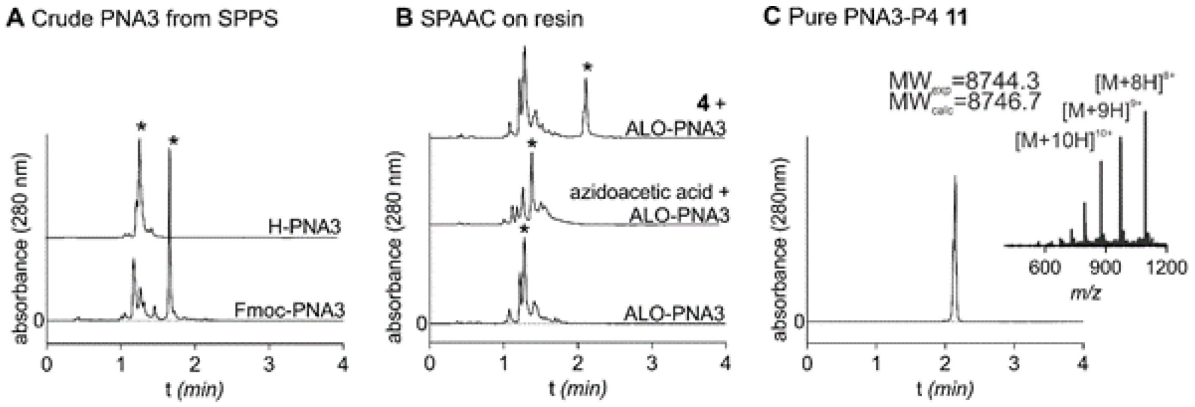

Figure 16 Synthesis of PNA3-P4 conjugate 11 on ChemMatrix RAM resin and analysis of test cleavages by UV-UPLC/ESI–MS. Asterix (*) denotes desired product at each step. **A)** Lower trace: Fmoc-PNA3 after SPPS; upper trace: crude H-PNA3 after Fmoc deprotection. **B)** Bottom trace: after coupling ALO to H-PNA3; middle trace: test SPAAC, ALO-PNA3 resin with excess azidoacetic acid in DMF; upper trace: SPAAC, ALO-PNA3 resin with 3 eq **4** (N_3-P4) in DMF to form **11**. **C)** Final conguate **11** after HPLC purification. tR= 2.12; two peaks correspond to two SPAAC isomers. Inlay: ESI–MS; UPLC gradient 8-80% mobile phase A in B.

for PNA3 and PNA1, respectively), swelled in minimal DMF, and ALO was coupled to the α-amino group with 10 eq PyBroP, 10 eq ALO, 20 eq DIPEA in DMF for 3 h. Since capping of incompletely coupled peptides had been carried out during SPPS to prevent elongation of these sequences, only the full-length PNA should have contained ALO. It was expected that this fact, combined with the large retention shift upon subsequent ligation with the N_3-donor peptide, would make purification of the final compounds straightforward. It also meant that much less of the cyclooctyne was

[§] For 2 umol scale of PNA (calculated from maximum potential amino acid loading of the batch of ChemMatrix RAM), 600 nmol of N terminal amine was recorded by Fmoc monitoring.

required for coupling, an advantage, since the cyclooctyne was not commercially available, and other commercially available cyclooctynes are expensive. The retention shift upon coupling ALO to the PNA was slight (Figure 17B, lower trace) and the correct mass was not found, as the cyclooctyne was not stable to the cleavage conditions. As a simple way to prove the reaction was successful, a test ligation was carried out. For this, ALO-PNA1 and ALO-PNA3 resin were treated with 30% azidoacetic acid/DMF for 2 h and a test cleavage carried out (Figure 17B, middle trace). The correct mass was found; however, most of the remaining PNA was found to be truncations from the initial SPPS. This suggesting the ALO coupling was largely successful, but the automated PNA synthesis had produced many truncations. The final SPAAC was therefore performed on the remaining resin beads. The resin, swelled in DMF, was transferred to a 1 mL micro-reaction vessel and 2 eq N_3-donor (**3** for ALO-PNA1 resin or **4** for ALO-PNA3 resin) in minimal DMF was added. The vessel was shaken at RT for 48 h before adding an extra 1 eq N_3-donor for a further 24 h at 35°C (Figure 17B, upper trace). Thioester hydrolysis products MPAA-P2 and MPAA-P4 peptide were identified in the ESI–MS analysis, indicating that some of the final thioester had hydrolysed in this time.

After washing out excess azido peptide, cleavage from the resin and HPLC purification gave the final PNA-donors **10** and **11** (3% and 6% respective yield from Fmoc-monitoring, 1% and 2% overall). Yields, though improved from the previous method to yield PNA1S-P2 **9**, were still rather low. Nonetheless, the amount was sufficient for later cellular experiments, the final products were obtained in excellent purity, and the synthesis only required a single HPLC purification of the PNA, saving time and resources. Still, a few obvious improvements could be suggested for a future synthesis: 1) a larger reaction scale, as there are universal vulnerabilities of nanomole scale organic synthesis. In this case transferal of resin and many test cleavages in particular lead considerable and noticeable loss of resin. A repeat synthesis would naturally involve fewer test cleavages; 2) treatment with a higher concentration and more equivalents of N_3-donor peptides would increase SPAAC speed, conversion, and may reduce potential thioester hydrolysis; 3) obtaining purer PNA from the automated SPPS would decrease non-productive resin mass and aid with point 2, since resin swelling was found to be the limiting factor for azide concentration; 3) use of a more strained cyclooctyne such as BCN (bicyclo[6.1.0]nonyne) or DIBO(dibenzocyclooctyne) would enable more rapid ligation; although these building blocks would add further hydrophobicity.

The author is confident that following only points 1–3 above, future synthesis would generate appreciably higher yields. PNA-donor thioester probes could also, theoretically, be synthesized in one long strand using Boc/Bzl SPPS, precluding the need for a ligation strategy. Strategic placement of positively charged residues at the N-terminal end of the sequence could aid in HPLC separation by decreasing the retention time and separating product from truncations. This could also be a tactic for more effective purification of ALO-PNA as carried out in strategy 1 (Scheme 3A), if C-terminal ligation to the donor peptide was, indeed, required.

4.1.2. Synthesis of Fluorophore-labelled Cys-Acceptor Peptides

To enable analysis of orthogonally-templated acyl transfer reactions by fluorescence UPLC (FLR–UPLC), acceptor peptides Cys-P1 and Cys-P3 were appended with 5(6)-carboxytetramethylrhodamine (TAMRA) or coumarin 343 (C343) fluorophores via a C-terminal lysine (Scheme 4). For this, Fmoc-P1-K(Mmt) and Fmoc-P1-K(Mmt) peptides were assembled on the resin by automated SPPS analogously to the donor peptides. Boc-Cys-(Trt)-OH was coupled with no preactivation of the amino acid and fewer DIPEA equivalents than ordinarily to prevent racemization. Then, selective deprotection of the Mmt from lysine with 2% TFA revealed the amino group. Coupling of the relevant dye to lysine was carried out using 4 eq of TAMRA or C343, 4 eq PyBOP and 8 eq NMM. After cleavage, HPLC gave the purified fluorophore-labelled Cys-acceptor peptides: Cys-P1-TAMRA **12**, Cys-P3-C343 **13**, and Cys-P3-TAMRA **14**. In preliminary FLR–UPLC experiments, it was noticed that the Cys-acceptors were not sufficiently pure; depletion of the peptides in the acyl transfer reaction revealed underlying peaks, which were not previously observed by UPLC–MS. To obtain purer peptides, they were first oxidised by bubbling the dissolved peptides (pH 8 phosphate buffer, 10% MeCN) with pressurised air overnight. Disulfide formation provided an adequate retention shift for HPLC purification. The $(\text{Cys-acceptor})_2$ disulfides **15**, **16** and **17** were thus used for further acyl transfer reaction analysis, reduced to the thiol in situ.

For analysis of the K3/E3-templated PNA transfer, Cys-E3-K(TAMRA) **18** was synthesized analogously, but conversion to the disulfide was omitted.

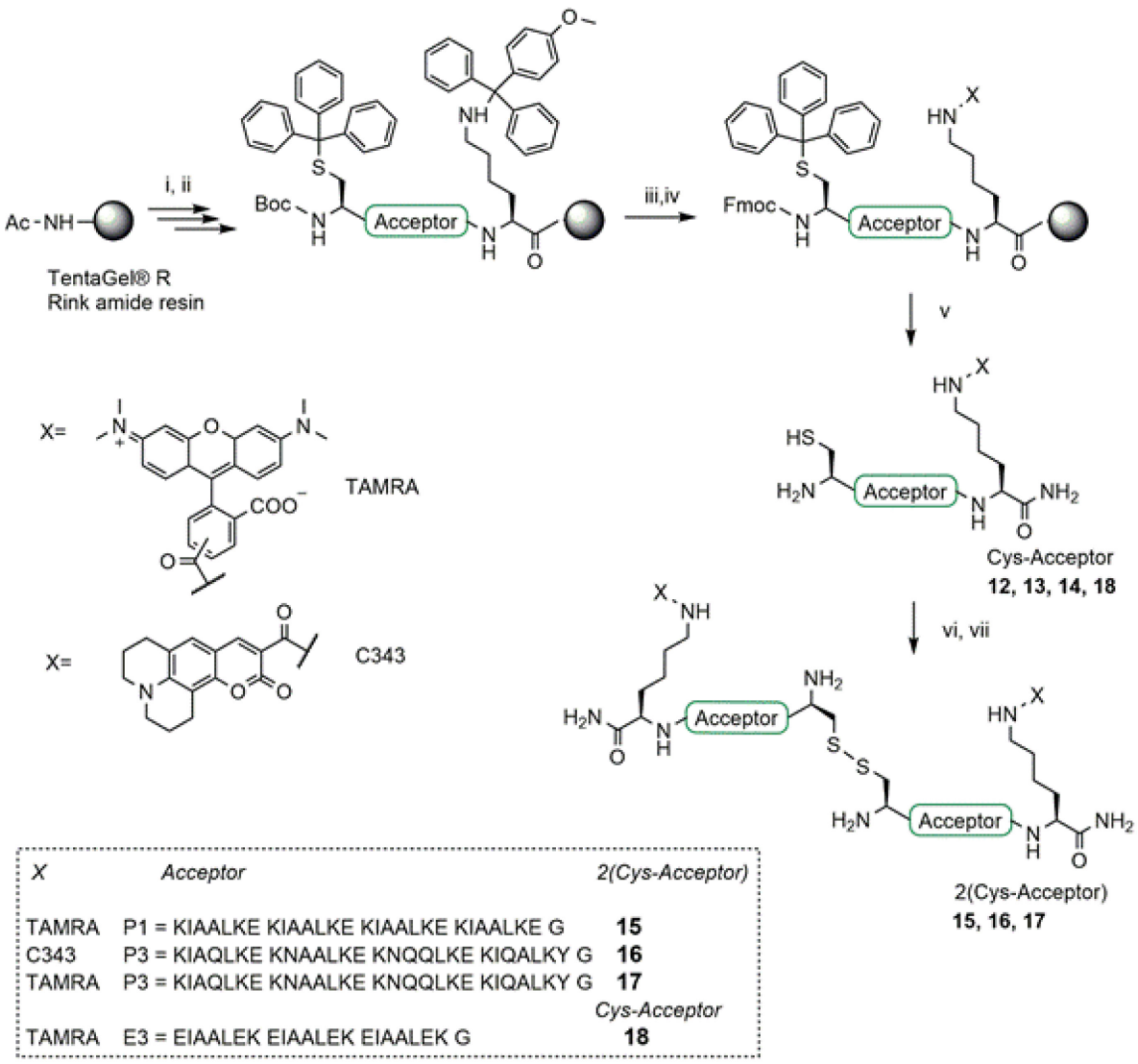

X	*Acceptor*	*2(Cys-Acceptor)*
TAMRA	P1 = KIAALKE KIAALKE KIAALKE KIAALKE G	**15**
C343	P3 = KIAQLKE KNAALKE KNQQLKE KIQALKY G	**16**
TAMRA	P3 = KIAQLKE KNAALKE KNQQLKE KIQALKY G	**17**
		Cys-Acceptor
TAMRA	E3 = EIAALEK EIAALEK EIAALEK G	**18**

Scheme 4 Synthesis of fluorophore-labelled Cys-acceptor peptides (i) automated Fmoc/tBu SPPS. Fmoc deprotection: 20% piperidine/DMF, 5+4 min; coupling: Fmoc-aa, OxymaPure, HCTU, NMM, DMF, 1 x 30 min (aa 2-7) or 2 x 30 min (aa 1; 8 onwards); capping: Ac_2O/2,6-lutidine/DMF (5:6:89), 5 min (ii) Fmoc deprotection; coupling: 4 eq Boc-L-Cys(Trt)-OH, 4 eq DIPEA, 3.6 eq HCTU (no preactivation) 2 x 15 min; 5 min capping (iii) trityl deprotection: DCM/TFA/TIS, 97:2:1 (iv) coupling: TAMRA or C343, pyBOP, NMM, DMF 3 x 30 min (v) cleavage: TFA/TIS/EDT/H_2O/, 93:3:2:2, 2 h; HPLC purification (vii) 150 nM NaCl, 50 mM PO_4^{2-}, pH 8.0, 10% MeCN, bubbled with pressurized air 24 h; HPLC purification.

4.1.3. SPPS of Peptides used for Acyl Transfer Analysis

For analysis of acyl transfer reactions, peptides **19-24** (Figure 18) were synthesized on Tentagel RAM resin using the same automated synthesis method as described for previous donor and acceptor peptides. Non-standard couplings will be briefly described here. For **19**, synthesis was as for N_3-donors **1**-**4** but Ac-Gly-OH was used in the final, terminal coupling rather than 6-azidohexanoic acid (Azhx). For **20**, Fmoc-Cys(Mmt)-OH was coupled to H-E3, followed by Fmoc deprotection then Azhx coupling (5 eq acid, 4.8 eq HATU and 8 eq DIPEA in DMF; 5 min preactivation; 2x 1 h). After removal of Mmt (DCM/TFA/TIS 97:2:1), Azhx coupling was repeated. **21-24** were synthesized by automated SPPS, then Fmoc-AEEAc-OH and Mmt-MPAA were coupled manually, as with the N_3-donor peptides. Finally, cysteine was coupled manually with 4 eq Boc-L-Cys(Trt)-OH, 4 eq DIPEA, 3.6 eq HCTU and no acid preactivation.

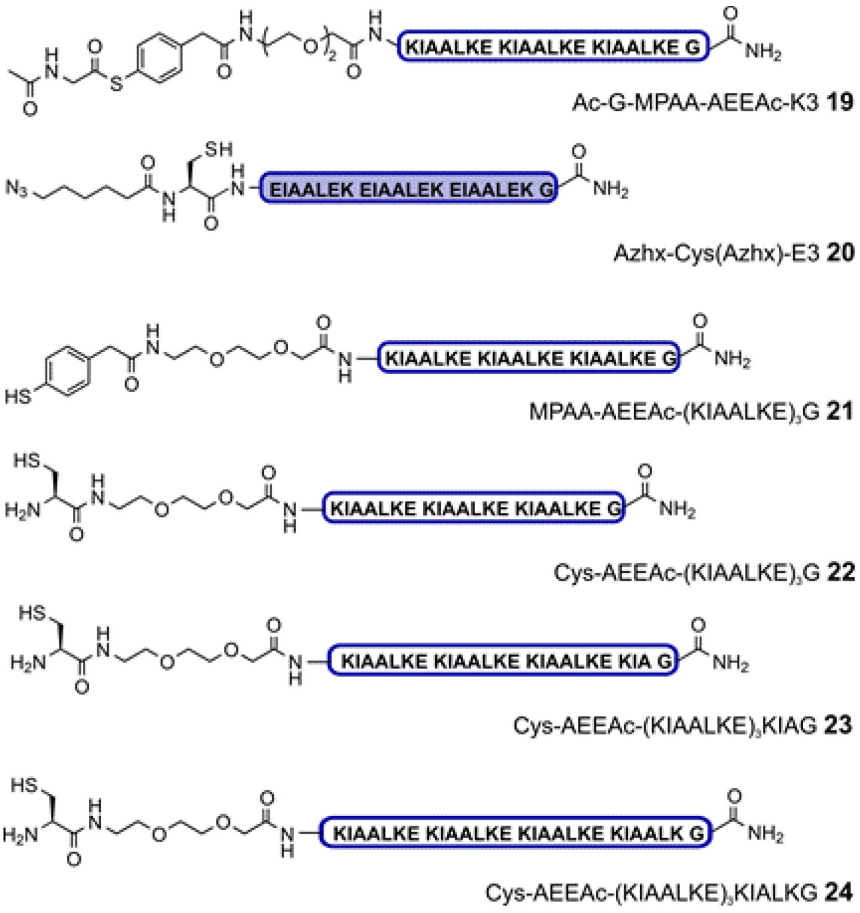

Figure 17 Peptides synthesized by SPPS for acyl transfer analysis (Chapter 4.2.3)

4.2. In vitro Acyl Transfer Reactions

In this chapter, templated acyl transfer of PNAs to synthetic acceptor coil peptides bearing an N-terminal cysteine was explored. The E3/K3 coiled-coil system had already been extensively studied for the transfer of different reporter fluorophores in the work of Ulrike Reinhardt, [142,153] and 3-mer or 11-mer PNAs strands by Katherina Gröger. [126] Preliminary studies carried out by Marc Reimann had shown that P1/P2 and P3/P4 coiled coils could template the acyl transfer of TAMRA and Coumarin343 simultaneously and orthogonally onto the target cysteinyl peptides. [126]

The aim of this work was to analyse both the single and simultaneous PNA transfer of 15-mer PNAs templated by the P1/P2 and P3/P4 coiled-coil systems. Of interest to orthogonal tag–probe labelling was determining the $t_{1/2}$ of the transfer reactions, and whether quantitative labelling of the acceptor peptide was attainable. To demonstrate whether the PNA transfer could be utilised for orthogonal protein labelling, it was important to identify any unwanted cross reactivity between PNA-donor thioester and Cys-acceptor peptides. Ideally, a simultaneous transfer reaction of the PNA strands could take place and for this, a 'one-pot' transfer reaction would be analysed. In addition to the main objective, some effort was put into resolving matters relevant the coiled-coil-templated transfer reaction itself, namely the occurrence of a species formed after a competing *S*-acylation, which leads to a product carrying two reporter groups.

Coiled-Coil-templated PNA Transfer Reaction

The general coiled-coil-templated transfer of PNA from a coil-peptide thioester to a Cys-acceptor coil-peptide and all anticipated products is illustrated in Scheme 5. The acyl transfer product PNA-Cys-acceptor (**P**) is formed from the reaction of PNA-donor and Cys-acceptor, after coiled coil formation brings both peptides into proximity. Competing reactions may also take place, which are non-productive for the purpose of labelling. One is the hydrolysis of the PNA-donor (an aryl thioester) or the cysteinyl-thioester intermediate Cys(PNA)-acceptor, both resulting in a practically irreversible PNA-OH acid formation (Scheme 5B). The second competing pathway is a second *S*-acylation of the desired transfer product (assigned as **P**) to form a product carrying two PNA strands (assigned as **PP'**, Scheme 5C); this consumes one more equivalent of PNA-donor for each Cys-acceptor and generates another HS-donor. Both side reactions were reported for coiled-coil-templated acyl transfers to varying degrees dependent on the reporter. [126,142]

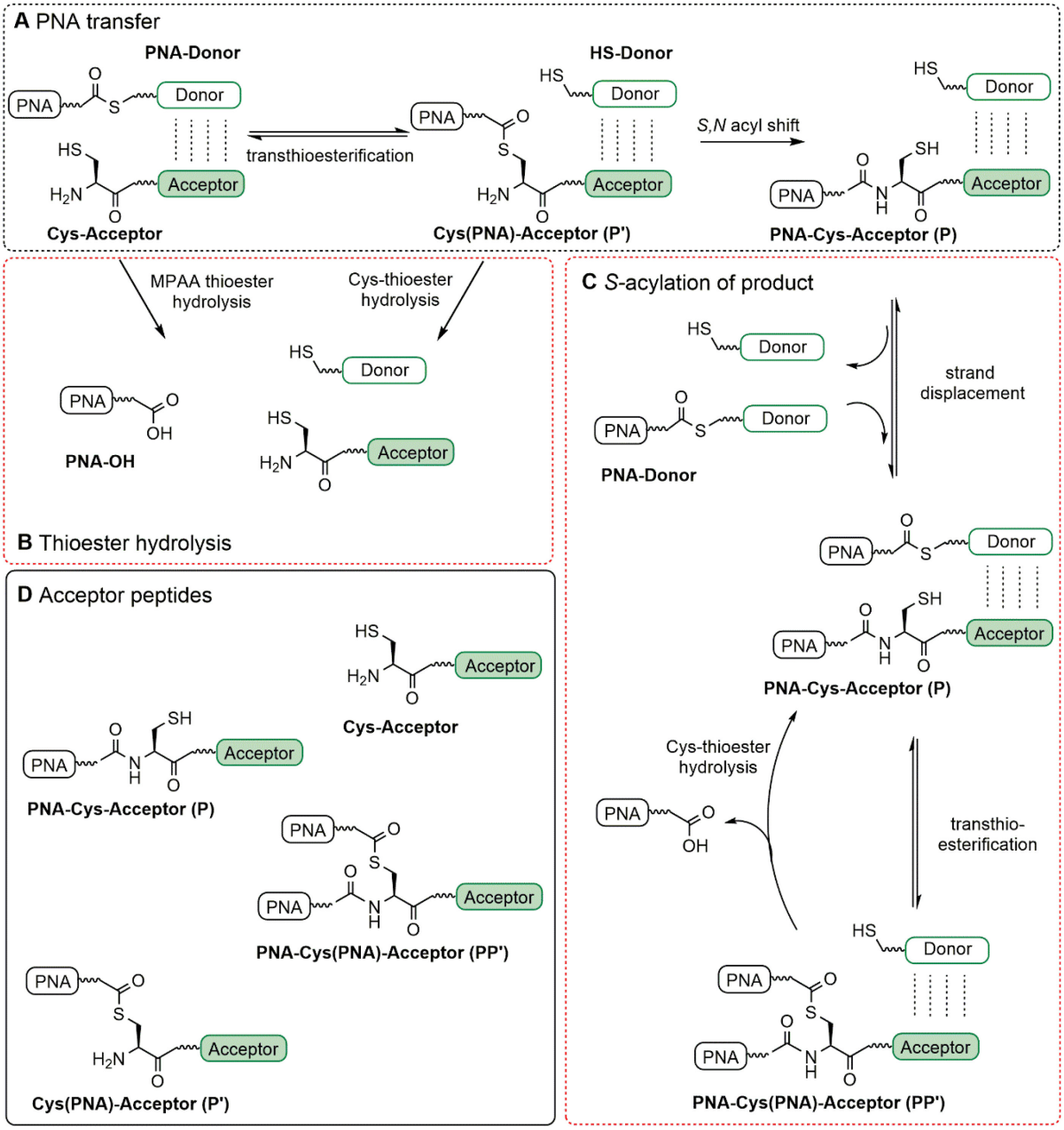

Scheme 5 General PNA transfer reaction: A) Transfer from PNA-donor coil peptide to Cys-acceptor coil peptide, where the donor and acceptor peptide form a coiled-coil interaction (dashed lines); **B)** and **C)** potential side reactions which deplete PNA-donor, B= hydrolysis of PNA-donor thioester or the intermediate Cys(PNA)-acceptor thioester, C= Formation of second acylation product **PP'** from *S*-acylation of PNA transfer product **P** with another equivalent of PNA-donor; **D) a**cceptor peptides featured in A-C; all potential species that are detectable in FLR–UPLC analysis when only the acceptor peptide is conjugated to a fluorophore.

4.2.1. PNA Transfer Templated by Orthogonal Coiled-Coil Pairs P1/P2 and P3/P4

The first objective was to separately analyse the reaction progress of PNA transfers templated by P1/P2 and P3/P4 coiled coils. For this, fluorescence UPLC (FLR–UPLC) was adopted. Since the desired outcome was a quantitative labelling of the Cys-acceptors, these peptides were labelled with a fluorophore. The reaction progress would then be considered only in relation to the more relevant goal of labelling the acceptor peptide, rather than consumption of the thioester (donor peptide). Fluorescence measurement had two advantages over conventional UV-UPLC; the first being that the peaks would be more easily resolved, since only acceptor peptides would be observable (Scheme 5D). Secondly, spectrally distinct fluorophores would be used for each coiled-coil system. This would be essential for independent detection of two simultaneous PNA transfer reactions. Lastly, the reaction could be carried out at lower peptide

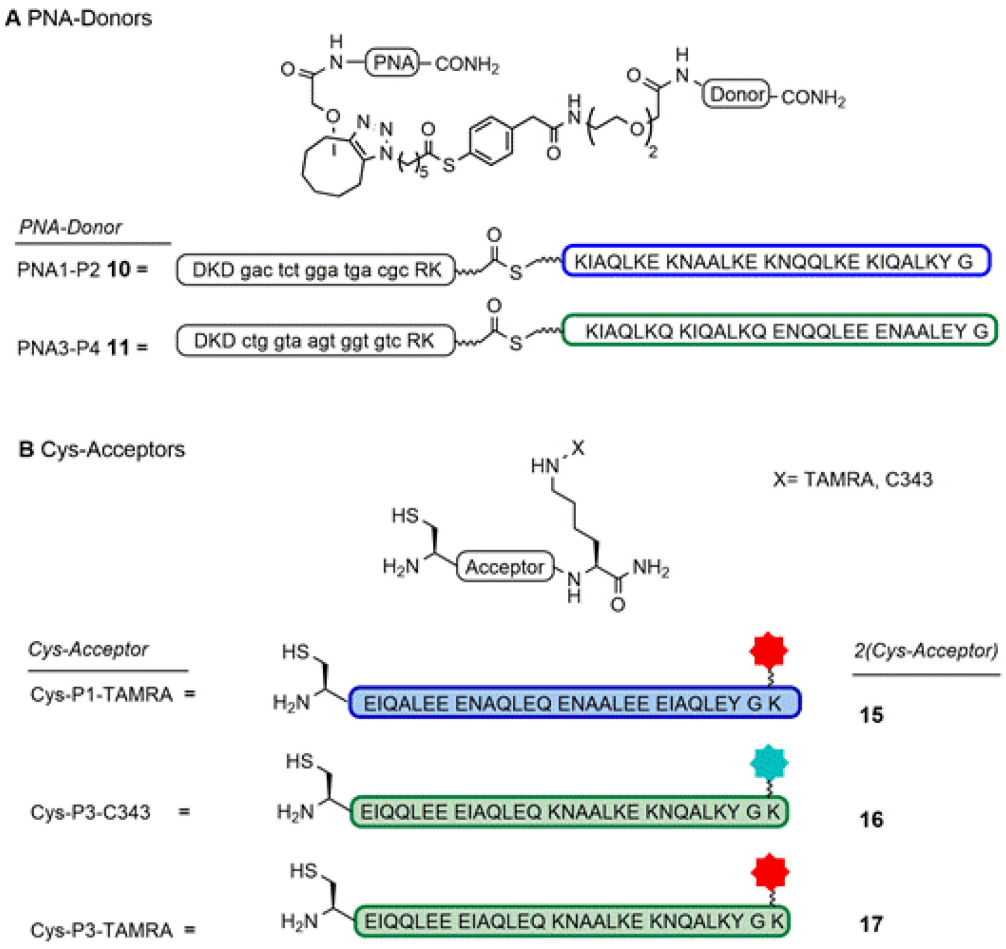

Figure 18 A) PNA-donors and **B)** fluorophore-labelled Cys-acceptors comprising the P1/P2 coiled coil (blue) and P3/P4 coiled coil (green) sets. Acceptor peptides: filled boxes; donor peptides: unfilled boxes. Cys-acceptor peptides were formed by in situ reduction of $(\text{Cys-acceptors})_2$ disulfides with TCEP.

concentration owing to the greater sensitivity of measured fluorescence emission. This means that a sub-nanomolar Cys-acceptor concentration could be used, which more closely represents the conditions encountered during live-cell protein labelling.

TAMRA and C343 were used to label the Cys-acceptors, as they are both cheap, compatible with SPPS, and are pH independent; therefore, they are able to fluoresce at the low pH (~pH 2) of the UPLC mobile phase and have distinct absorption and emission spectra, for analysis of a simultaneous transfer with the two coiled-coil systems. The PNA-donors and fluorophore-labelled Cys-acceptor peptides used in this chapter are shown in Figure 19.

UV-UPLC–MS

Before analysis of the reaction kinetics by FLR–UPLC, reaction species were verified by UV–UPLC–MS with a photodiode array (PDA) detector. Formic acid rather than the standard TFA was used in the mobile phase to improve electrospray ionization, but to the detriment of peak resolution. First, the P1/P2 system was analysed (Figure 20). Cys-P1-TAMRA (2 µM) was formed by stirring of the disulfide **15** in buffer A (200 mM Na_2HPO_4, 50 nM NaCl, 1 mM TCEP, pH 7.2) at 30°C for 10 min (Figure 20C). PNA1-P2 **10** was added for 5 sec before quenching the reaction by addition of 20 µL of reaction

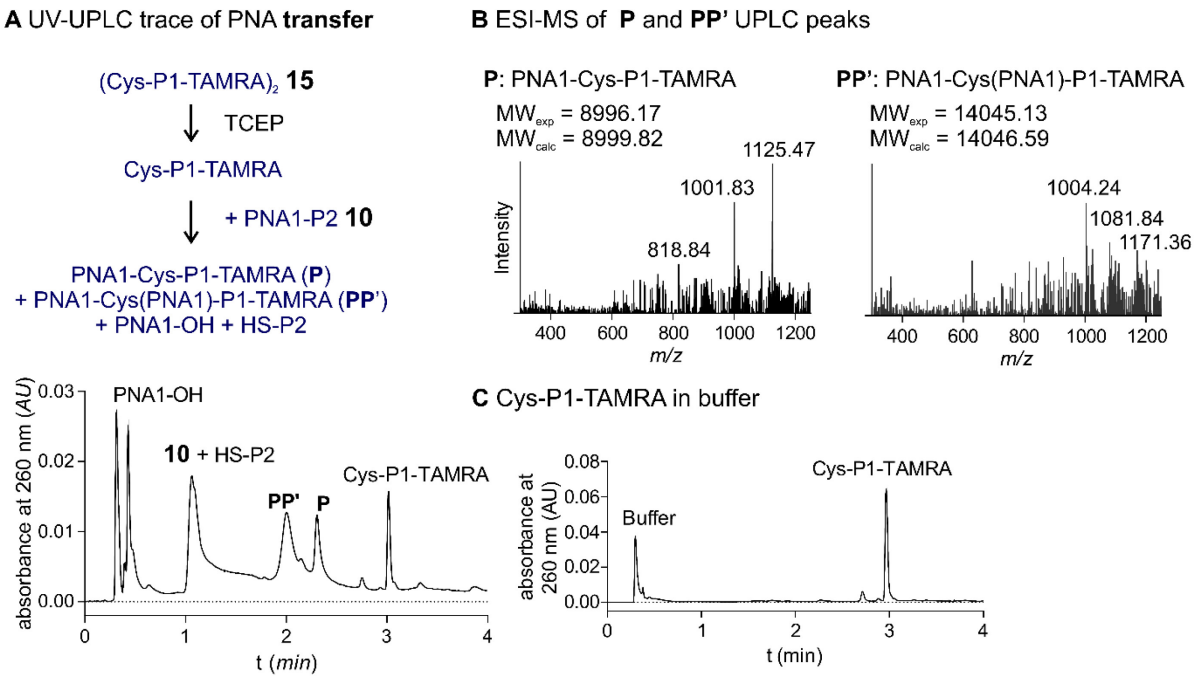

Figure 19 Verification of PNA-transfer reaction species by UV-UPLC–MS. Reaction with P1/P2 coiled-coil: 1 µM $(Cys\text{-}P1\text{-}TAMRA)_2$ **15** was stirred in buffer A for 10 min to form 2 µM Cys-P1-TAMRA, then 2 µM **10** was added for 5 sec before the reaction was quenched by addition of 10% TFA to a final concentration of 1% TFA (v/v); **A)** UPLC trace of the quenched reaction measured at 260 nm; **B)** ESI–MS spectra of peak maxima **P** and **PP'** in A; **C)** Cys-P1-TAMRA formed *in situ* from **15.** UPLC–MS gradient: 10-50 % eluent D in C. Buffer A: 200

of TFA to a final concentration of 1% (v/v). The UPLC peaks corresponding to ESI mixture to a UPLC glass vial insert, and addition masses of both the product **P** and *S*-acylated product **PP'** were observed at predictable retention times, i.e., retention times in between that of the PNA-donor and Cys-acceptor peptide, with **PP'** running at a higher retention time than **P**, owing to the extra PNA strand (Figure 20B). The mass of the predicted side product PNA1-OH was detected at a similar retention time to that of PNA1 during synthesis of PNA1-P2; HS-P2 was detected at the retention time matching the same compound during synthesis of N_3-P2. Given that the coil peptides P1 and P2 contain only one aromatic residue, they absorb very little at 260 nm, the wavelength at which the nucleobases of PNA strongly absorb. The approximate 214 /260 nm absorption ratios were therefore used to validate whether a species was comprised only of peptide, or of a PNA-polypeptide conjugate in a 1:1, or 2:1 ratio of PNA-to-peptide.

Similarly, a PNA transfer was carried out with $(Cys\text{-}P3\text{-}TAMRA)_2$ **17** and PNA3-P4 **11** (Figure 21). This time, peak resolution was more problematic, due to the lesser charge

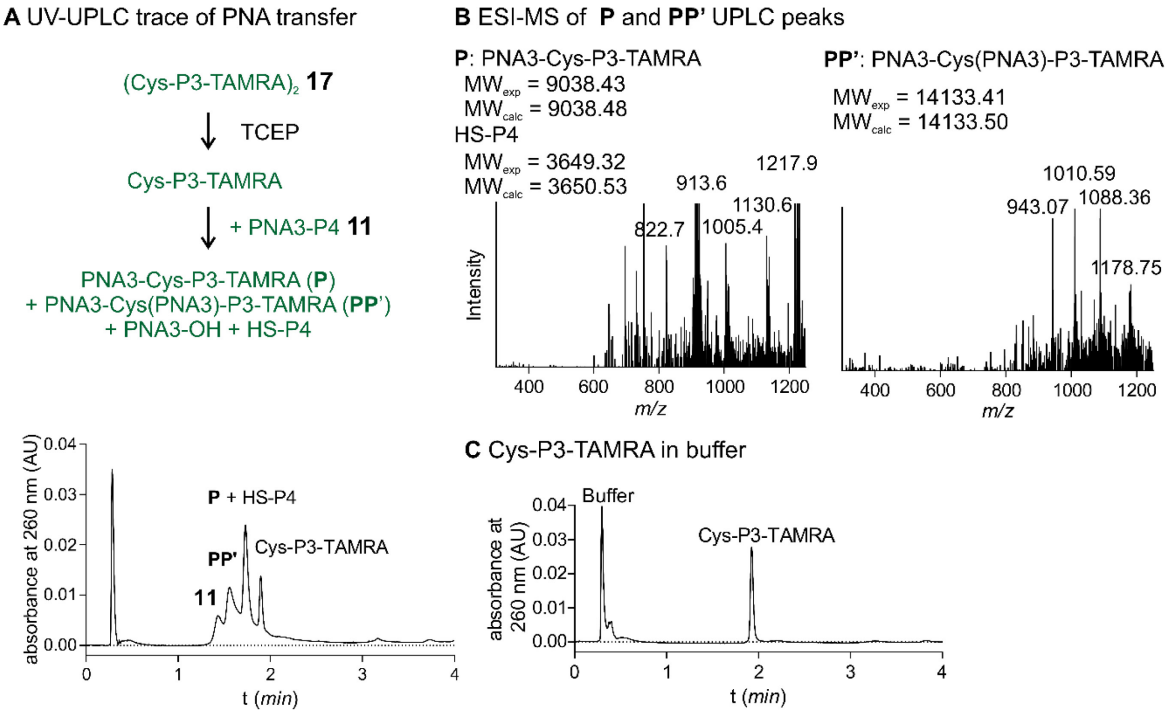

Figure 20 Verification of PNA transfer reaction species by UV-UPLC–MS. Reaction with P3/P4 coiled-coil: 1 µM $(Cys\text{-}P3\text{-}TAMRA)_2$ **17** was stirred in buffer A for 10 min to form 2 µM Cys-P3-TAMRA then 2 µM PNA3-P4 **11** was added to for 5 sec before the reaction was quenched by addition of 10% TFA to a final concentration of 1% TFA (v/v); **A)** UPLC trace of quenched reaction measured at 260 nm; **B)** ESI–MS spectra of peak maxima in A. HS-P4 and **P** have the same retention time and both masses are found in the ESI–MS; **C)** 2 µM Cys-P3-TAMRA formed in situ from **17.** UPLC–MS gradient: 10-50 % eluent D in C. Buffer A: 200 mM Na_2HPO_4, 50 nM NaCl, 1 mM TCEP, pH 7.2.

difference between P3 and P4 peptides compared with P1 and P2.[**] The product peak **P** coincided with that of the HS-P4 side product, and the remaining peaks could not be satisfactorily resolved. Still, the correct masses could be clearly identified for each compound in the peak maxima, with the mass for **P** and HS-P4 appearing together in the same peak. Additionally, absorption ratios (214/260 nm) corroborated results. During FLR–UPLC analysis, the HS-P4 peak would not be visible due to the lack of fluorochrome.

FLR–UPLC optimization

Before the reaction progress could be studied by FLR–UPLC, the setup was optimized with the P3/P4 system; PNA-donor **11** and (Cys-acceptor)$_2$ **17**. The reaction followed similar conditions described above in the UV–UPLC analysis but now 0.1% TFA (v/v) was included in the FLR–UPLC mobile phase rather than formic acid, to improve peak resolution and a ten-fold lower concentration of peptides (200 nM) was used. In general, three peaks were observed corresponding to: Cys-P3-TAMRA; transfer product PNA3-Cys-P3-TAMRA (**P)**; or *S*-acylated product PNA3-Cys(PNA3)-P3-TAMRA (**PP'**), i.e., all the expected acceptor peptides as outlined in Scheme 5D.[††] The identity of the three peaks were determined by comparison with the ESI–MS-corroborated UV–UPLC retention times; verification of the absorbance at 260 nm, via a TUV (tuneable ultraviolet) detector, though signal was very low; and by comparison of base- (1 M NaOH) vs. acid- (1% TFA) quenched samples. If the reactions were base quenched, the **PP'** peak would disappear, and **P** peak would increase in size, indicating hydrolysis of the cysteine thioester (Figure 22).

During optimization of the measurements, it became evident that FLR–UPLC peak intensities varied in magnitude depending on the timepoint at which they were measured, and how long after the reaction a sample was measured. Adsorption of reaction species occurred both during the reaction in the reaction vessels (Figure 23, Reaction 1A), as well as in the UPLC vials prior to measurement (Figure 23, Reaction 1B, comparing UPLC measurements or 'runs' of the same vial). This was of particular concern since the different reaction species adsorbed at unequal rates; the peaks corresponding to PNA transfer products **P** and **PP'** declined faster than the Cys-P3-

[**] Overall charges of coil peptides: P1 = -10, P2 = +5; P3 = -2 , P4= -1

[††] The thioester **P'**, formed before an *S*,*N* acyl shift was not observed, suggesting the rate limiting step is the acyl shift.

TAMRA peak. This effect was more pronounced in the UPLC vials, where the samples spent more time.

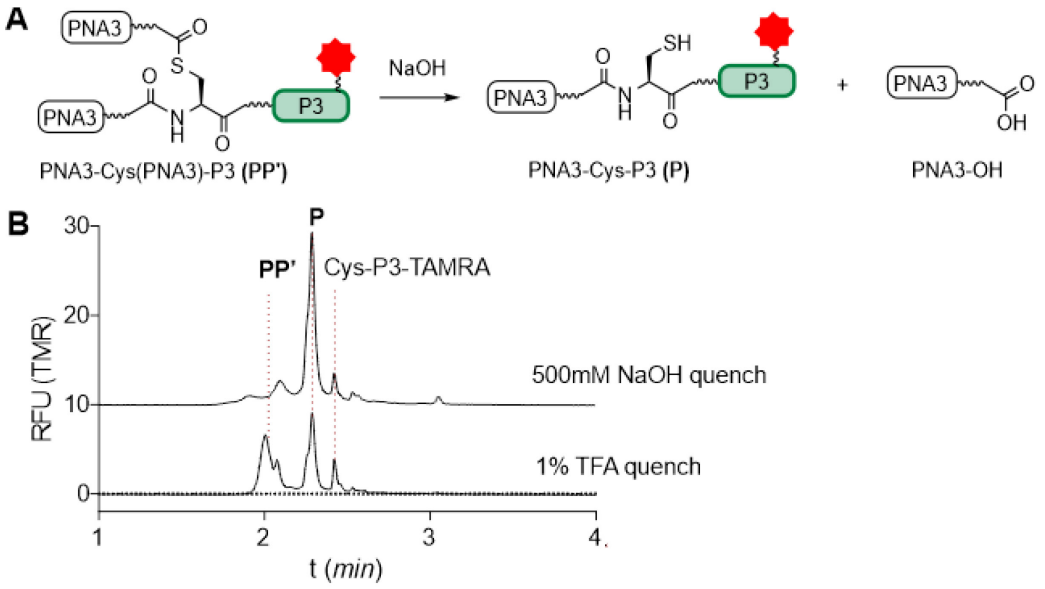

Figure 21 *S*-Acylated double transfer product hydrolysis: A) Base-induced hydrolysis of PNA3-Cys(PNA3)-P3-TAMRA (**PP'**) reforms PNA3-Cys-P3-TAMRA **(P)**; **B)** reaction of 100 nM $(Cys\text{-}P3\text{-}TAMRA)_2$ **17** and 1200 nM PNA3-P4 **11** in buffer B. After 15sec the reaction was quenched to final concentration of either 1% TFA (v/v) or 500 nM NaOH and analysed by FLR-UPLC.. RFU= relative fluorescence units measured at Ex: 550 nm and Em: 580 nm. Buffer B: 200 mM Na_2HPO_4, 50 nM NaCl, 1 mM TCEP, 0.1% CHAPS, pH 7.2.

It was suspected that acidic quenching of the overall-negatively-charged acceptor peptide species was detrimental to its solubility at low pH, and that addition of a hydrophobic TAMRA dye could aggravate this behaviour. Micromolar stock solutions of **17** alone required addition of 15 % MeCN to effectively solubilize in 0.1% TFA solution. Though the presence of charged amino acid residues on the PNA strand was thought to aid with aqueous solubility, addition of PNA strands to the Cys-P3-TAMRA evidently still intensified non-specific interactions with glass. For this reason, reactions were quenched with TFA in H_2O/MeCN 90:10. Switching from glass to polypropylene UPLC vial inserts significantly reduced the decline in peak intensities. Identical samples taken from the same reaction vessels and stored for 1 h prior to injection into the UPLC column provided an overall larger peak area when stored in plastic vials, compared with in glass vials (Figure 23 Reaction 1C). Unfortunately, even with plastic vials, the peak areas of PNA transfer products **P** and **PP'** shrunk to a greater extent than for Cys-P3-TAMRA after 1 h.

Addition of CHAPs (3-[(3-cholamidopropyl)-dimethylammonio]-1-propanesulfonate) to acyl transfer reactions involving PNA has been used to good effect in the Seitz lab. [194] CHAPs is a non-denaturing zwitterionic detergent[195] often used for solubilizing hydrophobic membrane proteins, whilst retaining protein function. [196] In a reaction with an excess of thioester, which almost fully converted Cys-P3-TAMRA to the *S*-acylated product **PP'**, addition of 0.1% CHAPs to the reaction buffer (a final concentration of 0.05% CHAPs in the UPLC vial) lead to a circa 5-fold increase in overall peak intensity when comparing two reactions quenched at identical time points (Figure 23, Reaction 2).

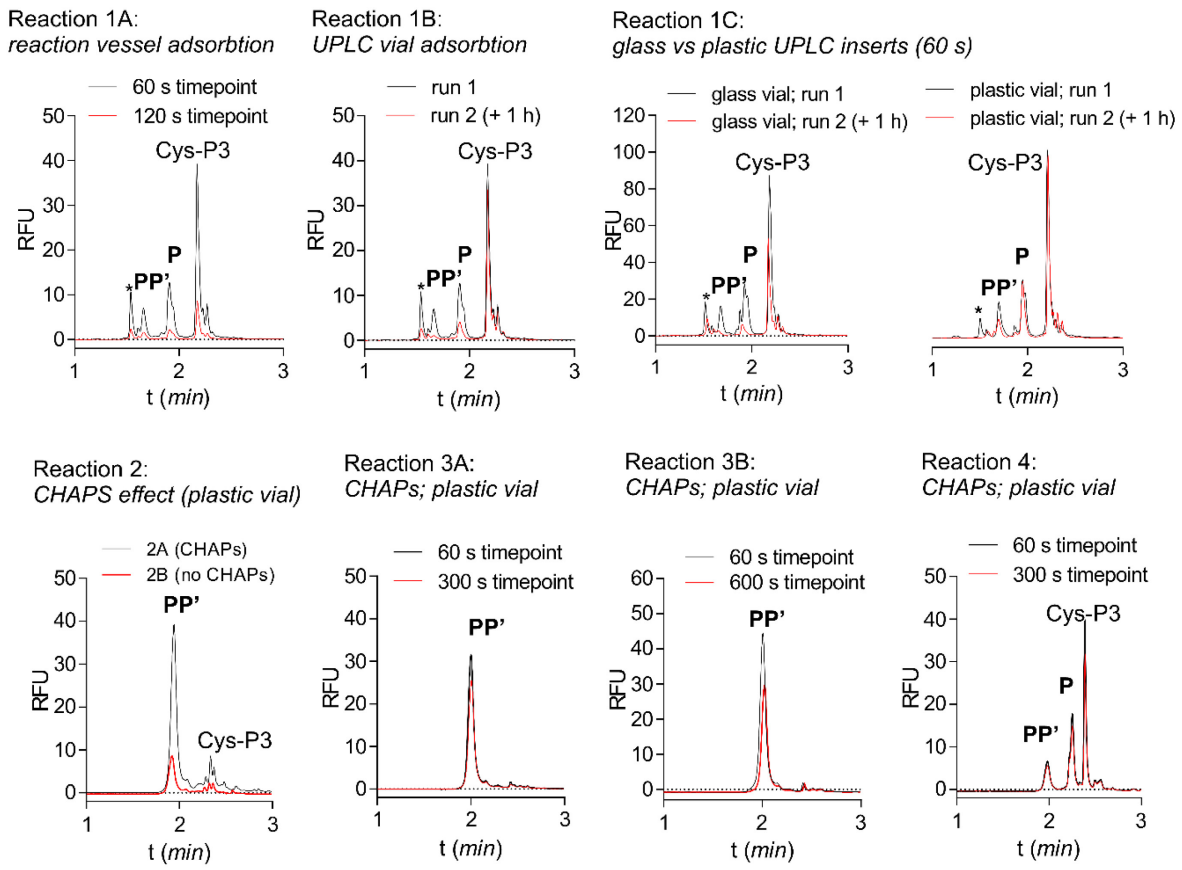

Figure 22 Assessing adsorption of reaction species during FLR–UPLC analysis. Reaction buffer: 200 mM Na_2HPO_4, 50 nM NaCl, 1 mM TCEP, pH 7.2, 30°C, with or without 0.1% CHAPS. Reactions quenched into UPLC vials with an equal volume of 2% TFA (v/v) in H_2O/MeCN (90:10). Reaction 1: 200 nM peptides **11** and **17**, UPLC gradient 10-60% eluent A in B. Reaction 2: 100 nM **17** (therefore 200 nM Cys-P3-TAMRA), 800 nM **11,** UPLC gradient 15-45% eluent A in B. Reaction 3: 100 nM **17**, 1200 nM **11**, UPLC gradient 15-45% eluent A in B. Reaction 4: 100 nM **17,** 200 nM **11**, UPLC gradient 15-45% eluent A in B. Cys-P3: Cys-P3-TAMRA; **P**: PNA3-Cys-P3-TAMRA; **PP'**: PNA3-Cys(PNA3)-P3-TAMRA; RFU: relative TAMRA fluorescence units measured at Ex: 550 nm and Em: 580 nm. 'Run': FLR–UPLC measurement. Asterisk (*) marked peaks: unidentified impurities observed when using an impure stock solution of **17**. Larger magnitude RFUs in reaction 1C due to a pipetting error.

To assess the improvements of CHAPs and plastic inserts together, two time points of already-completed reactions, i.e., Cys-P3-TAMRA was fully converted to (**PP'**), were compared. The aliquot from the second (300 s or 600 s) time point was measured after the 60 s time point in each case. The 300 s time point had an 8% smaller peak than for the 60 s sample, whereas up to 23% was lost in the 600 s aliquot (Figure 23, Reaction 3A, B), indicating that roughly 2% adsorption of **PP'** occurred in the reaction vial every minute. In a reaction which was virtually complete, but Cys-P3-TAMRA was not fully converted to the PNA-labelled transfer product (Figure 23, Reaction 4), all peaks decreased by roughly 10%. For all subsequent FLR–UPLC measurements up to 300 s, these conditions were considered acceptable. Though minor (10%) adsorption would still occur, randomization of the measurement order for the different vials, and setting the final time point to 300 s meant average peak ratios would not be significantly affected. The conditions were also verified for the P1/P2 system, with (Cys-acceptor)$_2$ **15** and PNA-donor **10**.

FLR–UPLC Analysis

Next, progress of the PNA transfer reactions were studied, with aliquots similarly quenched at set time points and analysed by FLR–UPLC in buffer B (200 mM Na_2HPO_4, 50 nM NaCl, 1 mM TCEP, 0.1% CHAPS, pH 7.2) at 30°C. Treatment of Cys-P3-TAMRA acceptor peptide formed in situ from **17** with just one equivalent (200 nM) of PNA3-P4 (**11**) resulted in 40% of Cys-P3-TAMRA labelled with a PNA. Roughly one third of that was the *S*-acylated product (**PP'**) and the rest was the regular transfer product **P** (Figure 24A, C). Adding three equivalents (600 nM) of PNA-donor **11** converted 90% of the acceptor, in this case mainly all the *S*-acylated product. For quantitative PNA labelling, at least 6 equivalents of thioester **11** were required, and with 6 eq the overall product (**P**+**PP'**) reached 100% within 60 s. Interestingly, this requirement of additional thioester equivalents could not be explained by its depletion via hydrolysis or the formation of the **PP'** product, as it was still present in the reaction after overall product formation reached a plateau. An equivalent analysis was carried out with PNA1-P2 **10** and 2(Cys-P1-TAMRA) **15** (Figure 24B, D). Similarly, a minimum of 6 equivalents of the PNA-donor thioester **10** was required to obtain quantitative PNA transfer, and this was in the form of the *S*-acylated product (**PP'**).

Previous acyl transfer reactions reported in the Seitz group had only shown near-quantitative transfer in one case: for a 3-mer PNA onto Cys-E3 peptide. [126] In this UPLC analysis, absorption at 260 nM was analysed and though 100% conversion of the

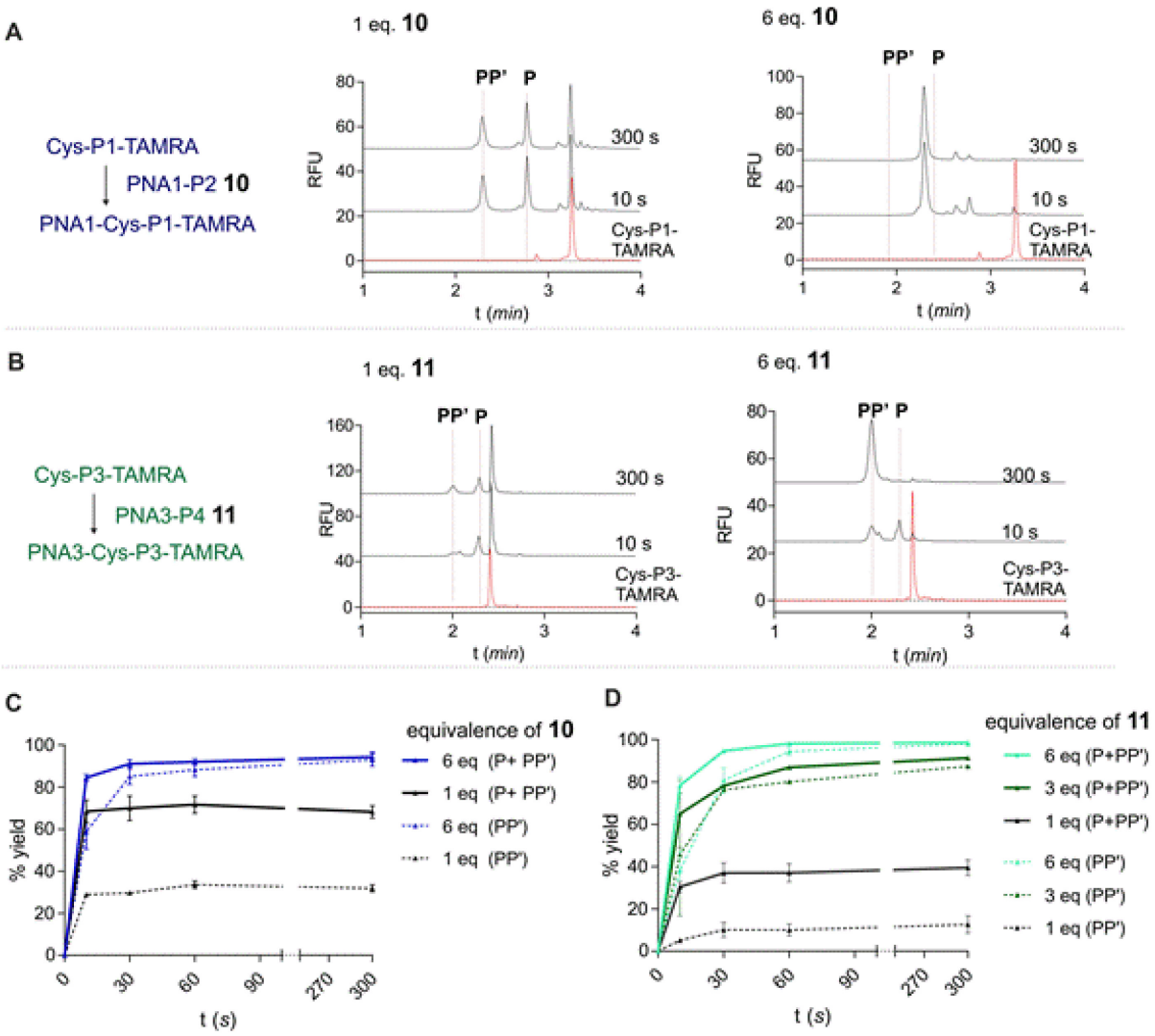

Figure 23 Products formed in coiled-coil-templated PNA transfer. FLR-UPLC analysis of reactions involving **A)** and **C)** $(Cys\text{-}P1\text{-}TAMRA)_2$ **15** and PNA1-P2 **10** or **B)** and **D)** $(Cys\text{-}P3\text{-}TAMRA)_2$ **17**, PNA3-P4 **11**. Conditions: 100 nM **15** or **17** stirred in buffer B (200 mM phosphate, 1 mM TCEP, 0.1% CHAPS, pH 7.2) at 30°C before addition of 200 (1 eq), 600 (3 eq) or 1200 nM (6 eq) **10** or **11** before quenching with an equal volume of 2% TFA in H_2O/MeCN (90:10). TAMRA, Ex: 550 nm; Em: 580 nm. UPLC gradient: 15-45% eluent B in A. Error bars = SEM of three or two (D; 3 eq) independent replicates.

thioester was recorded for a 1:1 reaction, conversion was measured with respect only to PNA-containing species rather than depletion of Cys-E3 acceptor peptide, since Cys-E3 has a low extinction coefficient at 260 nm. On closer examination, some *S*-acylated product (which consumed two thioester equivalents) was also recorded in the reaction, therefore it was deemed impossible for all Cys-E3 to be labelled with a PNA. In this case, either the reaction was not truly carried out with 1:1 stoichiometry or some Cys-E3 acceptor peptide remained undetected, due to the low concentration reaching the limit of detection of the UPLC assay.

Next, the specificity of the PNA transfer was examined. The mismatched peptides (P1 with P4; P2 with P3) were added together under identical experimental conditions as described for the previous experiments. For both reactions (**10** + **17**; **11** + **15**) no new peaks were observed at any measured time point (30, 60, 300, 600 sec), even after 10 min (Figure 25). This indicated that, as expected, PNA transfer could only proceed given a matching coiled-coil interaction between matching donor and acceptor coil peptides.

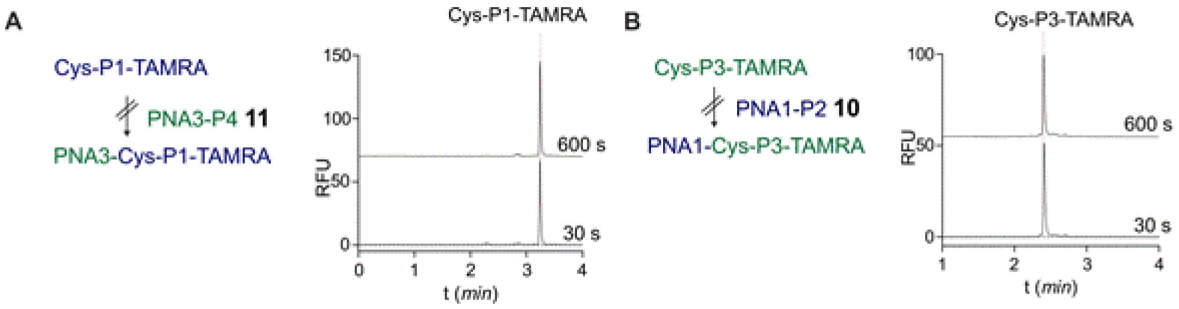

Figure 24 PNA transfer control reactions with mismatched acceptor and donor coil peptides. FLR–UPLC analysis of reactions with **A)** $(Cys\text{-}P1\text{-}TAMRA)_2$ **15** and PNA3-P4 **11** and **B)** Cys-P3-TAMRA **17** and PNA1-P2 **10**. Conditions: 100 nM **15** or **17** stirred in buffer B (200 mM phosphate, 1 mM TCEP, 0.1% CHAPS, pH 7.2) at 30°C before addition of **10** or **9.** Reactions quenched into UPLC vials with an equal volume of 2% TFA in H_2O/MeCN (90:10). TAMRA Ex: 550 nm; Em: 580 nm. UPLC gradient: 15-45% eluent B in A. Reaction was repeated three times with similar results.

Simultaneous PNA transfer

For measuring simultaneous dual PNA transfers, Cys-P3-C343 **16** was used in place of TAMRA-labelled Cys-P3 (**17**) to avoid overlapping FLR–UPLC peaks. PNA transfer with **11,** as described above, gave similar results with C343-labelled acceptor **16** as for the TAMRA labelled **17** (Figure 26).

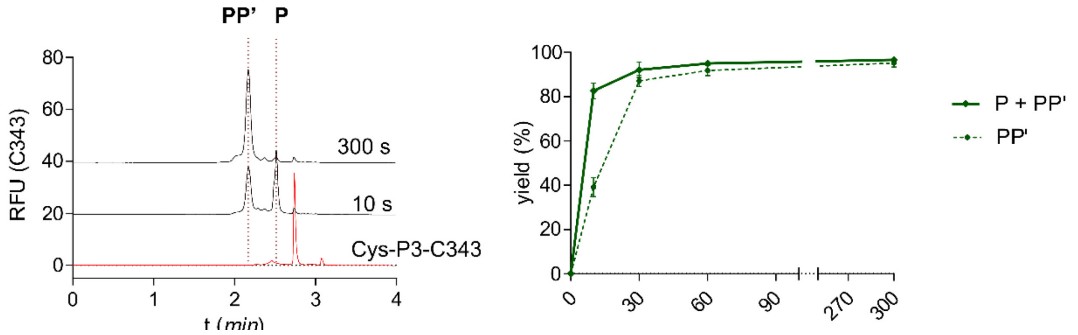

Figure 25 Products formed in coil-coil-templated PNA transfer. FLR–UPLC analysis of reactions involving $(Cys\text{-}P3\text{-}C343)_2$ **16** and PNA1- PNA3-P4 **11**. Conditions 100 nM **16** stirred in buffer B at 30°C before addition of 1200 nM **11**. Buffer B: 200 mM phosphate, 1 mM TCEP, 0.1% CHAPS, pH 7.2. Reactions quenched into UPLC vials with an equal volume of 2% TFA in H_2O/MeCN (90:10). C343, Ex: 420 nm, Em: 500 nm. UPLC gradient: 15-45% eluent B in A. Error bars = SEM of three independent replicates.

In the simultaneous transfer, it was anticipated that the self-assembly of the two coiled coils P1/P2 and P3/P4 would mean that each PNA transfer would proceed independently, with no cross-reactivity between mismatched coiled-coil peptides (Figure 27A). For the simultaneous 'one-pot' PNA transfer, the reaction was carried out similarly to the single transfers: disulfides of the Cys-acceptors, **15** and **16** (100 nM), were added to buffer B together for 10 min prior to addition both thioesters **10** and **11** (1200 nM). The PNA transfers were almost identical to the separately recorded transfers in speed and yield (Figure 27B); in fact, the FLR–UPLC traces could be superimposed (Figure 27C), indicating that no new products formed and that a specific, orthogonal transfer of the two PNA strands to the two acceptor peptides was feasible.

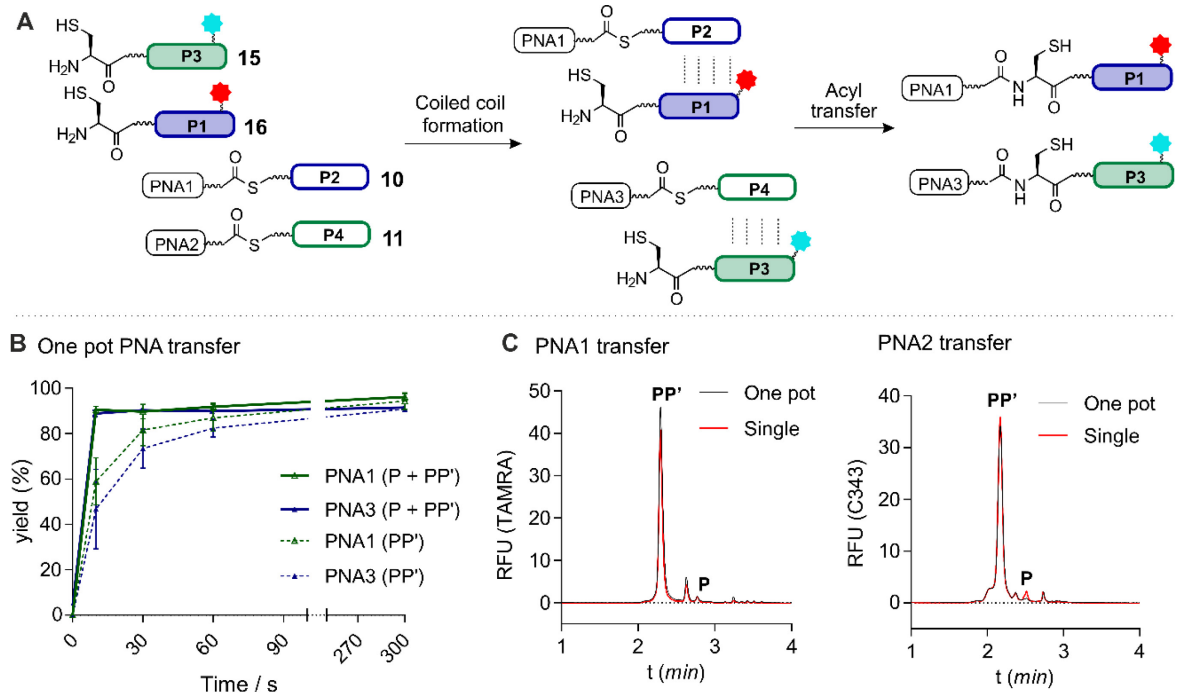

Figure 26 One-pot orthogonal-coiled-coil-templated PNA transfer with (Cys-P1-TAMRA)$_2$ **15**, (Cys-P3-C343)$_2$ **16**, PNA1-P2 **10** and PNA3-P4 **11**. **A)** Schematic of PNA transfer. Coiled-coil pairs of matching colours self-assemble before acyl transfer can take place. Red: TAMRA; Cyan: C343. **B)** Yield (%) of **P'** (PNA1-Cys-P1 or PNA3-Cys-P3) and **PP'** (PNA1-Cys-(PNA1)-P1 or PNA3-Cys-(PNA3)-P3) in relation to reaction time. **C)** Overlay of FLR–UPLC traces. Conditions: 100 nM **15** and **16** stirred in buffer B (200 mM phosphate, 1 mM TCEP, 0.1% CHAPS, pH 7.2) at 30°C before addition of 1200 nM **10** and **11**. Reactions quenched into UPLC vials with an equal volume of 2% TFA in H_2O/MeCN (90:10). TAMRA, Ex: 550 nm; Em: 580 nm. C343; Ex: 420 nm; Em: 500 nm. UPLC gradient: 15-45% eluent B in A. Error bars = SEM of three independent replicates.

4.2.2. Effect of Charged Residues on PNA Strands

K3/E3-templated PNA transfers had previously been carried out in the Seitz group with an 11-mer PNA strand. [126] In these experiments, it was observed that, whilst transfer of a 3-mer PNA proceeded to 98% within 2 min, transfer of the longer 11-mer required

much longer, taking 2 min to rise to 50%, and 10 min for 65%. It was speculated that the longer, hydrophobic PNA had a negative influence on the transfer. During preliminary experiments with PNA-donor **6** (Figure 28B), a K3 acceptor peptide linked via a thioester to the PNA strand PNA1H (which lacks charged amino acid residues), it was noted that adsorption of the products was substantial, especially in acidic quenched reactions. This became evident when comparing a basic vs acidic quench of the same reaction in glass vials (Figure 28A): the overall product yield appeared to be much less. At this stage, adsorption issues had not been considered in detail and plastic UPLC vials not yet adopted. It was decided to instead design more soluble PNA strands (PNA1S), and, gratifyingly, the observed overall yield of a 1:1 reaction of the new thioester PNA1S-K3 **8** with TAMRA-labelled Cys-E3 **18** (2.5 µM peptides, Buffer C: 100 mM phosphate, 1 mM TCEP, 0.1% CHAPs, pH 7.0) was almost two-fold (Figure 28C), though whether this observation was due to adsorption of PNA-tagged products was not

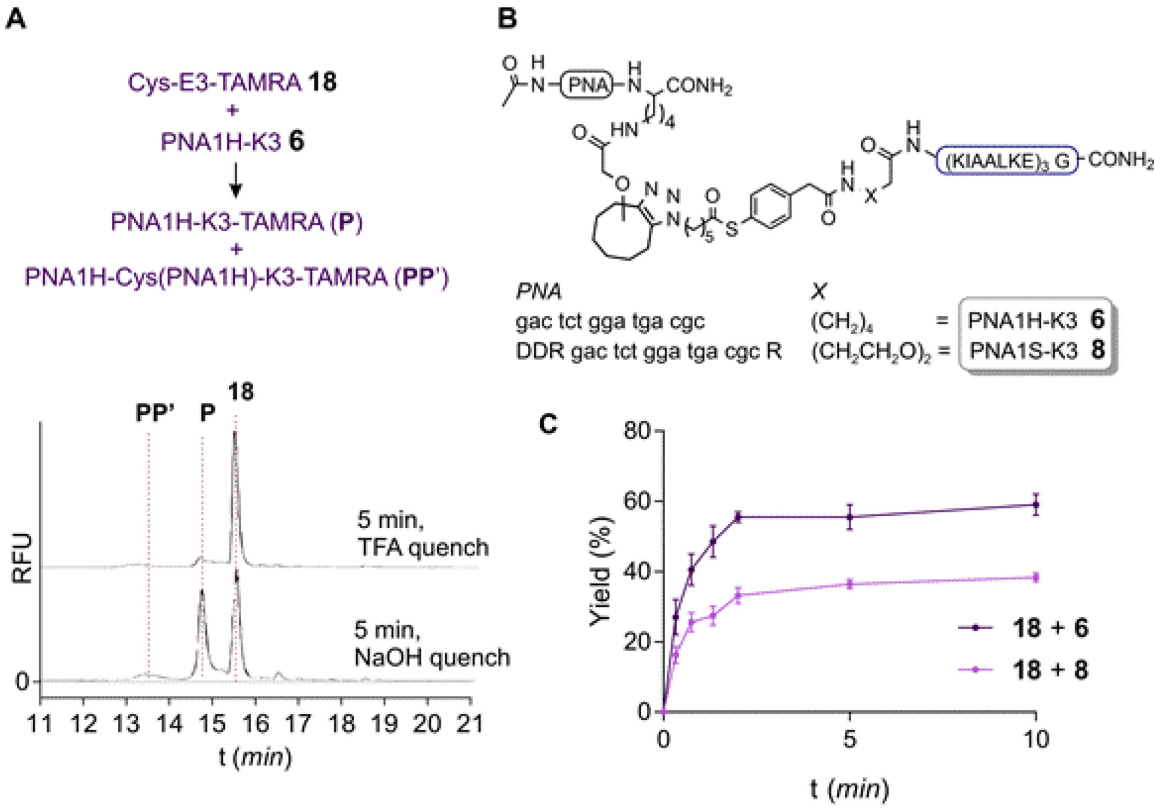

Figure 27 PNA transfer with Cys-E3-TAMRA 18. A) Comparison of quenching PNA transfer reaction of PNA1H-K3 **6** and **18** with an equal volume of acid (2% v/v TFA) or base (1 M NaOH). **B)** Structure of thioesters **6** and **8** used in C. **C)** PNA transfer yields with **6** or **8** and **18** (2.5 µM peptides). Conditions: **18** stirred in buffer C (100 mM phosphate, 0.1% CHAPS, 1 mM TCEP, pH 7.0) 10 min then **6** or **8** added. Quenched reaction analysed by FLR-HPLC: 25-65% A in B. TAMRA: Ex 550 nm, Em: 580 nm. Error bars = SEM of three independent replicates.

investigated at the time. The value of using a charged PNA strand was nonetheless apparent, and the strategy was adopted with the previously described PNA-donors **10** and **11** (PNA1 and PNA3). It was hoped that the decrease in non-specific interactions with the reaction vessel and UPLC vials would translate into reduced background staining in cellular experiments (see Chapter 4.3.2).

4.2.3. *S*-Acylated double transfer product

In previous works with the K3/E3, [153] P1/P2 and P3/P4[126] coiled-coil systems, a doubly (*N*- and *S*-) acylated product (**PP'** in Scheme 5) was, in most cases, generated and observed during PNA transfer. The fact that **PP'** had occurred to such an extent in the 1:1 orthogonal coiled-coil-templated reaction in chapter 4.2.1 (Cys-acceptors **15** and **17** with PNA-donors **10** and **11**; Figure 24) was surprising. Furthermore, the amount of the Cys-acceptors (**15** or **17**) would often reach a stable level where they reacted no further, however the product **P** would still be acylated once more to form **PP'**. In other words, reaction of the Cys-acceptor would seemingly 'stall'. Previous work had shown that the ratio of **P**:**PP**' in K3/E3-templated transfers was dependant on the fluorophore transferred. Furthermore, transfer of an 11-mer PNA resulted in more **PP'** formation than transfer of a 3-mer PNA. [126] These results hint at a scenario where reporter groups interact with one another, giving rise to extra stabilising (or destabilising) effects and leading to product inhibition.

To investigate whether this apparent increase in affinity of Cys-E3 for the acylated product is indeed due to the reporter groups interacting, a donor thioester capable of transferring an acetylated glycine residue (Ac-Gly-MPAA-AEEAc-K3, **19)** was synthesized (Figure 29A). Since two Ac-Gly were not expected to cause any meaningful interaction between **19** and its transfer product **P**, the Ac-Gly transfer represents a situation where there is no reporter–reporter stabilisation effect. Thioester **19** was reacted with Cys-E3-TAMRA **18** in buffer C. The masses and relative concentrations were verified by ESI–MS combined with UV-UPLC, then the reaction was examined by FLR-HPLC. The identity of the product **P** and doubly acylated product **PP'** were additionally verified by comparison of a base- and acid-quenched reaction (Figure 29B).

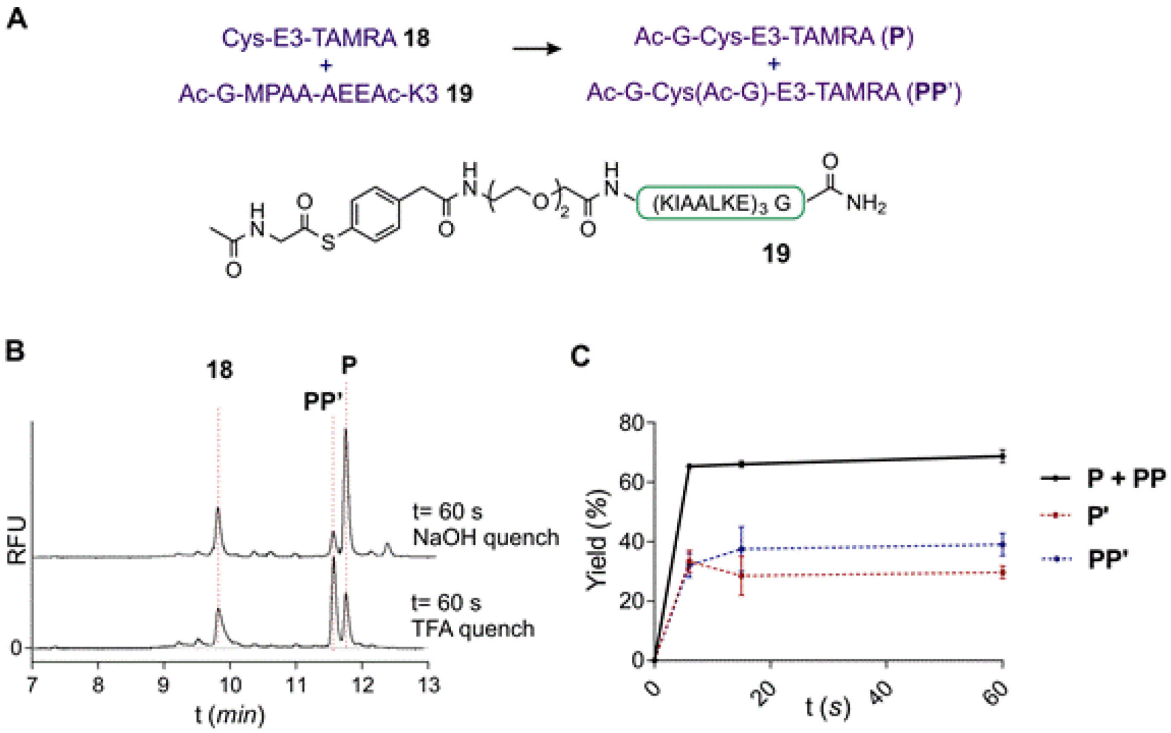

Figure 28 Acyl transfer of an acetylated glycine residue. Reaction of **18** with **19** at 1:1 (500 nM) in buffer C to yield the product Ac-G-Cys-E3-TAMRA **P** or the *S*-acylated product Ac-G-Cys(Ac-G)-E3-TAMRA **PP'. A)** Schematic of the reaction **B)** Time point t= 60 s point quenched with acid or base to a final concentration of 1% TFA or 500 mM NaOH. **C)** Reaction progress. Error bars = SEM of three independent replicates. Buffer C**:** 100 mM phosphate, 1 mM TCEP, 0.1% CHAPS, pH 7.0. HPLC gradient 40-60% A in B. TAMRA, Ex 550 nm, Em 580 nm. Error bars = SEM of three independent replicates.

With a 1:1 ratio **18** to **19**, the *S*-acylated Ac-Gly-Cys(Ac-Gly)-E3-TAMRA conjugate (**PP'**) formed half of the overall product after 5 s, yet after 1 min, this proportion had increased to 55% (Figure 29C). This was surprising as, given an equal affinity of **18** for **P** or the *S*-acylated product **PP'**, **P** would be expected to be the main product. This result therefore disfavours the hypothesis of interacting reporter groups or reporter hydrophobicity playing a role.

Another theory that could explain the behaviour is product inhibition, where the remaining thioester reactant **19** (donor peptide) preferentially binds to the reaction products (**P** or **PP'-** acceptor peptides) rather than the starting material **18** (acceptor peptide). The more product is formed, the further the reaction with starting material **18** is slowed down, leading to the eventual stalling. N-terminal 'capping' of α-helical peptides is known to be helix stabilising, [197] due to a mitigation of the repulsive interactions of the charged N-terminus. [198] This effect is even more pronounced in coiled-coil peptides; for example, acetylation of a tropomyosin peptide, able to form a dimeric coiled coil, was shown to stabilise coiled coiling of the peptide, especially in

conditions where the coiled coil was already formed. [199] This theory may also explain the observation of different reporters leading to different proportions of the *S*-acylated product. When comparing the *N*-cap preference of different amino acids, the positive effect on helix formation was particularly large when acetylating or acylation with non-positive amino acid residues, and residues which could accept hydrogen bonds. For acetylation, the lack of charged amino group was the distinction, but for residues such as Asp, Asn and Cys, H-bonding with the NH backbone groups was postulated. [198] ‡‡

Nevertheless, this theory does not explain the observation of the transfer reaction 'stalling' even in the presence of excess thioester. In Chapter 4.2.1, Figure 24, it was observed that performing the reaction with 3 eq of donor thioester **11** resulted in 90% conversion of Cys-acceptor **17** (mostly to the *S*-acylated **PP'**), and a further 3 eq of donor thioester was required to affect full conversion. Even with 4-5 eq thioester **11**, some Cys-acceptor reactant **17** remained (data not shown). In these scenarios, sequestering of reactant **11** by the product **P** (product inhibition) could not account for reaction stalling, due to the high excess of **11** used. It is possible that, instead, product inhibition of the Cys-acceptor reactant by the HS-donor (side product) occurs. This could theoretically be caused by a disulfide interaction, which are known to stabilise coiled coils, however, the reaction was carried out under reducing conditions. Alternatively, bearing in mind the *N*-cap preferences of hydrogen bonding residues, the MPAA of the HS-donor may interact with the coiled coil, imparting a stabilising effect. Though not further pursued in this work, a few experiments could shed light on this question of whether coiled-coil preference could be leading to product inhibition of the Cys-acceptor. One relatively simple solution would be to observe a reaction spiked with HS-donor peptide, to determine whether this significantly restricts the acyl transfer by inhibiting the Cys-acceptor peptide.

Another solution could be K_d measurements of the respective coiled-coil pairs (MPAA-AEEAc-K3; Ac-G-MPAA-AEEAc-K3; Ac-G-Cys-E3; Cys-E3). One approach to this would be to append a fluorophore, e.g., fluorescein, to the donor peptides and a quencher, e.g., Dabcyl, (4-((4-(dimethylamino)phenyl)azo)benzoyl)) to the acceptor peptides, and measuring the loss of fluorescence at particular concentrations. By titrating the Dabcyl peptide to a fixed concentration of the fluorescein acceptor peptide

‡‡In this work by Doig and Baldwin, the helical fractions of peptides with varying N-terminal residues were compared by circular dichroism, and from this the Gibbs free energy of *N*-acylation was calculated.

and measuring the fluorescence read out, binding affinities could be calculated and compared.

Hydrolysis of the S-Acylated Product

In a cellular labelling experiment, the *S*-acylated acceptor bearing two PNA strands (**PP'**) would likely be the main species. Whether this would pose a problem would depend much on the application. For instance, quantitative receptor tracking could be effected by hydrolysed reporter PNA, and when determining the oligomeric status of proteins by single molecule fluorescence imaging, the stoichiometry of labelling should be known. [10]

It was therefore valuable to determine whether this unwanted thioester linked PNA could be hydrolysed under conditions that would preserve cell viability, to yield a well-defined, irreversible, covalent linkage to a single reporter-PNA strand. A model peptide for the *S*-acylated species was synthesized using an azidohexanoic acid tether to represent the azido hexanoic acid-linked PNA **20** (Figure 30A). To assess hydrolysis rates, 40 μM of the model **PP' 20** was stirred in various buffers and the relative conversation to the thiol Azhx-Cys-E3 was assessed by UV-UPLC. At pH 8.0 (100 mM PBS), **20** was relatively stable: only 9% hydrolysis occurred after 2 h, and 55% after 16 h (data not shown). At a pH close to the thiol's pK_a of 9.2, 20 mM MESNA (in 100 mM PBS, pH 8.5) could afford full conversion of **20** via thiol-thioester exchange in only 5 min (Figure 30B), but the high concentration needed may affect cell viability. In comparison, MPAA was less effective, even above its pK_a of 6.6. To forgo high thiol concentrations, templated thiol-thioester exchange was attempted with MPAA-AEEAc-K3 **21** (Figure 30C). Transthioesterification was rapid, even with 1 equivalent of thiol **21,** due to the heightened effective concentration, however at only 20% conversion, a dynamic equilibrium was reached. This could be increased by using more equivalents of thiol **21**, and in the context of cell labelling, even 1 μM of **21** would be in orders of magnitude excess of the acceptor. It is expected that with repeat washes of *S*-acylated-Acceptor on adherent cells, complete conversion of 20 (and by extension, any *S*-acylated Acceptor) could be afforded, according to La Chatelier's principle. Alternatively, templated NCL with a peptide bearing an *N*-terminal cysteine residue, Cys-AEEAc-K3 **22**, could bring about a non-reversible thiol exchange owing to the sequestering of the thioester in an intramolecular S→N acyl transfer, similar to the original labelling reaction. With one equivalent of **22**, $t_{1/2}$ of **20** was 2.8 min. Increasing the length of the K coil peptide, and thereby the K_d of the coiled-coil interaction[116] by 3

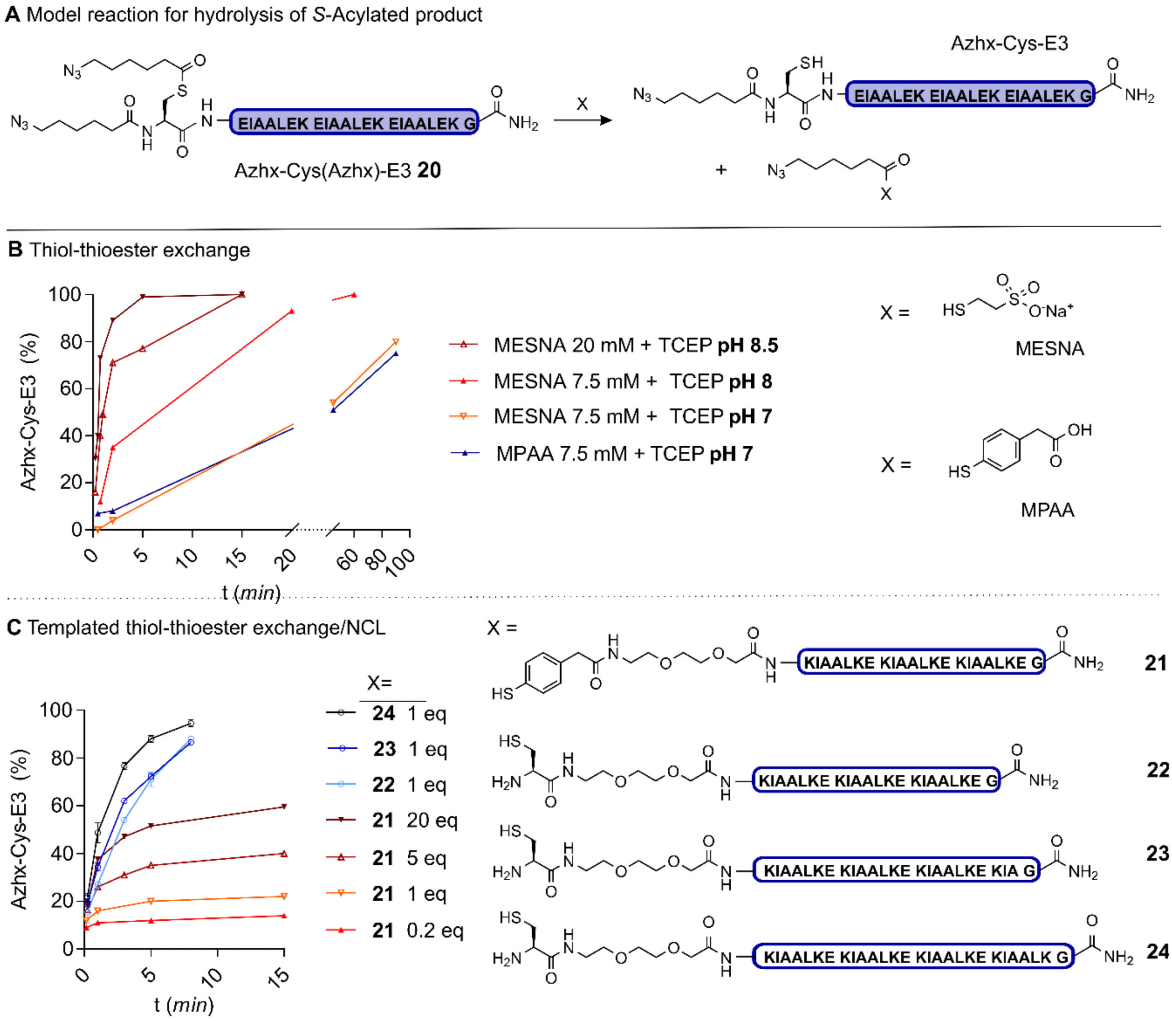

Figure 29 Stability of *S*-acylated product 20. A) Model reaction used to determine the stability of *S*-acylated PNA transfer product **PP'**. Stability to thiol thioester exchange **(B)** or templated thiol-thioester exchange or NCL **(C)** was determined. Conditions: thiol (X) at variable concentration was added to 40 µM **20** in buffer D (100 mM phosphate, 50 mM NaCl, 5 mM TCEP, with varied pH) or buffer E (100 mM phosphate, 50 mM NaCl, pH 7) at RT. The reaction was analysed by UV-UPLC–MS by measuring the ratio of the peak areas of **20** and Azhx-Cys-E3 at 210 nm.

amino acids in **23** reduced the $t_{1/2}$ to 2.2 min; lengthening by 6 amino acids, as for **24,** increased it to 1 min.

Acid- or base-catalysed hydrolysis of alkyl thioesters is generally very slow between pH 3 and pH 8, where thiol–thioester exchange is order of magnitudes faster. Thiol–thioester exchange becomes progressively more rapid as the pH increases up to the thiol's pK_a. [200] In cellular environments, the average concentration of the most abundant thiol, glutathione (pK_a: 8.66), is around 1-2 mM[201], while in some cellular compartments, such as the endoplasmic reticulum, values as high as 15 mM have been estimated. [202] Given the pH dependence of hydrolysis and thiol–thioester exchange, and the lower pH of endosomes (pH 5-6), stability of **20** would be compartment dependant.

At 7.5 mM MESNA at pH 7, the half-life of **20** was 1 h. It is likely that in more acidic endosomal compartments, the half-life of **20** would remain on the scale of hours, rather than minutes. A worthwhile addition to the above experiments therefore would be determining the different rates of hydrolysis for **20** firstly in cell media, as a model for cell surface protein hydrolysis of PNA during experiments; in cell lysate, as a model for the cellular matrix; and finally in acidified cell lysate, to mimic lysosomes. Fluorophore labelling of the peptide would allow using low micromolar concentrations of model thioester **20** in the experiments.

4.3. Live Cell PNA Transfer Experiments

The primary focus of this work was to establish the method of coiled-coil-templated PNA transfer as a versatile technique for labelling surface receptors. For this, a target protein must encode a 3-4 kDa acceptor coil tag bearing an N-terminal cysteine residue. Bioconjugation of this tag to a PNA strand is driven by the coiled-coil formation with a PNA-donor probe. After covalent attachment of the PNA strand, a hybridization step can install a fluorophore-conjugated DNA for fluorescence detection. Alternatively, an adaptor DNA strand may be recruited as a starting point for DNA nanotechnology.

Previous work in the group of Oliver Seitz had set the groundwork for the technique, demonstrating that K3/E3 coiled-coil-templated PNA transfer was effective for imaging Cys-E3-EGFR on live cells. [126] In this present thesis, the labelling technique will be validated on a number of receptors; the tyrosine kinase receptors EGFR and ErbB2 and the G protein-coupled receptor ET_BR. An advantage of coiled-coil motif-mediated labelling is that many de novo designed sets of these peptides exist, with well defined properties. [117,119,159,160] As the Beatty group showed for non-covalent labelling, [61,63,203] particular sets of coiled coils may be chosen that fit well with the specific application. The Jerala group also demonstrated this in their use of multiple sets of rationally designed orthogonal coiled coils were mutually orthogonal and functional in HEK293 cells experiments, and after tuning the coiled coil affinities, could use the peptides to upregulate gene expression.

This work will demonstrate that PNA transfer is compatible with two of the coiled coils used by the Jerala group, P1/P2 and P3/P4, [119] and that their orthogonality would be imparted on the PNA transfer, achieving the classically demanding task of simultaneous bioconjugation two protein targets on live cells. Lastly, the promise of the PNA tag as multifunctional oligonucleotide 'barcode' will be explored. Using DNA hybridization to build on the conjugated PNA tag, adaptor stands would recruit multiple fluorophores for brighter labelling, and the molecular tool of toehold mediated strand displacement used to pursue erasable labelling.

This chapter includes work in collaboration with Michael Bartoschek (Sebastian Bultmann, Ludwig-Maximilian's Universität München), who created the stable cell lines of Cys-P1-EGFR-eYFP and Cys-P3-ErbB2-eYFP, which were of great value to this work; and Philipp Wolf (Annette Beck-Sickinger, Universität Leipzig), who cloned the Cys-P1-ET_BR-GFPspark receptor, validated its activity and with whom PNA

labelling experiments of Cys-P1-ET_BR-GFPspark were carried out; all of which were vital during the review stages of a co-authored publication. [185]

4.3.1. Surface Protein Targets for Simultaneous PNA Conjugation

Cell surface receptor EGFR (epidermal growth factor receptor) and ErbB2 (also known as HER2; human epidermal growth factor receptor 2) were chosen as suitable candidates for single- and dual-protein-labelling experiments due to their clinical significance and abundance of scientific investigation on the two. Both are members of the tyrosine kinase super family and their roles in inducing cell proliferation, differentiation and migration means that when excessive signalling occurs, e.g. due to constitutive activation or overexpression, uncontrolled cell growth and tumour formation can result. [204,205] To restore the balance of signal transduction, many marketed cancer drugs have found success in targeting growth factor receptors, such as the tyrosine kinase inhibitor Gefitinib, [206] a high affinity EGFR binder; or the monoclonal antibodies Herceptin (tratuzumab), and Perjeta (pertuzumab), which target the extracellular domain of HER2 to prevent dimerization. [207]

Epidermal growth factor (EGF) is one of several native EGFR ligands whose binding allosterically activates a dimerization domain. [208] Dimerization results in autophosphorylation of tyrosine residues at an C-terminal intracellular domain, which in turn triggers signalling cascades that eventually lead to cell proliferation. ErbB2, conversely, has no native ligand but is constitutively active and more effective at eliciting a response than the EGFR homodimer, due to its downstream regulation resistance. [209] Both receptors have been widely studied, yet questions about their activation, [17] trafficking, [210] and mode of action of some drugs targeted to them[210] continue to perplex. Since ErbB2 has no known ligand, tag–probe labelling presents a suitable opportunity to install a fluorophore. Since both receptors contain an N-terminal extracellular domain and have proven to be functional with large N-terminal fusion tags, [17,105] the PNA transfer labelling method was deemed suitable.

To this end, coil acceptor tags Cys-P1 or Cys-P3 were required to be expressed at the N-terminus of EGFR and ErbB2. Three Chinese Hamster Ovary (CHO) cell lines were produced for this work by Michael Bartoschek in the Ludwig-Maximilians-Universität München: singly positive Cys-P1-EGFR-eYFP and Cys-P3-ErbB2-eCFP clones, and the double positive Cys-P1-EGFR-eYFP/ Cys-P3-ErbB2-eCFP clone. Enhanced yellow fluorescent protein (eYFP) and enhanced cyan fluorescent protein (eCFP) have distinct

absorption spectra and would be used to validate the PNA labelling. Adherent CHO cells were chosen, as they express very low levels of endogenous EGFR and ErbB2. [211] Briefly, Cys-P1-EGFR-eYFP and Cys-P3-HER2-eCFP constructs were cloned by *GenScript* (Piscataway, NJ, USA) into a donor vector[212] to produce two plasmids, pPBtet-Cys-P3-ErbB2-eCFP-PuroR and pPBtet-Cys-P1-EGFR-eYFP-PuroR, which both included a doxycycline inducible promoter and a puromycin resistance gene. These donor plasmids facilitated insertion of the genes into the genome as part of a PiggyBack transposon system, a genomic engineering tool for generating stable cell lines by a 'cut and paste' into TTAA chromosomal sites. [213] Puromycin selection followed by FACS sorting of the transfected cells both with and without doxycycline induction resulted in pools of cells, from which single clones were picked and expanded.

4.3.2. Comparison of PNA-donor Probes

Before carrying out dual labelling experiments, PNA transfer was tested with the differently designed PNA-donor probes. It had been postulated that the hydrophobicity of the PNA strands may adversely affect labelling in aqueous media, and experiments with synthetic Cys-E3 peptide (Chapter 4.2.2) had revealed that transfer of the more soluble, i.e., charged amino acid residue-modified, PNA-donor **8** was seemingly more effective than the less soluble PNA-donor **6.**

To compare their performance for live-cell labelling, experiments were carried out with Cys-E3-EGFR-GFP constructs transiently expressed in HEK293 cells as previously reported. [126] Cells were stained with Hoechst33342 nuclear stain before PNA transfer with **6** or **8** (100 nM in PBS, 4 min, RT). After washing with PBS, the PNA-conjugated receptors were stained with a complementary Atto565-conjugated DNA (**Atto565-DNA1**, 200 nM in PBS, 4 min, RT: Figure 31A) and, after washing with PBS to remove excess DNA, imaged. In a direct comparison with identical settings, it was found that the performance of probe **8** was superior, with visibly brighter labelling at the membrane regions compared with the background (Figure 31B vs C). As a result, all further labelling experiments were carried out with PNA-donors containing charged amino acids in the PNA portion.

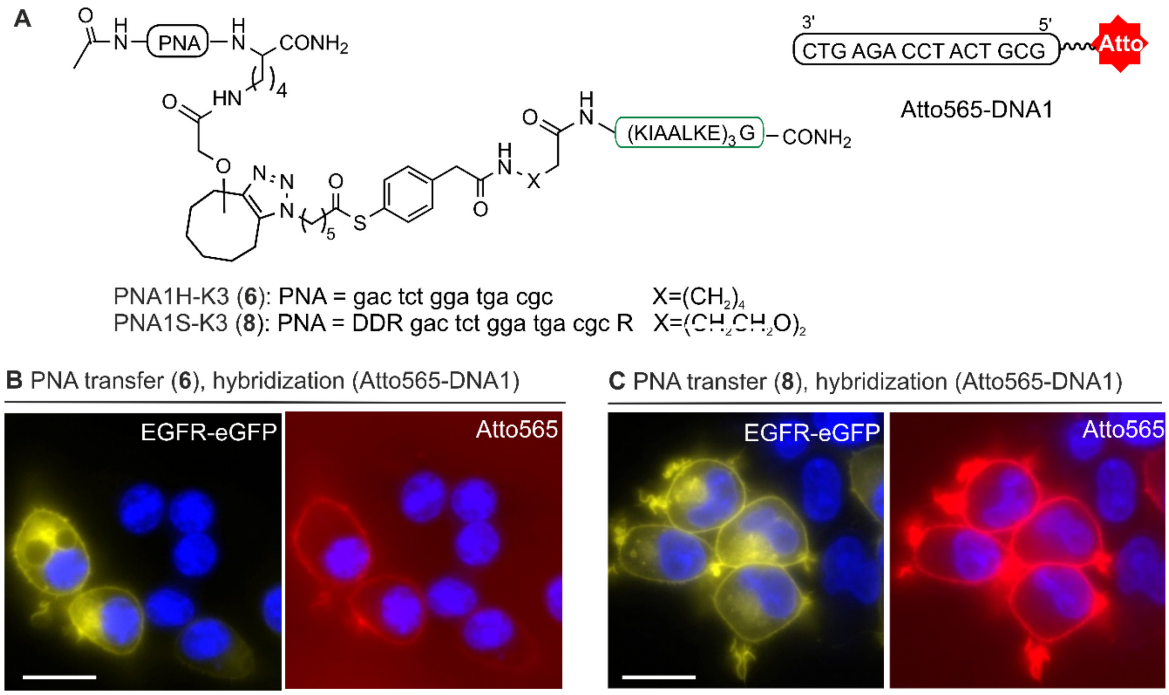

Figure 30 A) PNA donor probes and fluorescent DNA used for labelling of Cys-E3-EGFR-eGFP on transiently transfected (100 ng vector) HEK293 cells. Labelling with **B)** the 'less soluble' PNA donor probe **6** or **C)** the 'more soluble' PNA donor probe **8**. Labelling conditions: Hoechst33342 nuclear staining (10 min, 37°C, 5% CO_2, shown in blue), PNA transfer (100 nM **6** or **8** in PBS, 4 min, RT), Atto565-DNA1 hybridization (200 nM in PBS, 4 min, RT). Scale bars, 20 µm. Excitation times, YFP: 300 ms, TRITC: 1 s.

It should be noted that dead cells and cell debris were strongly stained by **Atto565-DNA1** in both experiments (not shown), something which is unsurprising due to the compromised membrane of dead cells allowing DNA to enter the cell. This effect has been noted for membrane staining[214] and is also the premise of marketed dead cell stains,[215] and was not an issue for labelling experiments.

4.3.3. Simultaneous Dual PNA Labelling using Orthogonal Coiled Coils

Orthogonal coiled-coil peptide pairs P1/P2 and P3/P4 were shown to be effective for in vitro selective transfer of PNA onto synthetic Cys-acceptor peptides (Chapter 4.2.1). Their performance in live-cell labelling experiments would next be tested on the stable cell lines Cys-P1-EGFR-eYFP, Cys-P3-ErbB2-eCFP, and the double positive Cys-P1-EGFR-eYFP/ Cys-P3-ErbB2-eCFP. PNA-donor probes PNA1-P2 (**10**) and PNA3-P4 (**11**) would again be used for the selective PNA transfer step (Figure 32A, B). For imaging after PNA conjugation, fluorescent DNAs **Atto565-DNA1** and the spectrally distinct **Cy7-DNA3** (complementary to **10** and **11,** respectively) would be hybridized

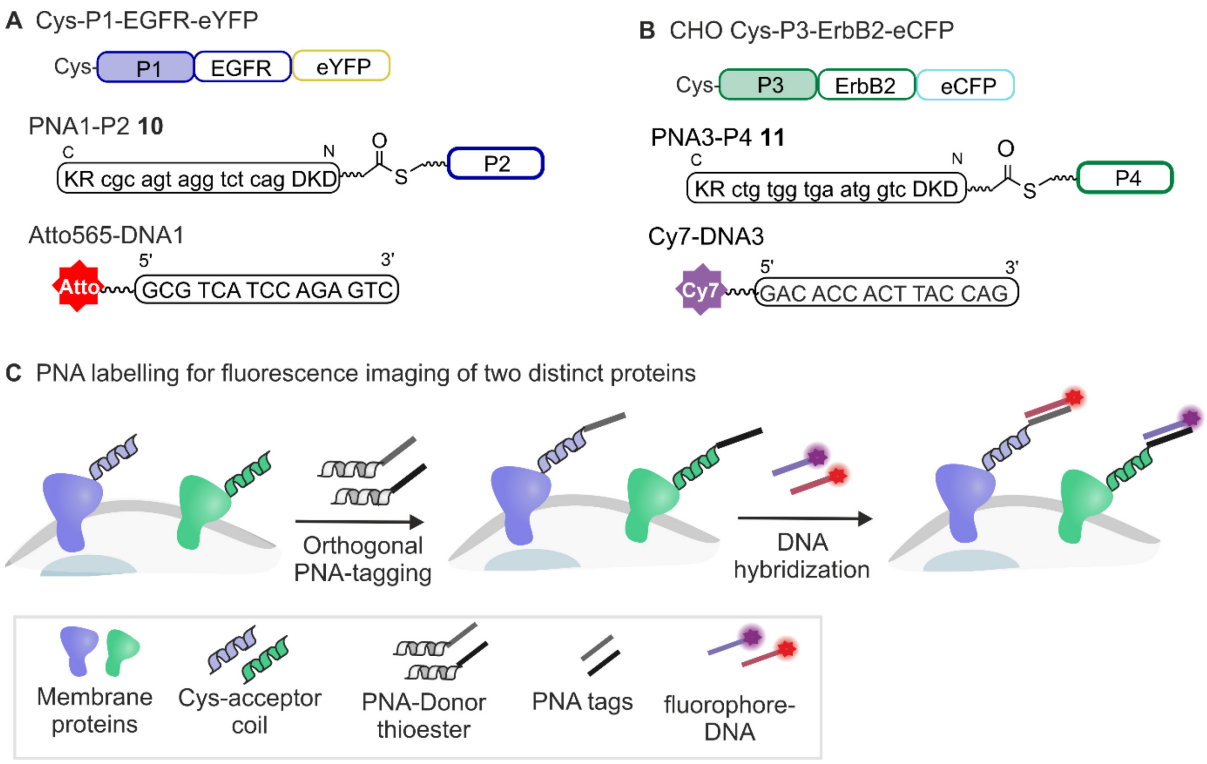

Figure 31 A) Schematic of construct and probes used for EGFR labelling. **B)** Schematic of constructs and probes used for ErbB2 labelling **C)** Schematic of orthogonal PNA labelling of two membrane proteins and subsequent DNA hybridization of fluorophore-DNA conjugate.

(Figure 32C). Stable cell lines, PNA-donor probes, and complementary DNA stains on hand, labelling experiments were commenced.

For experiments, Cys-P1-EGFR-eYFP and Cys-P3-HER2-eCFP stable CHO cell lines were prepared separately on 8-well µ-slides and grown to 80% confluency with 16 h doxycycline treatment to induce receptor expression. Prior to the experiments, nuclei were stained with Hoechst 33342 in Hank's Balanced Salt Solution (HBSS) containing magnesium and calcium to ensure cell adherence. Cys-P1-EGFR-eYFP and Cys-P3-HER2-eCFP expressing cells were then treated with PNA-donor **10** or **11,** respectively (100 nM in HBSS, 4 min, 37°C). After a washing step with HBSS, fluorophore conjugated DNA strands were added. Cys-P1-EGFR-eYFP CHO cells were stained with **Atto565-DNA1** and for Cys-P3-HER2-eCFP cells, **Cy7-DNA3** was applied (200 nM in HBSS, 4 min). After a final HBSS wash, fluorescence images were taken which confirmed the specificity for DNA staining only at membrane regions of the cells, where the YFP or CFP signal also occurred (Figure 33 A and D), a fact confirmed in scatter plots of the pixel intensities (Appendix Figure 1)

To check the specificity of the PNA conjugation to the correct coil peptide, Cys-P1-EGFR-YFP expressing cells were treated with the non-matching PNA-donor thioester

11 and hybridized with its complementary **Cy7-DNA3**, using the same protocol as described above. Similarly, Cys-P3-ErbB2-CFP cells were stained with non-matching **10** and hybridized with the complementary **Atto565-DNA1** (Figure 33 B and E). In both cases no labelling occurred, indicating that only with the correctly paired coil peptides could PNA conjugation take place. The specificity previously observed in the in vitro experiments was therefore maintained in the more complex environment of live-cell labelling. True validation of specificity of both the PNA transfer and DNA hybridization steps obligated every combination of PNA-donor and fluorophore-DNA to be tested on both cell lines. Labelling again did not occur when the non-complementary DNA was applied to PNA-conjugated or non-conjugated cells, confirming that DNA staining was selective (Figure 33 C and F). It was noted that the **Cy7-DNA3** stained images exhibited far more diffuse 'background' signal than Atto565-DNA images, even in the non-mismatched labelling. This was attributed to the lower solubility of Cy7 compared to Atto565 and the aggregation propensity of cyanine dyes compared with rhodamine dyes. [216]

The next logical stage was to label both receptors simultaneously in CHO-Cys-P1-EGFR-eYFP/ Cys-P3-ErbB2-eCFP cells. For this, the same conditions were applied as used for single colour labelling, but both thioesters **10** and **11**, and both oligonucleotides **Atto565-DNA1** and **Cy7-DNA3** were added together. Gratifyingly, the one-pot procedure performed seamlessly and Atto565 and Cy7 labelling correlated at the membrane regions expressing ErbB2 and EGFR (Figure 33 G; Appendix Figure 2). As an additional control, the same cells, but lacking doxycycline induced of protein expression, were subjected to the identical procedure, but no labelling occurred (Figure 33 H). These results demonstrated that orthogonal coiled-coil peptides could be successfully applied for simultaneous covalent PNA transfer of two distinct membrane proteins on the surface of a live cell. Following this, DNA hybridization could be used to selectively stain the PNA-conjugated receptors. Control experiments showed that both stages, PNA conjugation and DNA hybridization, were selective and specific.

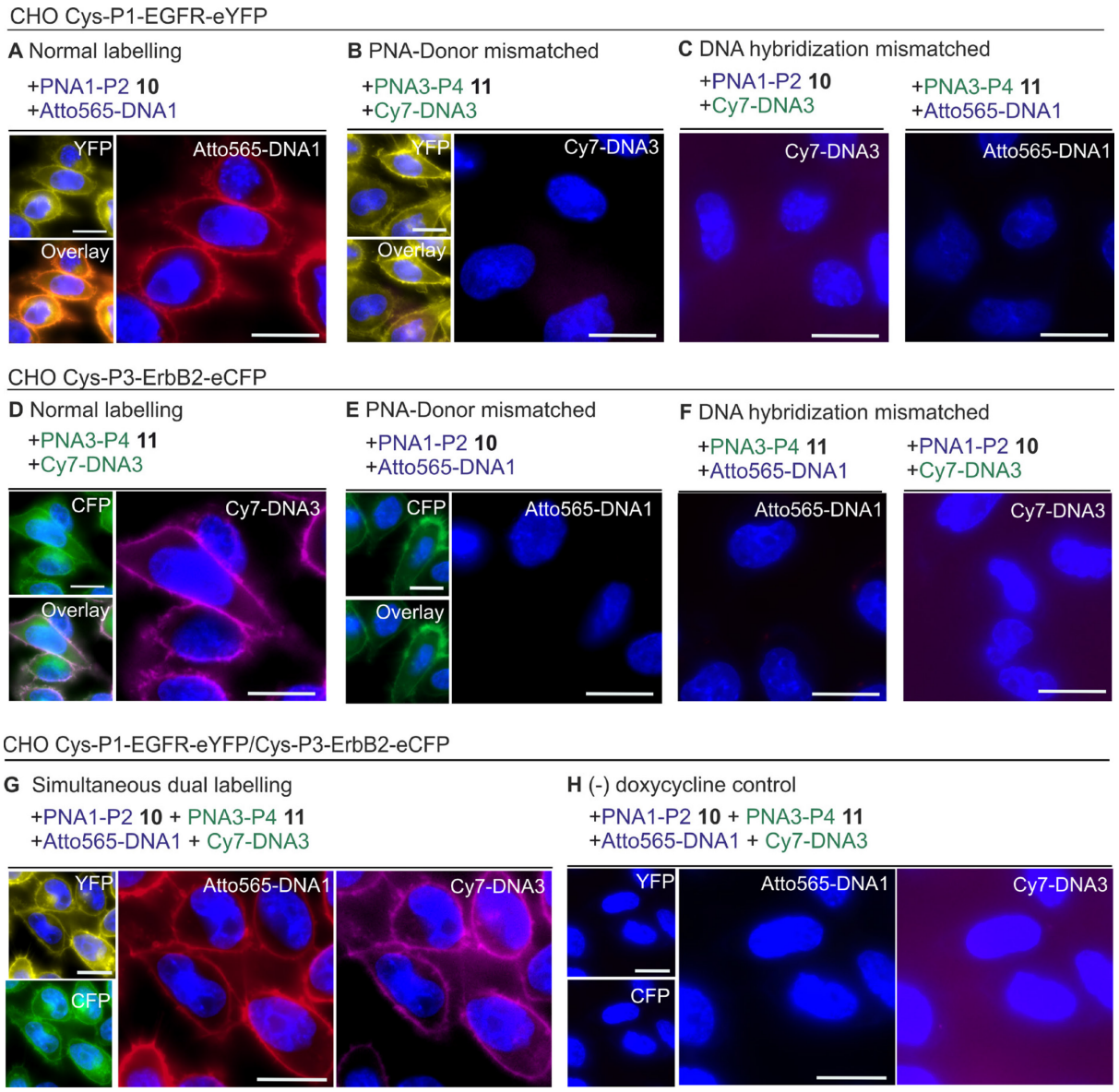

Figure 32 PNA labelling using orthogonal coiled-coils and imaging facilitated by DNA hybridization. **A-C)** Cys-P1-EGFR-eYFP stably expressing CHO cells were treated with A) PNA1-P2 **10** and **Atto565-DNA1** or (B,C) with mismatched PNA-donors and DNA. **D-F)** Cys-P3-ErbB2-eCFP stably expressing CHO cells were treated with A) PNA3-P4 **11** and **Cy7-DNA3** or (E,F) mismatched PNA-donors and DNA. **G)** Cys-P1-EGFR-eYFP/Cys-P3-EGFR-eCFP CHO cells treated with **10** and **11** then **Atto565-DNA1** and **Cy7-DNA3** for simultaneous dual labelling of both receptors. **H)** Same conditions as G but without doxycycline-induced receptor expression. Conditions: Hoechst33342 staining (shown in blue); PNA labelling with **10** and/or **11** (100 nM in HBSS, RT); hybridization of **Atto565-DNA1** or/and **Cy7-DNA3** (200 nM in HBSS, 4 min). Scale bar=10 µm. Excitation times: Cy7: 500 ms, Atto565: 500 ms, YFP: 200 ms, CFP: 150 ms. Experiments were repeated 3 times with similar results.

4.3.4. Validation of the PNA Labelling Method.

PNA Labelling of a G-Protein Coupled Receptor.

So far, three different coiled-coil sets had been used for PNA transfer experiments. To further demonstrate the general applicability of the method, labelling of another

receptor type, endothelin receptor type B (ET_BR) was also carried out. ET_BR is a G-protein coupled receptor responsible for vasoconstriction of endothelial cells and is rapidly internalized and degraded in response to endothelin 1 (ET-1). [217,218] For this, a Cys-P1 tag was cloned onto ET_BR-GFPspark, and receptor activity validation was carried out by Philipp Wolf. The inositol phosphate accumulation assay confirmed that introduction of the Cys-P1 tag did not affect downstream signalling of ET_BR-GFPspark. [185]

Next, PNA labelling experiments were carried out. For PNA transfer, donor **9** was used and for imaging, its complementary Atto565 conjugated 15-mer **Atto565-DNA1** (Figure 34A). Two concentrations of Cys-P1-ET_BR-GFPspark plasmid were transfected (750 ng and 250 ng) generating cells with differential expression levels. Serum starved cells were treated with 100 nM **9** for 4 min, washed, then **Atto565-DNA1** was hybridized (200 nM in HBSS, 4 min) and the cells imaged. Signals from GFPspark and

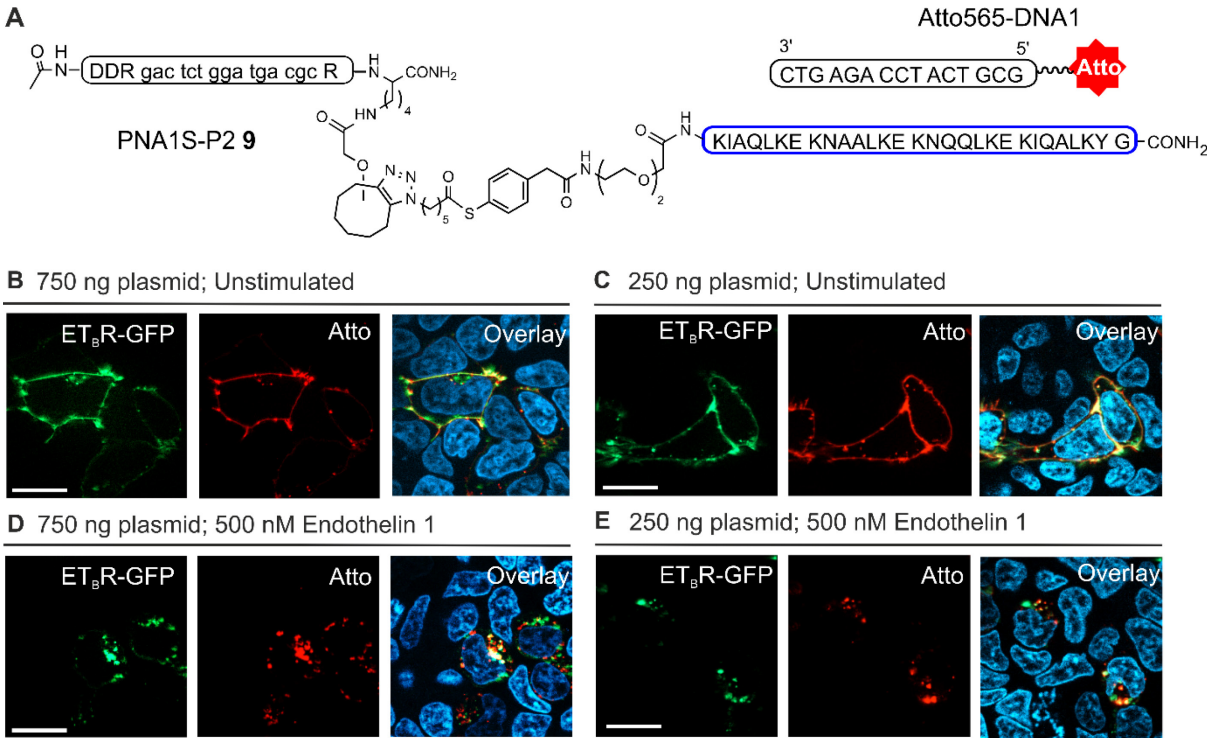

Figure 33 PNA enabled imaging Cys-P1-ET_BR-GFPspark on HEK293 cells at different transient expression levels. **A)** Schematic structures of the ET_BR construct, PNA-donor **9** and **Atto565-DNA1** used for imaging B-E) Labelling of ET_BR using either **B)** and **D)**, 750 ng or **C)** and **E)** 250 ng of pCMV3-Cys-P1-ET_BR-GFPspark plasmid for transient transfection. After nuclear staining with Hoechst3342 (shown in blue), PNA-tagging with **9** and subsequent hybridization with **Atto565-DNA1** cells were (B, C) imaged immediately or (D, E) stimulated with ET-1 (500 nM in HBSS, 1 h, 37°C) before imaging. Conditions: PNA transfer: 100 nM **9** in HBSS, 4 min, 37 °C. Hybridization: 200 nM **Atto565-DNA1** in HBSS, 4 min, 25°C. Scale bar = 20 µm. Excitation times B) and D): GFPspark 400 ms, Atto565 500 ms.C) GFPspark 340 ms, Atto565 370 ms. E) GFPspark 100 ms, Atto565 170 ms. All experiments were repeated independently with similar results 3 times.

Atto565 colocalized in clusters typical of this receptor type (Figure 34 B and C). [217] Satisfyingly, cells with differential expression level still afforded similarly well resolved labelling. To determine whether the receptors remained functional after PNA labelling, the same labelling was performed followed by ET-1 treatment. In response 1 h stimulation, the whole receptor population was internalized in both Atto565 and GFP channels. Some loss of localization did occur, but this was to be expected owing to the rapid degradation of ET_BR after internalization. [217]

EGFR Activity after PNA Labelling

ET_BR had shown to remain active after PNA labelling. To check whether PNA labelling, or DNA hybridization would influence receptor activity, an immunofluorescence assay was carried out in a 96-well plate format, measuring phosphorylation of Y1068 as a surrogate for receptor activation. Stable Cys-P1-EGFR-eYFP CHO cells were labelled with PNA donor **9** in PBS or just PBS as a control**,** hybridized with complementary DNA1 (non-fluorophore labelled) in HBSS or just HBSS, then stimulated with EGF or only serum-free medium (100 nm, 10 min). After fixation, incubation with a Phospho-EGF Receptor (Tyr1068) Rabbit mAb antibody followed by secondary AF647-labelled Goat anti-Rabbit IgG would give a AF647 fluorescence readout proportional to Y1068 phosphorylation. The EGFR-YFP signal was measured as an internal standard of EGFR levels to correct for variation in receptor concentration, and the ratio of Atto647N/YFP was defined as the phosphorylation level of Y1068. Results showed that phosphorylation of Tyrosine1068 was not significantly affected by either the PNA transfer step or subsequent hybridisation of the PNA with 10 min EGF stimulation, nor did the PNA label have an effect on Tyrosine1068 phosphorylation in non-stimulated cells (Figure 35A).

Labelling Stability Over Time

Under cellular conditions, the amide bond-linked PNA tag is stable and at 37°C, the 15-mer PNA/DNA duplex would not exhibit appreciable dissociation.[§§] In Chapter 4.2.1 it was discovered that most of the labelled Cys-acceptor peptide existed as the acyl transfer product with a second PNA attached via an *S*-acylation. In this double-transfer product one PNA was linked via its carboxylic acid in an amide bond to the peptide N terminus, and one via a thioester at the cysteine residue. Though it was shown that this may be hydrolysed if required (Chapter 4.2.3), this was not deemed necessary. It was

[§§] the predicted T_m for both conjugates was over 60°C (See Chapter 4.1.1)

also shown that the thioester bond was relatively stable, even at neutral pH with mM thiol additive ($t_{1/2}$ = 1 h in 7.5 mM MPAA; pH 7.0).

To determine if the PNA labelling method gave stable labelling over hours, **Atto565-DNA1** stained Cys-P1-EGFR-eYFP was measured, and the Atto565 signal was compared with the YFP signal. Atto565 was deemed a suitable fluorophore due to its high photobleaching resistance[219] and low excitation times were used Cys-P1-EGFR-

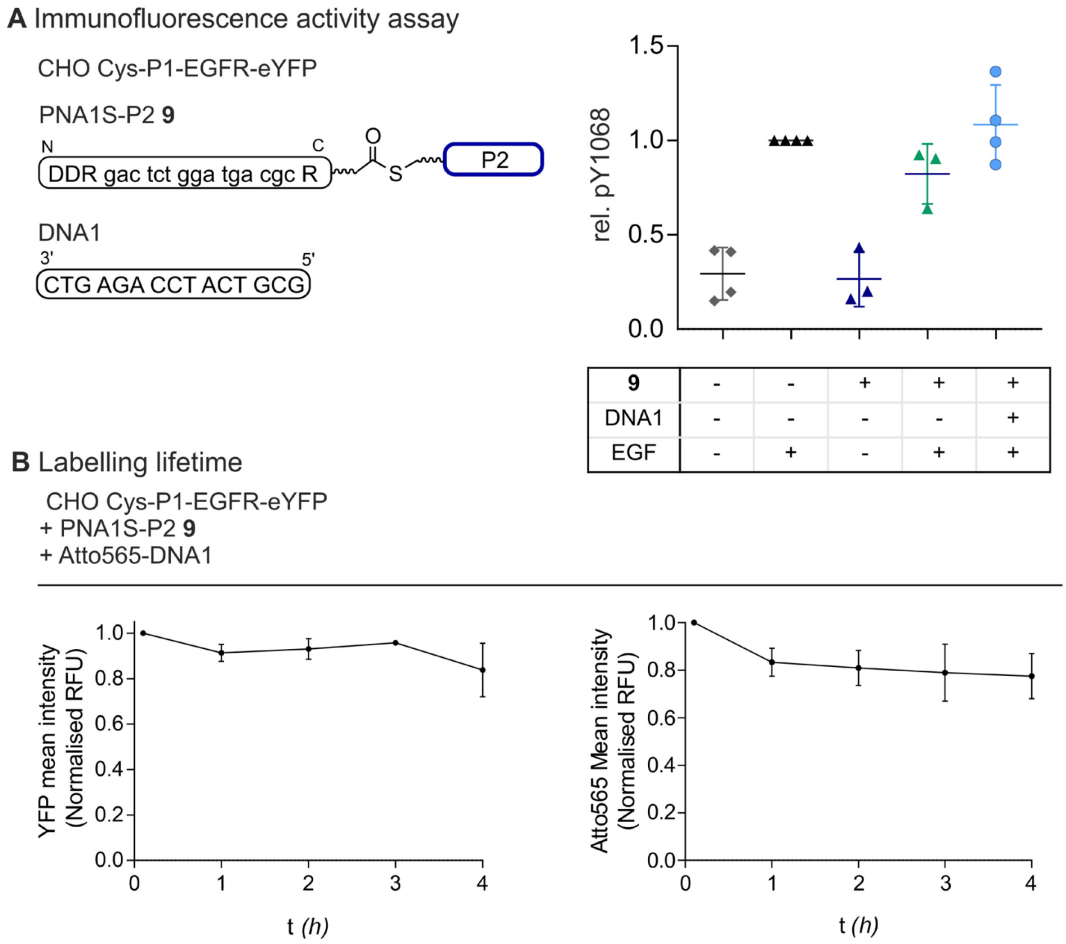

Figure 34 Effect of PNA labelling on EGFR phosphorylation and PNA labelling/DNA stain lifetime. A) Relative Y1068-EGFR phosphorylation of Cys-P1-EGFR-eYFP stably expressing CHO cells. Cells were serum starved for 12 h before PNA labelling with **9** (100 nM, 4 min), DNA1 hybridisation (100 nM, 3 min) and EGF stimulation (100 nM EGF, 10 min). Cells were fixed (4% PFA in PBS, 10 min) blocked (5% normal goat serum, 0.3% Triton in PBS, 1 h) and incubated with phospho-EGFR (Tyr1068) rabbit mAb (1:800; 1% BSA, 0.3% Triton in TBS; 4°C o/n) then with AF647-labelled Goat anti-Rabbit IgG (1:500; 1% BSA, 0.3% Triton in TBS; RT 1 h). AF647/YFP RFUs were normalised to the +EGF,-**9**,-DNA1 control. Dot plot presented as the mean +/- SD of independent biological replicates. YFP: λ_{ex} = 420±15 nm, λ_{em} = 532±10 nm. AF647: λ_{ex} = 665±10 nm λ_{em} = 640±10 nm. **B)** Analysis of signal loss over time after PNA transfer and **Atto565-DNA1** staining. Labelling: stable Cys-P1-EGFR-eYFP CHO cells treated with **9** (100 nM in DPBS, 4 min, 37°C) followed by **Atto565-DNA1** hybridization (200 nM in HBSS-BB, 4 min RT). Analysis: Fluorescence images was analysed by drawing a region of interest (ROI) around at least 20 cells in the YFP channel (Appendix Figure 3). Mean YFP and Atto565 fluorescence intensities of ROIs were recorded and normalised to the first time point. Data is presented as the mean +/- SD of n=3 independent experiments.

eYFP CHO cells were induced with doxycycline for 12 h before switching to serum free media without doxycycline to prevent new synthesis of protein and to limit basal internalization of EGFR by growth factors present in the media. After 4.5 h, cells were PNA conjugated with **9** and stained with **Atto565-DNA1**, then fluorescence images were taken in the YFP and Atto565 channel. Even with cell starvation, the EGF receptor was very gradually internalized. Therefore, rather than analysing the cell membrane only, whole cells were considered. Brightness of the cells was compared between the two channels. The mean Atto565 intensity dropped by 22% over 4 h whereas the YFP signal exhibited a loss of 16% (Figure 35B). The diminishing signal may be explained by the following: i) chromophore bleaching; ii) lysosomal degradation of the YFP protein and DNA (loss of YFP signal); iii) PNA/DNA duplex melting (loss of Atto565 signal); iii) hydrolysis of thioester (loss of Atto565 signal). This analysis of brightness loss was simplistic and would not distinguish these factors, but ratiometric and colocalization analysis was made more difficult by the presence of basal EGFR internalization. Nevertheless, it was assumed that if the PNA labelling or DNA hybridization was unstable, **Atto565-DNA1** would be lost to the surrounding extracellular media and result in a significant brightness decrease. Considering the signal loss of YFP and Atto565 was still similar, the results were encouraging and proved that, as expected, the Atto565 label persisted over hours.

If a more stable interaction were desired, the length of the PNA/DNA duplex could be extended, or a fluorophore-conjugated PNA could be employed instead, to offer a higher melting temperature. Additionally, if the signal were to be quantified, a hydrolysis step or templated native chemical ligation could be included to remove any thioester-linked PNA.

4.3.5. PNA transfer labelling with multiple fluorophores for brighter labelling

An advantage of using a PNA tag is that it may be used as a starting point to assemble DNA architectures. A simple and useful application of this feature is the assembly of multiple fluorophore-conjugated ssDNA strands on a single target protein. Obtaining sufficiently bright labelling can be a challenge for biologists, as fluorescence intensity is limited by the target concentration and fluorophore's photon output. Low sensitivity is often experiment limiting and increasing the excitation times is not an appropriate solution as it eventually leads to bleaching. [220] Some technologies try to overcome this by recruiting many fluorophores to the target, such as the SunTag, developed to

assemble up to 24 GFP proteins on a repeating epitope. As a result, these tags can achieve much longer labelling time frames, which is useful, for example, in single molecule tracking. [221] DNA 'nanotags' were also developed which consist of DNA scaffolds with many intercalating dyes. [214,222]

For our experiments to attempt brighter labelling by recruiting multiple fluorophores, stable Cys-P1-EGFR-eYFP expressing CHO cells were used, with PNA1-P2 **9** for the PNA transfer step. Two adaptor DNAs (Adaptor33 and Adaptor105) were designed, both ssDNA made up of (i) a region complementary to the PNA, (ii) a 3-mer gap to provide flexibility and (iii) either a 15-mer or an 87-mer portion designed to hybridize to one or five complementary Cy7 -15mer imager strands, respectively. The adaptors were prehybridized with one or five Cy7-DNA3 15-mers and named **Cy7-1xComplex** and **Cy7-5xComplex,** respectively (Figure 36A). To analyse brightness by fluorescence microscopy, Hoechst33342 stained cells were PNA labelled by treatment with **9** (100 nM in HBSS, 4 min, RT). Hybridization of the Cy7-DNA complexes (200 nM complex in HBSS, 4 min, 25°C) resulted in significant background staining, particularly for **Cy7-**

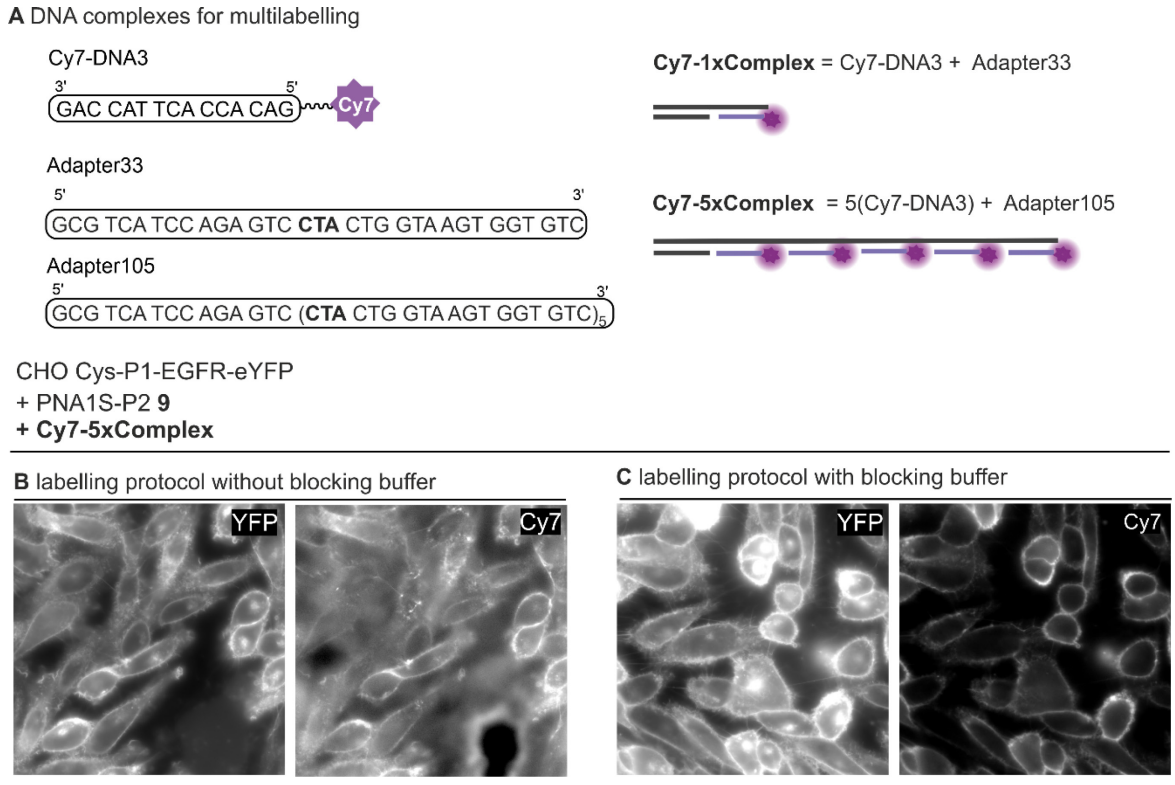

Figure 35 A) DNA sequences and complexes used for multilabelling with Cy7. **B)** Stable CHO Cys-P1-EGFR-eYFP labelling with five Cy7 dyes, without blocking buffer. Conditions: PNA labelling (100 nM **9**, 4 min), wash (HBSS 1x), hybridization (**Cy7-5xComplex**, 200 nM in HBSS, 4 min). **C)** Stable CHO Cys-P1-EGFR-eYFP labelling with five Cy7 dyes, using blocking buffer (HBSS-BB). Conditions: PNA labelling (200 nM **9**, 4 min); wash (HBSS-BB 1x); hybridization (**Cy7-5xComplex**, 100 nM in HBSS-BB, 4 min); wash (HBSS-BB 1x). Excitation times: YFP: 150 ms; Cy7: 500 ms. Figures shown in greyscale for clarity.

5xComplex (Figure 36B). This was likely due to the hydrophobic nature of Cy7 resulting in increased non-specific binding. To counteract this non-specific interaction, the complex concentration was decreased from 200 nM to 50 nM and a blocking buffer (HBSS-BB) containing 0.1 mg/ml salmon sperm DNA and 0.2% BSA was used in the hybridization step and in the wash steps before and after hybridization. With these changes to the protocol, significantly clearer microscopy images could be obtained (Figure 36C).

To compare the brightness of PNA-labelled cells stained with one fluorophore or five fluorophores, cells were treated with PNA **9** and stained with **Cy7-1xComplex** or **Cy7-5xComplex** as described. Line scan intensity profiles through the centre of the cells showed that only the membranous EGFR was stained with Cy7, and this was brighter in images stained with **Cy7-5xComplex** (Figure 37 A vs B). Using the line scan intensity profiles, signal to noise ratios were calculated from 20 cells (Appendix Figure 4). The 'noise' was assigned from a background region with no cells and was defined as the standard deviation of the pixel RFU (relative fluorescence units). The 'signal' was the max Cy7 RFU at the membranous region, corrected for the YFP RFU to account for cell-cell variation in expression level. Staining with five Cy7-DNA3 strands gave an almost 3x increase in signal/noise than staining with just one. (Figure 37C). Though not a five-fold increase, the results were encouraging since this would correspond to an immediate and easily won gain in sensitivity of any imaging/assay readout. The less than 5-fold increase may be attributed to the background staining, which was generally high for Cy7-stained cells. Additionally, assembling multiple fluorophores does not always relate linearly to an increase in fluorescence, and cyanine dyes in particular may aggregate[216,223] including in the environment of DNA conjugate. [224] To assess whether a linear increase in fluorescence intensity could be quantified, a moderately hydrophilic, red-spectral carbon-rhodamine dye (Atto647N) was employed. Flow cytometry analysis was used to analyse PNA-conjugated Cys-P1-EGFR-eYFP CHO cells stained with DNA carrying one, three or five Atto647N dyes.

In this case, the same 105-mer adaptor strand was prehybridized with either one, three or five complementary Atto647N-DNA 15-mers to give the three complexes: **Atto647N-1xComplex, Atto647N-3xComplex, Atto647N-5xComplex** (Figure 37E). After PNA labelling with **9** and staining with Atto647N complexes as before, cells were washed with PBS, detached with trypsin/EDTA, and then fixed with paraformaldehyde. Flow cytometric analysis (Appendix Figure 5) of the fixed cells was carried out and results revealed a linear relationship between brightness and number of hybridized

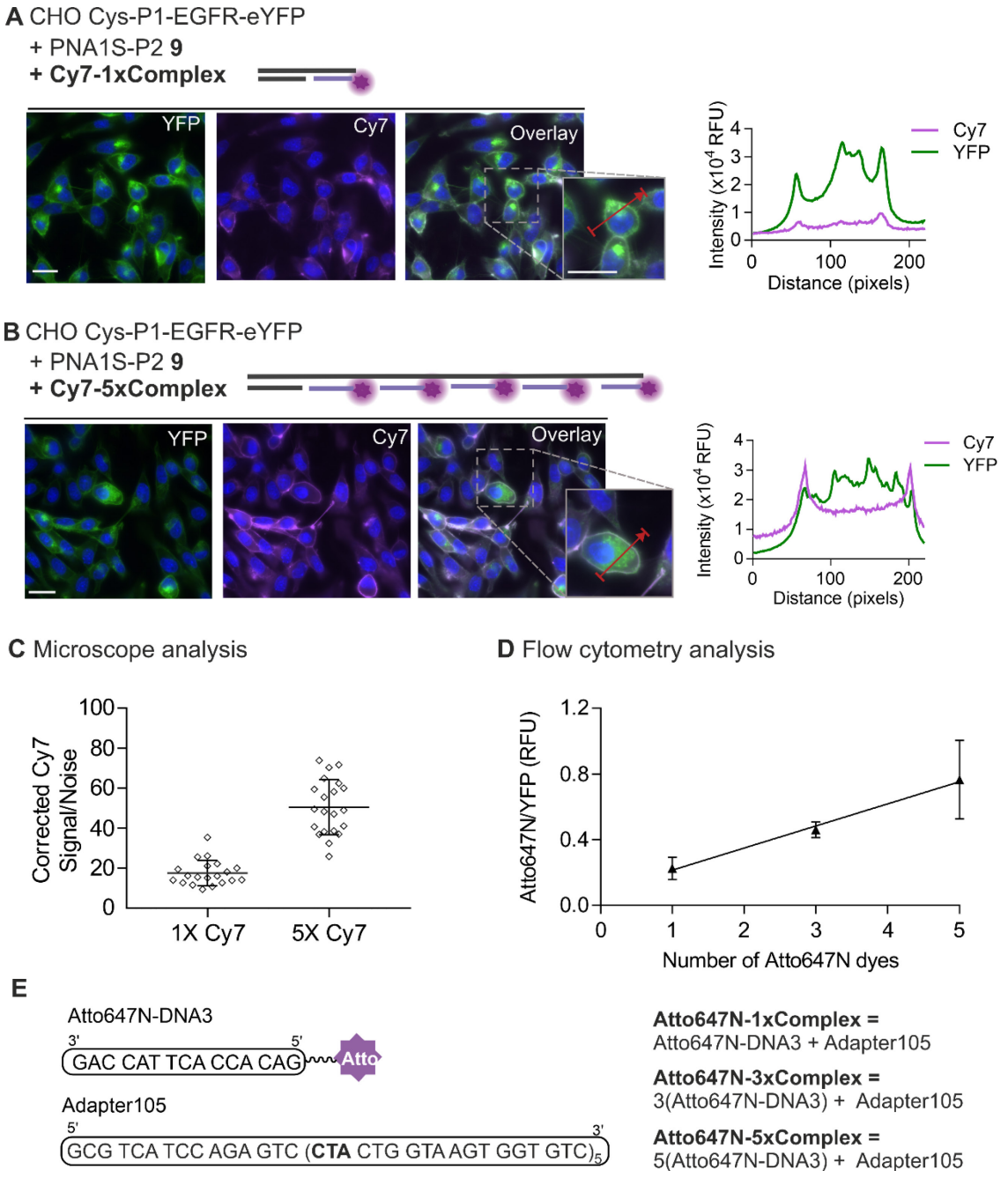

Figure 36 PNA labelled Cys-P1-EGFR-eYFP stable CHO cells stained with multiple fluorophores. **A-B)** Fluorescence images PNA-labelled EGFR stained with A) one, or B) five Cy7 dyes. Brightness of picture in B) was decreased comparative to A). Graphs represent signal intensity along the red lines shown in the zoomed inset. Conditions: PNA labelling (100 nM **9** in HBSS, 4 min) hybridization A) **Cy7-1xComplex** or B) **Cy7-5xComplex** (100nM in HBSS-BB, 4min). Excitation times: YFP: 150 ms; Cy7: 500 ms. **C)** Signal to noise ratio (SNR) calculated from line intensity profiles as shown in A and B. Dot plot shows SNR from n=30 cells from 3 independent experiments as shown in Appendix Figure 4. **D)** Flow cytometry analysis of PNA labelled Cys-P1-EGFR-eYFP cells stained with one, three or five Atto647N dyes. Conditions: PNA labelling (100nM **9** in HBSS, 4 min) hybridization **Atto647N-1xComplex, Atto647N-3xComplex, Atto647N-5xComplex** (50nM in HBSS-BB, 5min). Cells were detached with Trypsin/EDTA; fixed with PFA (4% in PBS, 10 min) and analysed by flow cytometry using excitation lasers: YFP) 488 nm; Atto647N) 640 nm and mission filters: YFP) 533/30 nm; Atto647N) 675/25 nm. The signal from cells not doxycycline induced or labelled, was subtracted and data presented as the mean +/- SD of n=3 three independent experiments. (Gating showed in Appendix Figure 5) **E)** DNA sequences and complexes used for counterstaining PNA with multiple fluorophores.

Atto647N dyes. On average, staining with five Atto647N dyes gave a 3.4x brighter cell than staining with one dye, a similar result to the previous experiment. Importantly, the experiment showed that the brightness increase was additive up to at least 5 dyes. Although this linearity was not assessed with more dyes, it is likely that more reporters could be added for further brightness enhancement. In this analysis, the labelling technique was also shown to be suitable with fixation protocols and flow cytometry analysis.

4.3.6. PNA transfer for erasable labelling

Brighter labelling had shown the advantage of DNA assembly for recruiting multiple fluorophores. Next, toehold-mediated strand displacement (TMSD) would be employed on to affect a reversible labelling system. TMSD is a molecular tool based the process of branch migration on double stranded DNA (dsDNA) [225] and forms the basis of dynamic DNA nanotechnologies including molecular machines[226] and logic gates. [227] In its simplest form a dsDNA with one strand containing an unhybridized overhang, or 'toehold' section may be invaded by a ssDNA fully complementary to the strand containing the toehold. Eventually the invading DNA becomes fully hybridized with this toehold containing strand, forming a new dsDNA hybridized pair in a displacement which is thermodynamically favoured by the increase of paired nucleobases. It was envisioned that for imaging, this technique could potentially be used for reversible of fluorescent labelling, by removing a fluorophore-conjugated imager strand using an invading eraser strand (Figure 38).

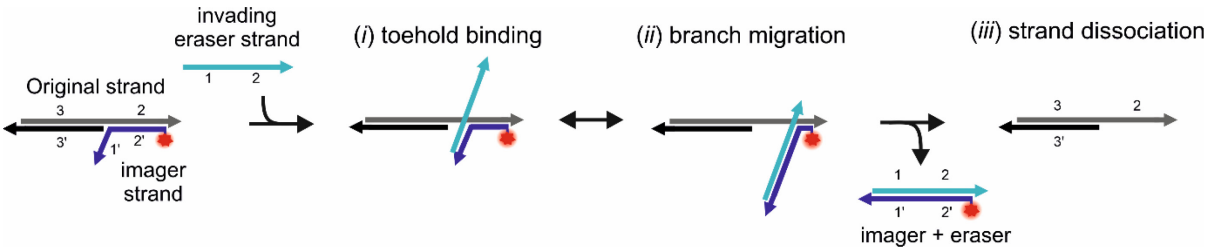

Figure 37 Principle of toehold mediated strand displacement (TMSD) to remove a fluorescent DNA (imager strand) from an 'original strand'. (*i*) An invading 'eraser strand' hybridises with a complementary toehold (unhybridized portion) of an imager strand. (*ii*) Branch migration, a reversible and random process, eventually leads to the thermodynamically favoured strand dissociation shown in (*iii*), where the eraser strand has displaced the imager strand from the original strand.

For this, the long adapter105 was again used to allow TMSD on a DNA/DNA duplex. Though carrying out TMSD on the PNA strand directly could preclude the use of an adaptor DNA, TMSD from DNA/DNA duplexes is much more established in literature.

A very recent study, however, defined TMSD in PNA/DNA duplexes and found that, though slower, behaved similarly. [228] Using DNA would therefore mean faster removal of the imaging strand, an advantage in a live-cell labelling experiments where rapid trafficking is investigated. A toehold of 8 nt was chosen. It is reported that the rate of toehold exchange increases linearly with toehold length, but levels off over 6 nt. [229] A 23-mer imager strand with a 15 nt section complementary to the adaptor strand, an 8-mer toehold, and an Atto565 dye conjugated to the 5' end was purchased and named Atto565-DNA4. A complex made up of Adapter105 and five erasable imager strands (Atto565-DNA4) was named **Atto565-5xImager.** The invading strand, which would remove the imaging strands from Adapter105 was a 23-mer fully complementary to Atto-DNA4 imager and named **EraserDNA4** (Figure 39).

Doxycycline-induced, stable Cys-P1-EGFR-eYFP CHO cells were serum starved before PNA labelling (100 nM **9** in HBSS, 4 min). **Atto565-5xImager** treatment (50 nM in HBSS-BB, 4 min) stained the membranous EGFR (Figure 39A). To ensure that the Adaptor105 strand was fully saturated with imager strands, **Cy7-DNA3** was added, and to ensure all PNA-conjugated EGFR was hybridized with **Atto565-5xImager**, cells were treated with **Cy7-5xComplex** (50 nM **Cy7-DNA4** and **Cy7-5xComplex** in HBSS-BB, 4 min). No signal was obtained in the Cy7 channel, suggesting that hybridization was largely saturated in both cases. To reverse the labelling, **EraserDNA4** (300 nM in HBSS) was applied twice for 5 min at 30 °C. This was sufficient for almost complete removal of the Atto565-DNA4 (Figure 39B) from the Adaptor105 stand. After that, Cy7-DNA3 treatment (100 nM in HBSS-BB, 3 min treatment) re-stained the unhybridized sections of the adaptor strand, proving that labelling with fluorophore-DNA could not only be erased but reinstated (Figure 39C).

A useful application of reversible labelling would be for studying membrane trafficking, by erasing signal from receptors that had not internalized. To demonstrate this, the same CHO cells were treated and labelled with **Atto565-5xImager** as described for the previous experiment and shown in Figure 39 (Figure 40A). Cells were then stimulated with 100 nM epidermal growth factor (EGF), which stimulates receptor dimerization and internalization. After 15 min confocal microscopy showed that some, but not all the EGFR had internalized (Figure 40B). Surface accessible Atto565 was removed by treatment with **EraserDNA4** (2 x 5 min in HBSS) to reveal only the internalized EGFR vesicles in the Atto565 channel (Figure 40B). Contrary to the YFP signal, only EGFR was internalized during the defined time frame was observed in the Atto565 channel. Moreover, internalized vesicles could be distinguished from surface accessible vesicles

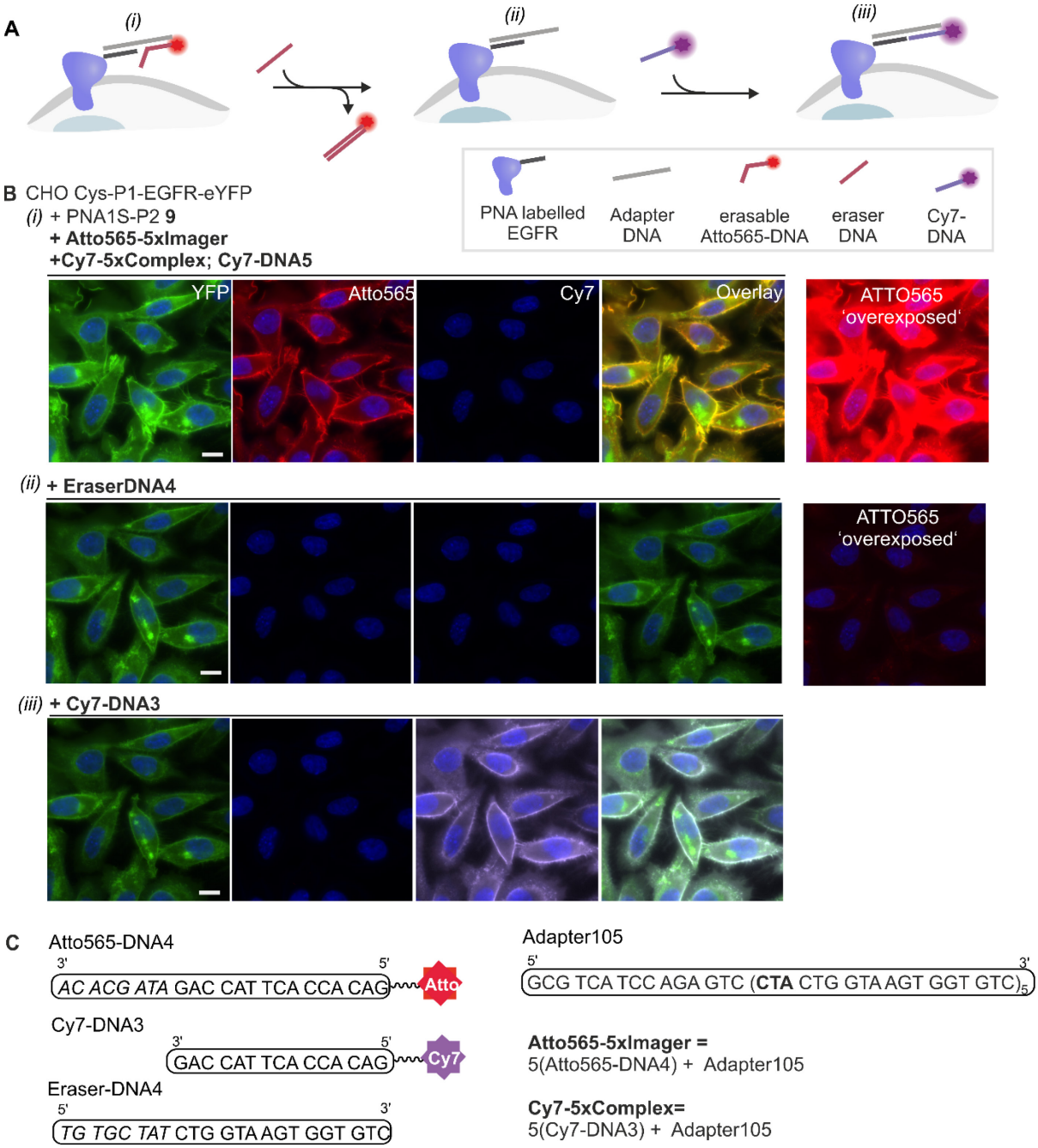

Figure 38 TMSD applied to live-cell labelling A) Schematic of live-cell labelling experiment shown in B (i) PNA labelled EGFR hybridised with Atto565-DNA imager strands via an adapter DNA (ii) treatment with an 'eraser DNA' complementary to the imager DNA displaces it via TMSD and the resultant dsDNA may be washed away. (iii) Treatment with complementary Cy7-DNA reinstates labelling. **B)** TMSD facilitated erasable labelling of Cys-P1-EGFR-eYFP on stable CHO cells. Conditions: (i) Hoechst 33342 staining in HBSS-BB, PNA labelling (100 nM **9** in HBSS, 4 min) then hybridization of **Atto565-5xImager** (100 nM in HBSS-BB, 4 min) before incubation with **Cy7-5xComplex** and **Cy7-DNA4** (50 nM, 4 min in HBSS-BB) to ensure saturation of hybridisation sites. (ii) Treatment with **EraserDNA4** (300 nM in HBSS-BB, 2 x 5 min, 30°C) removes membrane labelling. Brightness of Atto565 images in row (i) and (ii) were digitally increased to give 'overexposed' images which illustrate that Atto565 labelling was completely removed. (iii) Hybridisation of **Cy7-DNA3** (100 nM, 3 min) restores fluorescent labelling. Scale Bars = 10 µm. Excitation times: YFP: 150 ms; Atto565: 150 ms, Cy7: 500 ms. Experiment was repeated three times with similar results. **C)** Imager, adapter, and eraser DNAs used for experiment shown in B.

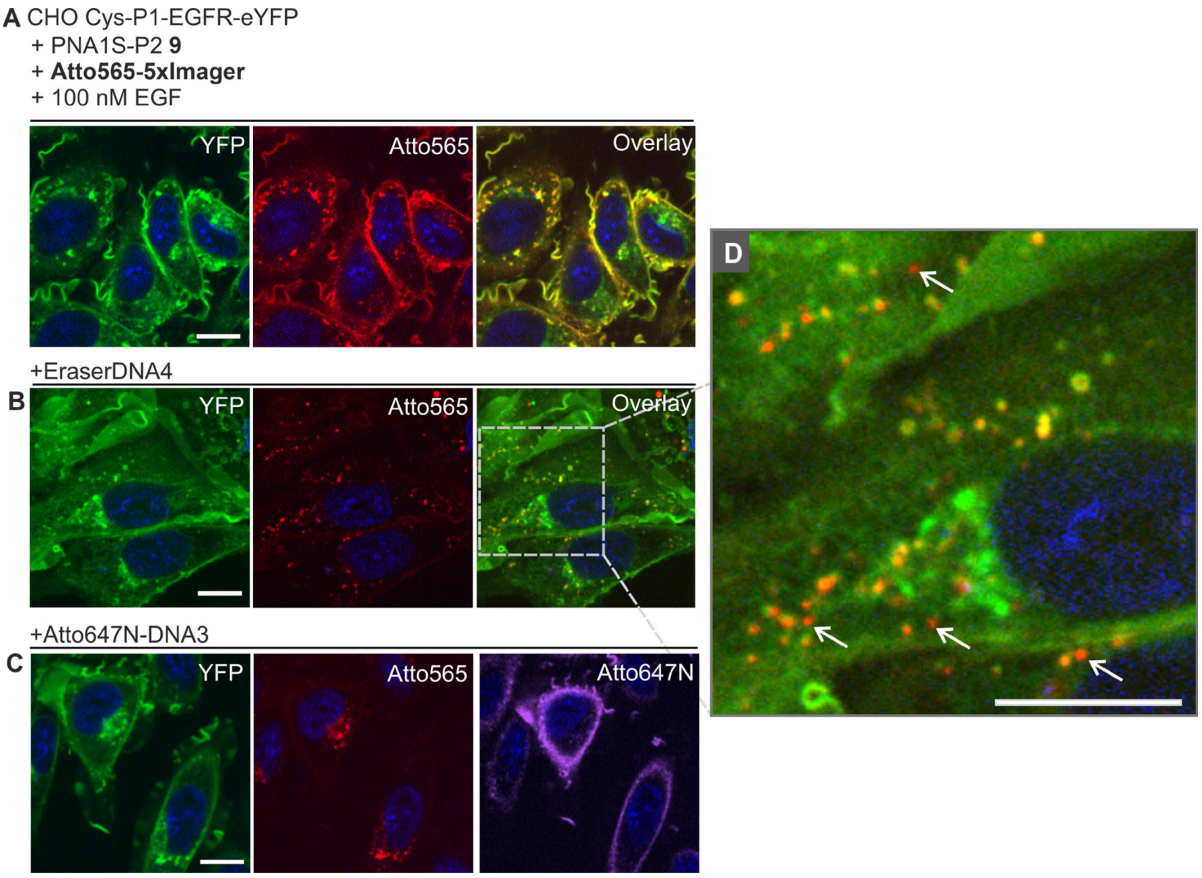

Figure 39 Confocal microscopy analysis of EGF stimulated EGFR with reversible labelling facilitated by DNA hybridization. A) Hoechst 33342 staining in HBSS-BB, PNA labelling (100 nM **9** in HBSS, 4 min) then hybridization of **Atto565-5xImager** (100 nM in HBSS-BB, 4 min). EGF treatment (15 min, 100 nM) **B)** TMSD displacement of Atto565-DNA4 with **EraserDNA4** (300 nM in HBSS-BB, 30°C) for 10 min and 1x wash. **C)** Hybridisation of **Atto647N-DNA3** (100 nM, 3 min) restores staining to surface PNA-labelled EGFR. **D)** Zoomed in overlay picture from B. Arrows highlight newly internalized vesicles, which are difficult to identify in the YFP channel. Scale bar= 10 µm. All experiments were repeated 3 times independently with similar results. Atto647N-DNA3= Atto647N-GAC ACC ACT TCA CAG.

4.3.7. Orthogonal PNA Transfer and Label Erasure for Internalization Analysis

To show how erasable labelling could be used for quantitative analysis, a fluorescence microscopy-based internalisation assay, to concurrently analyse EGFR and ErbB2, was developed (Figure 41 A). As shown in previous experiments, EGFR responds to EGF stimulation by receptor internalisation. Unlike EGFR, ErbB2 is known to be resistant to intracellular accumulation after EGFR stimulation. Both EGFR and ErbB2 will, however, internalise and be degraded in lysosomes in response to treatment with geldanamycin (GA). [230] GA is a heat shock protein 90 (Hsp90) inhibitor known to induce ubiquitinylation-mediated degradation of EGFR and ErbB2 by disrupting the growth factor receptor-Hsp90 interaction. [231] The internalisation assay would therefore compare the treatment of EGF and GA in cells expressing both EGFR and ErbB2. As

previously discussed, classical ligand-based internalisation assays are not suitable for the orphan receptor HER2, so internalisation of HER2 had to be measured using antibodies, [230] affibodies[210] or HALO tags[105] to circumvent this problem.

For the analysis, two new erasable imaging complexes were created, both designed to work independently with no cross hybridization. This time, new 60/59 nt long adaptor strands were designed (Adaptor60 and Adaptor59) to each carry 2 imager strands by hybridization with a complementary 22/21-mer portion. The imager strands still had an 8-mer toehold, but the longer overall length of 29/30 would ensure hybridization was maintained at 37°C and low concentration. For EGFR, an Atto565 imaging strand was used (Atto565-DNA5) and for ErbB2, the dye DY751 (DY751-DNA6), a similarly emitting but a more photostable analogue of Cy7. The complexes were named **Atto565-2xImager** for EGFR labelling and **DY751-2xImager** for ErbB2, respectively. **EraserDNA5** and **Eraser DNA6** were the corresponding eraser DNAs (Figure 41D).

CHO cells, expressing both Cys-P1-EGFR-eYFP and Cys-P3-ErbB2-eCFP following induction with doxycycline, were PNA-labelled with **10** and **11** (100 nM each in DPBS, 37°C) then stained with **Atto565-2xImager** and **DY751-2xImager** (200 nM in HBSS-BB, 4 min, RT). After staining with the DNA complexes, cells were incubated with either EGF (100 nM), GA (3 μM) or just serum free media. After 20 min in a cell culture incubator at 37°C, **EraserDNA5** and **EraserDNA6** (1 μM) were added for 4 min before replacing the medium with fresh eraser DNA in HBSS-BB for another 4 min. After a HBSS-BB wash, the cells were imaged by four-colour fluorescence microscopy in channels corresponding to the two imager DNAs along with YFP and CFP for controls. A control experiment was also carried out, where no PNA-donors were added in the PNA labelling step, as a measure of 'background'- where DNA had non-specifically interacted or internalised (Figure 41B; Appendix Figure 6 for CFP and YFP channels). The images were first segmented in the YFP channel, to facilitate picking individual cells as individual regions of interest (ROI) for analysis (Appendix Figure 7). After surface erasure, any remaining Atto565 or DY751 fluorescent signal in the ROI cellular regions would be owing to internalization. The average fluorescence intensity minus the average background signal (no PNA control) was therefore taken as a direct read-out of internalization, and this was normalized to the lowest value (Figure 41C).

The findings showed that with 20 min EGF stimulation, internalisation of EGFR had increased over basal levels (1.5x), whereas ErbB2 internalisation was insignificant. The

lack of EGF stimulated ErbB2 internalisation was expected but internalisation of EGFR seemed modest.

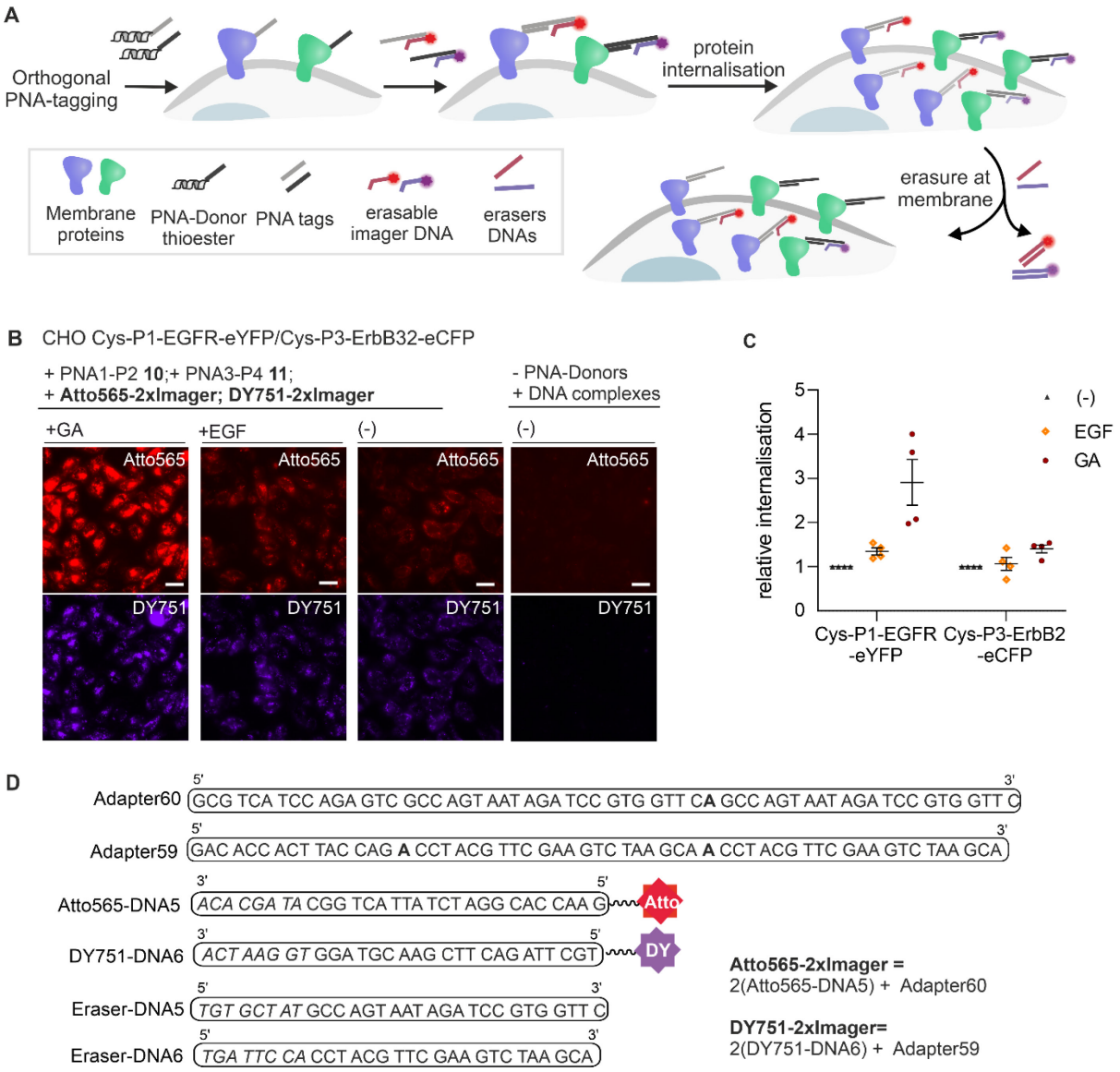

Figure 40 Assay for concurrent quantitative analysis of receptor internalisation of EGFR and ErbB2. A) Schematic of internalisation assay using erasable DNA imager strands **B)** Representative fluorescent microscopy images used for calculating receptor internalisation. Conditions: Cys-P1-EGFR-eYFP/Cys-P3-ErbB2-eCFP CHO cells induced with 0.035 µg/ml doxycycline for 20 h and starved for 4 h in 0% FBS media. PNA labelling (100 nM **10**, **11** in DPBS, 4 min) then hybridization of **Atto565-2xImager** and **DY751-2xImager** (200 nM in HBSS-BB, 4 min). Treatment with EGF (100 nM), geldanamycin (GA, 3 µM) or serum free media for 20 min followed by **EraserDNA5** and **EraserDNA6** (1 µM, 2 x 4 min). Two fluorescence microscopy images were taken for each condition for analysis. Excitation times: Atto565/Cy7: 600 ms. Scale bar = 30 µm. **C)** Relative internalisation of EGFR and ErbB2 calculated from microscopy images. An average RFU of individual cells was calculated for the Atto565/DY751 channels before background subtraction of a negative control where PNA-donor treatment was omitted. The resultant RFU was normalised to the control without EGF/GA treatment. conditions. For each replicate n = 100 cells from were counted. Scatter plots show mean with SEM **D)** DNA adaptors, imagers, erasers, and complexes used for receptor internalisation assay.

This may be explained in part by the high basal internalisation which, whilst somewhat optimised in this experiment,*** was observed under conditions of extreme starvation or stress, and has been reported in literature. [232,233] In this experiment, the negative control, where PNA-tagged cells stained with imager DNA were treated with media only, showed significant intracellular signal even without stimulation.

Another point to consider is that ErbB2 is known to impair EGF-stimulated EGFR endocytosis through preferential formation of heterodimers which are internalization deficient. [234] This may have reduced EGF internalization, as the level of ErbB2 in the cells line used in this work was artificially high.

GA-induced internalisation gave a much stronger response from both receptors, with a 2.9-fold increase for EGFR and 1.4-fold increase for ErbB2 compared to treatment with serum free media only. This finding was puzzling, as ErbB2 is reported more sensitive to GA induced downregulation than EGFR. However, these observations were based on the whole population of EGFR over hours by Western blot, rather than internalisation of a 'snapshot' surface population after 20 mins. [235] Another study showed that after only 1 h of GA stimulation, EGFR and HER2 internalisation were shown to be only moderately affected. [235] Our results do not completely correlate with literature, but the general outcome is consistent. This may be due to the measurement distinct cell populations within the independent studies. Different proteomes may lead to varying levels of basal signalling and internalisation, for instance, and this outcome highlights the importance for developing a variety of tools with different temporal and spatial controls. Methods which use fluorophore-labelled ligands do not consider basally internalised receptor, nor do antibody-based assays take into account receptor molecules that have degraded in the time frame of the experiment. Interestingly, these experiments also highlighted the surprising amount of basal internalisation of both EGFR and ErbB2 during the timeframe of the experiment.

Equally, this method should be optimized. A first improvement would be to use flow cytometry for analysis, rather than microscopy. This was not feasible at the time of the experiment as it would have required two laser/filter blocks orthogonal to each other and not in the range of the YFP/CFP channels, which were not available. Flow

*** High basal internalisation characteristic of stress-induced internalisation, i.e., very large vesicles, was observed after incubation of higher concentrations of doxycycline (possibly due to stress from high EGFR/ErbB2 expression and amplified cell replication, or from doxycycline itself); in the case of over-exposure to an oxidative atmosphere (observed via pH indicated in media); and after long starvation times.

cytometry measurements have the advantage of no background from microscopy plates, significantly higher throughput and much larger populations measured. Another point to consider is if the fluorophores themselves affect the results. For this, the same experiment could be repeated with the fluorophores exchanged, and consistency of the results verified.

5. Summary and Outlook

Live-cell post-translational conjugation techniques provide a means to link a reporter group to a protein of interest and thereby carry out functional studies. Though dozens of methods exist, which have provided valuable insights into the roles of proteins individually and within networks, [56,83] some aspects remain problematic; one being the simultaneous labelling of multiple targets, [9] the other the live-cell conjugation of proteins with DNA. [15] As DNA barcoding technologies become more advanced, the need for useful multiplexed nucleic acid conjugation methods is evident. At the same time, coiled-coil tag–probe labelling has shown to be suitable for protein membrane labelling methods both non-covalently[62,175] and covalently. [70,154] Through de novo programming, orthogonal coiled-coil sets (Figure 42) have been designed and used to target and control proteins in complex cell environments. [149] The potential for their use in multiplexed, covalent labelling is apparent, but before now, not exploited. This work described a technique which accomplished multiplexed labelling of surface proteins with distinct peptide nucleic acid barcodes using coiled coil peptide templates, whilst also maintaining qualities generally advantageous in labelling methods, namely, rapid conjugation, quantitative conversion, and modularity.

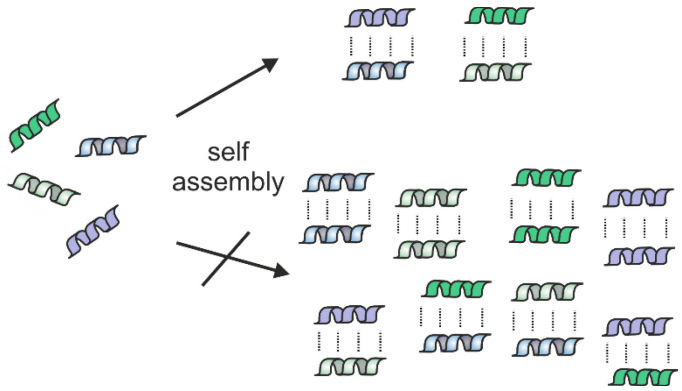

Figure 41 A set of orthogonal-coil peptides will self-assemble predictably, the peptides interacting only with the complementary 'matching' peptide (blue:light blue and green:light green). No self-interactions, or interaction between nonmatching peptides will occur.

For the acyl-transfer labelling reaction, PNA-donor thioesters designed with orthogonal coiled-coil peptides P2 and P4[119] were synthesized. A synthetic route was devised completely on the resin, resulting in easily purified final products. PNA 15-mers synthesised by SPPS were modified with a cyclooctyne (ALO), before strain-promoted

azide-alkyne cycloadditions were carried out with the purified azido-donor peptides. It was discovered that an important strategy in the design of these PNA-donor thioesters was to include charged amino acid residues on the PNA strand. This was shown to be advantageous to the efficiency of the final thioester probe, likely due to decreased hydrophobicity of the PNA part.

Test reactions between PNA-donor thioesters and synthetic Cys-acceptor peptides in buffer were analysed for speed, yield, side reactions and cross-reactivity. The orthogonal coiled coils P1/P2 and P3/P4 were used as acceptor–donor pairs for the acyl transfer reaction. In single reactions, transfer reactions of 15-mer PNAs were found to be rapid, with over 80% of the acceptor peptides carrying a PNA tag after only 10 s, making the method suitable for applications that require extremely fast labelling. Moreover, by using just 6 equivalents excess of the PNA-donor thioesters, quantitative labelling could be achieved in only one minute. Cross-reactivity between the two coiled-coil sets was also tested. Reactions with mismatched peptides would result in no change to the Cys-acceptor peptides, confirming specificity of the coiled-coil-templated reactions. A one-pot reaction was also carried out, which proceeded identically to the individual transfers, rendering the two systems suitable for simultaneous, quantitative PNA labelling of two distinct peptide targets.

During studies of the acyl transfer reaction, a potential downside was observed. When quantitative labelling was achieved, most of the acceptor peptide was doubly acylated with two PNA strands, i.e., another equivalence of the thioester had reacted with the desired product. This was unavoidable, since it was observed the there was a preference of the thioester to react with the desired product (PNA-Cys-acceptor), rather than the Cys-acceptor peptide itself (Figure 43A). This preference was hypothesised to be due to a hierarchy of coiled-coil-pair affinities between the different reaction species (Figure 43B), which could potentially lead to inhibition of the preferred reaction by sequestering the Cys-acceptor peptide in a ‘non-productive’ coiled-coil. Further experiments could shed light on this, such as K_d measurements of the various acceptor–donor species shown in Figure 43B, or by spiking the reaction with coil peptides predicted to inhibit the reaction, i.e., the HS-donor side product or doubly-acylated acceptor peptide. These experiments would further the understanding of the reaction and could potentially lead to a solution for mitigating the unwanted reaction. In this case, possible solutions could include a redesign of the labelling reagents, to destabilise/stabilise certain coiled coils within the reaction; altering of reaction conditions to favour the reaction over coiled-

coil strand displacement; or spiking the reaction with a coil peptide to favour the intended coiled-coil interactions.

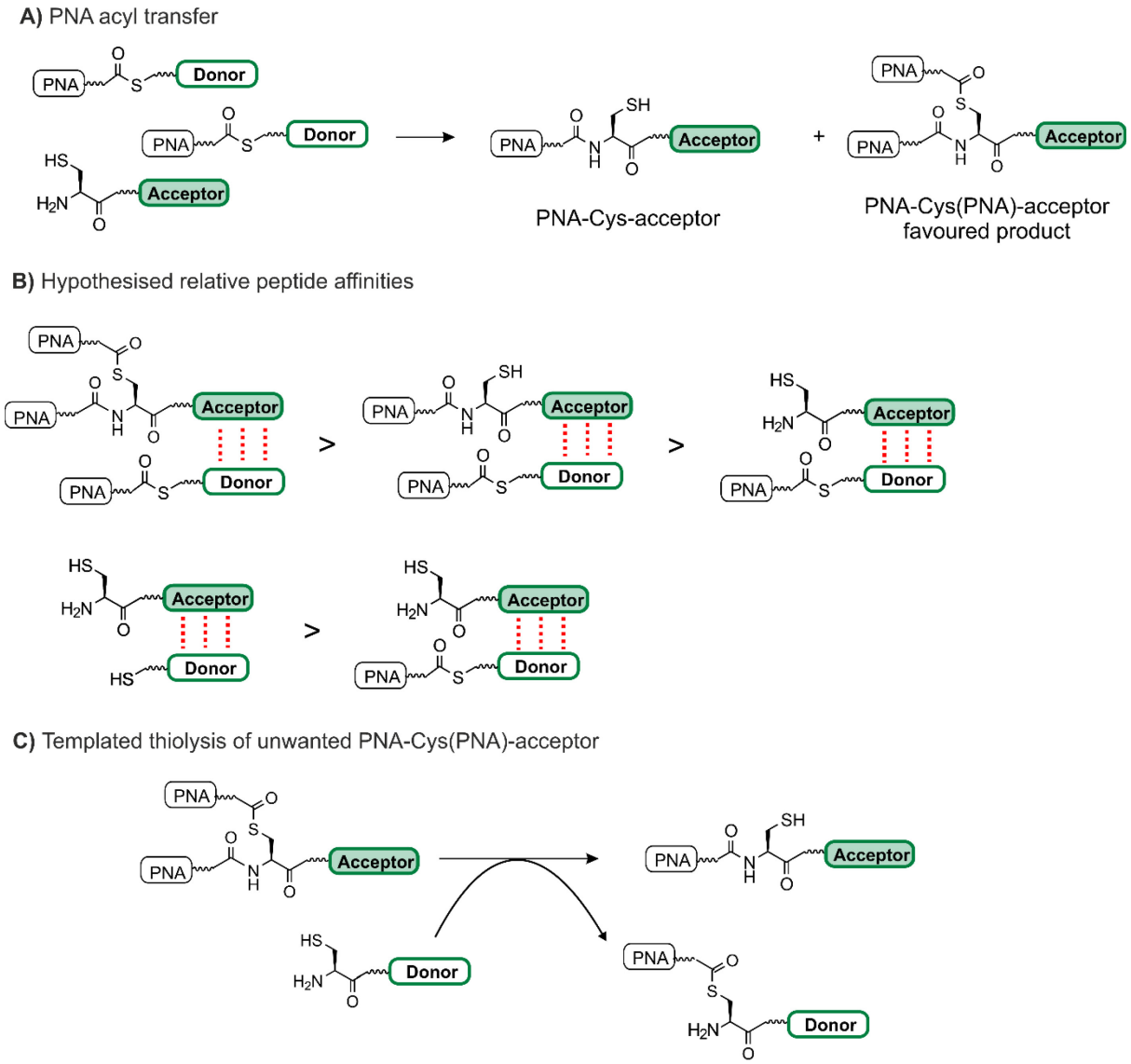

Figure 42 Doubly-acylated transfer product A) Products of acyl transfer; through experimentation it was found that the doubly (*S*- and *N*-)acylated product was favoured over the *N*-acylated product. **B)** Predicted hierarchy of coiled coil affinities. **C)** Templated reaction which would reform the wanted *N*-acylated product from the unwanted doubly-acylated product.

To gain an understanding of the stability of this unwanted doubly-acylated product, experiments were carried out on an analogous test peptide. Based on observed stabilities of this peptide toward the water-soluble thiol MESNA, it is likely that the species has a half-life in the magnitude of minutes during live-cell studies, and longer if the PNA-tagged receptor remains extracellular; however, to confirm this, further stability experiments would be required using cell lysates. Degradation of the thioester, releasing PNA strands and the hybridized DNA, may be unsuitable for some experiments. It was

shown that, if required, this unwanted second thioester-linked PNA strand could be removed in a second acyl-transfer reaction in only minutes, whereupon, in a live-cell setting, it could be simply washed away (Figure 42C).

Live-cell experiments showed that hybridization of fluorophore-DNA conjugates enabled visualization of the labelled proteins via fluorescence microscopy. The specificity of the labelling method, both the PNA transfer and the DNA hybridization steps, were verified on recombinantly expressed Cys-P1-EGFR-eYFP and Cys-P3-ErbB2-eCFP surface receptor constructs, expressed stably in cell lines created by Michael Bartoschek. The staining was specific and showed no cross-reactivity, an accomplishment which is not straightforward for live-cell labelling methods. Moreover, the tagging of both receptors was carried out in one step, meaning that the two receptors were conjugated in only a few minutes under mild conditions. In this work, two orthogonal coiled-coil sets were used for dual labelling; as previously remarked, larger sets do exist, and applying these to the methodology could allow specific labelling of even more targets.

Other aspects of the method were validated in live-cell experiments. In collaboration with Philipp Wolf, fluorescence microscopy of a GPCR construct Cys-P1-ET_BR-GFPspark was carried out, showing that the method works on different receptor types. To date, three different coiled-coil sets (E3/K3, P1/P2, P3/P4) have been utilized for live-cell PNA transfer, suggesting that the method is widely applicable. Furthermore, an immunofluorescence assay showed that the PNA tag did not significantly affect phosphorylation of Cys-P1-EGFR-eYFP and expression of the Cys-P1 fusion tag has been shown not to effect ET_B receptor activity. [185] Likewise, ET_AR and ET_BR (endothelin receptor A and B) constructs expressing Cys-P1 and Cys-P3 tags were shown by Wolf et al to have unchanged Ca^{2+} flux activity compared to the wildtype proteins, even after conjugation of organic fluorophores to the peptides. [236] It is therefore likely that the methodology is largely non-perturbing, especially in comparison with larger fusion proteins. However, analysis of further downstream signalling should be carried on PNA tagged, DNA hybridized receptors, to further substantiate this.

The notable feature of the presented method was the straightforward, specific, one-step conjugation of oligonucleotides to target proteins in a live-cell setting. To demonstrate the advantages of an oligonucleotide tag itself, hybridization of multiple fluorophore-DNAs and erasable fluorophore-DNAs was carried out (Figure 44). Multiple fluorophores recruited to single receptors resulted in a brightness gain, an advantage in

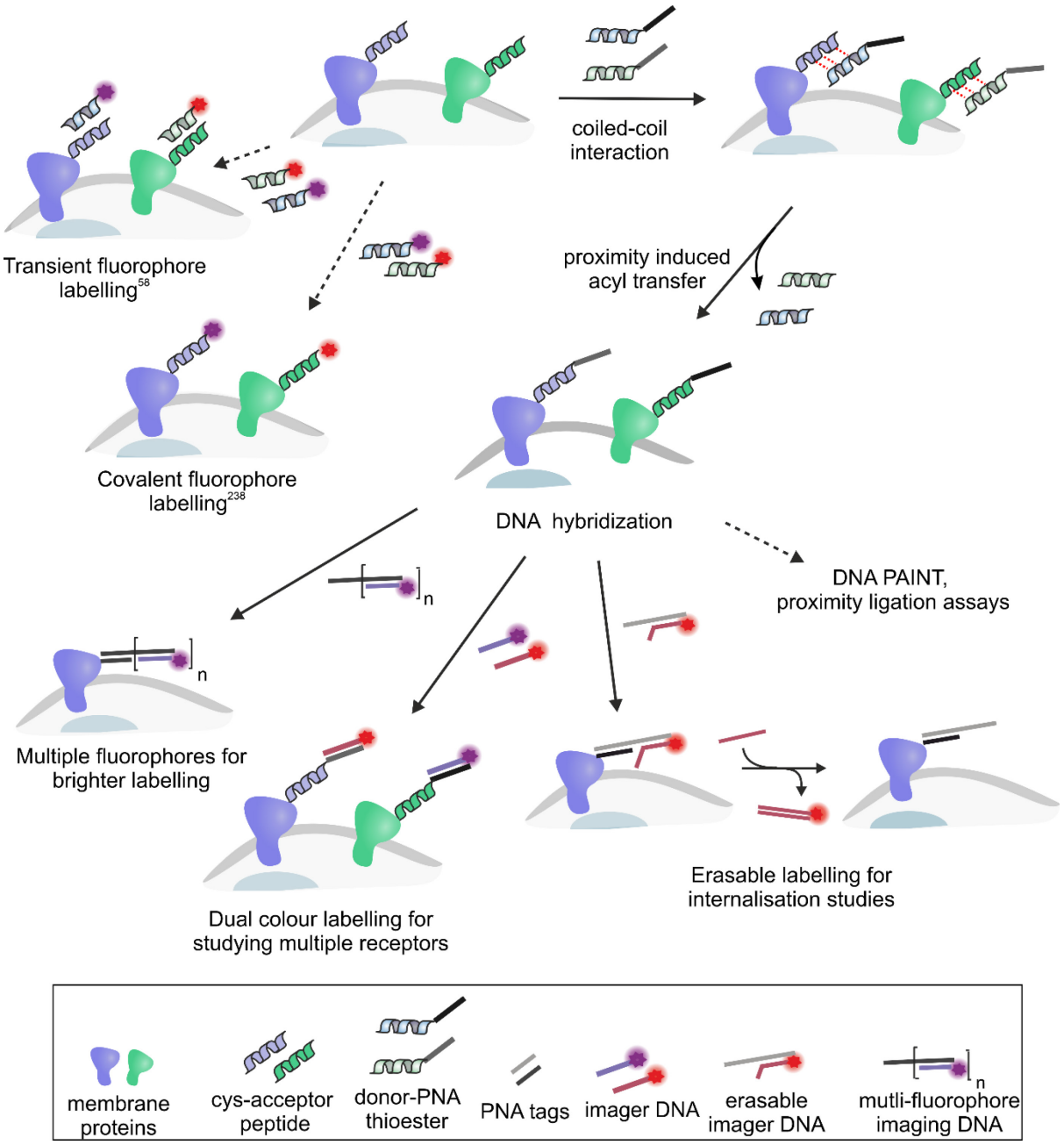

Figure 43 Live-cell experiments enabled by coiled-coil peptides. Block arrows show experiments carried out in this work. Dotted arrows represent potential experiments. These include: super resolution peptide-PAINT[59] using transient coiled coil interactions; FRET experiments enabled by covalent coiled coil templated labelling; [236] labelling methods based on DNA hybridisation.

experiments where the brightness of the label is limiting. Furthermore, the observation that addition of multiple fluorophores led to a linear increase in fluorescence was encouraging, implying that upscaling the method for super-bright labelling with many more fluorophore-DNA strands is feasible. Erasable labelling provided the opportunity for more complex, time-resolved receptor studies and the technology of toehold-mediated strand displacement was used to this effect. By removing surface hybridized fluorophore-DNA after receptor internalization, only internalized receptor remained

stained. This eliminated unwanted background signal and could be useful for quantification of internalization. In an exemplary, quantitative fluorescence microscopy-based assay, internalization of Cys-P1-EGFR-eYFP and Cys-P3-ErbB2-eCFP were simultaneously measured with a simple fluorescence readout, precluding the need for complex and time-consuming antibody assays. [230]

Importantly, these experiments showed two very simple strategies employed in DNA technology: hybridisation of multiple DNA strands by way of adaptors, and the process of toehold mediated strand displacement. The simple technique of TMSD is an integral one in DNA technology for the workings of such things as logic gates[227] and nanomachines, [237] and this was successfully carried out an adaptor-DNA directly hybridised to a PNA tag. The use of oligonucleotides as handles for DNA technologies is not new. DNA-conjugated antibodies are often used as a biochemical tool, e.g., for proximity ligation assays. [108] Though SNAP tag-labelled receptors conjugated with BG-oligos have been used for covalent installation of DNA, [17] the large fusion tag may impede certain applications, or downstream signalling. The only other reported method of this kind is from the Gordon lab, [16] and also suffers from large HUH-fusions and non-quantitative reactions.

Given the growing attention on coiled coils for tag–probe labelling, [63,125,203] the presented method is a valuable addition to this coiled-coil-labelling toolbox. Once the Cys-acceptor peptide tag is expressed with a target protein, the technique could be integrated with others that employ coiled-coil (covalent or transient) labelling (Figure 44). For instance, peptide-PAINT, [59] a super resolution imaging method using transient coiled coil interactions, could be used to deliver super resolution imaging of the target after PNA labelled studies have been performed. In recent work from the Beck-Sickinger group in collaboration with the Seitz group, [236] Wolf et al. showed that similar coiled-coil acyl transfers using the P1/P2 and P3/P4 peptides could be use to specifically label surface receptors with synthetic fluorophores. Using this labelling system and FRET methods, they could define the distribution and proximity of different interacting GPCR pairs. It would be straightforward to switch between this method and PNA labelling, taking advantage of both methods, and even to carry out multiparameter experiments.

In summary, this thesis detailed the development of a live-cell labelling reaction, and an important new opportunity to bring DNA nanotechnology to proteins in a live-cell setting. The labelling reaction covalently joins an oligonucleotide to the target protein

in a specific, rapid manner, and is easily applicable to different receptors. Furthermore, the coiled-coil templated reaction makes available multiplexed labelling by way of orthogonal coiled-coil sets. Thought this work showed that the method itself has many advantages, it also outlined the potential for combining with other coiled-coil-based methods, applying different DNA nanotechnologies, and widening the scope of multiplexing to a greater number of receptors.

6. Experimental

6.1. Materials and Reagents

6.1.1. Materials and Reagents for Templated Reactions and Synthesis

All solutions expressed as % refer to % v/v.

Micro reaction vessels and microcentrifuge tubes were ordered from *Sarstedt* (Nümbrecht, Germany). Polystyrene UPLC inserts were ordered from *Sigma-Aldrich* (Ward Hill, MA, USA)

The following building blocks were prepared as previously described: ALO (2-(cyclooct-2-yn-1-yloxy)acetic acid), [238] *S*-Mmt-protected 4-mercaptophenyl acetic. [190]

Ultrapure water was prepared using an Astacus system (*membraPure*, Henningsdorf, Germany).

Reagents were purchased from the following vendors:

Ac-Gly-OH	*Bachem* (Bubendorf, Switzerland)
Acetic anhydride, 99%	*abcr* (Karlsruhe, Germany)
Acetonitrile, >99% HPLC grade	*VWR* (Darmstadt, Germany)
Boc-Cys(Mmt)-OH	*Iris Biotech* (Marktredwitz, Germany)
CHAPS, >98%	*Alfa Aesar* (Ward Hill, MA, USA)
ChemMatrix® RAM resin	*Sigma-Aldrich* (St. Louis, USA)
Coupling reagents	
DIC, DCC, HCTU, HATU, PyBroP	*Carbolution* (St. Ingbert, Germany)
Coumarin343	*TCI* (Eschborn, Germany)
DIPEA, ≥99 %,	*Carl Roth* (Karlsruhe, Germany)
Dithiothreitol	*Iris Biotech* (Marktredwitz, Germany)
DMF, low in water (<150 ppm)	*VWR* (Radnor, Pa, USA)
Fmoc-protected amino acids (standard)	*Carbolution* (St. Ingbert, Germany)
Fmoc-6-amionohexanoic acid	*Iris Biotech* (Marktredwitz, Germany)
2-[2-(Fmoc-amino)ethoxy]ethoxy]acetic acid	*Iris Biotech* (Marktredwitz, Germany)
Fmoc-L-Lys(Mmt)-OH	*Iris Biotech* (Marktredwitz, Germany)
Fmoc-protected PNA monomers	*LGC Genomics* (Teddington, UK)

N-Methylmorpholine	*Alfa Aesar* (Ward Hill, MA, USA)
OxymaPure, ≤100 %	*Carbolutions* (Saarbrücken, Germany)
Piperidine, ≥99.5 %	*Carl Roth* (Karlsruhe, Germany)
TAMRA	*ChemPep Inc.* (Wellington, USA)
TentaGel®RAM Resin	*RAPP Polymers* (Tübingen, Germany)
Trifluoroacetic acid, ≥99.9 %	*Carl Roth* (Karlsruhe, Germany)
Triisopropylsilane, 98 %	*Sigma-Aldrich* (St. Louis, MO, USA)
Tris-(2-carboxyethyl)-phosphine·HCl	*Carl Roth* (Karlsruhe, Germany)

6.1.2. Materials and reagents for cell culture and cellular experiments

All solutions expressed as % refer to % v/v.

8-well sterilized µ-slides (ibiTreat: tissue culture treated) were acquired from *ibidi GmbH* (Gräfelfing, Germany).

Black Opaque 96-well Microplates Sterile and Tissue Culture Treated (CulturePlate-96) were purchased from *PerkinElmer LAS (Germany) GmbH.* (Rodgau, Germany)

Cellstar® 250 ml, 75 cm^2 Cell culture flasks were purchased from *Greiner Bio-One* (Kremsmünster, Austria).

Reagents were purchased from the following vendors:

Antibiotics	
Doxycycline, Penicillin-Streptomycin (10.000 U/ml)	*Thermo Fisher Scientific* (Waltham, MA, US)
Puromycin dihydrochloride	*Thermo Fisher Scientific* (Waltham, MA, US)
Bovine serum albumin (BSA), fraction V	*Carl Roth* (Karlsruhe, Germany)
DMEM (4.5 g/L glucose)	*Lonza Group Ltd.* (Basel, Switzerland)
DPBS (Ca, Mg, Product N°:14040*)*	*Thermo Fisher Scientific* (Waltham, MA, US)
ET-1	*Bachem* (Bubendorf, Switzerland
Fetal Bovine Serum (FBS) superior	*Sigma-Aldrich Chemie GmbH* (Taufkirchen, Germany)
Ham's F12 Nutrient mixture Ham (**N6658)**	*Sigma-Aldrich Chemie GmbH* (Taufkirchen, Germany)
HBSS (+Ca, +Mg, 14025092)	*Thermo Fisher Scientific* (Waltham, MA, US)

Hoechst 33342 (trichloride trihydrate, 10 mg/ml)	*Thermo Fisher Scientific* (Waltham, MA, US)
L-Glutamine 200 mM	*Thermo Fisher Scientific* (Waltham, MA, US)
Lipofectamine™ 2000	*Invitrogen* (Carlsbad, CA, USA)
Lipofectamine™ 3000	*Invitrogen* (Carlsbad, CA, USA)
NCL	*VWR* (Radnor, Pa, USA)
Normal goat serum (**31872)**	*Thermo Fisher Scientific* (Waltham, MA, US)
OptiMEM	*Thermo Fisher Scientific* (Waltham, MA, US)
PBS (18912014)	*Thermo Fisher Scientific* (Waltham, MA, US)
Poly-D-Lysine (0.1 mg/ml)	*Thermo Fisher Scientific* (Waltham, MA, US)
ProLong™ Live Antifade Reagent	*Thermo Fisher Scientific* (Waltham, MA, US**)**
Salmon Sperm DNA	*Carl Roth* (Karlsruhe, Germany)
Di-Sodium hydrogen phosphate anhydrous	*Merk* (Darmstadt, Germany)
Sodium dihydrogen phosphate dihydrate	*Merk* (Darmstadt, Germany)
Tris-HCl	*Thermo Fisher Scientific* (Waltham, MA, US)
Triton™ X-100	*Carl Roth* (Karlsruhe, Germany)
Trypsin-EDTA, 0.25 % (w/v)	*Thermo Fisher Scientific* (Waltham, MA, US)
Paraformaldehyde, 16% (w/v), methanol free	*Alfa Aesar* (Ward Hill, MA, USA)

Phospho-EGF Receptor (Tyr1068) ((D7A5), XP® Rabbit mAb #3777 Lot: TB264033) was purchased from *Cell Signalling* and used in an 800x dilution.

Goat anti-Rabbit IgG (H+L) Highly Cross-Adsorbed Secondary Antibody, Alexa Fluor Plus 647 (catalogue number A32733, Lot:10) was purchased from *Thermo Fisher Scientific* (Waltham, MA, US).

6.1.3. DNA and PNA Sequences, DNA complexes

Table 3 PNA sequences used.

PNA Name	**Sequence (N-C)**
PNA1H	gac tct gga tga cgc
PNA1S	Asp Asp Arg gac tct gga tga cgc Arg
PNA1	Asp Lys Asp gac tct gga tga cgc Arg Lys
PNA3	Asp Lys Asp ctg gta agt ggt gtc Arg Lys

Table 4 Modified and unmodified DNA oligonucleotides used in cellular experiments. All were ordered from Biomers.net (Ulm, Germany) with HPLC purification. Residues in bold remain unpaired after hybridisation. Toeholds and regions complementary to toeholds are in italics.

DNA name	**Purpose [hybridized with]**	**Sequence (5'-3')**
DNA1	Immunofluorescence assay [PNA1]	GCG TCA TCC AGA GTC
Atto565-DNA1	Imaging EGFR [PNA1]	ATTO565-GCG TCA TCC AGA GTC
Cy7-DNA3	Imaging ErbB2/EGFR [PNA3, Adaptor33/105]	Cy7- GAC ACC ACT TAC CAG
Atto647N-DNA3	Flow Cytometry EGFR [Adaptor105]	Atto647N- GAC ACC ACT TAC CAG
Atto565-DNA4	Erasable imaging EGFR [Adaptor105, Eraser4]	ATTO565- GAC ACC ACT TAC CAG *ATA GCA CA*
Atto565-DNA5	Erasable imaging EGFR [Adaptor60, Eraser5]	Atto565- GAA CCA CGG ATC TAT TAC TGG C *AT AGC ACA*
DY751-DNA6	Erasable imaging ErbB2 [Adaptor59, Eraser6]	DY751-TGC TTA GAC TTC GAA CGT AGG *TGG AAT CA*
Adapter33	Imaging EGFR [PNA1, DNA3]	GCG TCA TCC AGA GTC **CTA** CTG GTA AGT GGT GTC
Adapter105	Imaging EGFR [PNA1, DNA3]	GCG TCA TCC AGA GTC **CTA** CTG GTA AGT GGT GTC **CTA** CTG GTA AGT GGT GTC **CTA** CTG GTA AGT GGT GTC **CTA** CTG GTA AGT GGT GTC **CTA** CTG GTA AGT GGT GTC
Adaptor60	Imaging EGFR [PNA1, DNA5]	GCG TCA TCC AGA GCC AGT AAT AGA TCC GTG GTT C **A** GCC AGT AAT AGA TCC GTG GTT C

Adaptor59	Imaging ErbB2 [PNA3, DNA6]	GAC ACC ACT TAC CAG **A** CCT ACG TTC GAA GTC TAA GCA **A** CCT ACG TTC GAA GTC TAA GCA
Eraser4	Eraser EGFR [DNA4]	*TGT GCT AT* CTG GTA AGT GGT GTC
Eraser5	Eraser EGFR [DNA5]	*TGT GCT AT* GCC AGT AAT AGA TCC GTG GTT C
Eraser6	Eraser EGFR [DNA6]	*TGA TTC CA* CCT ACG TTC GAA GTC TAA GCA

Table 5 DNA complexes used for hybridization to PNA labelled receptors. Complexes were prehybridized in HBSS to a complex concentration of 10 µM. The DNA mixture was heated to 40°C before cooling to RT.

Complex Name	**Adapter**	**Imager**	**Imager/Adapter ratio**
Cy7-1xComplex	Adapter33	Cy7-DNA3	1
Cy7-5xComplex	Adapter105	Cy7-DNA3	5
Atto647N-1xComplex	Adapter105	Atto647N-DNA3	1
Atto647N-3xComplex	Adapter105	Atto647N-DNA3	3
Atto647N-5xComplex	Adapter105	Atto647N-DNA3	5
Atto565-5xImager	Adaptor105	Atto565-DNA4	5
Atto565-2xImager	Adaptor60	Atto565-DNA5	2
DY751-2xImager	Adaptor59	DY751-DNA6	2

6.2. Instrumentation

6.2.1. Liquid Chromatography

UPLC–MS

An analytical Acquity H-Class UPLC–MS system (*Waters Corporation*, Milford, MA, USA) was equipped with a PDA photodiode array detector (λ = 210 - 400 nm; 1.2 nm resolution) and QDa mass detector to record ESI spectra in positive ion mode in the range of 300-1250 Da. An Acquity UPLC CSH C18 (2.1 x 50 mm, 1.7 µM, 130 Å) column from *Waters Corporation*, *YMC Europe* (Dinslaken, Germany) was used for RP (reverse phase) separation at 50°C at a flow rate of 0.5 ml/ min

FLR–UPLC

An analytical Acquity UPLC system (*Waters Corporation*, Milford, MA, USA) was equipped with a TUV tuneable UV-detector and a multichannel FLR fluorescence detector. An Acquity UPLC CSH C18 column (1.7 µm, 50 x 2.1 mm) from *Waters Corporation*, *YMC Europe* (Dinslaken, Germany) was used for RP separation at 50°C at the flow rate of 0.5 ml/ min.

FLR-HPLC

An analytical Elite LaChrom HPLC system (*Merck-Hitachi)* was equipped with a Hitachi LaChrom Elite DAD (Diode Array Detector) and LaChrom Elite Fluorescence detector with a Xenon lamp. A Polaris C18 column (5 µm, C18-A 100 x 4.6 mm) from *Agilent Technologies* (Santa Clara, CA, USA) was used for RP separation with a flow rate of 0.8 ml/ min at 55 °C.

Preparative HPLC

A semi-preparative 1100 Series HPLC system (*Agilent Technologies*, Santa Clara, CA, USA) was equipped with a MWD multiple wavelength detector (λ = 210 nm, 260 nm, and 280 nm). A Nucleodur Gravity C18 column (10 x 250 mm, 5 µm, 110 Å) from *Macherey-Nagel* (Düren, Germany) was used for RP separation at RT with a flow rate of 6 ml/ min, respectively.

Mobile phases used for LC systems

All mobile phases are expressed in % v/v.

A	H_2O (with 1% MeCN, 0.1% TFA)
B	MeCN (with 1% H_2O, 0.1% TFA)

C	H_2O (with 1% MeCN, 0.1% formic acid)
D	MeCN (with 1% H_2O, 0.1% formic acid)

6.2.2. Microscopes and filter sets

Fluorescence Microscopy of Cys-P1-ET$_B$R-GFPspark on HEK293 cells

Fluorescence images were taken by using a Zeiss Axio Observer.Z1 microscope with an ApoTome.2 Imaging System, a C-Apochromat 63x/1.20 W Corr M27 objective, an AxioCamMR camera and the ZEN 2.0 software in the lab of Annette Beck-Sickinger (Leipzig University) in collaboration with Philipp Wolf. Cells were imaged using different Zeiss filter sets: Hoechst33342: λ_{ex}:365, beam splitter: 395; λ_{em}:420, GFP λ_{ex}: 470/40, beam splitter: 495: λ_{em}:525/50, Atto565 λ_{ex}: 565/30; beam splitter: 585; emission: λ_{em} 620/60.

Widefield Microscopy of Cys-E3-EGFR-eYFP, Cys-P1-EGFR-eYFP and Cys-P3-ErbB2-eCFP

Cells were imaged with a widefield IX83 microscope with a 60 x lens from *Olympus*. Cells were imaged using different Olympus filter sets: Hoechst33342: λ_{ex} = 350 ± 25 nm, λ_{em} = 460 ± 25 nm; CFP: λ_{ex} =438 ± 12 nm, λ_{em} 483 ± 12 nm; YFP: λ_{ex} = 500 ± 12 nm λ_{em} 545 ± 20 nm; Atto565: λ_{ex} = 575 ± 12 nm λ_{em} 628 ± 20 nm CY7/DY751: λ_{ex} = 710 ± 37 nm, λ_{em} 810 ± 40 nm. *Olympus* CellSens software and ImageJ was used for image processing.

Spinning-Disk Confocal Microscopy of Cys-P1-EGFR-eYFP

Cells were imaged with an a Visitron VisiScope with an *Olympus* IX83 microscope and a *Yokogawa* CSU-W1 spinning disk unit in the lab of Andreas Herrmann (Humboldt University of Berlin) under supervision of Thomas Korte. Confocal imaging: Diode lasers: Hoechst 33342: 405 nm; YFP: 488 nm; Atto565: 561 nm; Atto647N: 640 nm. Dichroic emission filters Hoechst 33342: λ_{em} = 460 ± 50 nm; YFP: λ_{em} 470 ± 24 nm; Atto565: λ_{em} 600 ± 50 nm. Atto647N: λ_{em} = 700 ± 75 nm. *Olympus* CellSens software was used for image processing.

6.2.3. Flow Cytometry

Flow cytometry was performed on a BD Accuri™ C6 ™ *(Beckton-Dickinson*, Franklin Lakes, NJ, USA) in the lab of Knut Rurak (Bundesanstalt für Materialforschung und Prüfung, Berlin) with blue (YFP: 488 nm) and red (Atto647N: 640 nm) laser and mirror/filters pairs. Emission filters: YFP: 533/30 nm; Atto647N: 675/25 nm. A flow rate of 66 µL/ min for 150 or 260 µL was used. Data was analyzed using BD CFlow Plus V1.0.227.4 (BD Biosciences).

6.2.4. Plate Reader

Fluorescence measurements in assay microplates were conducted on a Victor X5 Multilabel plate reader (*PerkinElmer*, Waltham, MA, USA), equipped with filters: YFP: λ_{ex} = 420±15, λ_{em} = 532±10 nm. AF647: λ_{ex} = 665±10 nm λ_{em} = 640±10 nm.

6.2.5. UV/VIS

Peptide/PNA/DNA concentration was determined by measuring the absorbance at 260 nm (PNA/DNA), 280 nm (peptides) on a NanoDrop ND-1000 (*PeqLab*, Erlangen, Germany) spectrophotometer against a 0.1% CHAPs water/buffer blank.

For PNA oligomers, the molar extinction coefficients at 260 nm were calculated from respective monomer extinction coefficients: ε_{260}(a) = 13 700 $M^{-1}\cdot cm^{-1}$, ε_{260}(c) = 6 600 $M^{-1}\cdot cm^{-1}$, ε_{260}(g) = 11 700 $M^{-1}\cdot cm^{-1}$, ε_{260}(t) = 8 800 $M^{-1}\cdot cm^{-1}$) using the PNA tool from *PNA Bio.* [239]

DNA molar extinction coefficients were calculated with OligoAnalyzer tool[240] by the nearest neighbour method, or for fluorescent DNA, using the value stated by the supplier.

For fluorescent peptides, extinction coefficients of the chromophore at max wavelength absorption were used as provided by the supplier. The following were used: ε_{478}(Dabcyl) = 3200 $M^{-1}\cdot cm^{-1}$, ε_{556}(TAMRA) = 95000 $M^{-1}\cdot cm^{-1}$ ε_{437}(C343) = 44000 $M^{-1}\cdot cm^{-1}$ ε_{564}(Atto565) = 120000 $M^{-1}\cdot cm^{-1}$

Peptides with no fluorophore, but with a tyrosine were measured at 260 nm using the sum of extinction coefficients: ε_{260}(MPAA) = 2139 $M^{-1}\cdot cm^{-1}$, ε_{260}(Tyr) = 484 $M^{-1}\cdot cm^{-1}$ as reported, [126] or measured at 214 nm with extinction coefficients calculated based on the sum of predicted residue and peptide bond extinction coefficients. [241]

Peptides with no Tyr, were measured at 214 nm and the extinction coefficients calculated based on the sum of predicted residue and peptide bond extinction coefficients. [241]

6.3. Synthesis Methods

All solutions used for synthesis are expressed in % v/v.

6.3.1. Automated peptide synthesis protocol

Automated peptide synthesis was carried out in a 25 or 50 µmol scale using a MultipepRS synthesizer from *Intavis* (Cologne, Germany) in 5 ml syringe reactors on Rink amide TentaGel® R RAM from *Rapp Polymere* (Tübingen, Germany, 0.23 mmol/g) or ChemMatrix® Rink Amide resin (0.5-0.7 mmol/g; *Sigma*-Aldrich, St. Louis, MO, USA). Fmoc/tBu SPPS strategy was employed, using standard Fmoc-protected amino acids unless otherwise stated. The washes from the first deprotection step before manual synthesis was used to calculate the Fmoc- concentration and used as a basis for subsequent reactant equivalence.

The following protocol was used for automated SPPS of peptides:

Swelling: Resins were swelled in DCM for 30-60 min prior to synthesis before washing with DMF.

Fmoc deprotection: The resin was treated with a mixture of DMF:piperidine (4:1) once for 5 min and again for 4 min before washing with DMF x 3.

Coupling: 5 eq Fmoc protected amino acid, 5 eq Oxyma, 4.5 Eq HCTU and 10 eq NMM in each coupling step. The following stock solutions were prepared: 0.5 M Fmoc-amino acid with *OxymaPure* in DMF; 0.4 M HCTU in DMF; 4 M NMM in NMP. Two 30 min couplings (double coupling) were carried for the first residue, then single 30 min couplings up to the 8th amino acid, after which two 20 min couplings were used with a DMF wash in between. After the coupling, resins were washed with DMF x 3.

Capping: Unreacted terminal amines from the coupling step were capped by treatment with a solution of acetic anhydride/2,6-lutidine/ DMF (5:6:89) for 5 min before washing with DMF x 3.

6.3.2. General automated PNA synthesis

PNA (including PNA sequences modified with amino acids) conjugate automated synthesis was carried out in a 2 or 5 µmol scale using a ResPep synthesizer from *Intavis* (Cologne, Germany) in 1-5 µmol miniscale columns (*Intavis Bioanalytical Instruments,* Cologne, Germany) on Rink amide TentaGel® R RAM from *Rapp Polymere*

(Tübingen, Germany, 0.23 mmol/g) or ChemMatrix® Rink Amide resin (0.5-0.7 mmol/g; *Sigma-Aldrich*, St. Louis, MO, USA). Fmoc/tBu SPPS strategy was employed, using standard Fmoc/Bhoc PNA monomers or standard Fmoc/tBu protecting groups. The absorbance (λ = 301 nm; ε = 7800 $cm^{-1}M^{1}$) of the filtrate from the first Fmoc deprotection step was used to calculate the loading (see 6.3.4) and used as a basis for subsequent reactant equivalents.

The following protocol was used for automated SPPS of PNA:

Swelling: Resins were swelled in DCM for 30-60 min prior to synthesis before washing with DMF x 3.

Fmoc deprotection: The resin was treated with a mixture of DMF:piperidine (4:1) once for 5 min and again for 4 min before washing with DMF x 3.

Coupling: For PNA monomers: 4 eq Fmoc- protected PNA monomer, 3.6 eq HATU and 8 eq NMM in NMP, final concentration of activated PNA monomers was 0.08 M. For amino acids: 6 eq Fmoc protected amino acid, 6 eq OxymaPure, 5.6 eq HATU and 12 eq NMM in NMP. Two 30 min couplings were carried out, with a DMF wash in between. After the coupling the resins were washed with DMF x 3.

Capping: Unreacted terminal amines from the coupling step were capped by treatment with a solution of acetic anhydride: 2,6-lutidine: DMF (5:6:89) for 5 min before washing with DMF x 3.

6.3.3. Manual SPPS of Peptides and PNA

Manual SPPS protocol

Resins were shaken at 120 rpm during each step

Swelling: Resins were swelled in DCM for 30-60 min prior to synthesis before washing with DMF x 3.

Fmoc deprotection: The resin was treated with a mixture of DMF:piperidine (4:1) three times for 2 + 4 + 4 min before washing with DMF x 3.

Coupling: Dependant on acid (see below). Acids were activated and coupled in DMF (dry). After coupling resin was washing with DMF x 2, DCM x2, DMF x2.

Capping: Unreacted terminal amines from the coupling step were capped by treatment with a solution of acetic anhydride/2,6-lutidine/DMF (5:6:89) for 8 min before washing with DMF x3.

Resin drying: To store the resin of incomplete synthesis, a final capping step was carried out and resin was washed with DCM x 3 before drying under vacuum.

The following amino acids were coupled manually according to the following procedures, unless stated otherwise.

Coupling of Ahx/AEEAC/MPAA

5 eq 6-(Fmoc-amino)hexanoic acid (Fmoc-Ahx), [2-[2-(Fmoc-amino)ethoxy]ethoxy]acetic acid (Fmoc-AEEAc) or Monomethoxytrityl protected mercaptophenylacetic acid (Mmt-MPAA), 5 eq pyBrOP and 10 eq DIPEA in DMF was preactivated for 4 min before coupling for 1 h. Coupling was repeated twice.

Coupling of Azhx/Ac-Gly-OH

5 eq 6-azidohexanoic acid (Azhx) or Ac-Gly-OH with 4.8 eq HATU and 8 eq DIPEA in DMF was preactivated for 5 min before adding to the resin for 1 h. Coupling was repeated twice.

Coupling of TAMRA/C343

4 eq 5(6)-Carboxytetramethylrhodamine (TAMRA) or coumarin 343 (C343), 4 eq pyBOP and 8 eq NMM in DMF for 30 min. Coupling was repeated twice, and no capping step was carried out. The resin was washed well for 5 times each with DMF and DCM.

Coupling of Cysteine

Cysteine was coupled by hand using 4 eq Boc-L-Cys(Trt)-OH or Fmoc-Cys(Mmt)-OH, 4 eq DIPEA, 3.6 eq HCTU for 2 x 15 min without preactivation of the amino acid to prevent racemization.

Coupling of ALO

Coupling of aryless-octyne (ALO) as a handle for SPAAC was specific to each final compound, and is described in 6.3.6

Removal of S-Mmt/N-Mmt group

Prior to Mmt deprotection, the resin was washed well with DCM x 5. Resin was washed with DCM/TFA/TIS, 97:2:1 repeatedly for 1 min each until the solution ran completely colourless. If an *S*-Trityl group was present on the peptide, TFA washes were ended when the solution was almost clear to prevent unwanted Trityl group deprotection. After Mmt removal, the resin was washed with DCM x5, 1% DIPEA in DCM x1, DCM x2 followed by DMF x3 before further coupling.

6.3.4. Fmoc Monitoring

A known weight of dry resin was swelled in DMF, excess DMF removed then treated with DMF:piperidine (4:1) three times (4 + 4 + 4 min) with a defined total volume. The washes were collected and mixed well along before diluting in DMF and measuring the absorbance at 301 nm. The concentration of the fulvene-piperidine adduct was calculated using an extinction coefficient of 7800 $M^{-1} \cdot cm^{-1}$.

6.3.5. Cleavage from resin and global deprotection

After synthesis, peptide and PNA oligomers cleavage from TentaGel® and ChemMatrix® RAM resins was carried out in fritted syringe reactors and prior to cleavage, resin was either dried under reduced pressure or rinsed 5 times with DCM.

General Peptide Cleavage (Standard Protocol)

Peptides were treated with TFA/TIS/H_2O/, 94:3:3 (1 ml for 5 µmol) for a total of 2 h; TFA for 20 min, then rinsed once with TFA. The combined filtrates were collected in a 15 ml falcon tube and evaporated under compressed air until to 20% of the total volume remained, or when precipitation already began. 6-10 volumes of cold (-18°C) diethylether was added and the falcon tube cooled for at least 30 min at -18°C before centrifugation at 4°C (10 min, 3345 x g). The diethylether was decanted and the pellet dried with a stream of compressed air before dissolving in MeCN/H_2O with 0.1% TFA for RP-HPLC purification.

N_3-donor Cleavage

Prior to cleavage, the resin was rinsed with DCM. Cleavage was carried out as in the standard protocol, but the resin was washed once with DCM (10 min) before the final TFA wash. The DCM filtrate was evaporated under compressed air to 5-10% its original volume before adding the TFA fractions and further evaporation as standard.

Thiol-Peptide Cleavage

Cys- or MPAA-peptides were treated with TFA/TIS/EDT/H_2O/, 93:3:2:2 (1 ml for 5 µmol) for a total of 2 h; TFA for 20 min, then rinsed once with TFA. The precipitate was collected as in the standard protocol, but compressed argon was used instead of compressed air.

PNA and PNA-Peptide Conjugates Cleavage

PNA was cleaved and deprotected as standard for peptides but with at least 1 ml cleavage solution per 1 µmol for 2.5 h.

6.3.6. Synthesis of Specific Compounds

For each batch of resin used for SPPS, Fmoc-Gly-OH was coupled to a portion of resin using standard methods, and subsequent Fmoc-monitoring was carried out to determine quantity of successfully coupled Fmoc-Gly-OH residue in mmol/g. SPPS yields in the following section are based on the resin loading (mmol/g) of a known weight of this resin. Absolute amounts of peptide and PNA were calculated from the measured absorbance at the appropriate wavelength as described in Chapter 6.2.5. using extinction coefficients for each product stated in Chapter 6.8. Several the following compounds were synthesized multiple times with slightly different methodologies. The following synthesis were found to be optimum.

1-4 Automated Fmoc-SPPS of donor peptides on TentaGel® Rink amide (RAM) was carried out as standard before Fmoc-monitoring to determine terminal amino group concentration. Either Fmoc-Ahx or Fmoc-AEEAc was coupled, followed by Mmt-MPAA. After Mmt group deprotection, 6-azidohexanoic acid (Azhx) was coupled to form the thioester. Peptide was cleaved and crude peptide precipitate purified by RP-HPLC with gradients of mobile phase B in A **1**: 10-70%, 60 min; **2**: 10-55% in 30 min, **3**: 10-50% in 25 min **4**: 20-50% in 35 min. Yields: **1** = 42% (3.5 µmol), **2** = 8% (470 nmol), **3** = 9%, (630 nmol), **4** = 12%, 740 nmol. Yields based on absorption at 214 nm.

5 Automated Fmoc-SPPS of the N-terminally acetylated PNA (PNA1H, Ac-gac tct gga tga cgc K-NH_2) with a C terminal lysine was carried out on TentaGel® Rink amide (RAM) as standard for PNA before cleavage and global deprotection. The crude precipitate was dissolved in DMF (50 µL) before addition of preactivated ALO (20 eq ALO, 20 eq DIC, 30 µL DMF, 15 min) to couple to the ε-amino group of lysine for 2 h followed by dilution into the stating mobile phase for the subsequent RF-HPLC (0%, 10 min then 5 -55% B in A in 30 min). Yield: 16% (148 nmol). Yield based on absorption at 260 nm.

6 1 eq of N_3-donor **1** was added to **5** (200 nmol of each, concentration calculated by measured absorption) in approximately 40 µL MeCN/H_2O/TFA (60:40:1) for 24 h before another 2 eq (400 nmol in approximately 40 µL) was added for 48 h followed by RP-HPLC purification (10-40% B in A, 40 min). Yield: 30% with respect to **5**, 5% overall (60 nmol). Yield based on absorption at 260 nm.

7 Automated Fmoc-SPPS of the N-terminally acetylated PNA (PNA1S: Ac-DDR gac tct gga tga cgc RK-NH_2) with a C terminal lysine was carried out on TentaGel® Rink amide (RAM) before cleavage and global deprotection. The crude precipitate was dissolved in DMSO (50 µL) before coupling of the preactivated ALO (40 eq ALO, 40 eq DCC, 3 eq DMAP, 30 µL DMF) to the ε-amino group of lysine for 20 h followed by dilution into the starting mobile phase for the subsequent RF-HPLC (10-50% B in A in 40 min). Yield 1.6% (31 nmol). Yield based on absorption at 260 nm.

8 3 eq of N_3-donor **2** (90 nmol) was added to **7** (30 nmol, concentration calculated by measured absorption) in 50 µL H_2O/TFA (100:1) at 30°C for 24 h before adding 2 x 3 eq in 30 µL (180 nmol) over the next 2 days, followed by HPLC purification (10-40% B in A, 40 min). Yield: 22% with respect to **7**, 0.5% overall from initial PNA resin loading (7 nmol). Yield based on absorption at 260 nm.

9 3 eq of N_3-donor **3** (420 nmol) was added to **7** (140 nmol, concentration calculated by measured absorption) in 30 µL MeCN/H_2O/TFA (75:25:1) at 30°C for 24 h before adding 3 eq over the next 24 h, followed by HPLC purification (10-40% B in A, 40 min). Yield: 7% with respect to **7**, 0.2% overall (10 nmol). Yield based on absorption at 260 nm.

10 Automated Fmoc-SPPS of Fmoc protected PNA (Fmoc-PNA1: Fmoc-DKD gac tct gga tga cgc RK) on ChemMatrix® Rink Amide resin following standard procedure in Chapter 6.3.2. After Fmoc removal, Fmoc-monitoring of the washes was used to determine the free amine concentration at the N-terminus, and to this was coupled ALO. From this calculation, 300 nmol worth of dry resin was weighed, taken in a 1.5 ml microcentrifuge tube, and swelled in minimal DMF (*circa* 20 µL, excess solvent removed by pipette after centrifugation). To this was added preactivated ALO (10 eq ALO, 10 eq pyBroP and 20 eq DIPEA from stock solutions in *circa* 20 µL total volume of DMF to make 3 µmol of 0.15 M activated acid; 10 min preactivation) for 3 h. The resin was transferred into a 1-5 µmol (500 µL) micro reactor syringe and washed with DMF x 2, DCM x2, DMF x2 then transferred back into a 1.5 ml microcentrifuge tube. Excess solvent was removed from the resin after centrifugation then 2 eq azide **3** (600 nmol, concentration calculated by measured absorption) in 15 µL dry DMF was added and shaken at RT for 24 h before addition of 1 eq (300 nmol) more of **3** for another 24 h at 35°C. The resin was transferred into a 3 ml fritted syringe for

cleavage and global deprotection as standard, followed by HPLC purification (2 min 20%, 20-60% B in A, 30 min). Yield: 3% with respect to Fmoc monitoring of Fmoc-PNA1, 1% overall from Gly loaded resin (9.2 nmol). Yield based on absorption at 260 nm.

11 Automated Fmoc-SPPS of Fmoc protected PNA (Fmoc-PNA3: Fmoc-DKD ctg gta agt ggt gtc RK) on ChemMatrix® Rink Amide resin following standard procedure in Chapter 6.3.2. After Fmoc removal, Fmoc-monitoring of the washes was used to determine the free amine concentration at the N-terminus, and to this was coupled ALO. From this calculation, 600 nmol worth of dry resin was weighed, taken in a 1.5 ml microcentrifuge tube, and swelled in minimal DMF (*circa* 30 µL, excess solvent removed by pipette after centrifugation). To this was added preactivated ALO (10 eq ALO, 10 eq pyBroP and 20 eq DIPEA from stock solutions in *circa* 30 µL total volume of DMF to make 6 µmol of 0.2 M activated acid; 10 min preactivation) for 3 h. The resin was transferred into a 1-5 µmol (500 µL) micro reactor syringe and washed with DMF x 2, DCM x2, DMF x2 then transferred back into a 1.5 ml microcentrifuge tube. Excess solvent was removed from the resin after centrifugation then 2 eq azide **4** (1200 nmol, concentration calculated by measured absorption) in 15 µL dry DMF was added and shaken at RT for 24 h before addition of 1 eq more of **4** (600 nmol) for another 24 h at 35°C. The resin was transferred into a 3 ml fritted syringe for cleavage and global deprotection as standard, followed by HPLC purification (2 min 20%, 20-65% B in A, 30 min). Yield: 6% with respect to Fmoc monitoring of Fmoc-PNA3, 2% overall from Gly loaded resin (36 nmol). Yield based on absorption at 260 nm.

12-14 Automated Fmoc-SPPS of donor peptides on TentaGel® Rink amide (RAM) was carried with Fmoc-Lys(Mmt) as the first coupled residue. Boc-L-Cys(Trt)-OH was coupled, Mmt deprotected then TAMRA/C343 coupled before global deprotection and cleavage and RP-HPLC purification of the crude precipitate with a mobile phase gradients **12:** 25-60% B in A, 40 min; **13**: 25-55% B in A in 40 min, **14**: 25-60% B in A in 40 min. Yields: **12** = 10 % (990 nmol), **13** = 11 % (480 nmol), **14** = 8 % (450 nmol). Yields based on absorption at 556 nm (TAMRA) or 437 nm (C343).

15-17 Peptides **12-14** were dissolved in buffer (150 nM NaCl, 50 mM PO_4^{2-}, pH 8.0) with 10% MeCN, bubbled with pressurized air 24 h or the thiol had oxidized to

the disulfide, before RP-HPLC purification of the crude precipitate with mobile phase gradients **15:** 25-60% B in A, 40 min; **16**: 25-55% B in A, 40 min; **17:** 25-60% B in A, 40 min. Yields: **15** = 40 % (290 nmol), **16** = 60 % (200 nmol), **17** = 54 % (204 nmol). Yields based on absorption at 556 nm (TAMRA) or 437 nm (C343).

18 Automated Fmoc-SPPS of donor peptide H-(EIAALEK)$_3$G on TentaGel® Rink amide (RAM) was carried with Fmoc-Lys(Mmt) as the first coupled residue. Boc-L-Cys(Trt)-OH was coupled, Mmt deprotected then TAMRA coupled before global deprotection and cleavage before HPLC purification of the crude precipitate with mobile phases gradient 30-60% B in A, 40 min. Yield: 25 % (450 nmol). Yield based on absorption at 214 nm.

19 Automated Fmoc-SPPS of H-(KIAALKE)$_3$G was carried out before manual coupling of Fmoc-AEEAc then Mmt-MPAA. After Mmt group deprotection, Ac-Gly-OH was coupled to form the thioester. Peptide was cleaved and crude peptide purified by RP-HPLC with mobile phase gradient 20-40% B in A in 30 min. Yield: 25% (565 nmol). Yield based on absorption at 214 nm.

20 Automated Fmoc-SPPS of H-(EIAALEK)$_3$G was carried out before Fmoc-Cys(Mmt)-OH, coupling, followed by Fmoc deprotection and Azhx coupling (5 eq acid, 4.8 eq HATU and 8 eq DIPEA in DMF; 5 min preactivation; 2x 1 h), removal of Mmt (DCM/TFA/TIS 96:3:1) and Azhx coupling to form a cysteinyl thioester (5 eq acid, 4.8 eq HATU and 8 eq DIPEA in DMF; 5 min preactivation; 2x 1 h). The peptide was cleaved and the crude purified by RP-HPLC with mobile phase gradient 60-80% B in A in 30 min. Yield: 42% (380 nmol). Yield based on absorption at 214 nm.

21-24 Automated Fmoc-SPPS of H-(KIAALKE)$_3$G was carried out before manual coupling of Fmoc-AEEAc then Boc-L-Cys(Trt)-OH or Mmt-MPAA. Peptides were cleaved and crude peptides purified by RP-HPLC with mobile phase gradients **21:** 30-55% B in A, 40 min; **22:** 25-55% B in A, 40 min; **23** 25-60% B in A, 40 min; **24** 25-60% B in A, 40 min. Yields: **21** = 37 % (630 nmol), **22** = 14 % (480 nmol), **23** = 8 % (220 nmol) **24** = 8 % (270 nmol). Yields based on absorption at 214 nm.

6.4. Chemical Methods

6.4.1. Buffers

The following buffers were used for in vitro reactions (chapter 4.2), and made up from a mixture of Na_2HPO_4 and NaH_2PO_4 to roughly the correct pH, before adjusting with NaOH or HCl.

Buffer A 200 mM PO_4^{2-}, 50 mM NaCl, 1 mM TCEP, pH 7.2

Buffer B 200 mM PO_4^{2-}, 50 mM NaCl, 1 mM TCEP, 0.1% CHAPS, pH 7.2

Buffer C 100 mM PO_4^{2-}, 1 mM TCEP, 0.1% CHAPS, pH 7.0

Buffer D 100 mM PO_4^{2-}, 50 mM NaCl, 5 mM TCEP pH 7.0 (pH was in some cases adjusted to 8.0 or 8.5)

Buffer E 100 mM PO_4^{2-}, 50 mM NaCl, pH 7.0

6.4.2. Acyl Transfer Reactions (Chapter 4.2.1)

UV-UPLC–MS analysis

Acyl transfer reactions between PNA1-P2 (**10**) and Cys-P1-TAMRA or PNA3-P4 (**11**) and Cys-P3-TAMRA were carried out in Buffer A (200 mM Na_2HPO_4, 50 nM NaCl, 1 mM TCEP, pH 7.2) at 30°C in 1.5 mL microcentrifuge tubes. Disulfide **15** or **17** from stock solutions (0.1% TFA, 20% MeCN in H_2O, 100 µM) were added to buffer (40 – 100 µl depending on number of measurements taken) at 2 µM and shaken for 10 min before addition of 2 µM **10** or **11** respectively, from stock solutions (0.1% TFA in H_2O, 50 µM). After 5 sec, 10 µL reaction was removed and quenched to 1% TFA by addition a 10% TFA solution in water. 10 µL was injected into a UPLC–MS and followed a 4 min gradient of 10-50% mobile phase D in C in 4 min, and absorption spectra recorded with a PDA detector and reported at 260 nm.

FLR–UPLC analysis

Acyl transfer reactions between PNA1-P2 (**10**) or PNA3-P4 (**11**) and Cys-P1-TAMRA, Cys-P3-C343, or Cys-P3-TAMRA were carried out in Buffer B (200 mM Na_2HPO_4, 50 nM NaCl, 1 mM TCEP, 0.1% CHAPS, pH 7.2) at 30°C in 1 ml microcentrifuge tubes. Disulfides **15 , 16** or **17** from stock solutions (0.1% TFA, 20% MeCN in H_2O, 50 µM) were added to buffer (50 – 100 µl depending on number of measurements taken) at 100 nM and shaken for 10 min to reduce the disulfide to the thiol before addition of 200 nm (1eq); 600 nm (3eq) or 1200 nm (6eq) **10** or **11** from stock solutions (0.1% TFA in H_2O, 50 µM). After the appropriate time point 10 µL reaction was removed and quenched by

adding to a polypropylene UPLC vial containing 10 µL of 2% TFA in H_2O/MeCN (90:10). 10 µL of this was injected into a FLR–UPLC system with a gradient of 15-45% mobile phase B in A in 4 min and measuring fluorescence of the fluorophore (either TAMRA, Ex: 550 nm, Em: 580 nm or C343: Ex 420 nm, Em 500 nm) along with absorbance at 260 nm. The UPLC vials for each time point (usually 10, 30, 60, and 300 s) were injected and measured in a different order for each replicate.

For simultaneous PNA transfer, reaction was carried out almost identically, but with the following differences: **15** and **17** added to the buffer simultaneously, and **10** and **11** also added simultaneously. 20 µL of reaction mixture was quenched into 10 µL of 3% TFA in H_2O/MeCN (90:10) and 10 µL reaction mixture was injected twice: once to measure TAMRA and once to measure C343.

Other deviations from this standard procedure include (where mentioned in the text):

Basic quench: for NaOH quench, reactions were quenched with an equal volume of 1M NaOH rather than 2% TFA in H_2O/MeCN (90:10).

No CHAPS: buffer A rather than buffer B was used for the reaction.

Glass vials: reactions were quenched into glass UPLC inserts rather than polypropylene UPLC inserts.

6.4.3. Acyl transfer reactions (Chapter 4.2.2)

Acyl transfer reactions between PNA1H-K3 (**6**) PNA1S-K3 (**8**) and Cys-E3-TAMRA (**18**) were carried out in Buffer C (100 mM PO_4^{2-}, 1 mM TCEP, 0.1% CHAPS, pH 7) at RT in 1.5 ml microcentrifuge tubes. **18** (from a stock solution: 50 µM peptide, 0.1% TFA, 20% MeCN in H_2O) was added to buffer at 2.5 µM and shaken for 10 min to reduce the disulfide to the thiol before addition of 2.5 µM **6** or **8** (from stock solutions, 50 µM peptides, 0.1% TFA in H_2O). After the appropriate time point 20 µL reaction was removed and quenched by adding to a polypropylene UPLC vial containing 20 µL of 2% TFA in H_2O (or 1M NaOH). 30 µL of this was injected into a FLR-HPLC system with a gradient of 25-65% mobile phase B in A in 25 min, measuring fluorescence of TAMRA: Ex 550 nm, Em 580 nm.

6.4.4. Acyl transfer reactions (Chapter 4.2.3)

Acyl transfer reactions between Ac-G-MPAA-AEEAc-K3 (**19**) and Cys-E3-TAMRA (**18**) were carried out in Buffer C (100 mM PO_4^{2-}, 1 mM TCEP, 0.1% CHAPS, pH 7)

at RT in 1.5 ml microcentrifuge tubes. **18** (from a stock solution: 50 µM peptide, 0.1% TFA, 20% MeCN in H_2O) was added to buffer at 500 nM and shaken for 10 min to reduce the disulfide to the thiol before addition of 500 nM **19** (from a stock solution, 10 µM peptide, 0.1% TFA in H_2O). After the appropriate time point 20 µL reaction was removed and quenched by adding to a polypropylene UPLC vial containing 20 µL of 2% TFA in H_2O (or 1M NaOH). 30 µL of this was injected into a FLR-HPLC system with a gradient of 40-60% mobile phase B in A in 25 min, measuring fluorescence of TAMRA: Ex 550 nm, Em 580 nm.

6.4.5. Hydrolysis reactions of peptide thioester **20** (Chapter 4.2.3)

Treatment with MESNA or MPAA

40 µM thioester **20** and either or MESNA (7.5 mM or 20 mM) or MPAA (7.5 mM), were added to buffer D (100 mM PO_4^{2-}, 50 mM NaCl, 5 mM TCEP; pH 7, pH 8 or pH 8.5) at RT. Reaction was quenched to 1% TFA with addition of an equal volume of 2% TFA and analysed immediately by UV-UPLC at 210 nm. Ratio of **20** to Azhx-Cys-E3 was calculated.

***Treatment thiols* 21-24**

40 µM thioester **20** and either thiol **21** (10, 40, 200, or 800 µM) or thiol **22, 23, 24** (40 µM) were added to buffer E (100 mM PO_4^{2-}, 50 mM NaCl, pH 7) at RT. Reaction was quenched to 1% TFA with addition of an equal volume of 2% TFA and analysed immediately by UV-UPLC at 210 nm. Ratio of **20** to Azhx-Cys-E3 was calculated.

6.5. Biological Methods

All solutions used are expressed in % v/v.

6.5.1. Buffers

The following standard buffers were used for cellular experiments:

HBSS 0.78 mM PO_4^{2-}, 138 mM NaCl, 1.3 mM $CaCl_2$, 0.4 mM $MgSO_4$, 0.5 $MgCl_2$, 5.3 mM KCl, 4.2 mM $NaHCO_3$, 5.6 mM D-Glucose, pH 7.2.

DPBS 9.5 mM PO_4^{2-}, 138 mM NaCl, 0.9 mM $CaCl_2$, 0.5 $MgCl_2$, 2.7 mM KCl, pH 7.2

PBS 10 mM PO_4^{2-}, 140 mM NaCl, 2.7 mM KCl, pH 7.2

TBS 20 nM Tris, 150 nM NaCl pH 8.0

The following specialized buffers were made from standard buffers and are expressed in % v/v.

HBSS-BB	0.1mg/ml salmon sperm DNA, 0.2% BSA in HBSS
Antibody blocking buffer	5% normal goat serum, 0.3% triton in PBS
Antibody incubation buffer	1% BSA, 0.3% triton in TBS
Fixation	4% paraformaldehyde in PBS

6.5.2. General cell culture

All cells were grown at 37 °C, 5 % CO_2, and 95% humidity.

Chinese Hamster Embryo (CHO) cells were grown as monolayers. Cells were cultured in Ham's F12 Nutrient mixture Ham (N6658 from *Sigma Aldrich Chemie GmbH*) with additional 2 mM L-Glutamine, and penicillin / streptomycin (10,000 units/ml), puromycin (8 µg/ml) and 10% FBS (*Sigma-Aldrich Chemie GmbH*). For plating cells were washed with PBS and detached with 1 ml 0.25% trypsin / 0.02% EDTA solution for 2min at 37°C. Cells were resuspended in cell culture medium and reseeded as needed. Experiments were aimed to be carried out on cells with 80% confluency.

HEK293 cells were grown as monolayers in DMEM/Ham's F12 (1:1 v/v), supplied with 15% (v/v) heat-inactivated FBS (*Biochrom*). After reaching around 95% confluence, cells were washed twice with DPBS and detached by incubation with 0.25% trypsin / 0.02% EDTA at 37 °C. Cells were resuspended in cell culture medium and reseeded as needed.

6.5.3. Plasmid Cloning

pPBtet-Cys-P3-ErbB2-eCFP-PuroR and pPBtet-Cys-P1-EGFR-eYFP-PuroR

Cys-P1-EGFR-eYFP and Cys-P3-HER2eCFP constructs were cloned from EGFR-eYFP-N1 and ErbB2-eCFP-pcDNA3.1(+)Zeo (kind gifts from Prof Thorsten Wohland in the Centre for Bioimaging Sciences, National University of Singapore). Synthesis of the Cys-P1 and Cys-P3 DNA and all their subsequent cloning was carried out by *GenScript Biotech* (Piscataway, NJ, USA). The Cys-P1 and Cys-P3 tags were inserted into the EGFR ErbB2 protein sequence respectively, directly before the N-terminal signal peptides (Table XX) to ensure that after receptor biosynthesis, translocation to the membrane and finally signal peptide cleavage, the mature protein would offer an N-terminal cysteine residue. The genes for Cys-P1-EGFR-eYFP and Cys-P3-HER2eCFP were amplified to include the addition of two unique SfiI restriction sites directly before and after the gene, before cloning into the donor vector pPBtet-3xFLAG-IRES-DsRed-Express-PuroR donor vector[242] using the SfiI restriction endonuclease to generate the vectors pPBtet-Cys-P3-ErbB2-eCFP-PuroR and pPBtet-Cys-P1-EGFR-eYFP-PuroR used for stable cell line generation. Vector maps are shown in Appendix (chapter 8.2).

Cys-P1-ET$_B$R-GFPspark

Cloning of pCMV3-Cys-P1-ETBR-GFPspark was carried out by Philipp Wolf and was previously reported[185]

Cys-E3-EGFR-eYFP

Cloning of Cys-E3-EGFR-eGFP plasmid was carried by *GenScript Biotech* (Piscataway, NJ, USA) and was previously reported[185]

Table 6 Amino acid sequences in cloned plasmids

Name	**Sequence:**
EGFR Signal peptide	MRPSGTAGAA LLALLAALCP ASRA
ErbB2 Signal peptide	MELAALCRWG LLLALLPPGA AS

Cys-P1 tag	C EIQALEE ENAQLEQ ENAALEE EIAQLEY GG
Cys-P3 tag	C EIQQLEE EIAQLEQ KNAALKE KNQALKY GG

6.5.4. Cell Line Generation

Generation of stable, doxycycline-inducible, single positive Cys-P3-ErbB2-eCFP and Cys-P1-EGFR-eYFP and double positive Cys-P1-EGFR-eYFP/ Cys-P3-ErbB2-eCFP CHO cells was carried out by Michael Bartoschek and was previously described (Appendix Figure 8). [185,186]

6.5.5. Immunofluorescence assay

Detection of EGFR phosphorylation in a well plate format was carried out by fluorescent labelling using AlexaFluo647 conjugated secondary antibodies against a phosphorylated EGFR mAb (Y1068), with YFP signal as an internal standard for expression level. Phospho-EGF Receptor mAb (Tyr1068, D7A5, XP® Rabbit mAb (#3777 Lot: TB264033)) was purchased from *Cell Signalling.* AlexaFluor647 conjugated Goat anti-Rabbit IgG (IgG (H+L) Highly Cross-Adsorbed Secondary Antibody, Alexa Fluor Plus 647 (#A32733, Lot:10)) was purchased from *Thermo Fischer Scientific*.

5000 cells/well of Cys-P1-EGFR-eYFP stably expressing CHO cells were plated on a 96-well culture plate (CulturePlate-96, *Perkin Elmer)*. After 18 h incubation, cells were induced by addition of 100 µL doxycycline to a final concentration of 0.1 µg/ml for 5 h before switching to FBS free media (0.1 µg/ml doxycycline) for a further 12 h. Media was removed and cells washed (HBSS x1) then incubated with PNA donor **9** (50 µL, 100 nM in HBSS, pH 7.0) or HBSS for 4 min at RT. Cells were washed (HBSS x1) then either DNA1 (100 nM in HBSS) or HBSS only was added for 3 minat RT. EGF in FBS free media (or FBS free media only) was added to a final concentration of 100 nM. Cells were added to an incubator (37° C, 5% CO_2) for 10 min before removal of media and fixation (4% paraformaldehyde in PBS, 100 µL/well).

Cells were washed (PBS x3) and treated with antibody blocking buffer (5% normal goat serum, 0.3% Triton in PBS) for 1h at RT. After rinsing with *Tris*-HCl Buffered Saline (TBS) x3 the Phospho-EGF Receptor mAb was added as 50 µL of a 1:800 dilution in

antibody incubation buffer (1% BSA, 0.3% Triton in TBS) and incubated overnight at 4 °C. After washing (TBS x3) cells were incubated with AF647-labelled Goat anti-Rabbit IgG as 50 µL of a 1:500 dilution in antibody incubation buffer (1% BSA, 0.3% Triton in TBS) for 1 h. After washing (5 min TBS x3), the plate was read in a Viktor X5 Multimode Plate Reader (*Perkin Elmer*) using the following filter sets: YFP: λ_{ex} = 420±15 nm, λ_{em} = 532±10 nm. AF647: λ_{ex} = 665±10 nm λ_{em} = 640±10 nm. The average AF647/YFP of three technical replicates was measured in relative fluorescence units (RFU). Each replicate was normalized to the (+EGF, -**9**, -DNA1) condition.

6.6. Microscopy Experiment Protocols

6.6.1. Labelling Transiently Expressed Cys-E3-EGFR-eYFP on HEK293 Cells (Chapter 4.2)

Prior to cell seeding 8-well µ-slides were coated with 0.01% poly-D-lysine by 10 min incubation before drying. HEK293 cells (10,000) were seeded and incubated in DMEM (10% FBS) overnight at 37°C. For transfection, 100 ng vector and 1 µL Lipofectamine2000 in Opti-MEM (200 µL) were added to each chamber. After 1 h, DMEM with (10% FBS, 100 µL) was added and cells incubated overnight (37°C, 5% CO_2). Cells were stained with Hoechst 33342 (0.5 mg/ml, 10 min, 37ºC) then donor **6** or **8** (100 nM in PBS) was added for 4 min.Cells were washed (PBS 2x) prior to addition of **Atto565-DNA1** (200 nM in PBS, 5 min) before washing (PBS x1). Fluorescence microscopy was performed in PBS using a widefield IX83 microscope from *Olympus*. Excitation times, YFP: 300 ms YFP, TRITC: 1 s.

6.6.2. Orthogonal Labelling Studies (Chapter 4.3.3)

Prior to cell seeding 8-well µ-slides were coated with 0.01% poly-D-lysine by 10 min incubation before drying. Cys-P1-EGFR-eYFP, Cys-P3-ErbB2-eCFP or Cys-P1-EGFR-eYFP/Cys-P3-ErbB2-eCFP stable CHO cells (20,000) were seeded and incubated in Hams F12 media (10% FBS, 200 µL) overnight at 37°C. Cells were induced with 0.1 µg/ml doxycycline by addition of 100 µL Hams F12 media (10% FBS, 0.3 µg/ml doxycycline) for 16 h. Cells were starved for 4 h in serum free (0% FBS) Hams F12 Media. Prior to labelling the cell nuclei were stained with Hoechst 33342 (0.5 mg/ml in HBSS, 10 min). After washing (HBSS 1x), PNA-donors **10, 11**, or both (100nM in HBSS) were added for 4 min. Cells were washed (HBSS 1x) prior to addition of **Atto565-DNA1**, **Cy7-DNA3** or both (200 nM in HBSS, 4 min). Cells were washed (HBSS 1x) and imaged in HBSS using a widefield IX83 microscope from *Olympus*. Excitation times: Cy7; 500 ms, Atto565: 500 ms, YFP: 200 ms, CFP: 150 ms.

6.6.3. Labelling transiently Expressed Cys-P1-ET_BR-GFPspark on HEK293 cells (Chapter 4.3.4)

Prior to cell seeding 8-well µ-slides were coated with 0.01% poly-D-lysine (10 min incubation then drying) before seeding 10,000 HEK293 cells. After reaching 70 % confluence, HEK293 cells were transiently transfected with the pCMV3-Cys-P1-ET_BR-GFPspark and Lipofectamine 2000 according to the manufacturer's protocol. Either 250 ng or 750 ng of plasmid DNA were used for transfection, while keeping the total amount of DNA 1,000 ng, balanced with pcDNA3 (empty vector). Labelling experiments and microscopic imaging was performed 24 h post transfection. The supernatant was exchanged with OptiMEM and cell nuclei were stained with Hoechst33342 (0.5 mg/ml in HBSS, 20 min). After medium exchange PNA1S-P2 **9** (100nM in HBSS, 4 min,37°C) was added. Cells were washed (HBSS x1) and the cells incubated with **Atto565-DNA1** (200 nM in HBSS, 4 min, RT) followed by (HBSS 2x). Cells were incubated with ET-1 (500 nM in OptiMEM, 1 h, 37°C) before washing (HBSS 1x) and microscopic analysis in HBSS. Fluorescence images were using a Zeiss Axio Observer Z1 microscope.

6.6.4. Measuring Labelling Lifetime of Cys-P1-EGFR-eYFP (Chapter 4.3.4)

CHO cells (25,000) stably expressing doxycycline-inducible Cys-P1-EGFR-eYFP were seeded on 8-well µ-slides and incubated in Hams F12 media (10% FBS, 200 µL) overnight at 37°C. Cells were induced with doxycycline by switching media (1% FBS, 500 ng/ml doxycycline) 16 h prior to experiments. 4.5 h prior to the experiment, medium was switched to 0% FBS Hams F12 medium with no doxycycline. After washing (DPBS 1x), cells were treated with **9** (100 nM in DPBS, 4 min). Cells were washed (HBSS-BB 1x) before incubation with **Atto565-DNA1** (200nM in HBSS-BB with 1x ProLong™ Live Antifade Reagent, 4 min, RT). Cells were kept at 37°C, with 5% CO_2, and 95% relative humidity. Fluorescence images were taken approximately 5 min after labelling with **Atto565-DNA1** and then hourly timepoints thereafter, with the same cells in frame for each experiment. Regions of interest (ROIs), encompassing the same cells per experiment and excluding areas without cells (Appendix Figure 3), were analyzed and mean intensity of the ROIs were compared between the Atto565 and YFP channels over time. Excitation times: Atto565: 300 ms, YFP: 100 ms.

6.6.5. Labelling Cys-P1-EGFR-eYFP with Multiple Fluorophores (Chapter 4.3.5)

Prior to cell seeding 8-well µ-slides were coated with 0.01% poly-D-lysine by 10 min incubation before drying. Cys-P1-EGFR-eYFP stable CHO cells (20,000) were seeded and incubated in Hams F12 medium (10% FBS, 200 µL) overnight at 37°C before exchange with 0.1 µg/ml doxycycline medium for 12 h before starvation for 5 h in serum free media (0% FBS, 0.1 µg/ml doxycyline). Prior to labelling, the cell nuclei were stained with Hoechst 33342 (0.5mg/ml in HBSS, 10 min).

After washing (HBSS 1x), PNA-donor **9** (100 nM in HBSS) was added for 4 min. Cells were washed (HBSS-BB 1x) prior to addition of **Cy7-1xComplex or Cy7-5xComplex** (50 nM in HBSS-BB, 4 min). Cells were washed (HBSS-BB 1x) and imaged in HBSS using a widefield IX83 microscope from *Olympus* with excitation times Cy7: 500 ms, YFP: 150 ms.

For Signal to Noise Ratio (SNR) calculations, cells (n=20) taken from three independent experiments were analyzed by taking a line intensity profile throughout the cell (Appendix Figure 4) For each cell, Cy7 or YFP signal was calculated as the max peak height at the membrane region, and the Noise calculated as the standard deviation of the signal from a background region. The background region was deemed as a nearby 'empty' region in the line intensity profile, with no cells, and where little to no YFP or Cy7 signal was observed. YFP signal for each cell was normalized to a 'Relative YFP signal' according to the equation:

$$\text{Relative YFP signal} = \frac{\text{YFP Signal}}{\text{YFP(min)}}$$

Where YFP(*min*) is the lowest YFP signal from all cells. To account for variation in peak signal between single cells due to different expression levels, Cy7 Signal was corrected according to the equation:

$$\text{Corrected Cy7 signal} = \frac{\text{Cy7 Signal}}{\text{Relative YFP signal}}$$

Finally, SNR was calculated for each cell:

$$\text{SNR} = \frac{\text{Corrected Cy7 Signal}}{\text{Cy7 Noise}}$$

6.6.6. Erasable Labelling of EGFR (Chapter 4.3.6)

Prior to cell seeding, 8-well µ-slides were coated with 0.01% poly-D-lysine by 10 min incubation before drying. Cys-P1-EGFR-eYFP stable CHO cells (20,000) were seeded and incubated in Hams F12 media (10% FBS, 200 µL) overnight at 37°C before exchange with 0.1 µg/ml doxycycline media for 12 h before starvation for 5 h in serum free medium (0% FBS, 0.1 µg/ml doxycyline). Prior to labelling, the cell nuclei were stained with Hoechst 33342(0.5 mg/ml in HBSS, 10 min). During measurement cells were maintained at 30°C with 5% CO_2.

After washing (HBSS 1x), PNA-donor **9** (100 nM in HBSS) was added for 4 min. Cells were washed (HBSS-BB 1x) prior to addition of **Atto565-5xImager** (50 nM in HBSS-BB, 4 min). Buffer was replaced with a solution of **Cy7-5xComplex** and **Cy7-DNA4** (50 nM in HBSS-BB, 4 min) before washing (HBSS-BB 1x). To reverse staining, **EraserDNA4** (300 nM in HBSS) was applied twice for 5 min at 30°C. To restain, Cy7-DNA3 (100 nM in HBSS-BB, 3 min) was added. Images were taken at each stage using an *Olympus* IX83 widefield microscope with the following excitation times: YFP: 150 ms; Atto565: 150 ms, Cy7: 500 ms.

6.6.7. Erasable Labelling of EGFR after EGF Stimulation (Chapter 4.3.6)

Prior to cell seeding, 8-well µ-slides were coated with 0.01% poly-D-lysine by 10 min incubation before drying. Cys-P1-EGFR-eYFP stable CHO cells (20,000) were seeded and incubated in Hams F12 medium (10% FBS, 200 µL) overnight at 37°C before exchange with 0.1 µg/ml doxycycline medium for 12 h before starvation for 5 h in serum free media (0% FBS, 0.1 µg/ml doxycyline). Prior to labelling, the cell nuclei were stained with Hoechst 33342(0.5 mg/ml in HBSS, 10 min). During measurement, cells were maintained at 30°C with 5% CO_2.

After washing (HBSS 1x), PNA-donor **9,** (100 nM in HBSS) was added for 4 min. Cells were washed (HBSS-BB 1x) prior to addition of **Atto565-5xImager** (50 nM in HBSS-BB, 4 min). After washing (HBSS-BB 1x), EGF was added (100 nM in HBSS, 15 min) and maintained at 30°C. To reverse membrane staining, **EraserDNA4** was added to the cells to a final concentration of 300 nM for 5 min at 30°C. Buffer was removed and replaced with **EraserDNA4** (300 nM in HBSS) for a further 5 min and 30°C. For restaining, **Atto647N-DNA3** (100 nM in HBSS-BB, 3 min, RT) was added. Images

were taken at each stage using a spinning disk (Visitron VisiScope) confocal *Olympus* IX83 microscope with the following excitation times: Atto565: 200 ms YFP: 100 ms, Hoechst 33342: 100 ms Atto647N: 300 ms.

6.6.8. Dual Colour Internalization Analysis of EGFR and ErbB2 (Chapter 4.3.7)

Cys-P1-EGFR-eYFP/Cys-P3-ErbB2-eCFP CHO cells (30,000) were seeded in in 200 µL Hams F12 medium (10% FBS) on 8-well µ-slides and incubated overnight at 37°C. Cells were induced with 0.035 µg/ml doxycycline by media change for 20 h. Cells were starved for 4 h in serum free Hams F12 medium with 0.035 µg/ml doxycycline. HBSS-BB and DPBS were prewarmed in a water bath at 37°C prior to experiment. After removing media and washing once with DPBS, both PNA-donors **10** and **11** (100 nM in DPBS, made from 50 µM stocks in 0.1% TFA) were added for 4 min in an incubator (37°C, 5% CO_2).

As a negative control, in one well no PNA thioester was added. Cells were washed (1x HBSS-BB) prior to addition of DNA complexes (**Atto565-complex I** and **DY751-complex III**; each 200 nM in HBSS-BB). After 4 min at room temperature cells were washed with HBSS-BB before addition of serum free Hams F12 medium with either epidermal growth factor (EGF, 100 nM), Geldanamycin (GA) 3 µM or no receptor agonist (negative control and no PNA control). The cells were returned to the incubator for 20 min before addition of 50 µM erasure DNAs to make up a final concentration of 1 µM. After 4 min, the medium was removed and replaced with eraser DNAs in HBSS-BB (1 µM) for a further 4 min before washing twice with HBSS-BB and leaving in HBSS-BB for microscopy.

Atto565-complex I: DNA_1-3-DNA_5*-1-DNA_5*: 2 x Atto565-DNA_5-TOE1
DY751-complex III: DNA_3-1-DNA_4*-1-DNA_4*: 2 x DY751-DNA_4-TOE2

DNA eraser I: TOE1*-DNA_5*
DNA eraser III: TOE2*-DNA_4*

To quantify internalisation of EGFR and ErbB2, two photos from the same well plate (2 viewpoints) were taken per experiment for each condition and analysed using Olympus *CellSens* software (excitation times Atto565/Cy7: 600 ms; CFP, YFP: 400 ms). For each photo, automatic segmentation was applied to the YFP channel and regions of interest (ROIs) were manually created based on the segmentation results.

Every cell, which was clearly segmented, was counted, and 50 cells from each photo were used for analysis. In the event that more than 50 cells were counted per photo, 50 cells were picked via random number generation in Microsoft Excel. In the event that less than 50 cells were counted, the number was made up to 50 from the second photo, also chosen by random number generation. 100 cells were therefore collected per condition per experiment. For each ROI, a measure of brightness was given in RFU (relative fluorescence units) and from this, a mean fluorescence value was calculated for each population. Appendix Figure 7 shows exemplary results from one replicate. From these mean fluorescence values, a 'background' value was subtracted. These were cells which had been treated with the relevant DNA, but not PNA and represented the nonspecific binding/internalisation of DNA-fluorophore to cells, or non-specific binding to the 8-well plate. The calculated means were then expressed as a relative to the negative control, i.e., cells treated with only media.

6.7. Flow Cytometry

Multiple Fluorophore Labelling (Chapter 4.3.5)

Prior to cell seeding, 8-well µ-slides were coated with 0.01% poly-D-lysine by 10 min incubation before drying. Cys-P1-EGFR-eYFP CHO cells (25,000) were seeded and incubated in Hams F12 medium (10% FBS, 200 µL) overnight at 37°C. Media was exchanged with serum free doxycyline media (0% FBS, 0.1 µg/ml doxycycline) for 15 h pior to the experiment.

Prior to labelling, the cell nuclei were stained with Hoechst 33342 (0.5 mg/ml in HBSS, 10 min).

After washing (HBSS 1x), PNA-donors **9,** (100 nM in HBSS) was added for 4 min. Cells were washed (HBSS-BB 1x) prior to addition of **Atto647N-1xComplex, Atto647N-3xComplex** or **Atto647N-5xComplex** (50 nM in HBSS-BB, 5 min). Cells were washed (HBSS-BB 1x; PBS 1x) before detachment with Trypsin/EDTA (0.25% trypsin / 0.02% EDTA in PBS, 30 µL, 5 min, RT). Hams F12 medium (10% FBS, 300 µL) was added and the detached cells pelleted by centrifugation (300 x g, 8 min).,The supernatant was removed and the cells resuspended in DPBS (200 µL). Paraformaldehyde (8% in PBS, 200 µL) was added for 10 min before centrifugation (300 g 8 min). The pellet was resuspended in DPBS (200 or 300 µL) before performing flow cytometry experiments on a BD Accuri™ C6 with a flow rate of 66 µL/ min for 150 or 260 µL of cells. Excitation lasers: YFP) 488 nm; Atto647N: 640 nm. Emission filters: YFP: 533/30 nm; Atto647N: 675/25 nm. Data was analysed using BD CFlow Plus V1.0.227.4.

After gating (Appendix Figure 5), mean intensities were obtained for YFP and Atto647N. An average of 444 (experiment 1), 6600 (experiment 2) or 9090 (experiment 3) cells were analyzed after gating was applied. Signal was recorded after application of 4 gates (debris, single cells, YFP, and Atto674N. Background was defined as the mean intensity obtained from the control without doxycycline (-Dox) after applying gates to exclude debris and non-single cells. For the -Dox control, cells were treated as described, but without doxycycline induction, addition of **9** or addition of DNA complexes. The background for the YFP signal and Atto647N signal were subtracted from the mean intensities. To correct for eYFP expression levels, a ratio of the mean Atto647N intensities to the mean eYFP intensity was calculated after the gating strategy was applied. To verify that the DNA complexes do not non-specifically bind to cells, an

additional control experiment, (-PNA) was carried out. Cells were treated as described, but no **9** was added to during the PNA tagging step, and **Atto647N-5xComplex** was added during the hybridization step.

6.8. Chromatograms and Mass Spectra

1 **N_3-MPAA-Ahx-K3** $N_3(CH_2)_5(CO)$-MPAA-$NH(CH_2)_5(CO)$-$(KIAALKE)_3G$-NH_2. ε_{214nm} = 28396 $L{\cdot}mol^{-1}cm^{-1}$; UPLC t_R = 2.73 min (3-80% B in 4 min). ESI–MS: *m/z* = 548.37, 685.18, 913.15 MW_{calc}=2736.84 $g{\cdot}mol^{-1}$ ($C_{127}H_{221}N_{33}O_{31}S$, MW_{exp}=2736.64 $g{\cdot}mol^{-1}$: $[M+3H]^{3+}$ = 913.21, $[M+4H]^{4+}$ = 685.17, $[M+5H]^{5+}$ = 548.33)

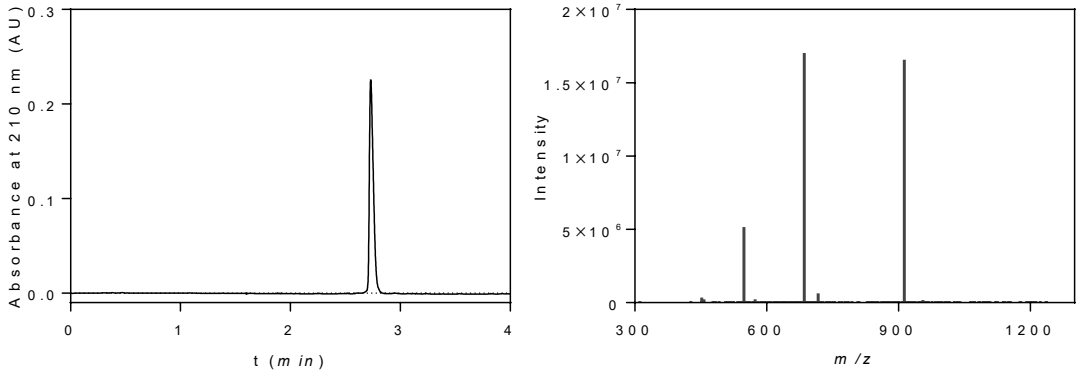

2 **N_3-MPAA-AEEAc-K3** $N_3(CH_2)_5(CO)$-MPAA-AEEAc-$(KIAALKE)_3G$-NH_2. E_{214nm} = 28396 $L{\cdot}mol^{-1}cm^{-1}$; UPLC t_R = 2.02 min (20-80% B in 4 min). ESI–MS: *m/z* = 924.48, 693.70, 555.28, MW_{calc}= 2770.88 $g{\cdot}mol^{-1}$ ($C_{127}H_{221}N_{33}O_{33}S_1$; MW_{exp}= 2770.39 $g{\cdot}mol^{-1}$: $[M+3H]^{3+}$ = 924.46, $[M+4H]^{4+}$ = 693.60, $[M+5H]^{5+}$ = 555.08)

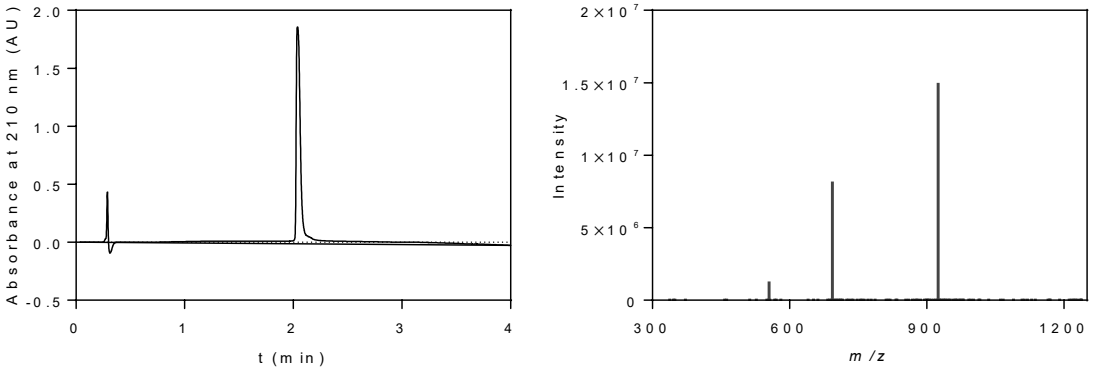

3 **N_3- P2** $N_3(CH_2)_5(CO)$-MPAA-AEEAc-KIAQLKE KNAALKE KNQQLKE KIQALKY G-NH_2. ε_{214}= 41008 $L{\cdot}mol^{-1}cm^{-1}$; UPLC t_R = 2.2 min (3 - 80% B in 4 min). ESI–MS: *m/z* = 948.01, 758.64, 632.2, MW_{calc}= 3787.93 $g{\cdot}mol^{-1}$ ($C_{170}H_{288}N_{48}O_{47}S$; MW_{exp}= 3788.48 $g{\cdot}mol^{-1}$: $[M+4H]^{4+}$ = 948.1, $[M+5H]^{5+}$ = 758.7, $[M+6H]^{6+}$ = 632.4)

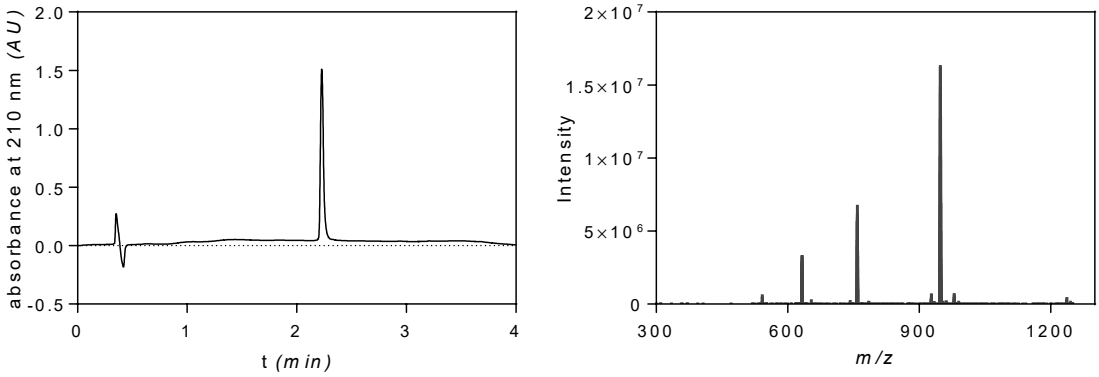

4 **N_3-P4** $N_3(CH_2)_5(CO)$-MPAA-AEEAc- KIAQLKQ KIQALKQ ENQQLEE ENAALEY G-NH_2. ε_{214}= 41394 L·mol^{-1}cm^{-1}; UPLC t_R = 2.53 min (3-80% B in 4 min). ESI–MS: *m/z* = 948.41, MW_{calc}= 3789.64 g·mol^{-1} ($C_{166}H_{270}N_{46}O_{53}S$: MW_{exp}= 3790.27 g·mol^{-1}: $[M+4H]^{4+}$ = 948.6)

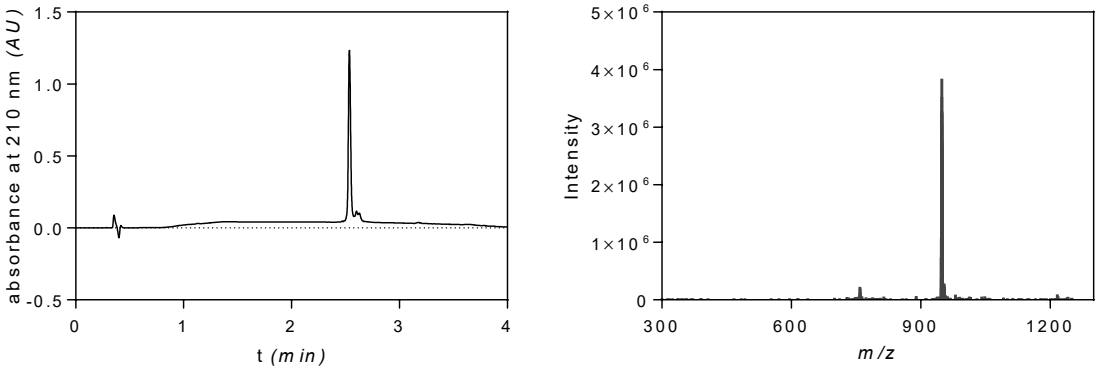

5 **ALO-PNA1H** *Ac*- ^{N}gac tct gga tga cgc^{C} K-$CONH_2$. ε_{260} = 151800 L·mol^{-1}cm^{-1}; UPLC t_R = 1.41 min (10-80% B in 4 min). ESI–MS: *m/z* = 899.71, 1124.32, MW_{calc} =4493.4 g·mol^{-1}, ($C_{181}H_{230}N_{92}O_{50,}$ MW_{exp} = 4491.82 g·mol^{-1}: $[M+4H]^{4+}$ = 1123.75, $[M+5H]^{5+}$ = 899.20)

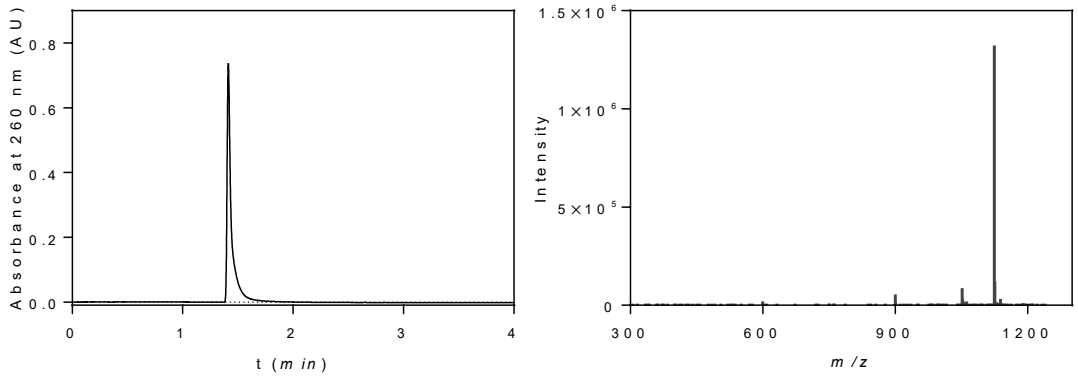

6 **PNA1H-K3** *Ac-* ^{N}gac tct gga tga cgc^{C} K-ALO-$N_3(CH_2)_5(CO)$-MPAA-$NH(CH_2)_5(CO)$-KIAALKE KIAALKE KIAALKE G-NH_2]G-*CONH₂*. ε_{260} = 153939 L·mol^{-1}cm^{-1}; UPLC t_R = 2.39 min (3- 80% B in 4 min). ESI–MS: *m/z* = 1206.47, 1034.28, 905.02, MW_{calc} =7232.67 g·mol^{-1} ($C_{308}H_{451}N_{125}O_{81}S_1$; MW_{exp} = 7232.744 g·mol^{-1} $[M+6H]^{6+}$ = 1206.5, $[M+7H]^{7+}$ = 1034.2, $[M+8H]^{8+}$ = 905.1, $[M+9H]^{9+}$ = 804.6)

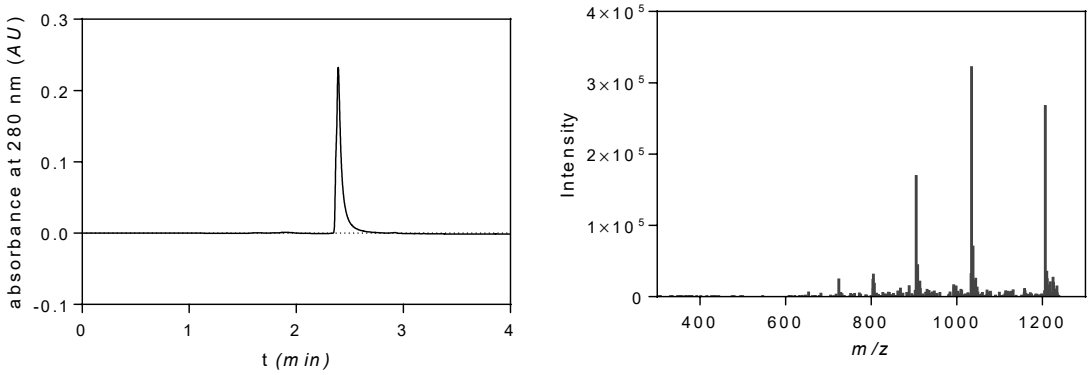

7 **ALO-PNA1S** Ac-DDR ^{N}gac tct gga tga cgc^{C} R-Lys(ALO)-NH_2. E_{260} = 151800 L·mol^{-1}cm^{-1}; UPLC t_R = 1.54 min (10- 60% B in 4 min). ESI–MS: *m/z* = 996.9, 831.9, MW_{calc} = 4982.45 g·mol^{-1} ($C_{199}H_{261}N_{101}O_{57}$, MW_{exp} = 4979.85 g·mol^{-1}: $[M+5H]^{5+}$ = 997.0, $[M+6H]^{6+}$ = 831.0)

The purity of ALO-PNA1S was deemed sufficient for use in the following synthetic step.

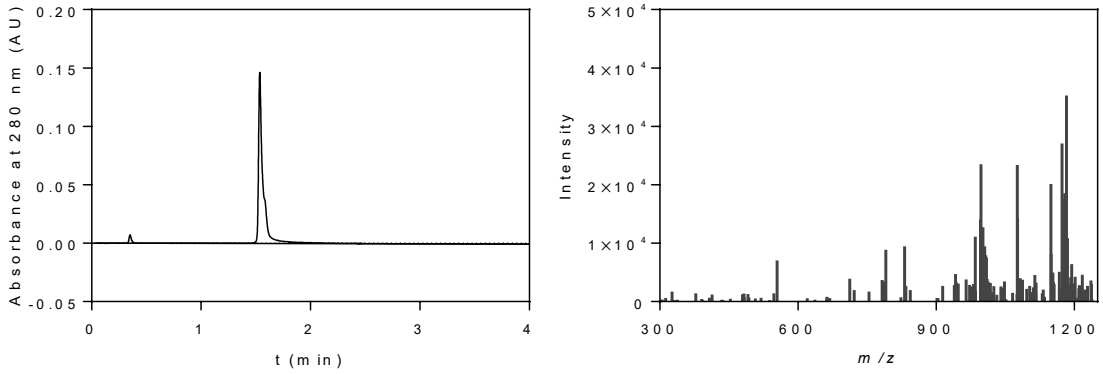

8 **PNA1S-K3** Ac- DDR ^{N}gac tct gga tga cgc^{C} R-Lys [ALO-$N_3(CH_2)_5(CO)$-MPAA-AEEAc-KIAALKE KIAALKE KIAALKEG-$CONH_2$]G-*CONH₂*. ε_{260} = 153939 L·mol^{-1}cm^{-1}; UPLC t_R = 2.64 min (3- 80% B in 4 min). ESI–MS: *m/z* = 860.98, 969.1, 1106.9, MW_{calc} = 7742. g·mol^{-1}0 ($C_{326}H_{483}N_{134}O_{90}S_1$; MW_{exp} = 7746.71 g·mol^{-1}: $[M+7H]^{7+}$ = 1107.67, $[M+8H]^{8+}$ = 969.34, $[M+9H]^{9+}$ = 861.75)

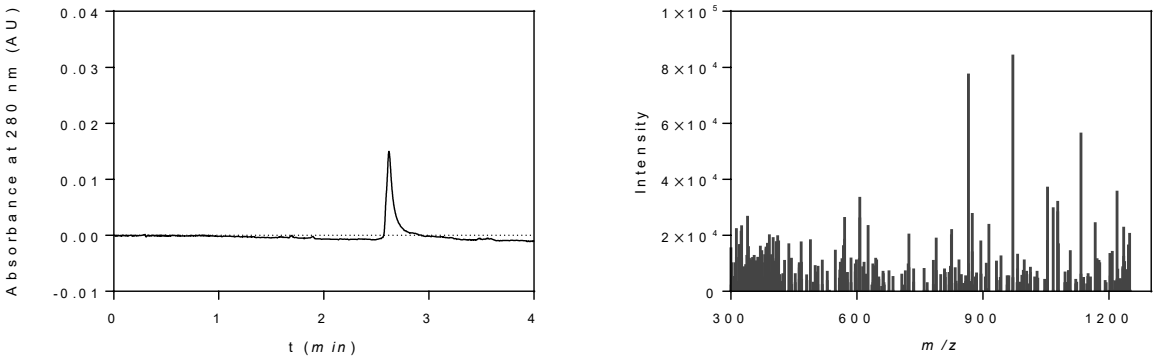

9 **PNA1S-P2** Ac- DDR ^{N}gac tct gga tga cgc^{C} R-Lys[(ALO)$N_3(CH_2)_5$(CO)-MPAA-AEEA-KIAQLKE KNAALKE KNQQLKE KIQALKY G-NH_2] ε_{260} = 154423 L·mol^{-1}cm^{-1}; UPLC t_R = 2.54 min (3- 80% B in 4 min). ESI–MS: *m/z* = 798.58, 877.63, 975.68, 1097.01 MW_{calc} =8769.97 g·mol^{-1} ($C_{369}H_{549}N_{149}O_{104}S_1$; MW_{exp} = 8763.197 g·mol^{-1}: $[M+8H]^{8+}$ = 1096.40, $[M+9H]^{9+}$ = 974.69, $[M+10H]^{10+}$ = 877.30, $[M+11H]^{11+}$ = 797.70)

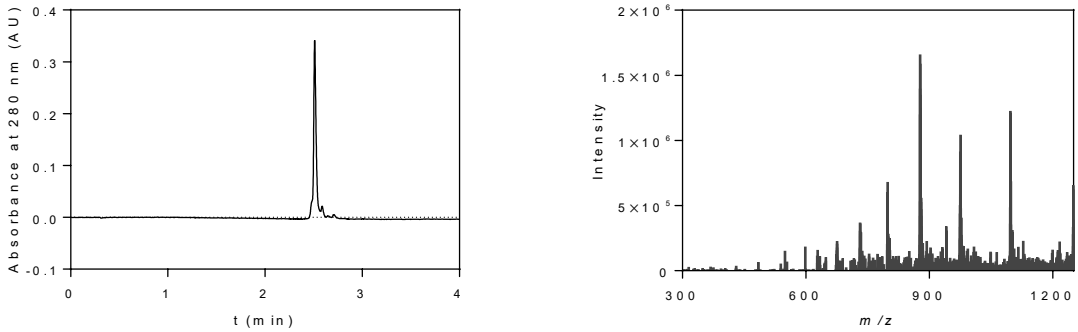

10 **PNA1-P2** NH_2- ^{C}KR cgc agt agg tct cag DKD ^{N} -ALO-$N_3(CH_2)_5$(CO)-MPAA-AEEAc-KIAQLKE KNAALKE KNQQLKE KIQALKY G-NH_2. ε_{260} = 154423 L·mol^{-1}cm^{-1}; UPLC t_R = 1.74 min (10 - 70% B in 4 min). ESI–MS: *m/z* = 791.73, 870.70, 967.48, 1088.09, 1244.04 MW_{calc} =8698.33 g·mol^{-1} ($C_{367}H_{547}N_{147}O_{103}S$, MW_{exp} = 8698.274 g·mol^{-1}: $[M+7H]^{7+}$= 1243.6, $[M+8H]^{8+}$= 1088.3, $[M+9H]^{9+}$= 967.5, $[M+10H]^{10+}$ = 870.8, $[M+11H]^{11+}$= 791.8)

The two UPLC peaks correspond to two isomers formed from SPAAC ligation

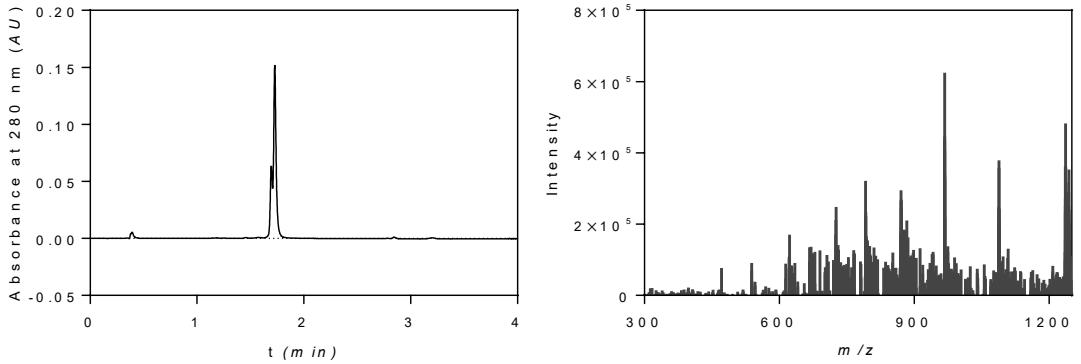

11 **PNA3-P4** NH_2-^{C} KR ctg tgg tga atg gtc DKD ^{N}-ALO-$N_3(CH_2)_5(CO)$-MPAA-AEEAc- KIAQLKQ KIQALKQ ENQQLEE ENAALEY G-NH_2. ε_{260} = 156423 $L \cdot mol^{-1}cm^{-1}$; UPLC t_R = 2.15 min (3- 80% B in 4 min). ESI–MS: *m/z* = 1094.43, 972.78, 875.76, 796.07, MW_{calc} = 8746.7 $g \cdot mol^{-1}$ ($C_{369}H_{549}N_{145}O_{106}S$; MW_{exp} = 8744.26 $g \cdot mol^{-1}$: $[M+8H]^{8+}$ = 1094.0, $[M+9H]^{9+}$ = 972.6, $[M+10H]^{10+}$ = 875.4, $[M+11H]^{11+}$ = 795.9)

The two UPLC peaks correspond to two isomers formed from SPAAC ligation

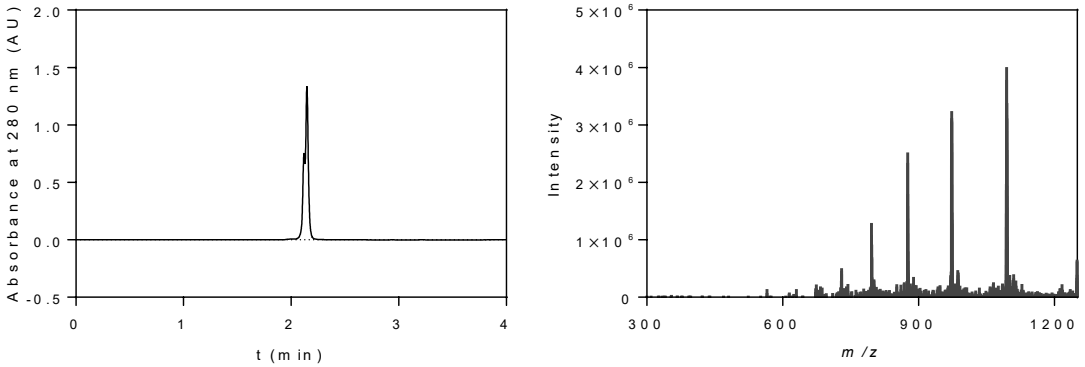

12 **Cys-P1-TAMRA** Cys-EIQALEE ENAQLEQ ENAALEE EIAQLEY G K(TAMRA)-$CONH_2$. ε_{556} = 95000 $L \cdot mol^{-1}cm^{-1}$; UPLC t_R = 2.23 min (20- 65% B in 4 min). ESI–MS: *m/z* = 987.28, 790.03, 658.93, MW_{calc} = 3945.95 $g \cdot mol^{-1}$ ($C_{174}H_{257}N_{41}O_{62}S$: MW_{exp} = 3947.212 $g \cdot mol^{-1}$: $[M+5H]^{5+}$ = 987.80; $[M+6H]^{6+}$ = 790.44 $[M+7H]^{7+}$ = 658.87)

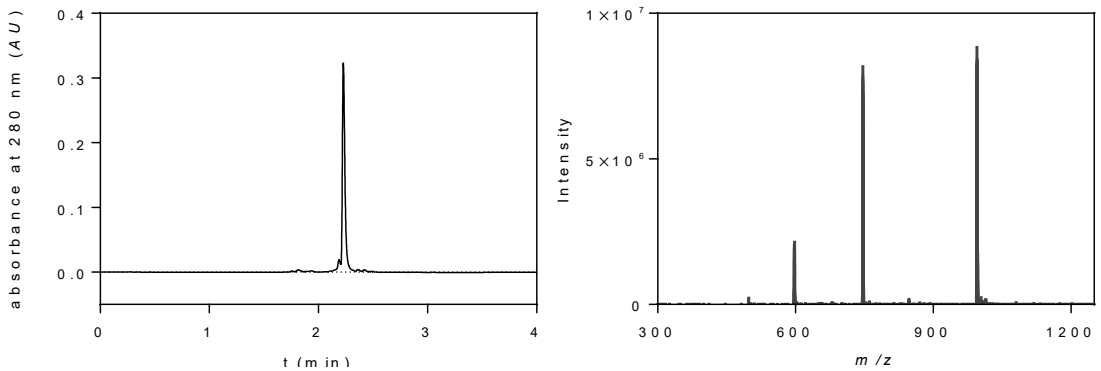

13 **Cys-P3-C343** Cys-EIQQLEE EIAQLEQ KNAALKE KNQALKY K(C343)-$CONH_2$. ε_{437} = 44000 L·mol^{-1}cm^{-1}; UPLC t_R = 1.97 min (20- 65% B in 4 min). ESI–MS: *m/z* = 950.7, 760.39 MW_{calc} = 3787.9 g·mol^{-1} ($C_{169}H_{270}N_{44}O_{53}S_1$: MW_{exp} = 3798.287 g·mol^{-1}: $[M+4H]^{4+}$ = 950.57, $[M+5H]^{5+}$ = 760.66)

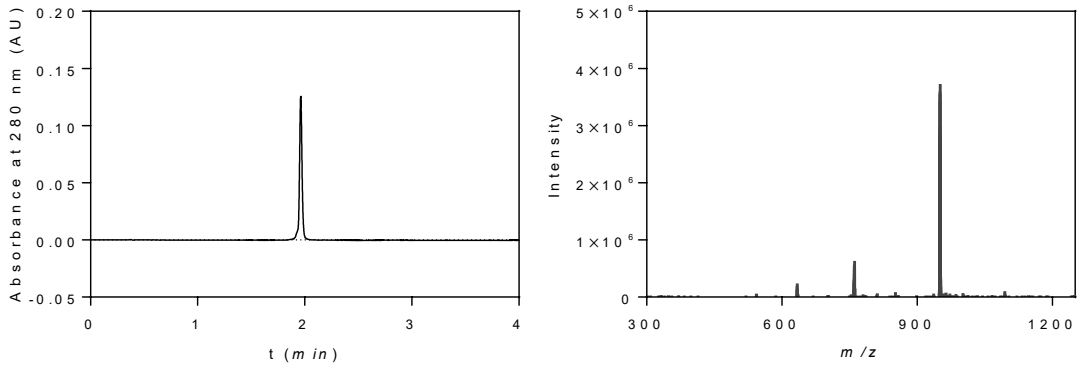

14 **Cys-P3-TAMRA** Cys-EIQQLEE EIAQLEQ KNAALKE KNQALKY K(TAMRA)-$CONH_2$. ε_{556} = 95000 L·mol^{-1}cm^{-1}; UPLC t_R = 1.73 min (20- 65% B in 4 min). ESI–MS: *m/z* = 986.95, 789.51, MW_{calc} = 3943.18 g·mol^{-1} ($C_{178}H_{277}N_{45}O_{54}S$: MW_{exp} = 3943.446 g·mol^{-1}: $[M+5H]^{5+}$ =986.86, $[M+6H]^{6+}$ = 789.69)

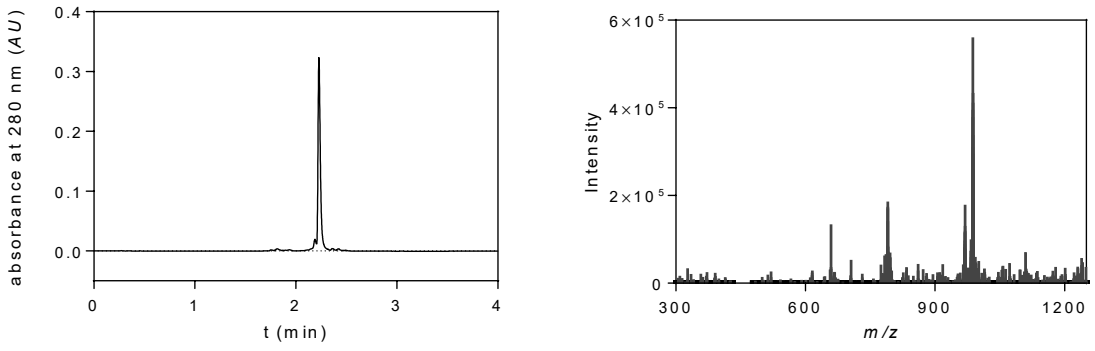

15 **2(Cys-P1-TAMRA)** disulfide of **12,** Cys-[EIQALEE EAQLEQ ENAALEE EIAQLEY G K(TAMRA)-$CONH_2$]$_2$. Yield: 40%. ε_{556} = 190000 L·mol^{-1}cm^{-1}; FLR–UPLC t_R = 2.86 min (15-45% B in 4 min). (ESI–MS: *m/z* = 790.46, 878.82, 987.78, 1128.54, MW_{calc} = 7895.5 g·mol^{-1} ($C_{348}H_{516}N_{82}O_{124}S_2$: MW_{exp} = 7896.441 g·mol^{-1}: $[M+7H]^{7+}$ = 1129.06, $[M+8H]^{8+}$ = 988.06, $[M+9H]^{9+}$ = 878.38, $[M+10H]^{10+}$ = 790.64)

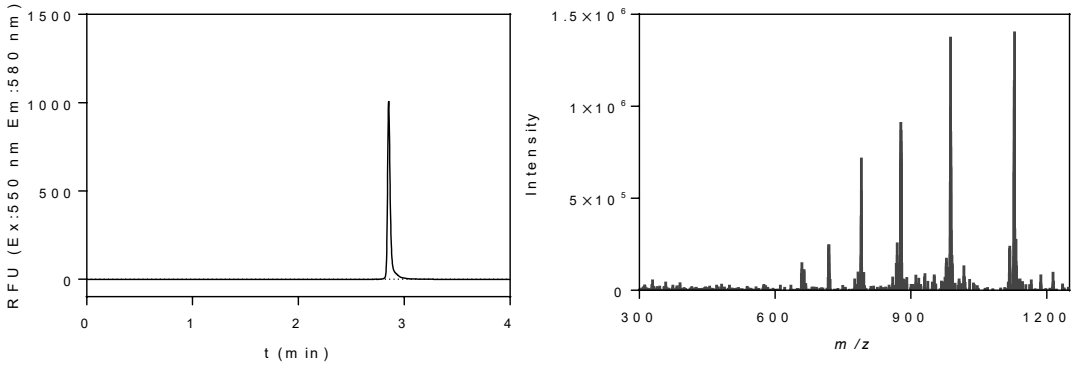

16 **2(Cys-P3-C343**) disulfide of **13,** Cys[Cys-EIQQLEE EIAQLEQ KNAALKE KNQALKY K(C343)-$CONH_2$]$_2$. Yield: 60 %. ε_{437} = 88000 L·mol^{-1}cm^{-1}; UPLC t_R = 2.15 min (20- 65% B in 4 min). ESI–MS: *m/z* = 1085.8, 950.1, 844.8, 760.5, MW_{calc} = 7593.9 g·mol^{-1} ($C_{338}H_{538}N_{88}O_{106}S_2$: MW_{exp} = 7594.569 g·mol^{-1}: $[M+7H]^{7+}$ = 1085.94, $[M+8H]^{8+}$ = 950.32, $[M+9H]^{9+}$ = 844.84, $[M+10H]^{10+}$ = 760.46)

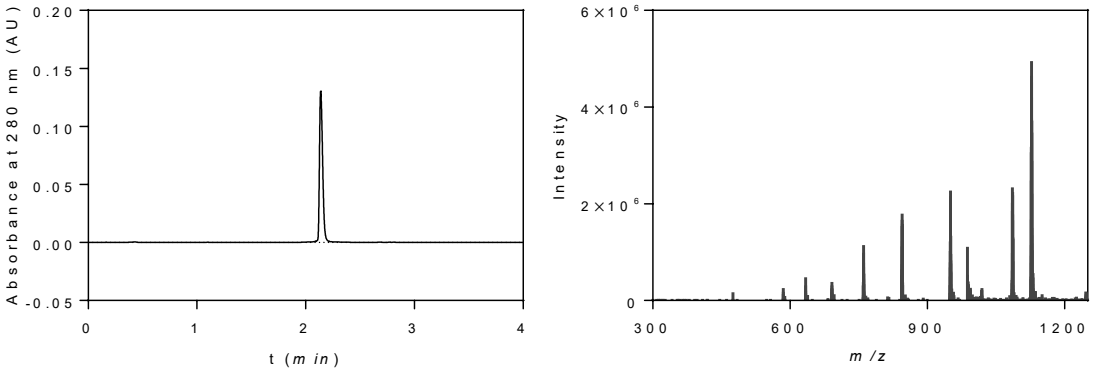

17 **2(Cys-P3-TAMRA**) disulfide of **14,** Cys[EIQQLEE EIAQLEQ KNAALKE KNQALKY K(TAMRA)-$CONH_2$]$_2$. Yield: 54 %. ε_{556} = 190000 L·mol^{-1}cm^{-1}; UPLC t_R = 1.90 min (20- 65% B in 4 min). ESI–MS: *m/z* = 1127.80, 986.95, 877.11, 789.51, MW_{calc} = 7885.7 g·mol^{-1} ($C_{178}H_{277}N_{45}O_{54}S$: MW_{exp} = 7884.875 g·mol^{-1}: $[M+7H]^{7+}$ =1227.41, $[M+8H]^{8+}$ =986.61, $[M+9H]^{9+}$ =877.10, $[M+10H]^{10+}$ = 789.49)

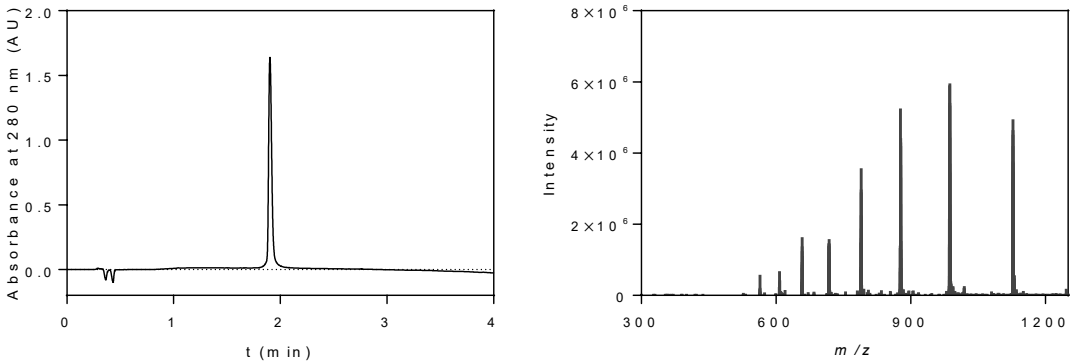

18 **Cys-E3-TAMRA** Cys-EIAALEK EIAALEK EIAALEK GK(TAMRA)-$CONH_2$. Yield: 18 %. ε_{556} = 95000 L·mol^{-1}cm^{-1}; UPLC t_R = 2.89 min (10-70% B in 4 min). ESI–MS: *m/z* = 995.14, 746.75, 597.41, MW_{calc} = 2982.49 g·mol^{-1} ($C_{138}H_{217}N_{31}O_{40}S$: MW_{exp} =2982.45 g·mol^{-1}: $[M+3H]^{3+}$ =995.2, $[M+4H]^{4+}$ = 746.6, $[M+5H]^{5+}$ = 597.5.

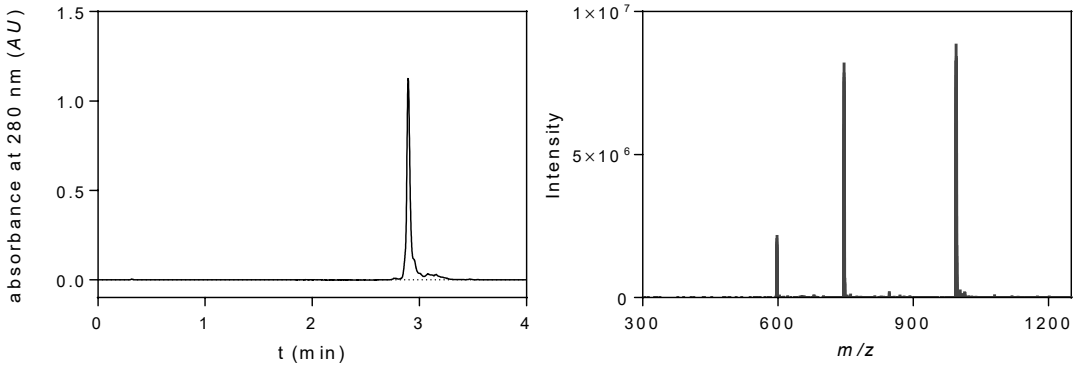

19 **Ac-G-MPAA-K3** Ac-G-MPAA-AEEAc-KIAALKE KIAALKE KIAALKE G-NH_2. ε_{214} =28942 L·mol^{-1}cm^{-1}; UPLC t_R = 1.39 min (20-60% B in 4 min). ESI–MS: *m/z* =910.78, 693.44, 546.76, MW_{calc} = 2729.3 g·mol^{-1} ($C_{125}H_{217}N_{31}O_{34}S$: MW_{exp} =2730.32 g·mol^{-1}: $[M+3H]^{3+}$ = 911.11, $[M+4H]^{4+}$ = 683.58, $[M+5H]^{5+}$ =547.06)

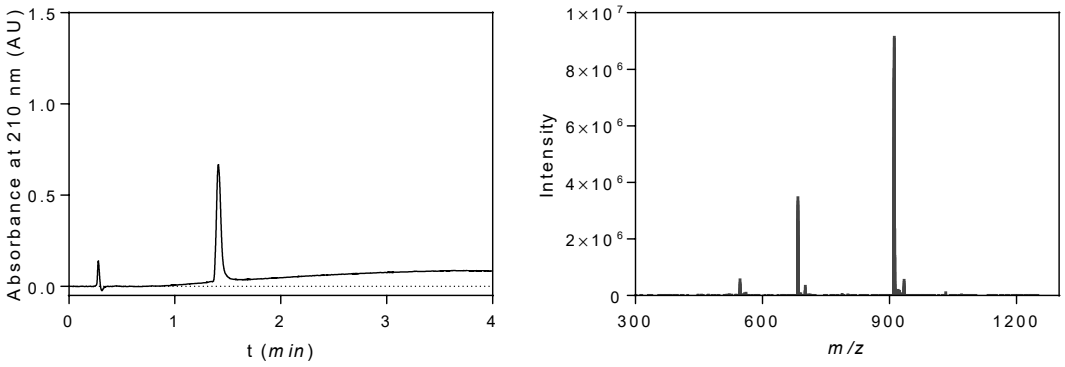

20 **Azhx-Cys(Azhx)-E3** $N_3(CH_2)_5(CO)$-Cys($N_3(CH_2)_5(CO)$)-EIAALEK EIAALEK EIAALKE G-NH_2. ε_{214} = 23972 $L \cdot mol^{-1}cm^{-1}$; UPLC t_R = 2.07 min (40-90% B in 4 min). ESI–MS: *m/z* = 907.57, MW_{calc} = 2719.71 $g \cdot mol^{-1}$ ($C_{119}H_{203}N_{33}O_{37}S$: MW_{exp} = 2720.15 $g \cdot mol^{-1}$; $[M+2H]^{2+}$ = 907.72)

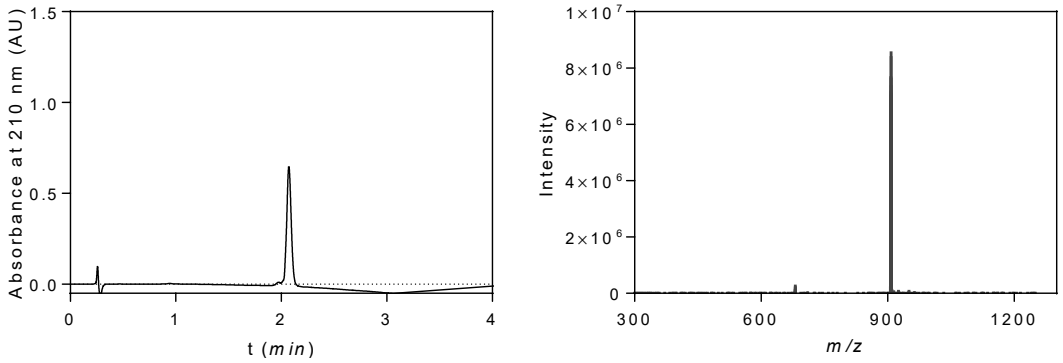

21 **MPAA-AEEAc-K3** MPAA-AEEAc-KIAALKE KIAALKE KIAALKE G-NH_2. ε_{214} = 27391 $L \cdot mol^{-1}cm^{-1}$; UPLC t_R = 1.76 min (25-55% B in 4 min). ESI–MS: *m/z* = 877.79, 658.75, MW_{calc} = 2630.69 $g \cdot mol^{-1}$. ($C_{121}H_{212}N_{30}O_{32}S$: MW_{exp} = 2631.23 $g \cdot mol^{-1}$: $[M+3H]^{3+}$ = 877.52, $[M+4H]^{4+}$ = 658.39)

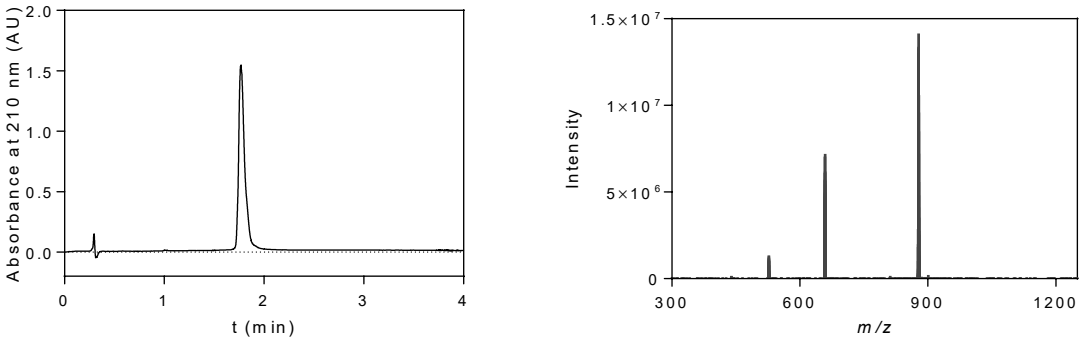

22 Cys-AEEAc-KIAALKE KIAALKE KIAALKE G-NH_2. ε_{214} = 23340 $L \cdot mol^{-1}cm^{-1}$, UPLC t_R = 2.25 min (10-70% B in 4 min). ESI–MS: *m/z* = 862.15,

646.98, 517.90, MW_{calc} = 2583.96 g·mol^{-1} ($C_{116}H_{211}N_{31}O_{32}S$: MW_{exp} = 2584.16 g·mol^{-1}: $[M+3H]^{3+}$ = 862.39, $[M+4H]^{4+}$ = 647.04, $[M+5H]^{5+}$ = 517.84)

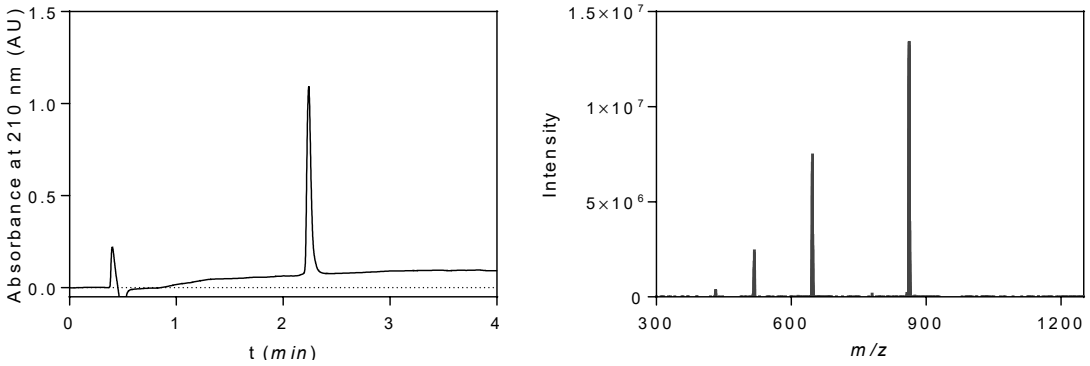

23 Cys-AEEAc-KIAALKE KIAALKE KIAALKE KIA G-NH_2. ε_{214} = 25304 L·mol^{-1}cm^{-1}; UPLC t_R = 2.02 min (10-70% B in 4 min). ESI–MS: *m/z* = 966.37, 725.09, 580.19, MW_{calc} = 2896.14 g·mol^{-1} ($C_{131}H_{239}N_{39}O_{38}S$: MW_{exp} = 2896.58 g·mol^{-1}: $[M+3H]^{3+}$ = 966.53, $[M+4H]^{4+}$ = 725.15, $[M+5H]^{5+}$ = 580.31)

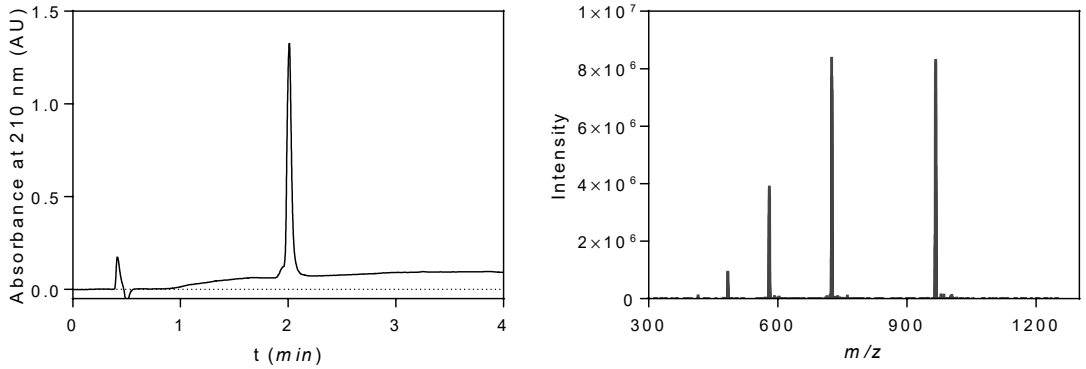

24 Cys-AEEAc-KIAALKE KIAALKE KIAALKE KIAAL G-NH_2. ε_{214} = 27227 L·mol^{-1}cm^{-1}; UPLC t_R = 2.30 min (10-70% B in 4 min). ESI–MS: *m/z* =1027.94, 771.28, 617.32, MW_{calc} = 3081.18 g·mol^{-1} ($C_{140}H_{255}N_{37}O_{37}S$: MW_{exp} = 3080.8 g·mol^{-1}: $[M+3H]^{3+}$ = 877.52 $[M+2H]^{2+}$ = 658.39.

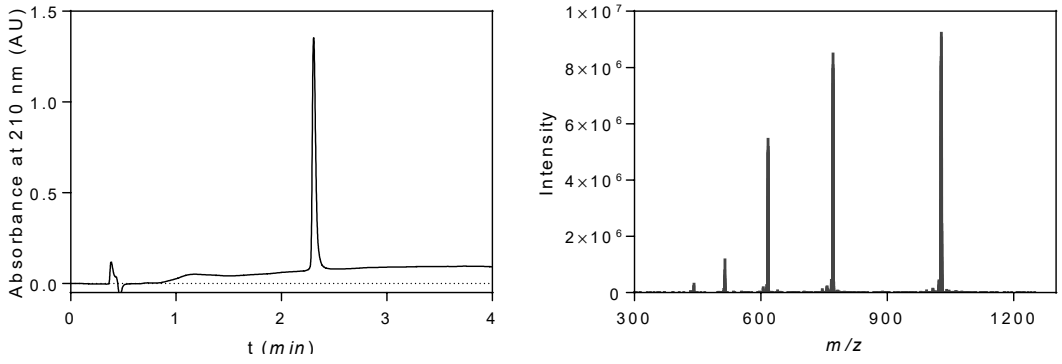

6.9. Abbreviations

Ac	Acetyl
ACP	Acyl carrier protein
ALO	Aryl-less octyne; 2-(cyclooct-2-yn-1-yloxy)acetic acid
Ahx	6-aminohexanoicacid
Azhx	6-azidohexanoic acid
AEEAc	[2-[2-amino)ethoxy]ethoxy]acetic acid
BCN	bicyclo[6.1.0]nonyne
Boc	*tert*-Butyloxycarbonyl
BRET	Bioluminescence resonance energy transfer
BSA	Bovine serum albumin
Bzl	Benzyl
ß2AR	ß2-adrenergic receptor
CHAPS	3-[(3-cholamidopropyl)-dimethylammonio]-1-propanesulfonate
CHO	Chinese hamster ovary
CLEM	Correlative light electron microscopy
CoA	Coenyzme A
CuAAC	Copper-catalyzed azide-alkyne cycloaddition
C343	Coumarin343
DCM	Dichloromethane
DIBO	Dibenzylcyclooctyne
DIC	*N,N'*-Diisopropylcarbodiimide
DCC	*N,N'*-Dicyclohexylcarbodiimide
DIPEA	*N,N*-Diisopropylethylamine
DMAP	4-Dimethylaminopyridine
DMF	*N,N*-Dimethylformamide
DMSO	Dimethylsulfoxide
DNA	Deoxyribonucleic acid
dsDNA	Double stranded DNA
dSTORM	Direct stochastic optical reconstruction microscopy
eDHFR	*Escherichia coli* dihydrofolate reductase
EDT	Ethane-(1,2)-dithiol
EGF	Epidermal growth factor
EGFR	Epidermal growth factor receptor
ErbB2	Human epidermal growth factor receptor 2
ESI	Electrospray ionization

ET-1	Endothelin 1
ET_BR	Endothelin receptor type B
E3	$(EIAALEK)_3$
FKBP	FK506 binding protein
FlAsH	Fluorescein Arsenical Helix binder
FLR–UPLC	Fluorescence Ultra Performance Liquid Chromatography
FP	Fluorescent protein
FRET	Fluorescence resonance energy transfer
GFP	Green fluorescent protein
GPCR	G-Protein coupled receptor
HATU	1-[Bis(dimethylamino)methylene]-1H-1,2,3-triazolo[4,5-b]pyridinium 3-oxid hexafluorophosphate
HCTU	2-(6-Chloro-1-H-benzotriazole-1-yl)-1,1,3,3-tetramethylaminium hexafluorophosphate
hAGT	Human O^6-alkylguanine-DNA alkyltransferase
HEK293	Human embryonic kidney 293 cells
HER2	Human epidermal growth factor receptor 2
hY2R	Human neuropeptide Y2 receptor
HPLC	High-performance liquid chromatography
K3	$(KIAALKE)_3$
LNA	Locked nucleic acid
mAb	Monoclonal antibody
MeCN	Acetonitrile
MESNA	2-Mercaptoethane sulfonate sodium salt
Mmt	4-Monomethoxytrityl
MPAA	4-Mercaptophenylacetic acid
MS	Mass spectrometry
NBD	Nitrobenzo-2-oxa-1,3-diazole
NCL	Native chemical ligation
NIR	Near-infrared
NK1R	Neurokinin 1
NMM	*N*-methylmorpholine
OxymaPure	Ethyl cyano(hydroxyamino)acetate
PAINT	Point Accumulation for Imaging in Nanoscale Topography
PALM	Photo-activated localization microscopy
PBS	Phosphate buffered saline
PCP	Peptidyl carrier protein
PCR	Polymerase chain reaction

PEG	Polyethylene glycol
PET	Photo induced electron transfer
PNA	Peptide nucleic acid
PyBroP	Bromo-tris-pyrrolidino-phosphonium hexafluorophosphate
RAM	Rink Amide
tBu	*tert*-Butyl
TCEP	Tris-(2-carboxyethyl)phosphine
TAMRA	(5/6)-Carboxytetramethylrhodamine
TFA	Trifluoroacetic acid
TIS	Triisopropylsilane
Trt	Trityl
TUV	Tuneableultraviolet
QDot	Quantum dot
RFU	Relative fluorescence units
RP	Reverse phase
RT	Room temperature
RTK	Receptor tyrosine kinase
SPAAC	Strain-promoted azide-alkyne cycloaddition
SPPS	Solid-phase peptide synthesis
SRM	Super resolution microscopy
ssDNA	Single stranded DNA
STED	Stimulated emission depletion microscopy
TBS	*tris*-buffered saline
TCEP	*tris*(2-carboxyethyl)phosphine
TfR1	Transferrin receptor 1
TMP	Trimethoprim
TMSD	Toehold-mediated strand displacement
Tris	*tris*(Hydroxymethyl)aminomethane
UPLC	Ultra-performance liquid chromatography
UV	Ultraviolet
VIP	Versatile interacting peptide
XIAP	X-Linked inhibitor of apoptosis protein
YFP	Yellow Fluorescence Protein

7. References

1 Gronemeyer, T., Chidley, C., Juillerat, A., Heinis, C. & Johnsson, K. Directed evolution of O6-alkylguanine-DNA alkyltransferase for applications in protein labeling. *Protein Engineering, Design and Selection* **19**, 309-316 (2006). https://doi.org:10.1093/protein/gzl014

2 Specht, E. A., Braselmann, E. & Palmer, A. E. A Critical and Comparative Review of Fluorescent Tools for Live-Cell Imaging. *Annual Review of Physiology* **79**, 93-117 (2017). https://doi.org:10.1146/annurev-physiol-022516-034055

3 Giepmans, B. N. G., Adams, S. R., Ellisman, M. H. & Tsien, R. Y. The Fluorescent Toolbox for Assessing Protein Location and Function. *Science* **312**, 217-224 (2006). https://doi.org:10.1126/science.1124618

4 Schneider, A. F. L. & Hackenberger, C. P. R. Fluorescent labelling in living cells. *Current Opinion in Biotechnology* **48**, 61-68 (2017). https://doi.org:10.1016/j.copbio.2017.03.012

5 Xue, L., Karpenko, I. A., Hiblot, J. & Johnsson, K. Imaging and manipulating proteins in live cells through covalent labeling. *Nature Chemical Biology* **11**, 917-923 (2015). https://doi.org:10.1038/nchembio.1959

6 Jung, D., Min, K., Jung, J., Jang, W. & Kwon, Y. Chemical biology-based approaches on fluorescent labeling of proteins in live cells. *Molecular BioSystems* **9**, 862-872 (2013). https://doi.org:10.1039/C2MB25422K

7 Schultz, C., Schleifenbaum, A., Goedhart, J. & Gadella Jr., T. W. J. Multiparameter Imaging for the Analysis of Intracellular Signaling. *ChemBioChem* **6**, 1323-1330 (2005). https://doi.org:10.1002/cbic.200500012

8 Weidtkamp-Peters, S. *et al.* Multiparameter fluorescence image spectroscopy to study molecular interactions. *Photochemical & Photobiological Sciences* **8**, 470-480 (2009). https://doi.org:10.1039/B903245M

9 Grecco, H. E., Imtiaz, S. & Zamir, E. Multiplexed imaging of intracellular protein networks. *Cytometry Part A* **89**, 761-775 (2016). https://doi.org:10.1002/cyto.a.22876

10 Xia, T., Li, N. & Fang, X. Single-Molecule Fluorescence Imaging in Living Cells. *Annual Review of Physical Chemistry* **64**, 459-480 (2013). https://doi.org:10.1146/annurev-physchem-040412-110127

11 Sahl, S. J., Hell, S. W. & Jakobs, S. Fluorescence nanoscopy in cell biology. *Nature Reviews Molecular Cell Biology* **18**, 685-701 (2017). https://doi.org:10.1038/nrm.2017.71

12 Yano, Y. & Matsuzaki, K. Tag–probe labeling methods for live-cell imaging of membrane proteins. *Biochimica et Biophysica Acta (BBA) - Biomembranes* **1788**, 2124-2131 (2009). https://doi.org:10.1016/j.bbamem.2009.07.017

13 Schnitzbauer, J., Strauss, M. T., Schlichthaerle, T., Schueder, F. & Jungmann, R. Super-resolution microscopy with DNA-PAINT. *Nature Protocols* **12**, 1198-1228 (2017). https://doi.org:10.1038/nprot.2017.024

14 Zieba, A., Ponten, F., Uhlén, M. & Landegren, U. In situ protein detection with enhanced specificity using DNA-conjugated antibodies and proximity ligation. *Modern Pathology* **31**, 253-263 (2018). https://doi.org:10.1038/modpathol.2017.102

15 Liszczak, G. & Muir, T. W. Nucleic Acid-Barcoding Technologies: Converting DNA Sequencing into a Broad-Spectrum Molecular Counter. *Angewandte Chemie International Edition* **58**, 4144-4162 (2019). https://doi.org:10.1002/anie.201808956

16 Lovendahl, K. N., Hayward, A. N. & Gordon, W. R. Sequence-Directed Covalent Protein–DNA Linkages in a Single Step Using HUH-Tags. *Journal of the American Chemical Society* **139**, 7030-7035 (2017). https://doi.org:10.1021/jacs.7b02572

17 Liang, S. I. *et al.* Phosphorylated EGFR Dimers Are Not Sufficient to Activate Ras. *Cell Reports* **22**, 2593-2600 (2018). https://doi.org:10.1016/j.celrep.2018.02.031

18 Stearns, T. Green Flourescent Protein: The green revolution. *Current Biology* **5**, 262-264 (1995). https://doi.org:10.1016/S0960-9822(95)00056-X

19 Adams, S. R., Harootunian, A. T., Buechler, Y. J., Taylor, S. S. & Tsien, R. Y. Fluorescence ratio imaging of cyclic AMP in single cells. *Nature* **349**, 694-697 (1991). https://doi.org:10.1038/349694a0

20 Gould, S. J. & Subramani, S. Firefly luciferase as a tool in molecular and cell biology. *Analytical Biochemistry* **175**, 5-13 (1988). https://doi.org:10.1016/0003-2697(88)90353-3

21 Stewaært, G. S. A. B. & Williams, P. lux genes and the applications of bacterial bioluminescence. *The Journal of General Microbiology* **138**, 1289-1300 (1992). https://doi.org:10.1099/00221287-138-7-1289

22 Shimomura, O., Johnson, F. H. & Saiga, Y. Extraction, Purification and Properties of Aequorin, a Bioluminescent Protein from the Luminous Hydromedusan, Aequorea. *Journal of Cellular Physiology* **59**, 223-239 (1962). https://doi.org:10.1002/jcp.1030590302

23 Morise, H., Shimomura, O., Johnson, F. H. & Winant, J. Intermolecular energy transfer in the bioluminescent system of Aequorea. *Biochemistry* **13**, 2656-2662 (1974). https://doi.org:10.1021/bi00709a028

24 Prasher, D. C., Eckenrode, V. K., Ward, W. W., Prendergast, F. G. & Cormier, M. J. Primary structure of the Aequorea victoria green-fluorescent protein. *Gene* **111**, 229-233 (1992). https://doi.org:10.1016/0378-1119(92)90691-H

25 Chalfie, M., Tu, Y., Euskirchen, G., Ward, W. W. & Prasher, D. C. Green fluorescent protein as a marker for gene expression. *Science* **263**, 802-805 (1994). https://doi.org:10.1126/science.8303295

26 Heim, R., Prasher, D. C. & Tsien, R. Y. Wavelength mutations and posttranslational autoxidation of green fluorescent protein. *Proceedings of the National Academy of Sciences* **91**, 12501-12504 (1994). https://doi.org:10.1073/pnas.91.26.12501

27 Heim, R., Cubitt, A. B. & Tsien, R. Y. Improved green fluorescence. *Nature* **373**, 663-664 (1995). https://doi.org:10.1038/373663b0

28 Day, R. N. & Davidson, M. W. The fluorescent protein palette: tools for cellular imaging. *Chemical Society Reviews* **38**, 2887-2921 (2009). https://doi.org:10.1039/B901966A

29 Renz, M. Fluorescence microscopy—A historical and technical perspective. *Cytometry Part A* **83**, 767-779 (2013). https://doi.org:10.1002/cyto.a.22295

30 Livet, J. *et al.* Transgenic strategies for combinatorial expression of fluorescent proteins in the nervous system. *Nature* **450**, 56-62 (2007). https://doi.org:10.1038/nature06293

31 Nobel Media AB 2021. *The Nobel Prize in Chemistry 2008*, <https://www.nobelprize.org/prizes/chemistry/2008/summary/> (

32 Hoffmann, C. *et al.* A FlAsH-based FRET approach to determine G protein–coupled receptor activation in living cells. *Nature Methods* **2**, 171-176 (2005). https://doi.org:10.1038/nmeth742

33 Vreja, I. C. *et al.* Super-resolution Microscopy of Clickable Amino Acids Reveals the Effects of Fluorescent Protein Tagging on Protein Assemblies. *ACS Nano* **9**, 11034-11041 (2015). https://doi.org:10.1021/acsnano.5b04434

34 Sokolovski, M., Bhattacherjee, A., Kessler, N., Levy, Y. & Horovitz, A. Thermodynamic Protein Destabilization by GFP Tagging: A Case of Interdomain Allostery. *Biophysical Journal* **109**, 1157-1162 (2015). https://doi.org:10.1016/j.bpj.2015.04.032

35 Gelman, H., Wirth, A. J. & Gruebele, M. ReAsH as a Quantitative Probe of In-Cell Protein Dynamics. *Biochemistry* **55**, 1968-1976 (2016). https://doi.org:10.1021/acs.biochem.5b01336

36 Lichtman, J. W., Livet, J. & Sanes, J. R. A technicolour approach to the connectome. *Nat Rev Neurosci* **9**, 417-422 (2008). https://doi.org:10.1038/nrn2391

37 Marshall, J., Molloy, R., Moss, G. W. J., Howe, J. R. & Hughes, T. E. The jellyfish green fluorescent protein: A new tool for studying ion channel expression and function. *Neuron* **14**, 211-215 (1995). https://doi.org:10.1016/0896-6273(95)90279-1

38 Neubert, F. *et al.* Bioorthogonal Click Chemistry Enables Site-specific Fluorescence Labeling of Functional NMDA Receptors for Super-Resolution Imaging. *Angew Chem Int Ed* **57**, 16364-16369 (2018). https://doi.org:10.1002/anie.201808951

39 Griffin, B. A., Adams, S. R. & Tsien, R. Y. Specific Covalent Labeling of Recombinant Protein Molecules Inside Live Cells. *Science* **281**, 269-272 (1998). https://doi.org:10.1126/science.281.5374.269

40 Adams, S. R. *et al.* New Biarsenical Ligands and Tetracysteine Motifs for Protein Labeling in Vitro and in Vivo: Synthesis and Biological Applications. *Journal of the American Chemical Society* **124**, 6063-6076 (2002). https://doi.org:10.1021/ja017687n

41 Fu, Y. & Finney, N. S. Small-molecule fluorescent probes and their design. *RSC Advances* **8**, 29051-29061 (2018). https://doi.org:10.1039/C8RA02297F

42 Grimm, J. B. *et al.* A general method to improve fluorophores for live-cell and single-molecule microscopy. *Nature Methods* **12**, 244-250 (2015). https://doi.org:10.1038/nmeth.3256

43 Zheng, Q. *et al.* Ultra-stable organic fluorophores for single-molecule research. *Chemical Society Reviews* **43**, 1044-1056 (2014). https://doi.org:10.1039/C3CS60237K

44 Hong, G., Antaris, A. L. & Dai, H. Near-infrared fluorophores for biomedical imaging. *Nature Biomedical Engineering* **1**, 0010 (2017). https://doi.org:10.1038/s41551-016-0010

45 Fölling, J. *et al.* Photochromic Rhodamines Provide Nanoscopy with Optical Sectioning. *Angew Chem Int Ed* **46**, 6266-6270 (2007). https://doi.org:10.1002/anie.200702167

46 Fernández-Suárez, M. & Ting, A. Y. Fluorescent probes for super-resolution imaging in living cells. *Nature Reviews Molecular Cell Biology* **9**, 929-943 (2008). https://doi.org:10.1038/nrm2531

47 Grimm, J. B. *et al.* Bright photoactivatable fluorophores for single-molecule imaging. *Nature Methods* **13**, 985-988 (2016). https://doi.org:10.1038/nmeth.4034

48 Li, P. *et al.* A near-infrared fluorescent probe for detecting copper(ii) with high selectivity and sensitivity and its biological imaging applications. *Chemical Communications* **47**, 7755-7757 (2011). https://doi.org:10.1039/C1CC11885D

49 Choi, C. P. *et al.* A photoactivatable crosslinking system reveals protein interactions in the Toxoplasma gondii inner membrane complex. *PLOS Biology* **17**, e3000475 (2019). https://doi.org:10.1371/journal.pbio.3000475

50 Resch-Genger, U., Grabolle, M., Cavaliere-Jaricot, S., Nitschke, R. & Nann, T. Quantum dots versus organic dyes as fluorescent labels. *Nature Methods* **5**, 763-775 (2008). https://doi.org:10.1038/nmeth.1248

51 Overington, J. P., Al-Lazikani, B. & Hopkins, A. L. How many drug targets are there? *Nature Reviews Drug Discovery* **5**, 993-996 (2006). https://doi.org:10.1038/nrd2199

52 Yano, Y., Kondo, K., Kitani, R., Yamamoto, A. & Matsuzaki, K. Cholesterol-Induced Lipophobic Interaction between Transmembrane Helices Using Ensemble and Single-Molecule Fluorescence Resonance Energy Transfer. *Biochemistry* **54**, 1371-1379 (2015). https://doi.org:10.1021/bi501528e

53 Yano, Y. *et al.* GXXXG-Mediated Parallel and Antiparallel Dimerization of Transmembrane Helices and Its Inhibition by Cholesterol: Single-Pair FRET and 2D IR Studies. *Angew Chem Int Ed* **56**, 1756-1759 (2017). https://doi.org:10.1002/anie.201609708

54 van Meer, G., Voelker, D. R. & Feigenson, G. W. Membrane lipids: where they are and how they behave. *Nature Reviews Molecular Cell Biology* **9**, 112-124 (2008). https://doi.org:10.1038/nrm2330

55 Mitra, K., Ubarretxena-Belandia, I., Taguchi, T., Warren, G. & Engelman, D. M. Modulation of the bilayer thickness of exocytic pathway membranes by membrane proteins rather than cholesterol. *Proceedings of the National Academy of Sciences* **101**, 4083-4088 (2004). https://doi.org:10.1073/pnas.0307332101

56 Wolf, P., Gavins, G., Beck-Sickinger, A. G. & Seitz, O. Strategies for Site-Specific Labeling of Receptor Proteins on the Surfaces of Living Cells by Using Genetically Encoded Peptide Tags. *ChemBioChem* **22** (2021). https://doi.org:10.1002/cbic.202000797

57 Yano, Y. & Matsuzaki, K. Live-cell imaging of membrane proteins by a coiled-coil labeling method—Principles and applications. *Biochimica et Biophysica Acta (BBA) - Biomembranes* **1861**, 1011-1017 (2019). https://doi.org:10.1016/j.bbamem.2019.02.009

58 Lotze, J. *et al.* Time-Resolved Tracking of Separately Internalized Neuropeptide Y2 Receptors by Two-Color Pulse-Chase. *ACS Chemical Biology* **13**, 618-627 (2018). https://doi.org:10.1021/acschembio.7b00999

59 Eklund, A. S., Ganji, M., Gavins, G., Seitz, O. & Jungmann, R. Peptide-PAINT Super-Resolution Imaging Using Transient Coiled Coil Interactions. *Nano Letters* **20**, 6732-6737 (2020). https://doi.org:10.1021/acs.nanolett.0c02620

60 Fernández-Suárez, M. *et al.* Redirecting lipoic acid ligase for cell surface protein labeling with small-molecule probes. *Nature Biotechnology* **25**, 1483-1487 (2007). https://doi.org:10.1038/nbt1355

61 Zane, H. K., Doh, J. K., Enns, C. A. & Beatty, K. E. Versatile Interacting Peptide (VIP) Tags for Labeling Proteins with Bright Chemical Reporters. *ChemBioChem* **18**, 470-474 (2017). https://doi.org:10.1002/cbic.201600627

62 Doh, J. K. *et al.* VIPER is a genetically encoded peptide tag for fluorescence and electron microscopy. *Proceedings of the National Academy of Sciences* **115**, 12961-12966 (2018). https://doi.org:10.1073/pnas.1808626115

63 Doh, J. K., Tobin, S. J. & Beatty, K. E. MiniVIPER Is a Peptide Tag for Imaging and Translocating Proteins in Cells. *Biochemistry* **59**, 3051-3059 (2020). https://doi.org:10.1021/acs.biochem.0c00526

64 Keppler, A. *et al.* A general method for the covalent labeling of fusion proteins with small molecules in vivo. *Nature Biotechnology* **21**, 86-89 (2003). https://doi.org:10.1038/nbt765

65 Jing, C. & Cornish, V. W. Chemical Tags for Labeling Proteins Inside Living Cells. *Accounts of Chemical Research* **44**, 784-792 (2011). https://doi.org:10.1021/ar200099f

66 Los, G. V. *et al.* HaloTag: A Novel Protein Labeling Technology for Cell Imaging and Protein Analysis. *ACS Chemical Biology* **3**, 373-382 (2008). https://doi.org:10.1021/cb800025k

67 Tamura, R., Jiang, F., Xie, J. & Kamiyama, D. Multiplexed labeling of cellular proteins with split fluorescent protein tags. *Communications Biology* **4**, 257 (2021). https://doi.org:10.1038/s42003-021-01780-4

68 Brotzel, F. & Mayr, H. Nucleophilicities of amino acids and peptides. *Organic & Biomolecular Chemistry* **5**, 3814-3820 (2007). https://doi.org:10.1039/B713778H

69 Uchinomiya, S.-h. *et al.* Site-specific covalent labeling of His-tag fused proteins with a reactive Ni(ii)–NTA probe. *Chemical Communications*, 5880-5882 (2009). https://doi.org:10.1039/B912025D

70 Yano, Y., Furukawa, N., Ono, S., Takeda, Y. & Matsuzaki, K. Selective amine labeling of cell surface proteins guided by coiled-coil assembly. *Biopolymers* **106**, 484-490 (2016). https://doi.org:https://doi.org/10.1002/bip.22715

71 Soh, N. Selective Chemical Labeling of Proteins with Small Fluorescent Molecules Based on Metal-Chelation Methodology. *Sensors* **8**, 1004-1024 (2008).

72 Martin, B. R., Giepmans, B. N. G., Adams, S. R. & Tsien, R. Y. Mammalian cell–based optimization of the biarsenical-binding tetracysteine motif for improved fluorescence and affinity. *Nature Biotechnology* **23**, 1308-1314 (2005). https://doi.org:10.1038/nbt1136

73 Nonaka, H., Fujishima, S.-h., Uchinomiya, S.-h., Ojida, A. & Hamachi, I. Selective Covalent Labeling of Tag-Fused GPCR Proteins on Live Cell Surface with a Synthetic Probe for Their Functional Analysis. *Journal of the American Chemical Society* **132**, 9301-9309 (2010). https://doi.org:10.1021/ja910703v

74 Gaietta, G. *et al.* Multicolor and Electron Microscopic Imaging of Connexin Trafficking. *Science* **296**, 503-507 (2002). https://doi.org:10.1126/science.1068793

75 Ojida, A. *et al.* Oligo-Asp Tag/Zn(II) Complex Probe as a New Pair for Labeling and Fluorescence Imaging of Proteins. *Journal of the American Chemical Society* **128**, 10452-10459 (2006). https://doi.org:10.1021/ja0618604

76 Kapanidis, A. N., Ebright, Y. W. & Ebright, R. H. Site-Specific Incorporation of Fluorescent Probes into Protein: Hexahistidine-Tag-Mediated Fluorescent Labeling with (Ni2+:Nitrilotriacetic Acid)n−Fluorochrome Conjugates. *Journal of the American Chemical Society* **123**, 12123-12125 (2001). https://doi.org:10.1021/ja017074a

77 Guignet, E. G., Hovius, R. & Vogel, H. Reversible site-selective labeling of membrane proteins in live cells. *Nature Biotechnology* **22**, 440-444 (2004). https://doi.org:10.1038/nbt954

78 Lata, S., Reichel, A., Brock, R., Tampé, R. & Piehler, J. High-Affinity Adaptors for Switchable Recognition of Histidine-Tagged Proteins. *Journal of the American Chemical Society* **127**, 10205-10215 (2005). https://doi.org:10.1021/ja050690c

79 Takahira, I. *et al.* Design of a binuclear Ni(II)–iminodiacetic acid (IDA) complex for selective recognition and covalent labeling of His-tag fused proteins. *Bioorganic & Medicinal Chemistry Letters* **24**, 2855-2858 (2014). https://doi.org:10.1016/j.bmcl.2014.04.096

80 Chen, I., Howarth, M., Lin, W. & Ting, A. Y. Site-specific labeling of cell surface proteins with biophysical probes using biotin ligase. *Nature Methods* **2**, 99-104 (2005). https://doi.org:10.1038/nmeth735

81 Yamamoto, T. & Nagamune, T. Expansion of the sortase-mediated labeling method for site-specific N-terminal labeling of cell surfaceproteins on living cells. *Chemical Communications*, 1022-1024 (2009). https://doi.org:10.1039/B818792D

82 Lin, C.-W. & Ting, A. Y. Transglutaminase-Catalyzed Site-Specific Conjugation of Small-Molecule Probes to Proteins in Vitro and on the Surface of Living Cells. *Journal of the American Chemical Society* **128**, 4542-4543 (2006). https://doi.org:10.1021/ja0604111

83 George, N., Pick, H., Vogel, H., Johnsson, N. & Johnsson, K. Specific Labeling of Cell Surface Proteins with Chemically Diverse Compounds. *Journal of the American Chemical Society* **126**, 8896-8897 (2004). https://doi.org:10.1021/ja048396s

84 Yin, J., Liu, F., Li, X. & Walsh, C. T. Labeling Proteins with Small Molecules by Site-Specific Posttranslational Modification. *Journal of the American Chemical Society* **126**, 7754-7755 (2004). https://doi.org:10.1021/ja047749k

85 Zhou, Z. *et al.* Genetically Encoded Short Peptide Tags for Orthogonal Protein Labeling by Sfp and AcpS Phosphopantetheinyl Transferases. *ACS Chemical Biology* **2**, 337-346 (2007). https://doi.org:10.1021/cb700054k

86 Stüber, J. C. & Plückthun, A. Labeling surface proteins with high specificity: Intrinsic limitations of phosphopantetheinyl transferase systems. *PLOS ONE* **14**, e0226579 (2019). https://doi.org:10.1371/journal.pone.0226579

87 Puthenveetil, S., Liu, D. S., White, K. A., Thompson, S. & Ting, A. Y. Yeast Display Evolution of a Kinetically Efficient 13-Amino Acid Substrate for Lipoic Acid Ligase. *Journal of the American Chemical Society* **131**, 16430-16438 (2009). https://doi.org:10.1021/ja904596f

88 Uttamapinant, C. *et al.* A fluorophore ligase for site-specific protein labeling inside living cells. *Proceedings of the National Academy of Sciences* **107**, 10914-10919 (2010). https://doi.org:10.1073/pnas.0914067107

89 Liu, D. S. *et al.* Computational design of a red fluorophore ligase for site-specific protein labeling in living cells. *Proceedings of the National Academy of Sciences* **111**, E4551-E4559 (2014). https://doi.org:10.1073/pnas.1404736111

90 Best, M., Degen, A., Baalmann, M., Schmidt, T. T. & Wombacher, R. Two-Step Protein Labeling by Using Lipoic Acid Ligase with Norbornene Substrates and Subsequent Inverse-Electron Demand Diels–Alder Reaction. *ChemBioChem* **16**, 1158-1162 (2015). https://doi.org:10.1002/cbic.201500042

91 Macias-Contreras, M., Little, K. N. & Zhu, L. in *Methods in Enzymology* Vol. 638 (ed David M. Chenoweth) 233-257 (Academic Press, 2020).

92 Hinner, M. J. & Johnsson, K. How to obtain labeled proteins and what to do with them. *Current Opinion in Biotechnology* **21**, 766-776 (2010). https://doi.org:10.1016/j.copbio.2010.09.011

93 Gautier, A. *et al.* An Engineered Protein Tag for Multiprotein Labeling in Living Cells. *Chemistry & Biology* **15**, 128-136 (2008). https://doi.org:10.1016/j.chembiol.2008.01.007

94 Marks, K. M., Braun, P. D. & Nolan, G. P. A general approach for chemical labeling and rapid, spatially controlled protein inactivation. *Proceedings of the National Academy of Sciences* **101**, 9982-9987 (2004). https://doi.org:10.1073/pnas.0401609101

95 Miller, L. W., Cai, Y., Sheetz, M. P. & Cornish, V. W. In vivo protein labeling with trimethoprim conjugates: a flexible chemical tag. *Nature Methods* **2**, 255-257 (2005). https://doi.org:10.1038/nmeth749

96 Jing, C. & Cornish, V. W. A Fluorogenic TMP-Tag for High Signal-to-Background Intracellular Live Cell Imaging. *ACS Chemical Biology* **8**, 1704-1712 (2013). https://doi.org:10.1021/cb300657r

97 Gallagher, S. S., Sable, J. E., Sheetz, M. P. & Cornish, V. W. An In Vivo Covalent TMP-Tag Based on Proximity-Induced Reactivity. *ACS Chemical Biology* **4**, 547-556 (2009). https://doi.org:10.1021/cb900062k

98 Stagge, F., Mitronova, G. Y., Belov, V. N., Wurm, C. A. & Jakobs, S. Snap-, CLIP- and Halo-Tag Labelling of Budding Yeast Cells. *PLOS ONE* **8**, e78745 (2013). https://doi.org:10.1371/journal.pone.0078745

99 Kohl, J. *et al.* Ultrafast tissue staining with chemical tags. *Proceedings of the National Academy of Sciences* **111**, E3805-E3814 (2014). https://doi.org:10.1073/pnas.1411087111

100 Nieves, D. J. *et al.* tagPAINT: covalent labelling of genetically encoded protein tags for DNA-PAINT imaging. *bioRxiv*, 604462 (2019). https://doi.org:10.1101/604462

101 Gu, G. J. *et al.* Protein tag-mediated conjugation of oligonucleotides to recombinant affinity binders for proximity ligation. *New Biotechnology* **30**, 144-152 (2013). https://doi.org:10.1016/j.nbt.2012.05.005

102 Srikun, D., Albers, A. E., Nam, C. I., Iavarone, A. T. & Chang, C. J. Organelle-Targetable Fluorescent Probes for Imaging Hydrogen Peroxide in Living Cells via SNAP-Tag Protein Labeling. *Journal of the American Chemical Society* **132**, 4455-4465 (2010). https://doi.org:10.1021/ja100117u

103 Prifti, E. *et al.* A Fluorogenic Probe for SNAP-Tagged Plasma Membrane Proteins Based on the Solvatochromic Molecule Nile Red. *ACS Chemical Biology* **9**, 606-612 (2014). https://doi.org:10.1021/cb400819c

104 Lukinavičius, G. *et al.* Selective Chemical Crosslinking Reveals a Cep57-Cep63-Cep152 Centrosomal Complex. *Current Biology* **23**, 265-270 (2013). https://doi.org:10.1016/j.cub.2012.12.030

105 Stüber, J. C., Kast, F. & Plückthun, A. High-Throughput Quantification of Surface Protein Internalization and Degradation. *ACS Chemical Biology* **14**, 1154-1163 (2019). https://doi.org:10.1021/acschembio.9b00016

106 Calebiro, D. *et al.* Single-molecule analysis of fluorescently labeled G-protein–coupled receptors reveals complexes with distinct dynamics and organization. *Proceedings of the National Academy of Sciences* **110**, 743-748 (2013). https://doi.org:10.1073/pnas.1205798110

107 Bosch, Peter J. *et al.* Evaluation of Fluorophores to Label SNAP-Tag Fused Proteins for Multicolor Single-Molecule Tracking Microscopy in Live Cells. *Biophysical Journal* **107**, 803-814 (2014). https://doi.org:10.1016/j.bpj.2014.06.040

108 Söderberg, O. *et al.* Direct observation of individual endogenous protein complexes in situ by proximity ligation. *Nature Methods* **3**, 995-1000 (2006). https://doi.org:10.1038/nmeth947

109 Belousov, V. V. *et al.* Genetically encoded fluorescent indicator for intracellular hydrogen peroxide. *Nature Methods* **3**, 281-286 (2006). https://doi.org:10.1038/nmeth866

110 Tompkins, K. J. *et al.* Molecular underpinnings of ssDNA specificity by Rep HUH-endonucleases and implications for HUH-tag multiplexing and engineering. *Nucleic Acids Research* **49**, 1046-1064 (2021). https://doi.org:10.1093/nar/gkaa1248

111 Vega-Rocha, S., Byeon, I.-J. L., Gronenborn, B., Gronenborn, A. M. & Campos-Olivas, R. Solution Structure, Divalent Metal and DNA Binding of the Endonuclease Domain from the Replication Initiation Protein from Porcine Circovirus 2. *Journal of Molecular Biology* **367**, 473-487 (2007). https://doi.org:https://doi.org/10.1016/j.jmb.2007.01.002

112 Boer, D. R. *et al.* Plasmid replication initiator RepB forms a hexamer reminiscent of ring helicases and has mobile nuclease domains. *EMBO J* **28**, 1666-1678 (2009). https://doi.org:10.1038/emboj.2009.125

113 Datta, S., Larkin, C. & Schildbach, J. F. Structural Insights into Single-Stranded DNA Binding and Cleavage by F Factor TraI. *Structure* **11**, 1369-1379 (2003). https://doi.org:https://doi.org/10.1016/j.str.2003.10.001

114 Wolf, E., Kim, P. S. & Berger, B. MultiCoil: A program for predicting two-and three-stranded coiled coils. *Protein Sci* **6**, 1179-1189 (1997). https://doi.org:10.1002/pro.5560060606

115 Cohen, C. & Parry, D. A. D. α-Helical coiled coils — a widespread motif in proteins. *Trends in Biochemical Sciences* **11**, 245-248 (1986). https://doi.org:10.1016/0968-0004(86)90186-6

116 Litowski, J. R. & Hodges, R. S. Designing heterodimeric two-stranded α-helical coiled-coils: the effect of chain length on protein folding, stability and specificity. *Journal of Peptide Science* **58**, 477-492 (2001). https://doi.org:10.1034/j.1399-3011.2001.10972.x

117 Litowski, J. R. & Hodges, R. S. Designing heterodimeric two-stranded α-helical coiled-coils. Effects of hydrophobicity and α-helical propensity on protein folding, stability, and specificity. *Journal of Biological Chemistry* **277**, 37272-37279 (2002). https://doi.org:10.1074/jbc.M204257200

118 Moutevelis, E. & Woolfson, D. N. A Periodic Table of Coiled-Coil Protein Structures. *Journal of Molecular Biology* **385**, 726-732 (2009). https://doi.org:10.1016/j.jmb.2008.11.028

119 Gradišar, H. & Jerala, R. De novo design of orthogonal peptide pairs forming parallel coiled-coil heterodimers. *Journal of Peptide Science* **17**, 100-106 (2011). https://doi.org:10.1002/psc.1331

120 Negron, C. & Keating, A. E. A Set of Computationally Designed Orthogonal Antiparallel Homodimers that Expands the Synthetic Coiled-Coil Toolkit. *Journal of the American Chemical Society* **136**, 16544-16556 (2014). https://doi.org:10.1021/ja507847t

121 Woolfson, D. N. Building fibrous biomaterials from α-helical and collagen-like coiled-coil peptides. *Peptide Science* **94**, 118-127 (2010). https://doi.org:10.1002/bip.21345

122 Thomas, F., Burgess, N. C., Thomson, A. R. & Woolfson, D. N. Controlling the Assembly of Coiled–Coil Peptide Nanotubes. *Angewandte Chemie International Edition* **55**, 987-991 (2016). https://doi.org:10.1002/anie.201509304

123 Robson Marsden, H. & Kros, A. Self-Assembly of Coiled Coils in Synthetic Biology: Inspiration and Progress. *Angewandte Chemie International Edition* **49**, 2988-3005 (2010). https://doi.org:10.1002/anie.200904943

124 Lupas, A. N. & Gruber, M. in *Advances in Protein Chemistry* Vol. 70 37-38 (Academic Press, 2005).

125 Yano, Y. *et al.* Coiled-Coil Tag−Probe System for Quick Labeling of Membrane Receptors in Living Cells. *ACS Chemical Biology* **3**, 341-345 (2008). https://doi.org:10.1021/cb8000556

126 Gröger, K. *Peptide und Peptidnukleinsäuren zur Markierung und Organisation von Rezeptoren auf lebenden Zellen*, Humboldt-Universität zu Berlin, (2018).

127 Kawano, K., Yano, Y., Omae, K., Matsuzaki, S. & Matsuzaki, K. Stoichiometric Analysis of Oligomerization of Membrane Proteins on Living Cells Using Coiled-Coil Labeling and Spectral Imaging. *Analytical Chemistry* **85**, 3454-3461 (2013). https://doi.org:10.1021/ac400177a

128 Kawano, K., Yagi, T., Fukada, N., Yano, Y. & Matsuzaki, K. Stoichiometric analysis of oligomeric states of three class-A GPCRs, chemokine-CXCR4, dopamine-D2, and prostaglandin-EP1 receptors, on living cells. *Journal of Peptide Science* **23**, 650-658 (2017). https://doi.org:10.1002/psc.3020

129 Yamashita, H., Yano, Y., Kawano, K. & Matsuzaki, K. Oligomerization–function relationship of EGFR on living cells detected by the coiled-coil labeling and FRET microscopy. *Biochimica et Biophysica Acta (BBA) - Biomembranes* **1848**, 1359-1366 (2015). https://doi.org:10.1016/j.bbamem.2015.03.004

130 Yano, Y. & Matsuzaki, K. Fluorescence ratiometric detection of ligand-induced receptor internalization using extracellular coiled-coil tag–probe labeling. *FEBS letters* **585**, 2385-2388 (2011). https://doi.org:10.1016/j.febslet.2011.06.012

131 Takeda, Y., Yano, Y. & Matsuzaki, K. High-Throughput Analysis of Ligand-Induced Internalization of β2-Adrenoceptors Using the Coiled-Coil Tag–Probe Method. *Analytical Chemistry* **84**, 1754-1759 (2012). https://doi.org:10.1021/ac203231n

132 Lambert, N. A. & Javitch, J. A. CrossTalk opposing view: Weighing the evidence for class A GPCR dimers, the jury is still out. *The Journal of Physiology* **592**, 2443-2445 (2014). https://doi.org:10.1113/jphysiol.2014.272997

133 Bouvier, M., Heveker, N., Jockers, R., Marullo, S. & Milligan, G. BRET analysis of GPCR oligomerization: newer does not mean better. *Nature Methods* **4**, 3-4 (2007). https://doi.org:10.1038/nmeth0107-3

134 Lohse, M. J. G protein—coupled receptors: too many dimers? *Nature Methods* **3**, 972-973 (2006). https://doi.org:10.1038/nmeth1206-972

135 Asher, W. B. *et al.* Single-molecule FRET imaging of GPCR dimers in living cells. *Nature Methods* **18**, 397-405 (2021). https://doi.org:10.1038/s41592-021-01081-y

136 James, J. R., Oliveira, M. I., Carmo, A. M., Iaboni, A. & Davis, S. J. A rigorous experimental framework for detecting protein oligomerization using bioluminescence resonance energy transfer. *Nature Methods* **3**, 1001-1006 (2006). https://doi.org:10.1038/nmeth978

137 Schnell, U., Dijk, F., Sjollema, K. A. & Giepmans, B. N. G. Immunolabeling artifacts and the need for live-cell imaging. *Nature Methods* **9**, 152-158 (2012). https://doi.org:10.1038/nmeth.1855

138 Salahpour, A. *et al.* Homodimerization of the β2-Adrenergic Receptor as a Prerequisite for Cell Surface Targeting*. *Journal of Biological Chemistry* **279**, 33390-33397 (2004). https://doi.org:10.1074/jbc.M403363200

139 Meyer, B. H. *et al.* FRET imaging reveals that functional neurokinin-1 receptors are monomeric and reside in membrane microdomains of live cells. *Proceedings of the National Academy of Sciences* **103**, 2138-2143 (2006). https://doi.org:10.1073/pnas.0507686103

140 Reinke, A. W., Grant, R. A. & Keating, A. E. A Synthetic Coiled-Coil Interactome Provides Heterospecific Modules for Molecular Engineering. *Journal of the American Chemical Society* **132**, 6025-6031 (2010). https://doi.org:10.1021/ja907617a

141 Moll, J. R., Ruvinov, S. B., Pastan, I. & Vinson, C. Designed heterodimerizing leucine zippers with a ranger of pIs and stabilities up to 10−15 M. *Protein Science* **10**, 649-655 (2001). https://doi.org:10.1110/ps.39401

142 Reinhardt, U. *et al.* Peptide-Templated Acyl Transfer: A Chemical Method for the Labeling of Membrane Proteins on Live Cells. *Angewandte Chemie International Edition* **53**, 10237-10241 (2014). https://doi.org:10.1002/anie.201403214

143 Fegan, A., White, B., Carlson, J. C. T. & Wagner, C. R. Chemically Controlled Protein Assembly: Techniques and Applications. *Chemical Reviews* **110**, 3315-3336 (2010). https://doi.org:10.1021/cr8002888

144 Pollock, R. & Clackson, T. Dimerizer-regulated gene expression. *Current Opinion in Biotechnology* **13**, 459-467 (2002). https://doi.org:10.1016/S0958-1669(02)00373-7

145 Thompson, K. E., Bashor, C. J., Lim, W. A. & Keating, A. E. SYNZIP Protein Interaction Toolbox: in Vitro and in Vivo Specifications of Heterospecific Coiled-Coil Interaction Domains. *ACS Synthetic Biology* **1**, 118-129 (2012). https://doi.org:10.1021/sb200015u

146 Fernandez-Rodriguez, J. & Marlovits, T. C. Induced heterodimerization and purification of two target proteins by a synthetic coiled-coil tag. *Protein Science* **21**, 511-519 (2012). https://doi.org:10.1002/pro.2035

147 Itakura, E., Sawada, I. & Matsuura, A. Dimerization of the ATRIP protein through the coiled-coil motif and its implication to the maintenance of stalled replication forks. *Mol Biol Cell* **16**, 5551-5562 (2005). https://doi.org:10.1091/mbc.e05-05-0427

148 Jungmann, R. *et al.* Multiplexed 3D cellular super-resolution imaging with DNA-PAINT and Exchange-PAINT. *Nature Methods* **11**, 313-318 (2014). https://doi.org:10.1038/nmeth.2835

149 Lebar, T., Lainšček, D., Merljak, E., Aupič, J. & Jerala, R. A tunable orthogonal coiled-coil interaction toolbox for engineering mammalian cells. *Nature Chemical Biology* (2020). https://doi.org:10.1038/s41589-019-0443-y

150 Lovejoy, B. *et al.* Crystal Structure of a Synthetic Triple-Stranded α-Helical Bundle. *Science* **259**, 1288-1293 (1993).

151 Tsutsumi, H. *et al.* Fluorogenically Active Leucine Zipper Peptides as Tag–Probe Pairs for Protein Imaging in Living Cells. *Angew Chem Int Ed* **48**, 9164-9166 (2009). https://doi.org:10.1002/anie.200903183

152 Nomura, W. *et al.* Development of crosslink-type tag-probe pairs for fluorescent imaging of proteins. *Biopolymers* **94**, 843-852 (2010). https://doi.org:10.1002/bip.21444

153 Reinhardt, U., Lotze, J., Mörl, K., Beck-Sickinger, A. G. & Seitz, O. Rapid Covalent Fluorescence Labeling of Membrane Proteins on Live Cells via Coiled-Coil Templated Acyl Transfer. *Bioconjugate Chemistry* **26**, 2106-2117 (2015). https://doi.org:10.1021/acs.bioconjchem.5b00387

154 Wang, J., Yu, Y. & Xia, J. Short Peptide Tag for Covalent Protein Labeling Based on Coiled Coils. *Bioconjugate Chemistry* **25**, 178-187 (2014). https://doi.org:10.1021/bc400498p

155 Hopkins, A. L., Mason, J. S. & Overington, J. P. Can we rationally design promiscuous drugs? *Current Opinion in Structural Biology* **16**, 127-136 (2006). https://doi.org:10.1016/j.sbi.2006.01.013

156 Strack, R. Highly multiplexed imaging. *Nature Methods* **13**, 35-35 (2016). https://doi.org:10.1038/nmeth.3706

157 Gautier, A. *et al.* An Engineered Protein Tag for Multiprotein Labeling in Living Cells. *Chemistry & Biology* **15**, 128-136 (2008). https://doi.org:10.1016/j.chembiol.2008.01.007

158 Wilmes, S. *et al.* Triple-Color Super-Resolution Imaging of Live Cells: Resolving Submicroscopic Receptor Organization in the Plasma Membrane. *Angew Chem Int Ed* **51**, 4868-4871 (2012). https://doi.org:10.1002/anie.201200853

159 Bromley, E. H. C., Sessions, R. B., Thomson, A. R. & Woolfson, D. N. Designed α-Helical Tectons for Constructing Multicomponent Synthetic Biological Systems. *Journal of the American Chemical Society* **131**, 928-930 (2009). https://doi.org:10.1021/ja804231a

160 Thomas, F., Boyle, A. L., Burton, A. J. & Woolfson, D. N. A Set of de Novo Designed Parallel Heterodimeric Coiled Coils with Quantified Dissociation Constants in the Micromolar to Sub-nanomolar Regime. *Journal of the American Chemical Society* **135**, 5161-5166 (2013). https://doi.org:10.1021/ja312310g

161 Crooks, R. O., Lathbridge, A., Panek, A. S. & Mason, J. M. Computational Prediction and Design for Creating Iteratively Larger Heterospecific Coiled Coil Sets. *Biochemistry* **56**, 1573-1584 (2017). https://doi.org:10.1021/acs.biochem.7b00047

162 Seitz, O. Templated chemistry for bioorganic synthesis and chemical biology. *Journal of Peptide Science* **25**, e3198 (2019). https://doi.org:10.1002/psc.3198

163 Dawson, P. E., Muir, T. W., Clark-Lewis, I. & Kent, S. B. H. Synthesis of Proteins by Native Chemical Ligation. *Science* **266**, 776-779 (1994).

164 Camarero, J. A., Fushman, D., Cowburn, D. & Muir, T. W. Peptide chemical ligation inside living cells: in vivo generation of a circular protein domain. *Bioorganic & Medicinal Chemistry* **9**, 2479-2484 (2001). https://doi.org: 10.1016/S0968-0896(01)00217-6

165 Vázquez, O. & Seitz, O. Templated native chemical ligation: peptide chemistry beyond protein synthesis. *Journal of Peptide Science* **20**, 78-86 (2014). https://doi.org:10.1002/psc.2602

166 Lee, D. H., Granja, J. R., Martinez, J. A., Severin, K. & Ghadiri, M. R. A self-replicating peptide. *Nature* **382**, 525-528 (1996). https://doi.org:10.1038/382525a0

167 Grossmann, T. N., Strohbach, A. & Seitz, O. Achieving Turnover in DNA-Templated Reactions. *ChemBioChem* **9**, 2185-2192 (2008). https://doi.org:10.1002/cbic.200800290

168 Ficht, S., Dose, C. & Seitz, O. As Fast and Selective as Enzymatic Ligations: Unpaired Nucleobases Increase the Selectivity of DNA-Controlled Native Chemical PNA Ligation. *ChemBioChem* **6**, 2098-2103 (2005). https://doi.org:10.1002/cbic.200500229

169 Catalano, M. J., Price, N. E. & Gates, K. S. Effective molarity in a nucleic acid-controlled reaction. *Bioorg Med Chem Lett* **26**, 2627-2630 (2016). https://doi.org:10.1016/j.bmcl.2016.04.022

170 Bruick, R. K., Dawson, P. E., Kent, S. B. H., Usman, N. & Joyce, G. F. Template-directed ligation of peptides to oligonucleotides. *Chemistry & Biology* **3**, 49-56 (1996). https://doi.org:10.1016/S1074-5521(96)90084-8

171 Ficht, S., Mattes, A. & Seitz, O. Single-Nucleotide-Specific PNA−Peptide Ligation on Synthetic and PCR DNA Templates. *Journal of the American Chemical Society* **126**, 9970-9981 (2004). https://doi.org:10.1021/ja048845o

172 Grossmann, T. N. & Seitz, O. DNA-Catalyzed Transfer of a Reporter Group. *Journal of the American Chemical Society* **128**, 15596-15597 (2006). https://doi.org:10.1021/ja0670097

173 Egholm, M. *et al.* Pna Hybridizes to Complementary Oligonucleotides Obeying the Watson-Crick Hydrogen-Bonding Rules. *Nature* **365**, 566-568 (1993).

174 Erben, A., Grossmann, T. N. & Seitz, O. DNA-Triggered Synthesis and Bioactivity of Proapoptotic Peptides. *Angewandte Chemie International Edition* **50**, 2828-2832 (2011). https://doi.org:10.1002/anie.201007103

175 Yano, Y. *et al.* Coiled-coil tag - Probe system for quick labeling of membrane receptors in living cells. *ACS Chemical Biology* **3**, 341-345 (2008). https://doi.org:10.1021/cb8000556

176 Johnson, E. C. B. & Kent, S. B. H. Insights into the Mechanism and Catalysis of the Native Chemical Ligation Reaction. *Journal of the American Chemical Society* **128**, 6640-6646 (2006). https://doi.org:10.1021/ja058344i

177 Agouridas, V. *et al.* Native Chemical Ligation and Extended Methods: Mechanisms, Catalysis, Scope, and Limitations. *Chemical Reviews* **119**, 7328-7443 (2019). https://doi.org:10.1021/acs.chemrev.8b00712

178 Seeman, N. & Sleiman, H. DNA nanotechnology. *Nature Reviews Materials* **3**, natrevmats201768 (2017). https://doi.org:10.1038/natrevmats.2017.68

179 Sano, T., Smith, C. & Cantor, C. Immuno-PCR: very sensitive antigen detection by means of specific antibody-DNA conjugates. *Science* **258**, 120-122 (1992). https://doi.org:10.1126/science.1439758

180 Wade, O. K. *et al.* 124-Color Super-resolution Imaging by Engineering DNA-PAINT Blinking Kinetics. *Nano Letters* **19**, 2641-2646 (2019). https://doi.org:10.1021/acs.nanolett.9b00508

181 Guo, S.-M. *et al.* Multiplexed and high-throughput neuronal fluorescence imaging with diffusible probes. *Nature Communications* **10**, 4377 (2019). https://doi.org:10.1038/s41467-019-12372-6

182 Zhao, Y., Sarkar, A. & Wang, X. Peptide nucleic acid based tension sensor for cellular force imaging with strong DNase resistance. *Biosensors and Bioelectronics* **150**, 111959 (2020). https://doi.org:/10.1016/j.bios.2019.111959

183 Gu, L. *et al.* Multiplex single-molecule interaction profiling of DNA-barcoded proteins. *Nature* **515**, 554-557 (2014). https://doi.org:10.1038/nature13761

184 Trads, J. B., Tørring, T. & Gothelf, K. V. Site-Selective Conjugation of Native Proteins with DNA. *Accounts of Chemical Research* **50**, 1367-1374 (2017). https://doi.org:10.1021/acs.accounts.6b00618

185 Gavins, G. C. *et al.* Live cell PNA labelling enables erasable fluorescence imaging of membrane proteins. *Nature Chemistry* **13**, 15-23 (2021). https://doi.org:10.1038/s41557-020-00584-z

186 Gavins, G. C. *et al.* Orthogonal coiled coils enable rapid covalent labelling of two distinct membrane proteins with peptide nucleic acid barcodes. *RSC Chemical Biology* **2**, 1291-1295 (2021). https://doi.org:10.1039/D1CB00126D

187 SantaLucia, J., Allawi, H. T. & Seneviratne, P. A. Improved Nearest-Neighbor Parameters for Predicting DNA Duplex Stability. *Biochemistry* **35**, 3555-3562 (1996). https://doi.org:10.1021/bi951907q

188 Panjkovich, A. & Melo, F. Comparison of different melting temperature calculation methods for short DNA sequences. *Bioinformatics* **21**, 711-722 (2004). https://doi.org:10.1093/bioinformatics/bti066

189 Giesen, U. *et al.* A formula for thermal stability (Tm) prediction of PNA/DNA duplexes. *Nucleic Acids Research* **26**, 5004-5006 (1998). https://doi.org:10.1093/nar/26.21.5004

190 Mourtas, S., Gatos, D., Kalaitzi, V., Katakalou, C. & Barlos, K. S-4-Methoxytrityl mercapto acids: synthesis and application. *Tetrahedron Letters* **42**, 6965-6967 (2001). https://doi.org:10.1016/S0040-4039(01)01423-X

191 Bernardin, A. *et al.* Copper-Free Click Chemistry for Highly Luminescent Quantum Dot Conjugates: Application to in Vivo Metabolic Imaging. *Bioconjugate Chemistry* **21**, 583-588 (2010). https://doi.org:10.1021/bc900564w

192 Simmons, C. G., Pitts, A. E., Mayfield, L. D., Shay, J. W. & Corey, D. R. Synthesis and membrane permeability of PNA-peptide conjugates. *Bioorganic & Medicinal Chemistry Letters* **7**, 3001-3006 (1997). https://doi.org:10.1016/S0960-894X(97)10136-6

193 Braasch, D. A. & Corey, D. R. Synthesis, Analysis, Purification, and Intracellular Delivery of Peptide Nucleic Acids. *Methods* **23**, 97-107 (2001). https://doi.org:https://doi.org/10.1006/meth.2000.1111

194 Di Pisa, M., Hauser, A. & Seitz, O. Maximizing Output in RNA-Programmed Peptidyl-Transfer Reactions. *Chembiochem* **18**, 872-879 (2017). https://doi.org:10.1002/cbic.201600687

195 Hjelmeland, L. M. A nondenaturing zwitterionic detergent for membrane biochemistry: design and synthesis. *Proceedings of the National Academy of Sciences* **77**, 6368-6370 (1980). https://doi.org:10.1073/pnas.77.11.6368

196 Kalipatnapu, S. & Chattopadhyay, A. Membrane Protein Solubilization: Recent Advances and Challenges in Solubilization of Serotonin1A Receptors. *IUBMB Life* **57**, 505-512 (2005). https://doi.org:10.1080/15216540500167237

197 Fairman, R., Shoemaker, K. R., York, E. J., Stewart, J. M. & Baldwin, R. L. Further studies of the helix dipole model: Effects of a free α-NH3+ or α-COO− group on helix stability. *Proteins* **5**, 1-7 (1989). https://doi.org:10.1002/prot.340050102

198 Doig, A. J. & Baldwin, R. L. N- and C-capping preferences for all 20 amino acids in alpha-helical peptides. *Protein Sci* **4**, 1325-1336 (1995). https://doi.org:10.1002/pro.5560040708

199 Greenfield, N. J., Stafford, W. E. & Hitchcock-Degregori, S. E. The effect of N-terminal acetylation on the structure of an N-terminal tropomyosin peptide and αα-tropomyosin. *Protein Science* **3**, 402-410 (1994). https://doi.org:10.1002/pro.5560030304

200 Bracher, P. J., Snyder, P. W., Bohall, B. R. & Whitesides, G. M. The Relative Rates of Thiol–Thioester Exchange and Hydrolysis for Alkyl and Aryl Thioalkanoates in Water. *Origins of Life and Evolution of Biospheres* **41**, 399-412 (2011). https://doi.org:10.1007/s11084-011-9243-4

201 Forman, H. J., Zhang, H. & Rinna, A. Glutathione: Overview of its protective roles, measurement, and biosynthesis. *Molecular Aspects of Medicine* **30**, 1-12 (2009). https://doi.org:10.1016/j.mam.2008.08.006

202 Montero, D., Tachibana, C., Rahr Winther, J. & Appenzeller-Herzog, C. Intracellular glutathione pools are heterogeneously concentrated. *Redox Biology* **1**, 508-513 (2013). https://doi.org:10.1016/j.redox.2013.10.005

203 Morgan, E., Doh, J., Beatty, K. & Reich, N. VIPERnano: Improved Live Cell Intracellular Protein Tracking. *ACS Applied Materials & Interfaces* **11**, 36383-36390 (2019). https://doi.org:10.1021/acsami.9b12679

204 Yarden, Y. & Sliwkowski, M. X. Untangling the ErbB signalling network. *Nature Reviews Molecular Cell Biology* **2**, 127-137 (2001). https://doi.org:10.1038/35052073

205 Sekhon, N., Kumbla, R. A. & Mita, M. in *Cardio-Oncology* (eds Roberta A. Gottlieb & Puja K. Mehta) 1-24 (Academic Press, 2017).

206 Ciardiello, F. *et al.* Antitumor Effect and Potentiation of Cytotoxic Drugs Activity in Human Cancer Cells by ZD-1839 (Iressa), an Epidermal Growth Factor Receptor-selective Tyrosine Kinase Inhibitor. *Clinical Cancer Research* **6**, 2053-2063 (2000).

207 Nami, B. M., H.; Wang, Z. . The Effects of Pertuzumab and Its Combination with Trastuzumab on HER2 Homodimerization and Phosphorylation. . *Cancers* **11**, 375 (2019).

208 Zhang, X., Gureasko, J., Shen, K., Cole, P. A. & Kuriyan, J. An Allosteric Mechanism for Activation of the Kinase Domain of Epidermal Growth Factor Receptor. *Cell* **125**, 1137-1149 (2006). https://doi.org:10.1016/j.cell.2006.05.013

209 Shramova, E. I., Proshkina, G. M. & Deyev, S. M. The Cause of ErbB2 Receptor Resistance to Downregulation. *Russian Journal of Bioorganic Chemistry* **44**, 279-288 (2018). https://doi.org:10.1134/S1068162018030147

210 Fehling-Kaschek, M., Peckys, D. B., Kaschek, D., Timmer, J. & Jonge, N. d. Mathematical modeling of drug-induced receptor internalization in the HER2-positive SKBR3 breast cancer cell-line. *Scientific Reports* **9**, 12709 (2019). https://doi.org:10.1038/s41598-019-49019-x

211 Hosseinzadeh Colagar, A., Amjadi, O., Valadan, R. & Rafiei, A. Minimal HER1 and HER2 expressions in CHO and HEK-293 cells cause them appropriate negative cells for HERs-related studies *Research in Molecular Medicine* **1**, 6-12 (2013). https://doi.org:10.18869/acadpub.rmm.1.3.6

212 Stief, S. M. *et al.* Loss of KDM6A confers drug resistance in acute myeloid leukemia. *Leukemia* **34**, 50-62 (2020). https://doi.org:10.1038/s41375-019-0497-6

213 Kim, A. & Pyykko, I. Size matters: versatile use of PiggyBac transposons as a genetic manipulation tool. *Molecular and Cellular Biochemistry* **354**, 301-309 (2011). https://doi.org:10.1007/s11010-011-0832-3

214 Benvin, A. L. *et al.* Fluorescent DNA Nanotags: Supramolecular Fluorescent Labels Based on Intercalating Dye Arrays Assembled on Nanostructured DNA Templates. *Journal of the American Chemical Society* **129**, 2025-2034 (2007). https://doi.org:10.1021/ja066354t

215 Thermo Fisher Scientific Inc. *Nonfixable Viability Dyes for Flow Cytometry*, <https://www.thermofisher.com/de/de/home/life-science/cell-analysis/flow-cytometry/flow-cytometry-assays-reagents/cell-viability-assays-flow-cytometry/nonfixable-viability-dyes-flow-cytometry.html> (2021).

216 Bricks, J. L., Slominskii, Y. L., Panas, I. D. & Demchenko, A. P. Fluorescent J-aggregates of cyanine dyes: basic research and applications review. *Methods and Applications in Fluorescence* **6**, 012001 (2017). https://doi.org:10.1088/2050-6120/aa8d0d

217 Mazzuca, M. Q. & Khalil, R. A. Vascular endothelin receptor type B: Structure, function and dysregulation in vascular disease. *Biochemical Pharmacology* **84**, 147-162 (2012). https://doi.org:10.1016/j.bcp.2012.03.020

218 Yamaguchi, T., Murata, Y., Fujiyoshi, Y. & Doi, T. Regulated interaction of endothelin B receptor with caveolin-1. *European Journal of Biochemistry* **270**, 1816-1827 (2003). https://doi.org:10.1046/j.1432-1033.2003.03544.x

219 Yeow, E. K. L., Melnikov, S. M., Bell, T. D. M., De Schryver, F. C. & Hofkens, J. Characterizing the Fluorescence Intermittency and Photobleaching Kinetics of Dye Molecules Immobilized on a Glass Surface. *The Journal of Physical Chemistry A* **110**, 1726-1734 (2006). https://doi.org:10.1021/jp055496r

220 Baker, M. Bright light, better labels. *Nature* **478**, 137-142 (2011). https://doi.org:10.1038/478137a

221 Tanenbaum, Marvin E., Gilbert, Luke A., Qi, Lei S., Weissman, Jonathan S. & Vale, Ronald D. A Protein-Tagging System for Signal Amplification in Gene Expression and Fluorescence Imaging. *Cell* **159**, 635-646 (2014). https://doi.org:10.1016/j.cell.2014.09.039

222 Fouz, M. F. *et al.* Bright Fluorescent Nanotags from Bottlebrush Polymers with DNA-Tipped Bristles. *ACS Central Science* **1**, 431-438 (2015). https://doi.org:10.1021/acscentsci.5b00259

223 Mooi, S. M., Keller, S. N. & Heyne, B. Forcing Aggregation of Cyanine Dyes with Salts: A Fine Line between Dimers and Higher Ordered Aggregates. *Langmuir* **30**, 9654-9662 (2014). https://doi.org:10.1021/la502124b

224 Garoff, R. A., Litzinger, E. A., Connor, R. E., Fishman, I. & Armitage, B. A. Helical Aggregation of Cyanine Dyes on DNA Templates: Effect of Dye Structure on Formation of Homo- and Heteroaggregates. *Langmuir* **18**, 6330-6337 (2002). https://doi.org:10.1021/la025742f

225 Yurke, B., Turberfield, A. J., Mills, A. P., Simmel, F. C. & Neumann, J. L. A DNA-fuelled molecular machine made of DNA. *Nature* **406**, 605-608 (2000). https://doi.org:10.1038/35020524

226 Zhang, D. Y. & Seelig, G. Dynamic DNA nanotechnology using strand-displacement reactions. *Nature Chemistry* **3**, 103 (2011). https://doi.org:10.1038/nchem.957

227 Luo, T., Fan, S., Liu, Y. & Song, J. Information processing based on DNA toehold-mediated strand displacement (TMSD) reaction. *Nanoscale* **13**, 2100-2112 (2021). https://doi.org:10.1039/D0NR07865D

228 Kundu, N., Young, B. E. & Sczepanski, J. T. Kinetics of heterochiral strand displacement from PNA–DNA heteroduplexes. *Nucleic Acids Research* (2021). https://doi.org:10.1093/nar/gkab499

229 Yurke, B. & Mills, A. P. Using DNA to Power Nanostructures. *Genetic Programming and Evolvable Machines* **4**, 111-122 (2003). https://doi.org:10.1023/A:1023928811651

230 Lerdrup, M., Hommelgaard, A. M., Grandal, M. & van Deurs, B. Geldanamycin stimulates internalization of ErbB2 in a proteasome-dependent way. *Journal of Cell Science* **119**, 85-95 (2006). https://doi.org:10.1242/jcs.02707

231 Ahsan, A. *et al.* Destabilization of the Epidermal Growth Factor Receptor (EGFR) by a Peptide That Inhibits EGFR Binding to Heat Shock Protein 90 and Receptor Dimerization. *Journal of Biological Chemistry* **288**, 26879-26886 (2013). https://doi.org:10.1074/jbc.M113.492280

232 Tan, X., Lambert, P. F., Rapraeger, A. C. & Anderson, R. A. Stress-Induced EGFR Trafficking: Mechanisms, Functions, and Therapeutic Implications. *Trends in Cell Biology* **26**, 352-366 (2016). https://doi.org:10.1016/j.tcb.2015.12.006

233 Peng, K. *et al.* Stress-induced endocytosis and degradation of epidermal growth factor receptor are two independent processes. *Cancer Cell International* **16**, 25 (2016). https://doi.org:10.1186/s12935-016-0301-x

234 Hendriks, B. S., Opresko, L. K., Wiley, H. S. & Lauffenburger, D. Quantitative Analysis of HER2-mediated Effects on HER2 and Epidermal Growth Factor Receptor Endocytosis: DISTRIBUTION OF HOMO- AND HETERODIMERS DEPENDS ON RELATIVE HER2 LEVELS. *Journal of Biological Chemistry* **278**, 23343-23351 (2003). https://doi.org:10.1074/jbc.M300477200

235 Xu, W. *et al.* Sensitivity of Mature ErbB2 to Geldanamycin Is Conferred by Its Kinase Domain and Is Mediated by the Chaperone Protein Hsp90*. *J. Biol. Chem.* **276**, 3702-3708 (2001). https://doi.org:10.1074/jbc.M006864200

236 Wolf, P. *et al.* Orthogonal Peptide-Templated Labeling Elucidates Lateral ETAR/ETBR Proximity and Reveals Altered Downstream Signaling. *ChemBioChem* **n/a** https://doi.org:https://doi.org/10.1002/cbic.202100340

237 Wang, Y. *et al.* Toehold-mediated DNA strand displacement-driven super-fast tripedal DNA walker for ultrasensitive and label-free electrochemical detection of ochratoxin A. *Analytica Chimica Acta* **1143**, 21-30 (2021). https://doi.org:https://doi.org/10.1016/j.aca.2020.11.013

238 Roloff, A. *Templatgesteuerte Reaktionen von Peptidnukleinsäuren* PhD thesis, Humboldt-Universität zu Berlin, (2014).

239 PNA Bio Inc. *PNA Bio Tool*, <https://www.pnabio.com/support/PNA_Tool.htm> (

240 Integrated DNA technologies. *OligoAnalyzer Tool*, <https://eu.idtdna.com/pages/tools/oligoanalyzer > (

241 Kuipers, B. J. H. & Gruppen, H. Prediction of Molar Extinction Coefficients of Proteins and Peptides Using UV Absorption of the Constituent Amino Acids at 214 nm To Enable Quantitative Reverse Phase High-Performance Liquid Chromatography−Mass Spectrometry Analysis. *Journal of Agricultural and Food Chemistry* **55**, 5445-5451 (2007). https://doi.org:10.1021/jf070337l

242 Stief, S. M. *et al.* Loss of KDM6A confers drug resistance in acute myeloid leukemia. *Leukemia* (2019). https://doi.org:10.1038/s41375-019-0497-6

8.1. Additional Figures

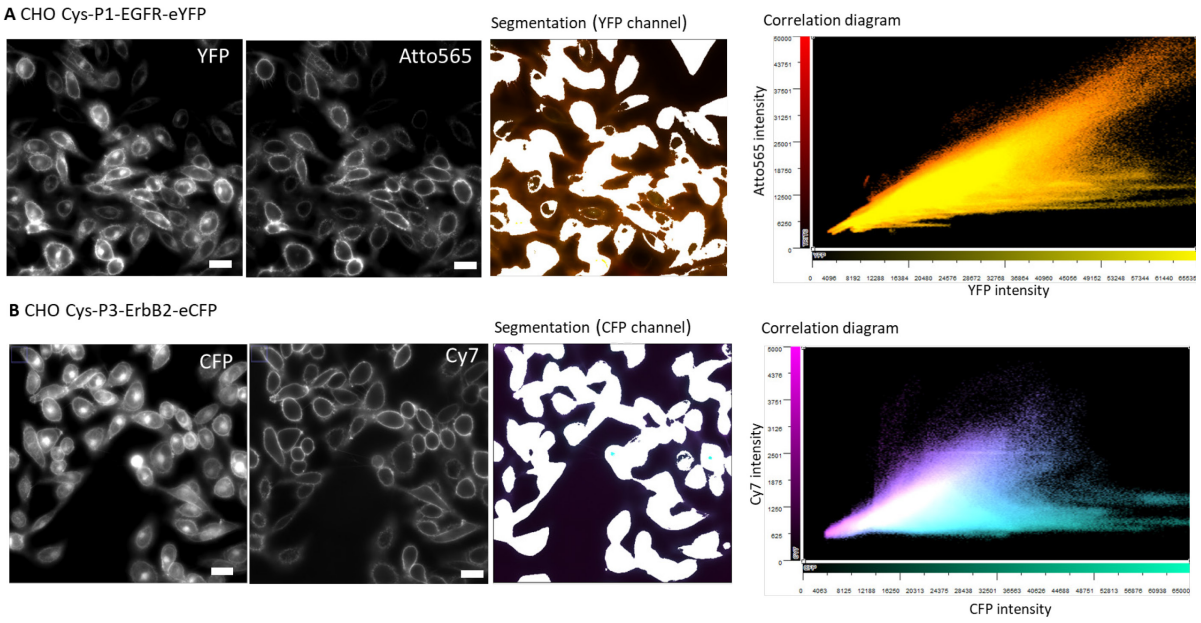

Appendix Figure 1 Correlation plots for colocalization. Fluorescence microscopy images and correlation diagram for stable CHO cells expressing A) Cys-P1-EGFR-eYFP and B) Cys-P3-ErbB2-eCFP as shown in Figure 33. After PNA labelling and DNA hybridisation with A) **10** and **Atto565-DNA1** or B) **11** and **Cy7-DNA3**, images were segmented in the fluorescent protein (YFP or CFP) channel. The pixel intensities in different channels were plotted in correlation diagrams using *cellSens* software (*OLYMPUS EUROPA SE & CO. KG*, Hamburg, Germany**)**. Excitation times: Cy7: 500 ms, Atto565: 500 ms, YFP: 200 ms, CFP 150 ms. Scale bar = 20 µm.

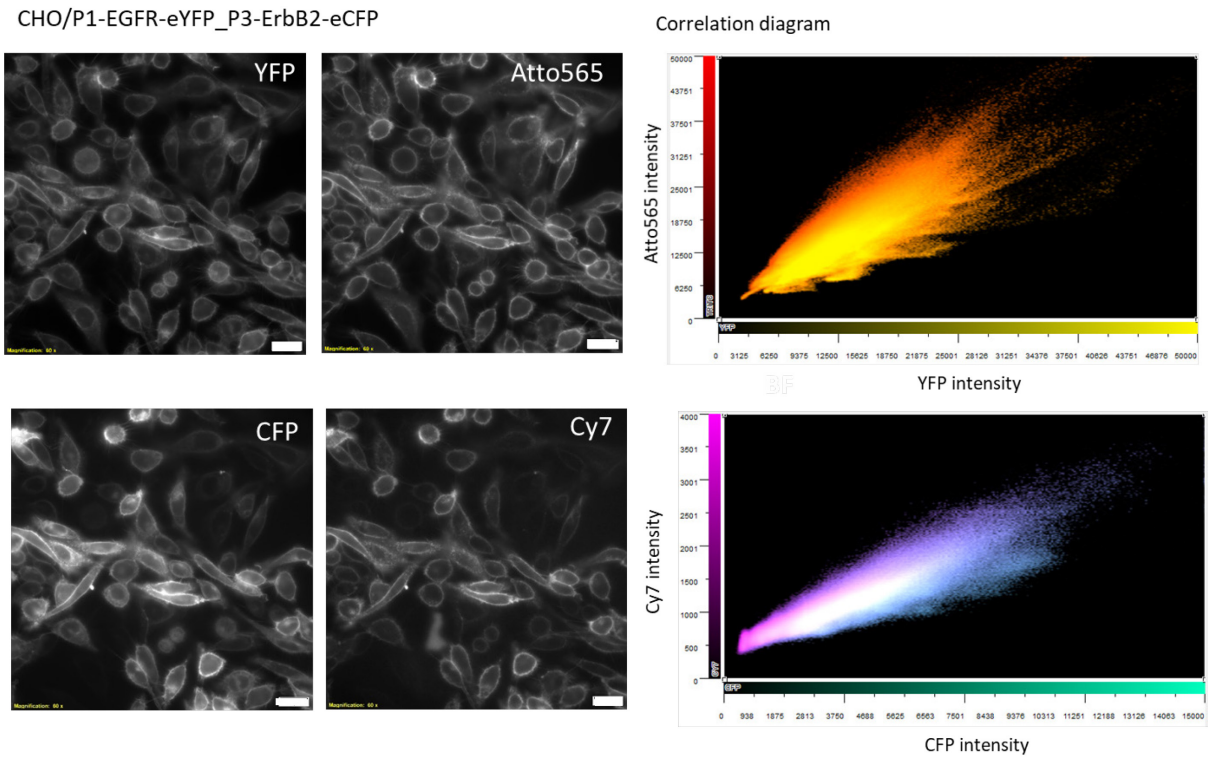

Appendix Figure 2 Correlation plots for colocalization. Fluorescence microscopy and correlation diagram for images of stable CHO cells expressing Cys-P1-EGFR-eYFP and Cys-P3-ErbB2-eCFP as shown in Figure 33G. After PNA labelling with **10** and **11,** followed by DNA hybridisation with **Atto565-DNA1** and **Cy7-DNA3,** images were segmented in the fluorescent protein (YFP or CFP) channel. The pixel intensities in different channels were plotted in correlation diagrams using *cellSens* software (*OLYMPUS EUROPA SE & CO. KG*, Hamburg, Germany**)**. Excitation times: Cy7: 500 ms, Atto565: 500 ms, YFP: 200 ms, CFP 150 ms. Scale bar = 20 µm.

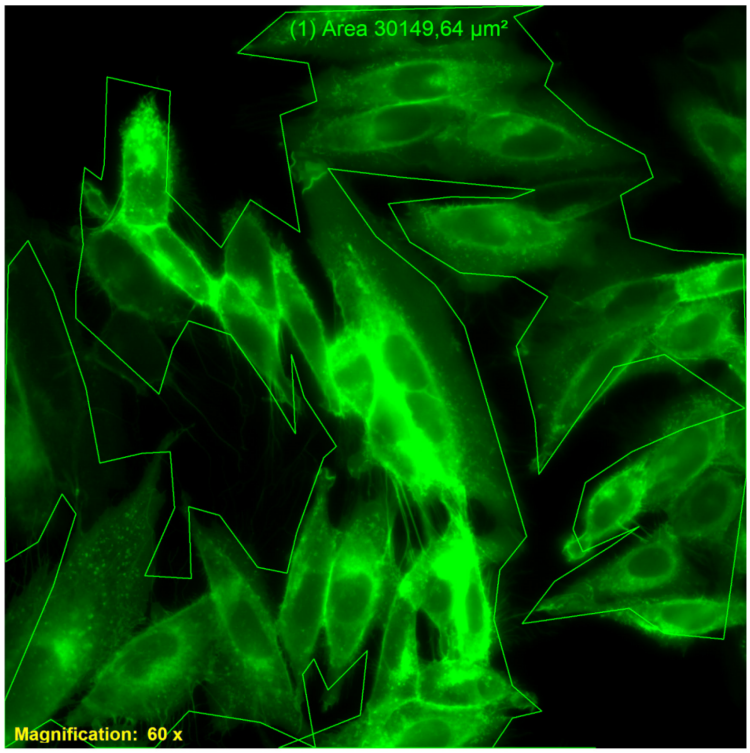

Appendix Figure 3 Measuring labelling lifetime after PNA transfer and DNA hybridization. Representative image (screenshot) from labelling stability analysis in Figure 35B showing region of interest (ROI) drawn in the YFP channel around the cells. In the analysis, mean ROI intensities in the Atto565 and YFP channels were analysed. Excitation time: YFP: 100 ms.

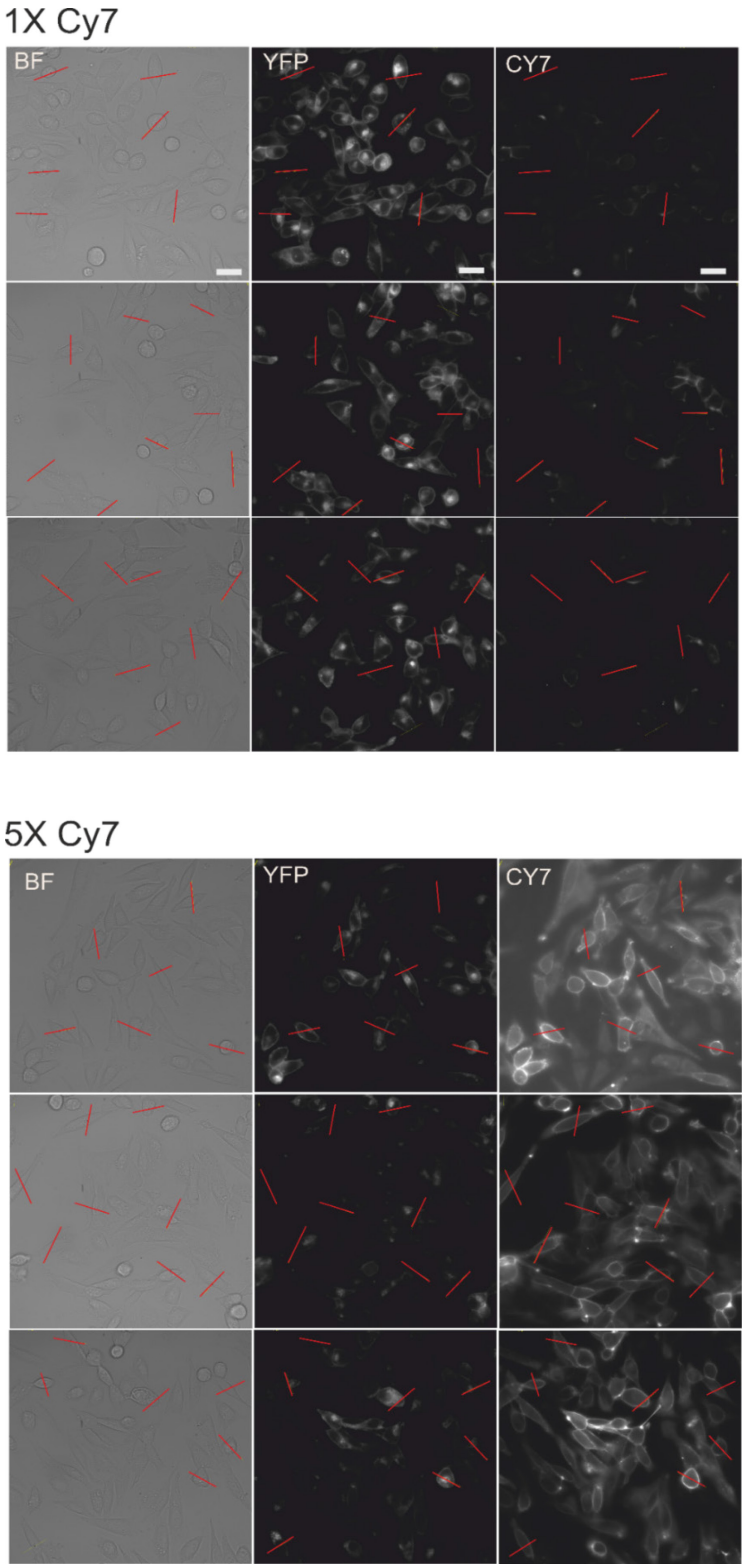

Appendix Figure 4 Line intensity Profiles for multilabelling analysis. Greyscale images and vectors (red) used to create line intensity profiles for calculation of signal-to-noise ratios as shown in Figure 37C. ImageJ was used to generate line scan intensity profiles. Conditions: PNA labelling (100 nM **9** in HBSS, 4 min). DNA hybridization; Cy7-1xComplex or Cy7-5xComplex (100 nM in HBSS-BB, 4 min). Excitation times: YFP: 150 ms; Cy7: 500 ms. n=30 cells from three independent experiments.

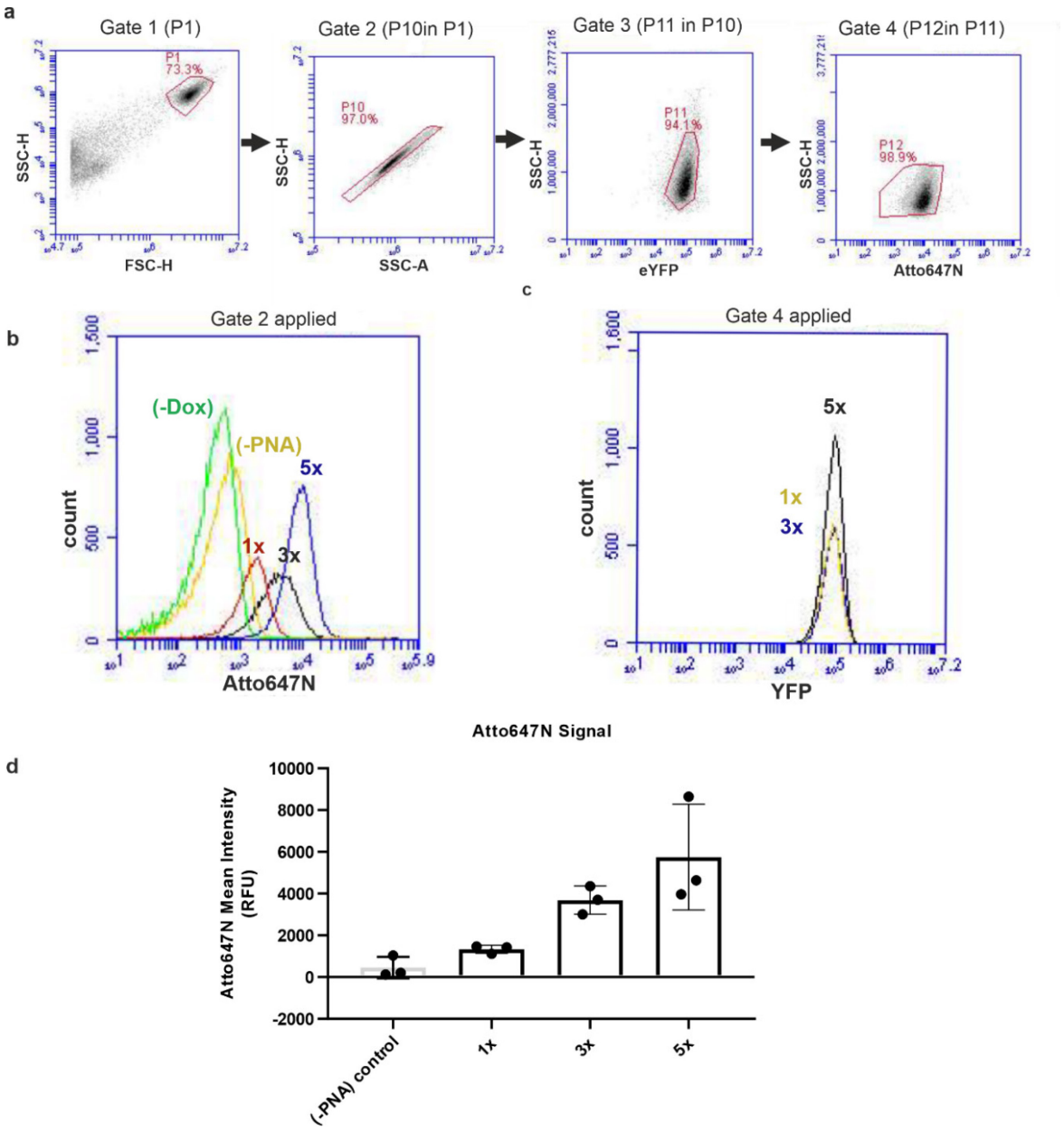

Appendix Figure 5 Flow Cytometry for multilabelling analysis. Flow cytometry analysis of PNA labelled Cys-P1-EGFR-eYFP CHO cells labelled with multiple Atto647N dyes as shown in Figure 37D. **a)** Exemplified gating strategy for the analysis of CHO cells expressing Cys-P1-EGFR-eYFP upon induction with doxycycline and after tagging with PNA and hybridization with Atto647N-labelled nucleic acid complexes. Debris (FSC-A, SSC-A; Gate 1) and doublets (SSC-H, SSC-W; Gate 2) were excluded and the main populations (eYFP; Gate 3) and (Atto647N; Gate 4) were identified. Histograms were analysed by fluorescence flow cytometry after PNA labelling and hybridization with 1, 3 or 5 Atto647N dyes (**Atto647N-1xComplex**, **Atto647N-3xComplex** and **Atto647N-5xComplex,** respectively). A control without doxycycline addition (-Dox) was included to identify background signal and a (-PNA) control where non PNA- tagged cells were treated **Atto647N-5xComplex**. **b)** Atto647N channel after applying gate 2 **c)** YFP channel after applying gate 4. Fluorescence intensity of eYFP and Atto647N is indicated in arbitrary units (A.U.) **d)** Mean intensity of PNA-tagged cells treated with 1, 3 or 5 Atto647N reporter strands, and a (-PNA) control where non-PNA- tagged cells were treated with 5x reporter strands. For analysis, gate 4 was applied, or gate 2 for the control (-Dox). Data is presented as the mean +/- SD of three independent experiments.

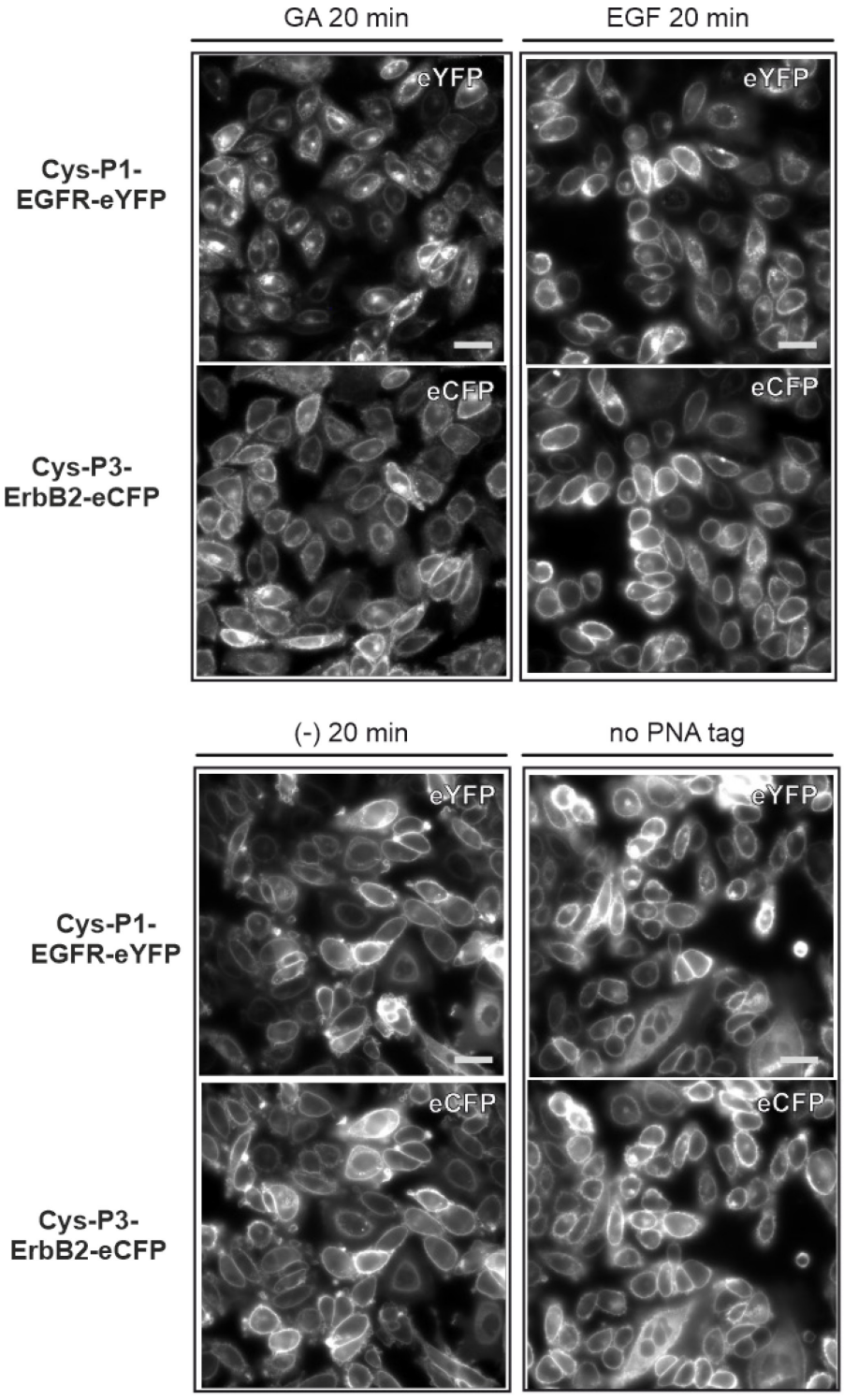

Appendix Figure 6 CFP and YFP channel images from fluorescence microscopy experiment shown in Figure 41B. Representative fluorescence microscopy images from internalization analysis experiment on stable Cys-P1-EGFR-eYFP/Cys-P3-ErbB2-eCFP CHO cells. Excitation time eCFP/eYFP: 400 ms. Conditions: Cys-P1-EGFR-eYFP/Cys-P3-ErbB2-eCFP CHO cells induced with 0.035 µg/ml doxycycline for 20 h and starved for 4 h in 0% FBS media. PNA labelling (100 nM **10**, **11** in DPBS, 4 min) then hybridization of **Atto565-2xImager** and **DY751-2xImager** (200 nM in HBSS-BB, 4 min). Treatment with EGF (100 nM), geldanamycin (GA, 3 µM) or serum free media for 20 min followed by **EraserDNA5** and **EraserDNA6** (1 µM, 2 x 4 min).

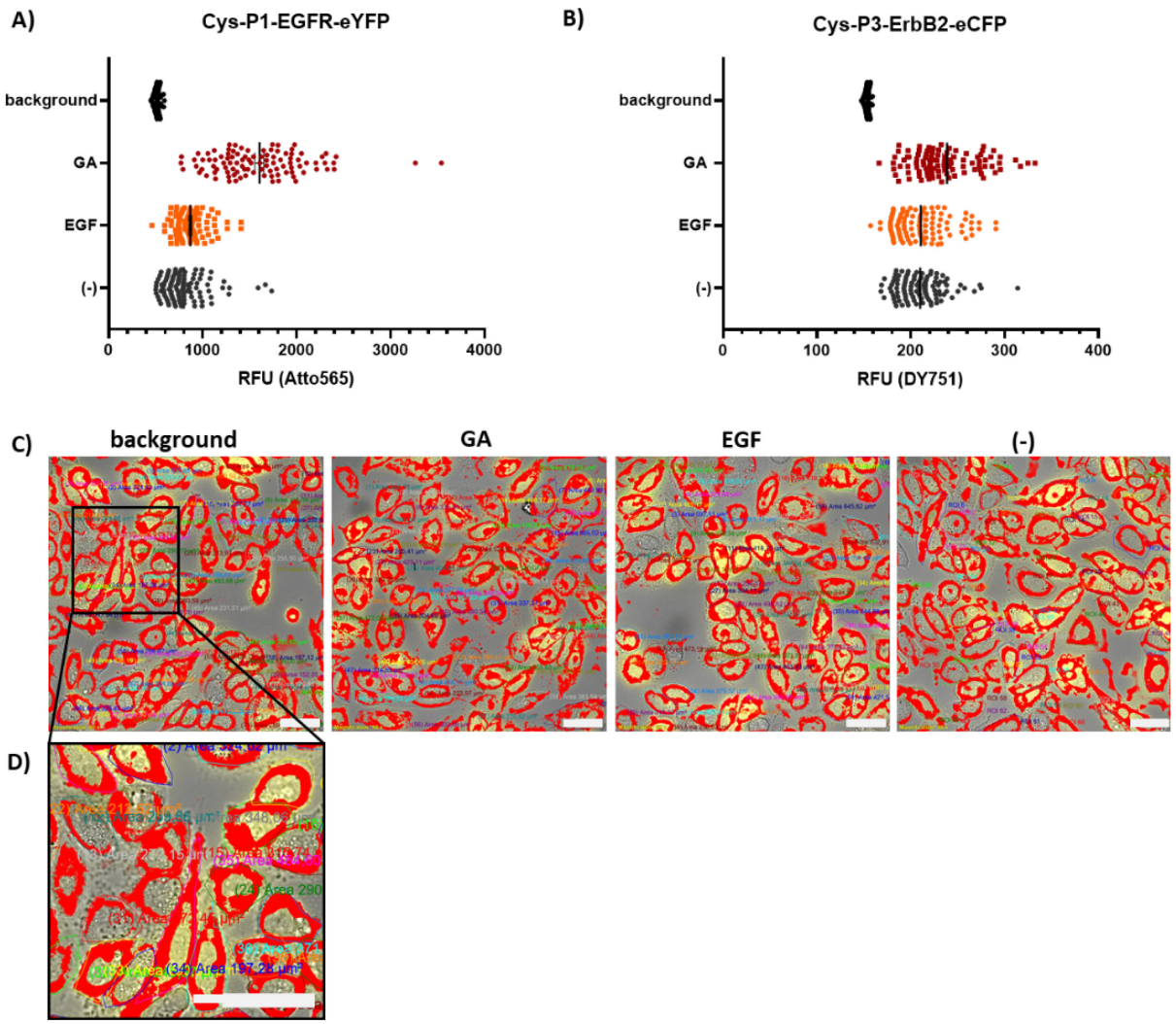

Appendix Figure 7 Internalization analysis methodology. A) and **B)** Scatter plots from a single replicate from experiment shown in Figure 41. Each dot represents one ROI (region of interest), which represents one cell. The brightness (RFU) of the ROI in an indication of internalization in response to the given conditions. For each condition, 100 cells were counted, from two images (viewpoints) of the same well. Scatter plots show mean with SEM. **C)** Examples of automatic segmentation (red) and manual picking of ROIs. Pictures show brightfield images (grey) overlaid with the YFP signal(yellow), segmentation and ROIs (mulitcoloured lines). Scale bar = 30 µm. D) Enlarged image of the black inset in (C). Experiments were repeated three times with similar results and combined data is shown in Figure 41C.

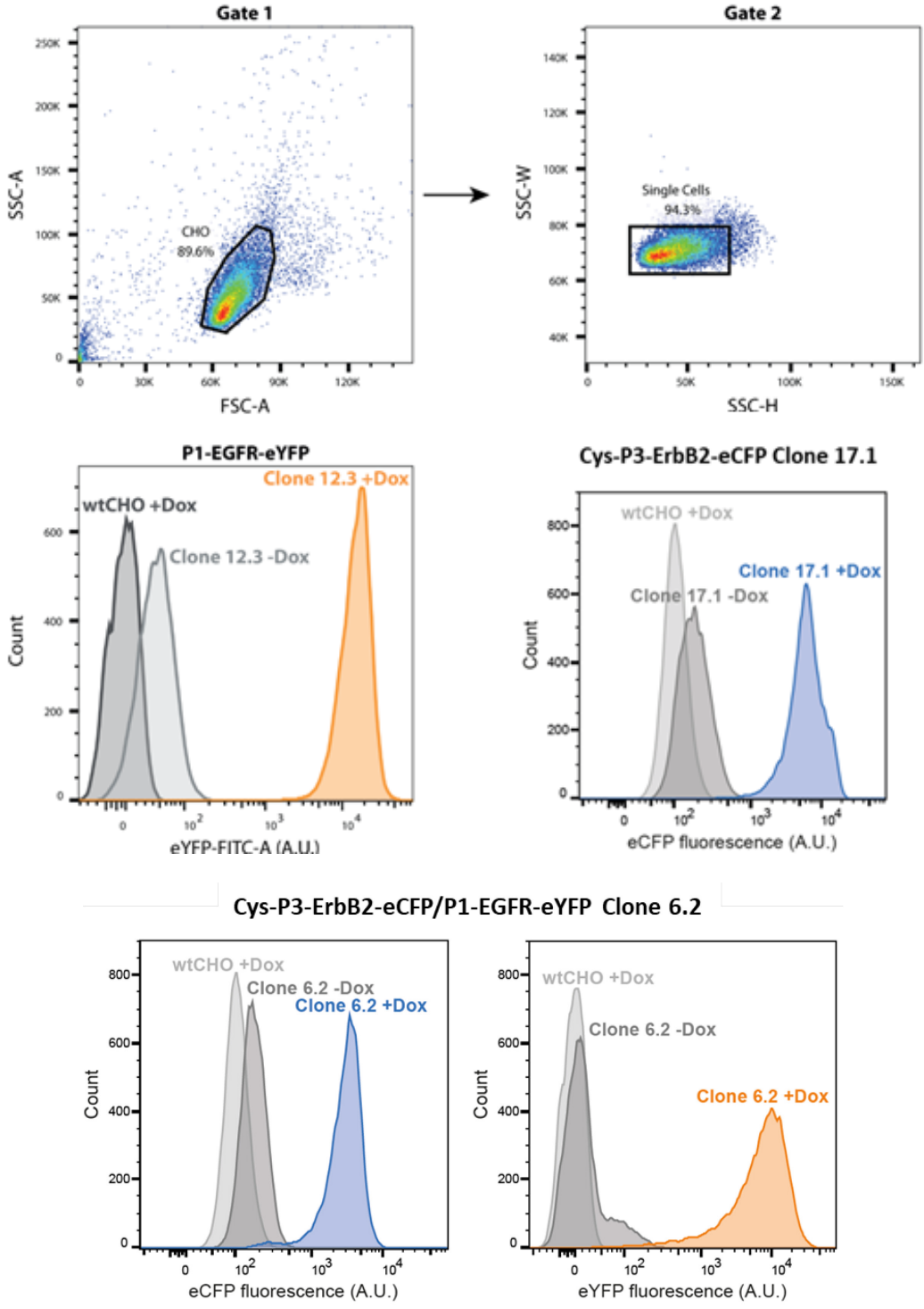

Appendix Figure 8 Generation of doxycycline inducible, stable CHO cell lines. Exemplified gating strategy (Gate 1 and 2),displaying wild-type CHO cells (wtCHO). Debris (FSC-A, SSC-A; Gate 1) and doublets (SSC-H, SSC-W; Gate 2) were excluded and 18,000 cells per sample were analysed for eYFP fluorescence intensity. Expression of P1-EGFR-eYFP (stable CHO clone 12.3), Cys-P3-ErbB2-eCFP only (stable CHO clone 17.1) or Cys-P3-ErbB2-eCFP/Cys-P1-EGFR-eYFP (stable CHO clone 6.2) as analysed by fluorescence flow cytometry in the absence of doxycycline (-Dox) and 18 h after induction with 100 ng/ml doxycycline (+Dox). wtCHO (+Dox) are plotted as negative control. Fluorescence intensity of eCFP/eYFP is indicated in arbitrary units (A.U.).

8.2. Plasmid Maps

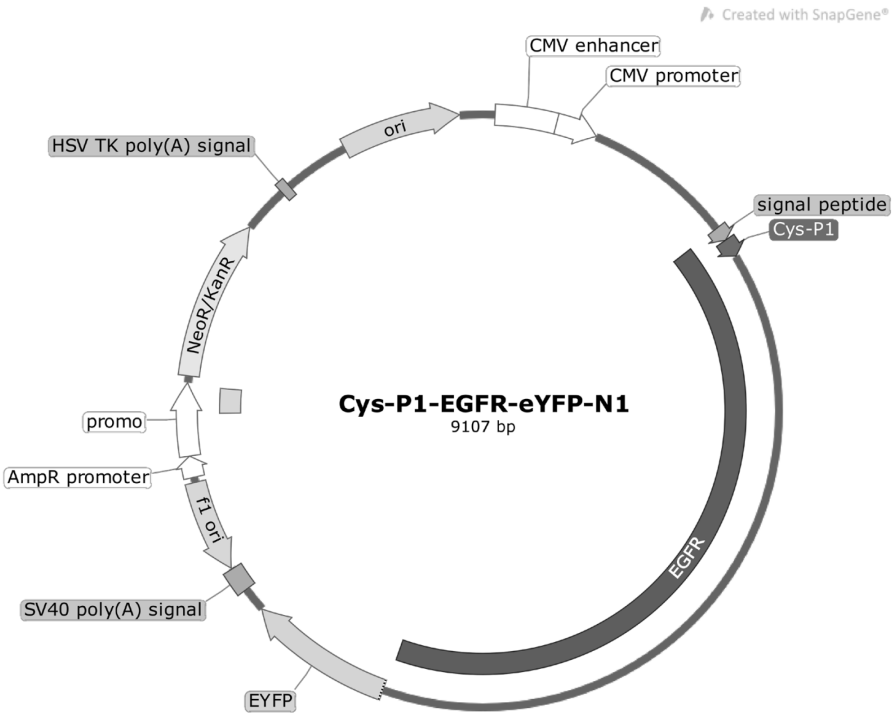

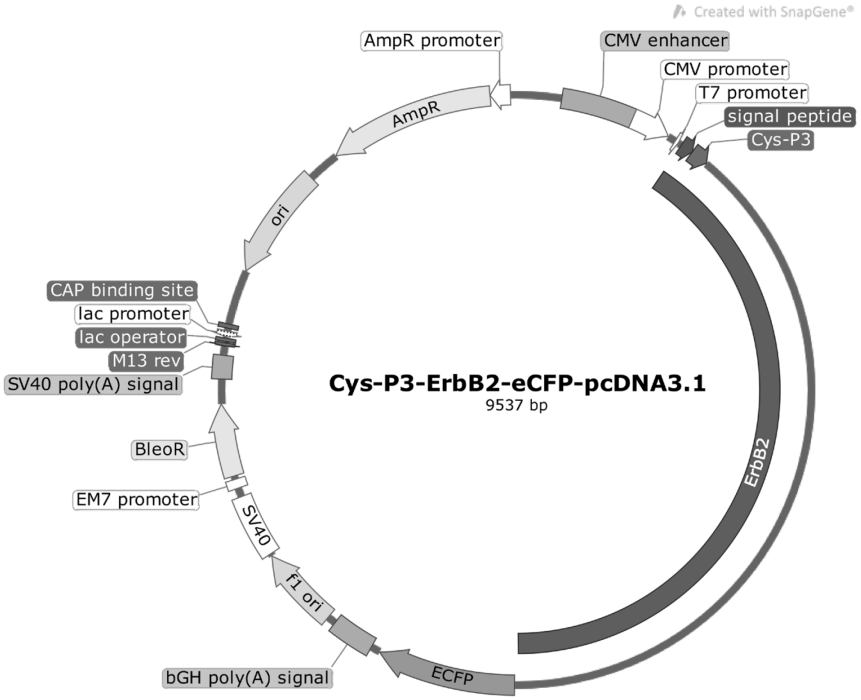

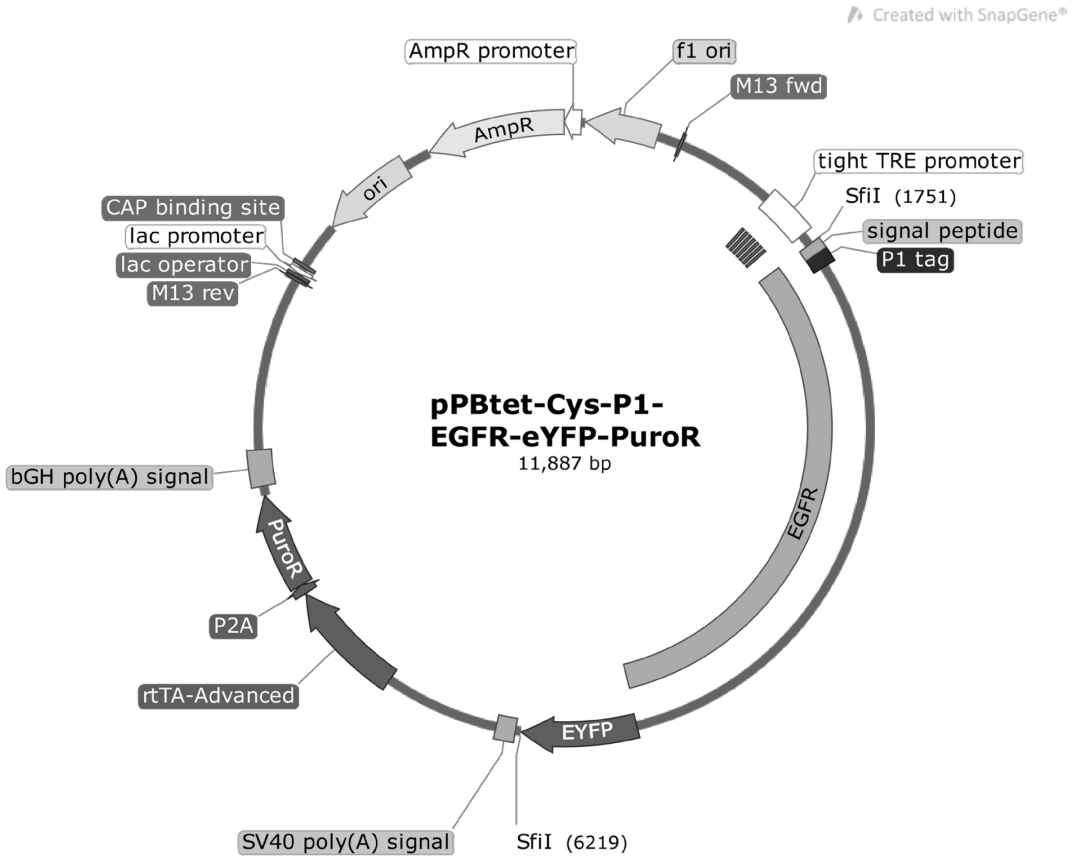
Created with SnapGene®
AmpR promoter
f1 ori
M13 fwd
AmpR
ori
tight TRE promoter
SfiI (1751)
signal peptide
P1 tag
CAP binding site
lac promoter
lac operator
M13 rev
pPBtet-Cys-P1-
EGFR-eYFP-PuroR
11,887 bp
EGFR
bGH poly(A) signal
PuroR
P2A
rtTA-Advanced
EYFP
SV40 poly(A) signal
SfiI (6219)

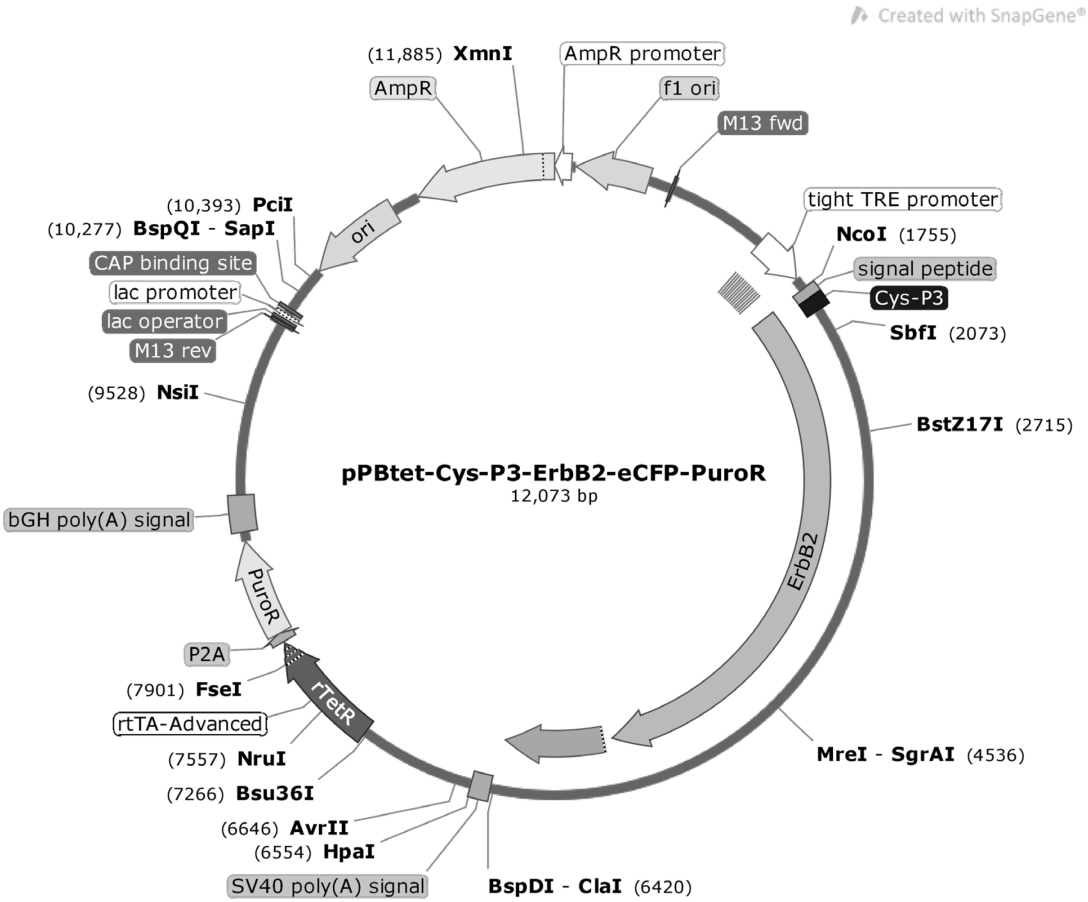
Created with SnapGene®
(11,885) XmnI
AmpR promoter
AmpR
f1 ori
M13 fwd
tight TRE promoter
(10,393) PciI
(10,277) BspQI - SapI
ori
NcoI (1755)
signal peptide
CAP binding site
lac promoter
lac operator
M13 rev
Cys-P3
SbfI (2073)
(9528) NsiI
BstZ17I (2715)
pPBtet-Cys-P3-ErbB2-eCFP-PuroR
12,073 bp
bGH poly(A) signal
ErbB2
PuroR
P2A
(7901) FseI
rTetR
rtTA-Advanced
MreI - SgrAI (4536)
(7557) NruI
(7266) Bsu36I
(6646) AvrII
(6554) HpaI
SV40 poly(A) signal
BspDI - ClaI (6420)

8.3. DNA Sequences for Cloning

Table 7 DNA sequences cloned into expression plasmids

Name	Sequence (5' → 3'):
Cys-P1	TGC GAG ATC CAG GCC CTG GAG GAG GAG AAC GCC CAG CTG GAG CAG GAG AAC GCC GCC CTG GA GGA GGA GAT CGC CCA GCT GGA GTA CGG CGG C
Cys-P3	TGC GAG ATC CAG CAG CTG GAG GAG GAG ATC GCC CAG CTG GAG CAG AAG AAC GCC GCC CTG AAG GAG AAG AAC CAG GCC CTG AAG TAC GGC GGC
SfiI (start)	GGC CTC TGA GGC C
SfiI (stop)	GGC CTG TCA GGC C

9. Declaration

I, Georgina Gavins, declare that I have completed the thesis independently using only the aids and tools specified. I have not applied for a doctor's degree in the doctoral subject elsewhere and do not hold a corresponding doctor's degree. I have taken due note of the Faculty of Mathematics and Natural Sciences PhD Regulations, published in the Official Gazette of Humboldt-Universität zu Berlin no. 42/2018 on 11/07/2018.

…… ……

Place, Date Signature